

Rochester Institute of Technology

**RIT Digital Institutional Repository**

---

Theses

---

5-2023

## **Advanced Control of Vapor Compression Liquid Chillers**

Suliman Awad  
saa9231@rit.edu

Follow this and additional works at: <https://repository.rit.edu/theses>

---

### **Recommended Citation**

Awad, Suliman, "Advanced Control of Vapor Compression Liquid Chillers" (2023). Thesis. Rochester Institute of Technology. Accessed from

This Thesis is brought to you for free and open access by the RIT Libraries. For more information, please contact [repository@rit.edu](mailto:repository@rit.edu).



**Advanced Control of Vapor Compression Liquid Chillers**

**By**

**Suliman Awad**

**A Thesis Submitted in Partial Fulfilment of the Requirements for the  
Degree of Master of Science in Electrical Engineering**

**Department of Electrical Engineering and Computing Sciences**

**Rochester Institute of Technology**

**RIT Dubai**

**May 2023**

## Committee Approval

---

Dr. Abdulla Ismail

Date

Professor of Electrical Engineering, RIT Dubai

Thesis Advisor

---

Dr. Ghalib Y. Kahwaji

Date

Professor and Chair of Mechanical & Industrial Engineering, RIT Dubai

Committee Member

---

Dr. Jinane Mounsef

Date

Assistant Professor of Electrical Engineering, RIT Dubai

Committee Member

## **Acknowledgement**

I would like to acknowledge and extend my gratefulness to my thesis advisor Dr. Abdula Ismail for his continuous support and his motivation of exploring different approaches to tackle the control problem. I, also, would like to extend my appreciation to my family and friends who encouraged and supported me to complete this work.

## **Abstract**

Chillers are one of the most sophisticated and most important equipment in cooling plants. Due to its complexity and importance, a cost effective and accurate control technique is a necessity to ensure system reliability and longevity. As the chiller contains multiple inputs and outputs, two advanced multivariable control techniques were selected to control the chillers cooling capacity, exit chilled liquid temperature of the evaporator as well as to reject disturbances. The advanced techniques covered in this framework are the Linear Quadratic Integral (LQI) and Model Predictive Control (MPC). Both were successfully applied to the chiller's model for multiple testing cases and simulations. Then the results were compared to the industry standard control technique, the PID. Successful use of Genetic Algorithm (a machine learning method) is also presented in this thesis as a method for tuning the controller weights. It was deduced from the simulation test results that the LQI and MPC outperformed the traditional PID controllers in terms of energy efficiency and transient response. An energy savings of around 10% to 20% is seen on the compressor's electric power, lower overshoot/undershoot for most outputs and faster settling time. Also, the MPC controller had the ability to incorporate input constraints into the problem formulation and use quadratic programming to find a solution to the constraint optimization problem.

# Table of Contents

Acknowledgement.....	iii
Abstract .....	iv
Table of Contents.....	v
List of Figures.....	viii
List of Tables .....	xiii
Nomenclature .....	xiv
Chapter 1 Introduction.....	1
1.1 Background .....	1
1.2 District Cooling System Loops.....	2
1.2.1 Loop 1: Air System.....	3
1.2.2 Loop 2: Chilled Water System.....	4
1.2.3 Loop 3: Condenser Water System .....	4
1.3 Temperature Design Basis .....	5
1.4 Major Components of a District Cooling Plant.....	5
1.4.1 Chiller .....	5
1.4.2 Cooling Tower .....	8
1.4.3 Condenser Water Pump .....	9
1.4.4 Chilled Water Pumps .....	10
1.5 Capacity Control of Water-Cooled Centrifugal Chillers .....	10
1.6 Thesis Objective .....	12
1.7 Research Contributions .....	13
1.8 Thesis Organization.....	13
Chapter 2 Literature Review .....	14
2.1 Modeling Techniques of Vapor Compression Systems.....	16
2.1.1 White-Box Modeling (Physical) .....	16
2.1.2 Black-Box Modeling (Data-Driven).....	20
2.1.3 Grey-Box Modeling (Hybrid) .....	25
2.2 Control Techniques of Vapor Compression Systems.....	31
2.2.1 Classical Control.....	32
2.2.2 Hard Control.....	33

2.2.3 Soft and Hybrid Controls.....	40
Chapter 3 Dynamic Modeling of Single-stage Liquid Chiller .....	44
3.1 Model Formulation.....	44
3.1.1 Working Principles of Vapor Compression Cycle in Liquid Chillers.....	44
3.1.2 Modeling Approach and Assumptions.....	46
3.1.3 Fundamental Equations.....	46
3.1.4 Key Parameters Determination .....	49
3.2 State-Space Representation.....	52
3.3 Simulation Results of the Open-Loop Model.....	59
3.3.1 Open-loop Response of Case 1 .....	61
Chapter 4 Liquid Chiller Control using PID Controllers .....	68
4.1 The Control Problem .....	68
4.1.1 Trajectory Tracking .....	69
4.1.2 Disturbance Rejection.....	71
4.2 PID Control of Liquid Chiller .....	72
4.3.1 Trajectory Tracking – Cooling Load.....	77
4.3.2 Trajectory Tracking – Leaving Chilled liquid Temperature .....	81
4.3.3 Disturbance Rejection – Entering Chilled liquid Temperature .....	83
Chapter 5 Linear Quadratic Integral Control of Liquid Chiller .....	86
5.1 The Solution to the Linear Quadratic Regulator .....	86
5.2 Linear Quadratic Integral Problem Formulation .....	87
5.3 Implementation and Simulation Results of the LQI Controller .....	89
5.3.1 Trajectory Tracking – Cooling Load.....	91
5.3.2 Trajectory Tracking – Leaving Chilled liquid Temperature .....	95
5.3.3 Disturbance Rejection – Entering Chilled liquid Temperature .....	97
Chapter 6 Model Predictive Control of Liquid Chiller and Controller Tuning using Genetic Algorithms .....	100
6.1 Fundamentals of Model Predictive Control (MPC) .....	100
6.2 Solution to Model Predictive Control with Direct Feedthrough .....	102
6.2.1 Augmented State-space Model Formulation.....	102
6.2.2 Prediction of Controlled Inputs, States and Output Variables .....	104
6.2.3 Optimization.....	105
6.2.4 Block Diagram Representation of the Model Predictive Control System .....	107

6.3 Model Predictive Controller Weight Tuning using Genetic Algorithm .....	109
6.4 Implementation and Simulation Results of the MPC Controller .....	111
6.4.1 Trajectory Tracking – Cooling Load.....	114
6.4.2 Trajectory Tracking – Leaving Chilled liquid Temperature .....	118
6.4.3 Disturbance Rejection – Entering Chilled liquid Temperature .....	121
Chapter 7 Analysis and Performance Comparison between the Control Approaches.....	123
7.1 Trajectory Tracking – Cooling Load .....	124
7.2 Trajectory Tracking – Leaving Chilled liquid Temperature.....	130
7.3 Disturbance Rejection – Entering Chilled liquid of Evaporator .....	133
Chapter 8 Conclusions and Future Work .....	137
Bibliography .....	139

## List of Figures

Figure 1-1: District Cooling System Network [1] .....	1
Figure 1-2: Water-Cooled HVAC System Schematic [3].....	3
Figure 1-3: Components of a Vapor Compression Refrigeration System [3] .....	7
Figure 1-4: Cooling Tower [3].....	9
Figure 1-5: Centrifugal Chiller, Courtesy of Trane [6].....	11
Figure 1-6: Hot Gas By-Pass [5].....	12
Figure 2-1: Discretization of the shell-and-tube heat exchangers for the finite-volume formulations [12] .....	17
Figure 2-2: Discretization of the shell-and-tube heat exchangers for the moving boundary formulations [12] .....	17
Figure 2-3: Block diagram of a condenser [16] .....	19
Figure 2-4: Data-driven Models in HVAC Systems [18].....	21
Figure 2-5: Series-parallel Identification Structure [19].....	22
Figure 2-6: ARX, AMX, OE and BJ Model Architectures [21].....	24
Figure 2-7: Predicted vs Actual Dynamic Response of Chilled Water Output using four methods [21] .....	24
Figure 2-8: State-space chiller model directed graph [28].....	29
Figure 2-9: Block diagram for the dynamic simulation of refrigeration system [29] .....	30
Figure 2-10: Control System Block Diagram with Gain Scheduling [34] .....	34
Figure 2-11: Block diagram of the non-linear predictive control system .....	35
Figure 2-12: Block diagram of the closed-loop system [37] .....	37
Figure 2-13: Overall GA Optimization Controller Process [43] .....	42
Figure 2-14: Overall Block diagram of the Prediction System with GA Trial Computations [43] .....	42
Figure 2-15: Average COP according to the control method [45].....	43
Figure 3-1: Block-diagram of a single-stage vapor compression liquid chiller [28].....	45
Figure 3-2: Pressure-enthalpy plot of a single-stage vapor compression system [28] .....	45
Figure 3-3: State-space Representation Block Diagram .....	53
Figure 3-4: State-space Representation with Disturbance Input Block Diagram .....	53
Figure 3-5: Output Responses of Exit Coolant Temperature of Condenser at Different Inputs.....	62

Figure 3-6: Output Responses of Exit Chilled liquid Temperature of Evaporator at Different Inputs.....	62
Figure 3-7: Output Responses of Compressor Electric Power, Chiller Cooling Capacity and COP due to Step Increase of Inlet Coolant Temperature of Condenser.....	63
Figure 3-8: Output Responses of Compressor Electric Power, Chiller Cooling Capacity and COP due to Step Increase of Coolant Flow Rate of Condenser .....	63
Figure 3-9: Output Responses of Compressor Electric Power, Chiller Cooling Capacity and COP due to Step Increase of Inlet Chilled liquid Temperature of Evaporator.....	64
Figure 3-10: Output Responses of Compressor Electric Power, Chiller Cooling Capacity and COP due to Step Increase of Chilled liquid Flow Rate of Evaporator.....	64
Figure 3-11: Output Responses of Compressor Electric Power, Chiller Cooling Capacity and COP due to Step Increase of the Refrigerant Flow Rate .....	65
Figure 4-1: PID controller block diagram of a SISO system .....	72
Figure 4-2: Decentralized PID control for a model with 4 inputs and 4 outputs.....	74
Figure 4-3: Decentralized PID control implementation on Simulink .....	76
Figure 4-4: Decentralized Closed-loop System with only Dominant Controllers .....	77
Figure 4-5: Output responses due to a step change in cooling load by 600 W .....	78
Figure 4-6: Output responses due to a step change in cooling load by 1200 W .....	78
Figure 4-7: Output responses due to a step change in cooling load by 3000 W .....	79
Figure 4-8: Applied control inputs signals due to a step change in cooling load by 600 W ...	79
Figure 4-9: Applied control inputs signals due to a step change in cooling load by 1200 W .	80
Figure 4-10: Applied control inputs signals due to a step change in cooling Load by 3000 W .....	80
Figure 4-11: Output responses due to a step change in exit chilled liquid temperature of the evaporator by 1 °C .....	81
Figure 4-12: Output responses due to a step change in exit chilled liquid temperature of the evaporator by 2 °C .....	82
Figure 4-13: Control signals due to a step change in exit chilled liquid temperature of the evaporator by 1 °C .....	82
Figure 4-14: Control signals due to a step change in exit chilled liquid temperature of the evaporator by 2 °C .....	83
Figure 4-15: Output responses due a step change in inlet chilled liquid temperature of evaporator by 0.5 °C .....	84

Figure 4-16: Output responses due a step change in inlet chilled liquid temperature of evaporator by 2.5 °C .....	84
Figure 4-17: Control signals due to a step change in inlet chilled liquid temperature of evaporator by 0.5 °C .....	85
Figure 4-18: Control signals due to a step change in inlet chilled liquid temperature of evaporator by 2.5 °C .....	85
Figure 5-1: Block diagram representation of an LQR controller [49] .....	87
Figure 5-2: Block diagram representation of an LQI controller.....	88
Figure 5-3: Simulink implementation of the LQI controller on the chiller model.....	90
Figure 5-4: Implementation of the open-loop chiller model subblock in discrete time.....	90
Figure 5-5: Output responses due to a step change in cooling load by 600 W .....	92
Figure 5-6: Output response due to a step change in cooling load by 1200 W.....	92
Figure 5-7: Output responses due to a step change in cooling load by 3000 W .....	93
Figure 5-8: Control signals due to a step change in cooling load by 600 W .....	93
Figure 5-9: Control signals due to a step change in cooling load by 1200 W .....	94
Figure 5-10: Control signals due to a step change in cooling load by 3000 W .....	94
Figure 5-11: Output responses due to a step change in exit chilled liquid temperature of evaporator by 1 °C .....	95
Figure 5-12: Output response due to a step change in exit chilled liquid temperature of evaporator by 2 °C .....	96
Figure 5-13: Control signals due to a step change in exit chilled liquid temperature of evaporator by 2 °C .....	96
Figure 5-14: Control signals due to a step change in exit chilled liquid temperature of evaporator by 2 °C .....	97
Figure 5-15: Output response due to a step change in inlet chilled liquid temperature of evaporator by 0.5 °C .....	98
Figure 5-16: Output response due to a step change in inlet chilled liquid temperature of evaporator by 1 °C .....	98
Figure 5-17: Control signals due to a step change in inlet chilled liquid temperature of evaporator by 0.5 °C .....	99
Figure 5-18: Control signals due to a step change in inlet chilled liquid temperature of evaporator by 1 °C .....	99
Figure 6-1: Illustration of the MPC control operation [52] .....	101

Figure 6-2: Block diagram of discrete-time predictive control system with direct feedthrough and measured input disturbance.....	108
Figure 6-3: Flow chart of the Genetic algorithm optimization process [55].....	110
Figure 6-4: Illustration of the various steps performed by GA [54] .....	111
Figure 6-5: Performance of the GA on liquid chiller tuning as the generations evolve.....	113
Figure 6-6: Output responses due to a step change in cooling load by 600 W .....	115
Figure 6-7: Output responses due to a step change in cooling load by 1200 W .....	115
Figure 6-8: Output responses due to a step change in cooling load by 3000 W .....	116
Figure 6-9: Control signals due to a step change in cooling load by 600 W .....	116
Figure 6-10: Control signals due to a step change in cooling load by 1200 W .....	117
Figure 6-11: Control signals due to a step change in cooling load by 3000 W .....	117
Figure 6-12: Output response due to a step change in exit chilled liquid temperature of evaporator by 1 °C .....	118
Figure 6-13: Output response due to a step change in exit chilled liquid temperature of evaporator by 2 °C .....	119
Figure 6-14: Control signals due to a step change in exit chilled liquid temperature of evaporator by 1 °C .....	120
Figure 6-15: Control signals due to a step change in exit chilled liquid temperature of evaporator by 2 °C .....	120
Figure 6-16: Output response due to a step change in entering chilled liquid temperature of evaporator by 0.5 °C .....	121
Figure 6-17: Output response due to a step change in entering chilled liquid temperature of evaporator by 2.5 °C .....	122
Figure 6-18: Control signals due to a step change in entering chilled liquid temperature of evaporator by 0.5 °C .....	122
Figure 6-19: Control signals due to a step change in entering chilled liquid temperature of evaporator by 2.5 °C .....	123
Figure 7-1: Output responses due to step change in cooling load by 200 W .....	125
Figure 7-2: Output responses due to step change in cooling load by 600 W .....	126
Figure 7-3: Output responses due to step change in cooling load by 1200 W .....	126
Figure 7-4: Output responses due to step change in cooling load by 2000 W .....	127
Figure 7-5: Output responses due to step change in cooling load by 3000 W .....	127
Figure 7-6: Control signals due to step change in cooling load by 200 W .....	128

Figure 7-7: Control signals due to step change in cooling load by 600 W .....	128
Figure 7-8: Control signals due to step change in cooling load by 1200 W .....	129
Figure 7-9: Control signals due to step change in cooling load by 2000 W .....	129
Figure 7-10: Control signals due to step change in cooling load by 3000 W .....	130
Figure 7-11: Output responses due to a step change in exit chilled liquid temperature of evaporator by 1 °C .....	131
Figure 7-12: Output responses due to a step change in exit chilled liquid temperature of evaporator by 2 °C .....	132
Figure 7-13: Control signals due to a step change in exit chilled liquid temperature of evaporator by 1 °C .....	132
Figure 7-14: Control signals due to a step change in exit chilled liquid temperature of evaporator by 2 °C .....	133
Figure 7-15: Output responses due to a step change in entering chilled liquid temperature of evaporator by 0.5 °C .....	134
Figure 7-16: Output responses due to a step change in entering chilled liquid temperature of evaporator by 2.5 °C .....	135
Figure 7-17: Control signals due to a step change in entering chilled liquid temperature of evaporator by 0.5 °C .....	135
Figure 7-18: Control signals due to a step change in entering chilled liquid temperature of evaporator by 2.5 °C .....	136

## List of Tables

Table 1-1: Chiller Technology [1] .....	6
Table 2-1: Some of HVAC Control Methods [10] .....	15
Table 2-2: Performance Comparison of the Models Under Different Experiments [21] .....	24
Table 3-1: Initial Conditions of Case 1 [28][46] .....	59
Table 3-2: Initial Conditions of Case 2 and its Subcases [28][46] .....	59
Table 3-3: Initial Conditions of Case 3 and its Subcases [28][46] .....	60
Table 3-4: Initial Conditions of Case 4 and its Subcases [28][46] .....	60
Table 3-5: Applied Changes on Input Value of the Open-loop System .....	61
Table 4-1: Saturations of the Control Input Signals .....	69
Table 4-2: Reference Values for Testing the Trajectory Tracking Performance of the Controller due a to Step Change in the Cooling Capacity .....	70
Table 4-3: Reference Values for Testing the Trajectory Tracking Performance of the Controller due a to Step Change in the Exit Chilled liquid Temperature of the Evaporator .....	71
Table 4-4: Reference Values for Testing the Disturbance Rejection of the Controller due a to Step Change in the Entering Chilled liquid Temperature of the Evaporator .....	71
Table 5-1: Weights of Q and R Matrices of the LQI controller .....	91
Table 6-1: Tuning Parameters and Weights of the MPC Controller .....	114

# Nomenclature

## Abbreviations

A, B, C, D	State-space representation coefficient matrices
$A_{co}$	Area between condenser and refrigerant, $m^2$
$A_{cw}$	Area of condenser secondary fluid (coolant liquid) channel, $m^2$
$A_{eo}$	Area between evaporator and refrigerant, $m^2$
$A_{ew}$	Area of evaporator secondary fluid (chilled liquid) channel, $m^2$
$a_{co}$	Heat transfer coefficient between condenser and refrigerant, $W m^2 \text{ }^\circ C^{-1}$
$a_{cw}$	Heat transfer coefficient of convection of condenser secondary fluid (coolant liquid), $W m^2 \text{ }^\circ C^{-1}$
$a_{eo}$	Heat transfer coefficient between evaporator and refrigerant, $W m^2 \text{ }^\circ C^{-1}$
$a_{ew}$	Heat transfer coefficient of convection of evaporator secondary fluid (chilled liquid), $W m^2 \text{ }^\circ C^{-1}$
$c_{cr}$	Specific heat of refrigerant in condenser, $J kg^{-1} \text{ }^\circ C^{-1}$
$c_{cw}$	Specific heat of condenser secondary fluid (coolant liquid), $J kg^{-1} \text{ }^\circ C^{-1}$
$c_{cg}$	Specific heat of shell wall of condenser, $J kg^{-1} \text{ }^\circ C^{-1}$
$c_{er}$	Specific heat refrigerant in evaporator, $J kg^{-1} \text{ }^\circ C^{-1}$
$c_{ew}$	Specific heat of evaporator secondary fluid (chilled liquid), $J kg^{-1} \text{ }^\circ C^{-1}$
$c_{eg}$	Specific heat of shell wall of evaporator, $J kg^{-1} \text{ }^\circ C^{-1}$
com	compressor
d	Hydraulic diameter, m
FV	Finite Volume
GA	Genetic Algorithms
$G_{cw}$	Mass flow rate of condenser secondary fluid or coolant liquid (additional subscript L denotes to leaving/outlet and E for entering/inlet), $kg s^{-1}$
$G_{ew}$	Mass flow rate of evaporator secondary fluid or chilled liquid (additional subscript L denotes to leaving/outlet and E for entering/inlet), $kg s^{-1}$
$G_{rm}$	Mass flow rate of the refrigerant, $kg s^{-1}$
$h_{\#}$	Enthalpy (subscripts # 1, 2, 3 or 4 denote to the state in the vapor compression cycle), $J kg^{-1}$
$h_{r,\Delta t}$	Enthalpy of sub-cooled liquid refrigerant, $J kg^{-1}$
$h_o$	Reference enthalpy, $J kg^{-1}$

LQI	Linear Quadratic Integral
LQR	Linear Quadratic Regulator
$M_{cr}$	Mass of refrigerant in condenser, kg
$M_{cw}$	Mass of condenser secondary fluid (coolant liquid), kg
$M_{cg}$	Mass of shell wall of condenser, kg
$M_{er}$	Mass of refrigerant in evaporator, kg
$M_{ew}$	Mass of evaporator secondary fluid (chilled liquid), kg
$M_{eg}$	Mass of shell wall of evaporator, kg
MB	Moving Boundary
MIMO	Multi-Input-Multi-Output
MPC	Model Predictive Control
$p_{atm}$	Atmospheric pressure, Pa
$p_{r,bg}$	Saturated vapor refrigerant pressure, Pa
$p_{r,bl}$	Saturated liquid refrigerant pressure, Pa
PID	Proportional-Integral-Derivative
Qc	Cooling Capacity, W
QP	Quadratic Programming
$q_r$	Latent heat of vaporization refrigerant, $\text{kJ kg}^{-1}$
$R_r$	Gas constant of refrigerant, $\text{kJ kg}^{-1}$
r	Reference Signal
REF	Reference (or setpoint) signal
SISO	Single-Input-Single-Output
T	time, s
$t_c$	Condensing temperature, °C
$t_{cw,E}$	Entering/inlet condenser secondary fluid or coolant liquid temperature, °C
$t_{cw,L}$	Leaving/outlet condenser secondary fluid or coolant liquid temperature, °C
$t_{cg}$	Shell wall temperature of condenser, °C
$t_k$	Evaporating temperature, °C
$t_{ew,E}$	Entering/inlet evaporator secondary fluid or chilled liquid temperature, °C
$t_{ew,L}$	Leaving/outlet evaporator secondary fluid or chilled liquid temperature, °C
$t_{eg}$	Shell wall temperature of evaporator, °C
$T_{cc}$	Critical state temperature, K

$T_{r,bg}$	Saturated vapor refrigerant temperature, K
$T_{r,g}$	Vapor refrigerant temperature, K
$T_{r,q}$	Refrigerant temperature in evaporation process, K
$u$	Velocity of flow $m\ s^{-1}$
$N$	Electric power, W
$Nu$	Nusselt number
$Re$	Reynolds number
VCS	Vapor Compression Systems
$Z$	Compressibility factor
$\tau$	Time, s
$\rho$	Density, $kg\ m^{-3}$
$K_p$	Proportional controller constant
$K_i$	Integral controller constant
$K_d$	Derivative controller constant
$k_s$	Adiabatic compression
$\eta$	Efficiency
$\Delta t_{e,shr}$	Superheated temperature, °C
$\lambda$	Thermal conductivity, $W\ m^{-1}\ ^\circ C^{-1}$
$\mu$	Dynamic viscosity coefficient, $kg\ m^{-1}\ s^{-1}$
$\nu$	Kinematic viscosity coefficient, $m^2\ s^{-1}$ ; or specific volume, $m^3\ kg^{-1}$

# Chapter 1 Introduction

## 1.1 Background

A District Cooling Plant (DCP) is a centralized approach in distributing chilled water to Heating, Ventilation and Air Conditioning (HVAC) equipment such as an Air Handling Unit (AHU) and a Fan Coil Unit (FCU) in medium to large residential, commercial, educational, medical and industrial buildings/facilities for the purpose of cooling and dehumidification [1][2]. Figure 1-1 depicts a typical DCP building and its piping or distribution system to each respective building [1]. Thus, it is a replacement of the traditional decentralized approach of having all the equipment installed within each building; or in other words, each building produces its own chilled water for its respective equipment.

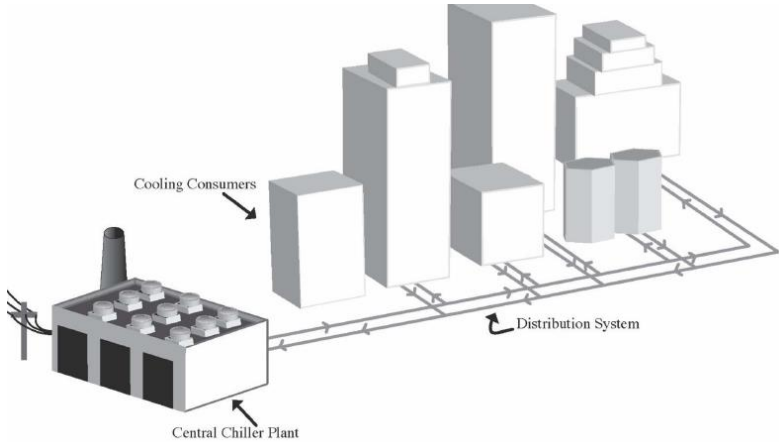


Figure 1-1: District Cooling System Network [1]

Albeit the high initial cost of constructing a DCP, the long run benefits can be viewed from different angles, including, but not limited to economic, environmental and performance benefits. [1][2]. The economic benefits for the investor and operator include having a smaller number of personnel for operation for their other equipment, more free space which can be

utilized for other purposes, lower electricity consumption, insurance and liability benefits, the cost of equipment maintenance will be less, lower electrical and mechanical costs during construction (i.e. chillers and other equipment are in a centralized location inside the DCP) [1][2].

A DCP uses fewer chillers – to cool a certain district - whose rating is higher and more efficient (i.e. higher cooling output produced per electrical input) compared to smaller units installed within each consumers' building [1][2]. Moreover, many DCPs utilize Thermal Energy Storage (TES) tanks that can be used to supply chilled water to the load during high demand hours, power failure or to shed off the load from the chiller(s) during the day when the electricity cost is higher (i.e. charging the TES tank(s) during night when electricity cost is lower and discharging the tank(s) during the day when the cost of electricity is higher) [1][2]. Thus, the environmental and performance gains of a centralized approach for cooling is higher due to higher overall efficiency of equipment, lower electricity consumption, reduced carbon emission and redundancy [1][2].

## **1.2 District Cooling System Loops**

The main components of a District Cooling System are presented in Figure 1-2, these components are sub-divided into three loops, namely, chilled water loop, condenser water loop and the air system loop [3]. The main components of a District Cooling System include:

1. Chillers
2. Cooling Towers
3. Condenser Water Pumps (CWP)
4. Chilled Water Pumps. These are split into two parts: Primary Chilled Water Pump (PCHWP) and Secondary Chilled Water Pumps (SCHWP).
5. Auxiliary Equipment such as valves, make-up pumps, chemical dosing system, expansion tanks, chilled/condenser water filtration system, air separators and expansion tanks.
6. Loads in the form of HVAC Equipment such as AHUs and FCUs.

Other main component that may be included in a district cooling system depending on design criteria - is a Thermal Energy Storage (TES) Tank [1][3].

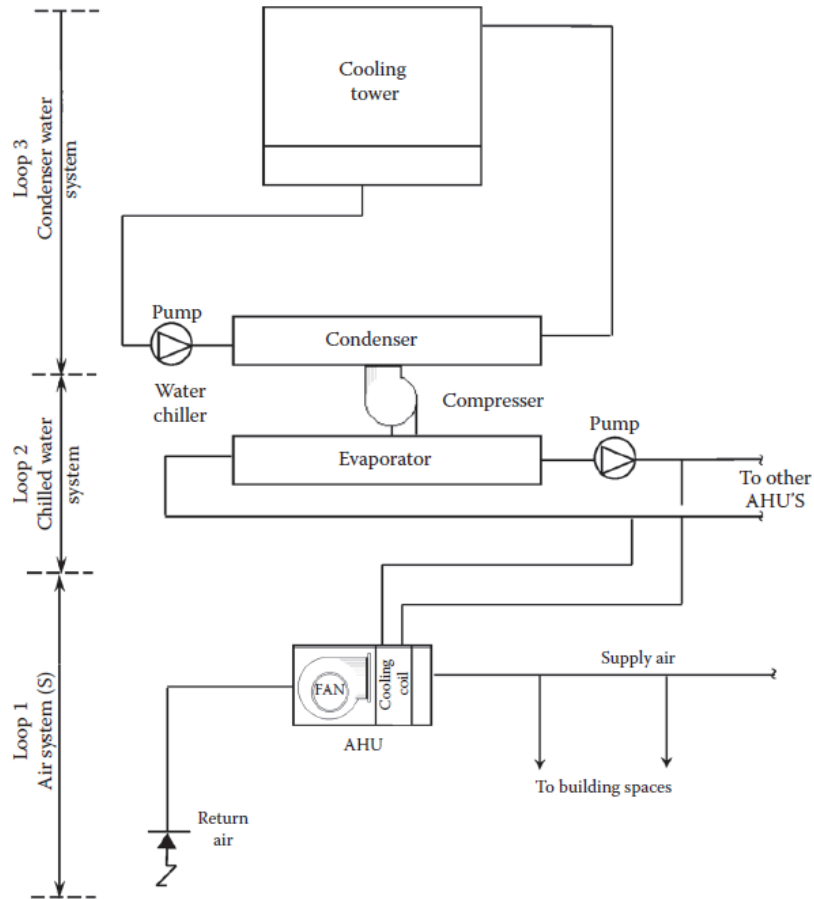


Figure 1-2: Water-Cooled HVAC System Schematic [3]

### 1.2.1 Loop 1: Air System

The load side or the air system represented by loop 1, consists of the buildings (or loads) the DCP is producing and distributing chilled water to. The chilled water produced by the DCP will be utilized by the HVAC equipment installed inside the buildings – such as the AHU and the FCU - to produce and distribute cold air - through the process of heat extraction - to the building’s areas or rooms. The warmer chilled water or chilled water return – which is the result of the heat transfer process - flows back from the load side to loop 2, and more specifically, to the chiller’s evaporator [3]. The total cooling capacity required for these buildings is the deciding factor of the overall cooling capacity of the DCP; the load required for cooling the areas and rooms inside a DCP must be considered as well. The load required can be estimated through charts that list down the unit-area cooling-load values for various building types, including, but not limited to hospitals, shopping malls and apartments in various building types [1].

### **1.2.2 Loop 2: Chilled Water System**

Located inside the DCP, the chilled water system, or loop 2, is responsible for producing chilled water to the loads. The main component of this loop is the chiller, which is comprised of an evaporator, a condenser and a compressor. As the chilled water return line is received from the load side through the underground (or aboveground) piping system, the chilled water return enters the chiller's evaporator. The heat in the chilled water return line is extracted and transferred through a refrigerant from the evaporator to the condenser via the compressor [3]. Hence, producing chilled water supply at the evaporator's output.

The pump, shown in Figure 1-2, can be split into 2 pumps, namely, a Primary Chilled Water Pump (PCHWP) and a Secondary Chilled Water Pump (SCHWP). The former will transfer the chilled water return from the loads to the evaporator at a predetermined flow and pressure, whereas the latter transfers the chilled water supply from the evaporator to the loads [1][2][3][4]. The Primary and Secondary Chilled Water Pumps are designed in several configurations, and the pumps may be constant or variable speed pumps [1][2]. In some designs, where the network is not large, SCHWP is omitted inside the DCP, and instead, these pumps will be located inside the consumer's building [2]. Otherwise, a primary-secondary pumping system is utilized, that is, when the length of network is long [1]. Depending on the design of the DCP, loop 2 may be configured to include a TES tank that is charged by the evaporator's output (i.e. chilled water supply) and discharges the stored chilled water to the loads [1][2][3].

### **1.2.3 Loop 3: Condenser Water System**

The third and final loop is the condenser water system loop (located inside the DPC). This loop has no physical connection with the chilled water system loop (loop 2). However, the condenser water and chilled water loops are linked together through chiller's compressor, whose is to transfer the heat generated by the loads from the evaporator circuit to the condenser circuit [3]. The heat collected by the condenser - in the form of warm water - is then transferred to a cooling tower that dissipates the heat to the air. Through another heat transfer process within the cooling tower, cooler condenser water is transferred back to the condenser to repeat the same process of heat collection and dissipation [3]. Moreover, a Condenser Water Pump (CWP) pumps the cooler condenser water from the cooling tower to the condenser as illustrated in Figure 1-2 [3].

### 1.3 Temperature Design Basis

The first and most important variable in the design of DC System is temperature. Due to its importance, temperature takes place in all DC System loops as reflected in Figure 1-2, and as within the chiller in the refrigeration loop. The latter will be discussed in more detail in the Chiller subsection.

The concept of temperature difference or differential, denoted as  $\Delta T$ , between the CHW supply and CHW return lines is the key factor of the system's overall design, including, but not limited to, the pumping energy, pipe sizing and pipe insulation [2]. Since, the optimal goal of any DCS design is to minimize the cost of production whilst maintaining the design specification, it is highly favorable to have the temperature differential to be high, usually about 9-12 °C [1][2][3]. However, there is a constraint of the maximum allowable temperature differential to avoid other implication in performance such as the ability to maintain the humidification requirements. Thus, a typical industry standard values of the CHW supply and return temperatures are 4.4 °C and 13.3 °C, respectively [1].

### 1.4 Major Components of a District Cooling Plant

#### 1.4.1 Chiller

The chiller is the heart of any cooling system. The chiller produces chilled water through the process of refrigeration, which is derived from the Second Law of Thermodynamics. The second law provides insights into the behavior of heat transfer as the heat flows from hot to cold regions due to temperature differences and the inherent drive of nature to equalize temperature disparities. The refrigeration process or cycle in a chiller can be accomplished either through the *vapor compression cycle* or through *absorption cycle*. Thus, there are two types of chiller technologies, namely, *compression* type and *absorption* type chillers [3].

Under each type, a chiller is classified based on the type of compressor or absorption stage [1]. Table 1-1 illustrates the chiller technology and tabulates the Coefficient of Performance (COP) for each chiller. COP is a dimensionless coefficient that indicates the efficiency of the chiller. The higher the COP, the more cooling a chiller can produce per electrical kW. Since the Centrifugal compression type chiller has the highest COP for large capacity chillers, it is the most utilized chiller in DCPs [1]. The following discussion will primarily focus on the centrifugal compression type chiller, although many of the general concepts would still be applicable to other types of chillers listed in Table 1-1 [1].

Table 1-1: Chiller Technology [1]

	Compression Chillers			Absorption Chillers	
Parameter	Reciprocating	Screw	Centrifugal	One-Stage	Two-Stage
Primary Energy	Electric Motor	Electric Motor	Electric Motor	Hot Water	Steam or fire
COP $\left(\frac{\text{Removed Heat (W)}}{\text{Input Work (W)}}\right)$	4-6	4-6	>7.0	0.6-0.76	1.2

Chillers can also be classified based on the process used to reject the condenser heat. The two processes for rejecting the condenser heat are air-cooled and water-cooled chillers [1]. Air cooled chillers are of smaller capacity in comparison to water cooled chillers. An air -cooled chiller has a capacity of slightly more than 450 tons or 16,000 kW. Whereas the capacity water-cooled chillers may go as high as 10,000 tons or 35,170 kW when fitted in series counter flow orientation [1]. In terms of the expected life span of air-cooled and water-cooled chillers is 15 and 25 years, respectively. Air-cooled chillers are packaged units, meaning that the chiller’s controls, compressor, evaporator and air-cooled condenser are mounted on the same skid [1]. On the contrary, water-cooled chillers reject the heat from the condenser circuit through water. The warm water carried from the condenser circuit may be diffused in different ways, the most common and efficient way is through cooling towers [1]. In the gulf region, DCPs utilize water-cooled chillers instead of air-cooled chillers due to their higher cooling capacity, overall efficiency (lower electrical cost per produced cooling tonnage) and the overall expected life span.

The three main circuits within a chiller are the refrigeration, condenser water and chilled water circuits. All three circuits are physically separated from one another. In other words, the chilled water does not get mixed with the condenser water, and the condenser water does not get mixed with the refrigerant. However, the refrigeration circuit will be the common link since it collects the hot water from the chilled water return line and dumps in the condenser. The refrigeration or vapor compression cycle is demonstrated through four steps, from which, a certain refrigerant changes its physical state from liquid to vapor in alternating manner. This is achieved through changes in pressure and temperature [3]. Figure 1-3 depicts the stages of the vapor compression or refrigeration cycle [3].

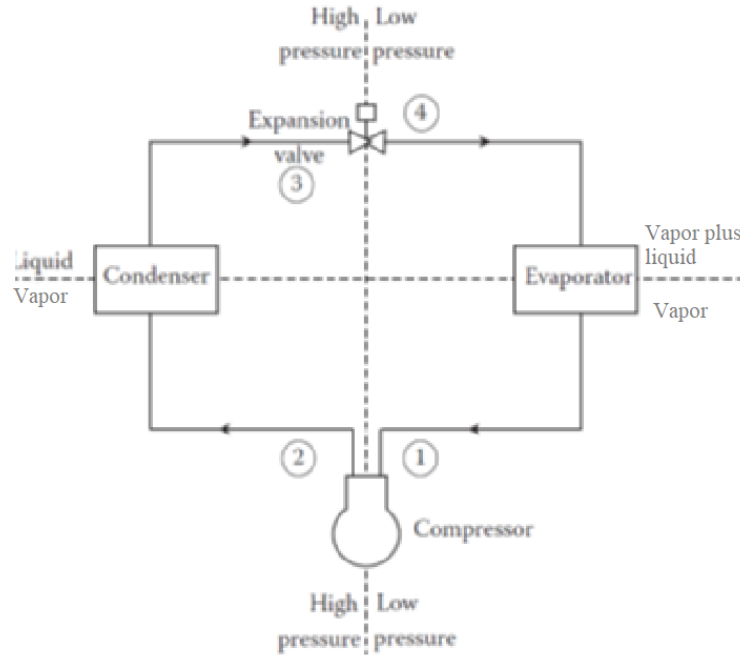


Figure 1-3: Components of a Vapor Compression Refrigeration System [3]

1. Stage 1: Compression.

In this stage, the compressor – such as the centrifugal type – absorbs and compresses the low-pressure and low-temperature refrigerant vapor (*saturated vapor state*) from the evaporator. Consequently, the process of compression produces a high-pressure and high temperature *superheated vapor* at its output [3].

2. Stage 2: Condensation.

In the condensation stage, the output of stage 1 is cooled down by the cooler water that enters the chiller’s condenser from the cooling tower. The water leaving the condenser to the cooling tower plays the role of a “heat sink”. The result would be a high-pressure and medium temperature refrigerant at the *saturated liquid* state [3].

3. Stage 3: Expansion

In the third stage, the high-pressure and medium temperature refrigerant at the saturated liquid state undergoes a pressure and temperature drop as it flow through the expansion valve. Hence, the output of the expansion valve is a low-pressure and low temperature refrigerant. A state from which the refrigerant becomes a *mixture of liquid and vapor* [3].

#### 4. Stage 4: Evaporation

In the final stage of the cycle, evaporation occurs in the refrigerant when the low-pressure and low-temperature refrigerant absorbs the heat from the chilled water return line. The refrigeration or vapor compression cycle then repeats [3].

### 1.4.2 Cooling Tower

The water flowing through and out of the chiller's condenser as depicted in Figure 1-2 goes into a cooling tower. A typical cooling tower used along with a water-cooled chiller is shown in Figure 1-4. As discussed under the chiller subsection, the refrigerant collects the heat from the evaporator circuit and transfers it to the condenser, and then uses the condenser water as a media to dispose the heat. The process of disposing the heat to air is accomplished through a cooling tower, once the heat is disposed to air, a cooler condenser water flows back to the chiller's condenser and the process repeats [1][3].

A typical cooling tower is composed of the following components as depicted in Figure 1-4 [3]:

- *Inlet Louvers*. Located in the lower portion of a cooling tower, they permit the ambient cool air to enter the cooling tower to work in rejecting the heat and to stops the water from exiting the cooling tower [3].
- *Fan*. The fan – located on the cooling tower - is driven through an induction motor and coupled together using a gear box or belt. Typically, in a DCP, the fan is controlled via a variable frequency drive. Which increases the energy savings and adds to the overall efficiency of the system [3].

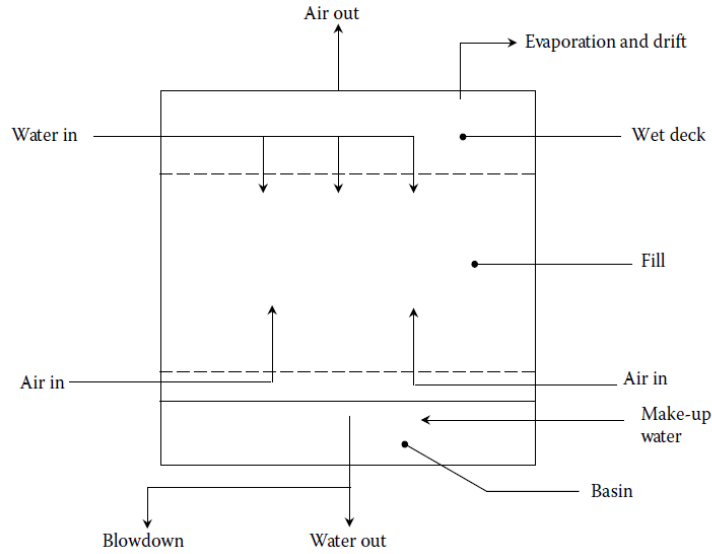


Figure 1-4: Cooling Tower [3]

- *Hot Water Distribution.* The warm water from the chiller’s condenser circuit enters the cooling tower and is sprayed through nozzles down to the fill packaging as illustrated in Figure 1-4 [3].
- *Fill.* The fill packaging is made of thin slices from which the heat exchanging process in a cooling tower occurs within it [3]. In other words, as the fan is continuously exerting force on the positive z-axis, the fill packaging receives the warm condenser water from the chiller directed on the negative z-axis. The cooler air – from the atmosphere – enters the cooling tower and flows to the fill packaging in the positive z-axis. The result of this heat exchanging process is cooler condenser water flowing in the negative z-axis down to the cold-water basin [3].
- *Basin.* The cold-water basin located at the bottom of the cooling tower receives the cooled condenser water from the fill packaging. The cooled condenser water or the condenser water supply will then flow back from the basin to the chiller as depicted in Figure 1-4 [3].

### 1.4.3 Condenser Water Pump

The role of the Condenser Water Pump (CWP) as depicted in loop 3 in Figure 1-2 is to receive the cooler condenser water from the cooling tower outlet and pump it to the chiller’s condenser water inlet at a pre-defined flow and pressure. Thereby, the CWP circulates condenser water between the chiller’s condenser and the cooling tower [3]. The total required

flow rate for the CWP is determined based on the total heat rejection (cooling system load + heat of compression) and the condenser water temperature range [3]. A CWP is mostly of the centrifugal type, and it is driven by an electric induction motor. The speed of the CWP may be constant or varied, each has its advantages and disadvantages [1]. Irrespective of the CWPs arrangement and their connection to the chiller, variable-speed CWPs offer greater energy savings at part-load, low starting current and possible increase in the chiller's performance [1]. Thus, making them more attractive in modern DCP designs.

#### **1.4.4 Chilled Water Pumps**

Like the condenser water pump, the primary and secondary chilled water pumps are mainly centrifugal and are driven by an electric induction motor [3]. Moreover, these pumps are installed in a system to have constant or variable flow. The flow rate of the primary chilled water pump is determined by the cooling load and chilled water temperature differential [3]. The pressure or the head required is then calculated based on the summation of pressure drops in the piping system - due to friction - and through the chiller's evaporator, cooling coils and the loop's valves [3].

The Secondary Chilled Water Pump (SCHWP) - located at the outlet of the evaporator - transfers the chilled water at around 4.4 °C to the loads [4]. Hence, forming the primary-secondary pumping or the primary-secondary-tertiary pumping system; the latter includes smaller pumps at the consumer side to make-up for the pressure drop in the network [1]. The pump's speed is controlled through a variable frequency (or speed) drive that modulates the speed of the motor as per the cooling load requirements [1].

#### **1.5 Capacity Control of Water-Cooled Centrifugal Chillers**

Controlling the cooling capacity (represented in kW, tons of refrigeration or BTU/h) of a water-cooled centrifugal chiller is basically varying the volumetric flow rate of the refrigerant that is passing from the evaporator to the condenser [3]. The flow rate of a centrifugal compressor and subsequently the cooling capacity is a function of the condensation pressure (or lift) and refrigerant flowrate [5]. That is, a change in either or both variables affect the chiller's cooling capacity. Moreover, the load requirement is a function of the chilled water

flow rate, temperature differential and a constant coefficient [5]. Thus, a reduction in the chilled water return temperature or flow rate is an indication of load reduction, or vice versa.

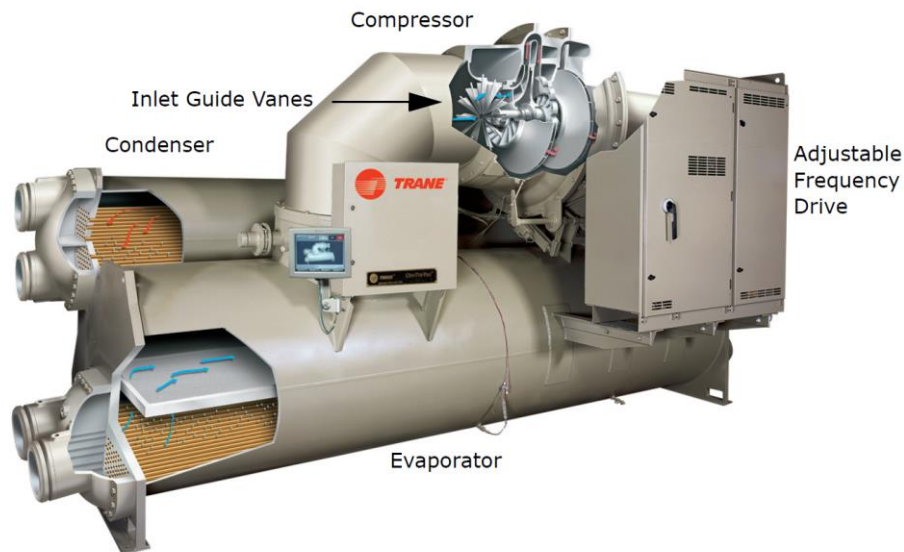


Figure 1-5: Centrifugal Chiller, Courtesy of Trane [6]

In constant speed chillers, the refrigerant flow (or the cooling capacity) is varied using Inlet Guide Vanes (IGV) as illustrated in Figure 1-5 [3][6]. The IGV is placed on the compressor's input to restrict or allow the flow of refrigerant to move from the evaporator to the compressor. Consequently, the cooling capacity of the chiller is controlled. Furthermore, this method yields to high efficiencies around chiller's design points (i.e., at high load requirements) where the IGV is fully open [7]. However, at low load requirements, the IGV position is almost closed to permit less refrigerant flow. Consequently, this yield to low levels of efficiency and the chance of surge is high [7]. A surge is an unwanted phenomenon where the pressure rises or lift in a chiller exceeds a predesigned value [5]. If the surge persists for long periods of time, it yields to high current consumption and may cause the chiller to trip, produces noise from the chiller and damages the compressor [3].

Another known method to vary the cooling capacity of a chiller is to use a Hot Gas By-Pass (HGBP) [3][5]. However, this method yields to low performance and high electricity input per cooling output (i.e., kW/ton) at part-load [5]. This is due to the constant refrigerant flow rate, and the machine unloads only through by-passing the gas going from the evaporator to the condenser back to the evaporator as shown in Figure 1-6 [5].

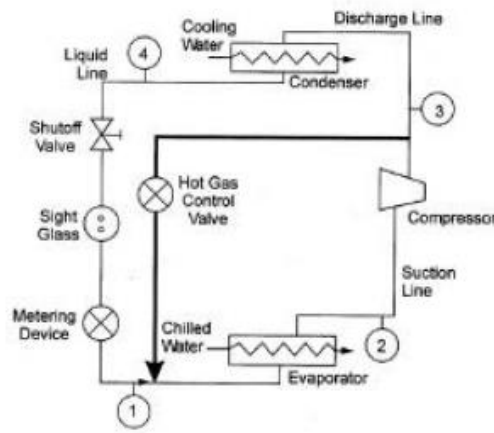


Figure 1-6: Hot Gas By-Pass [5]

The most recent approach to control the cooling capacity of a chiller is by varying the speed of the compressor's motor through a Variable Frequency Drive (VFD) [3]. Other common names of a VFD include Variable Speed Drive (VSD) and Adjustable Frequency Drive (AFD). A VFD can be mounted on the chiller module – as depicted in Figure 1-5 - or it can be provided as a stand-alone panel for large motor rating. Speed control in a centrifugal chiller increase the efficiency of a chiller at part-load and lower condenser water inlet temperature [7]. Thus, providing energy savings up to 30% [8]. However, an IGV control is more efficient at full load at any condenser water inlet temperature [7]. On the other side, VFD drive, or speed control efficiency drops at high loads and high lift conditions (high condenser water temperature) due to drive losses introduced by the VFD [5][6]. Therefore, capacity control of a centrifugal chiller is applied through a combination of VFD and IGV control to ensure maximum overall efficiency at various operating conditions [7]. Figure 1-5 depicts a Trane centrifugal chiller with both IGV (located at the inlet of the compressor) and built-in VFD (or AFD).

## 1.6 Thesis Objective

The aim of this thesis is to investigate two advanced multivariable control techniques and compare them with an array of PID controllers. Linear Quadratic Integral (LQI) and Model Predictive Control (MPC) methods are chosen due to their versatile characteristics, wide use in the industry and effectiveness to tackle multi-input-multi-output (MIMO) system seamlessly such as a chiller. Furthermore, the MPC will be implemented with direct feedthrough and tuned common and widely using technique, namely, Genetic Algorithm.

## 1.7 Research Contributions

The contributions in this work include the following:

1. Adopted a published multi-input-multi-output (MIMO) model of a vapor compression liquid chiller and used its linearized state-space published data to develop several controllers. The controllers' performance was evaluated based on their ability to track a set of setpoints whilst regulating other outputs simultaneously and to reject measured input disturbance.
2. The number of outputs of the chiller model was altered and the inputs were classified into two categories (i.e. control or disturbance input) to suit the control problem.
3. Designed a Proportional-Integral-Derivative (PID) controllers fitted in a multi-input-multi-output environment.
4. Designed a discrete-time Linear Quadratic Integral (LQI) and tuned its output and input weights to achieve the design objectives.
5. Designed a discrete-time Model Predictive Controller (MPC) with a nonzero direct feed through term. The model's input constraints (or saturations) were integrated into the cost function. The weights of the MPC controller's cost function were tuned using Genetic Algorithms to meet the design requirements.
6. The LQI and MPC controllers showed various improvements in terms of overshoot, steady-state error, settling time and lower input power requirements with respect to the PID controller.

## 1.8 Thesis Organization

Literature review of the various modeling and control techniques of chillers and/or vapor compression systems (VCS) are presented in Chapter 2. The dynamic model of the chiller in state-space is demonstrated in Chapter 3. The control problem and PID control of the chiller are provided in Chapter 4. Chapter 5 shows the design and implementation of LQI control on the chiller. The derivation of the MPC with direct feedthrough, its weight tuning using Genetic Algorithms (GA) and its implementation on the chiller are detailed in Chapter 7. In Chapter 8, the performance of the three controllers was analyzed and discussed.

## Chapter 2 Literature Review

This chapter discusses the modeling and control techniques previously done on liquid chillers or vapor compression systems (VCS). The modeling techniques presented are divided into three categories, namely, white-box, black box and grey-box models. Each of the three modeling techniques exhibit the below properties [9]:

- Linear or nonlinear.
- Static or dynamic.
- Explicit or implicit.
- Discrete or continuous time.
- Deterministic or probabilistic.
- Deductive, inductive or floating.

In white-box modeling, the system is modeled using physics-based mathematical formulations (such as differential equations) through the fundamental laws such as mass balance, heat transfer and momentum equations. On the contrary, black-box models are derived through input-output relations with little or without having any prior knowledge of how the system works. These models are often referred to as data-driven or empirical, since they require system real or manufacturer's performance data to derive the input-output relations using artificial intelligence or mathematical algorithms. As the name suggests, Grey-box modeling, or hybrid modeling, is a blend of white-box and black-box techniques. In this approach, the system is initially modeled using physics-based formulations. However, model parameters or coefficients of these equations are computed through input-output relationships of measured data [9]. A VCS model can be classified as white-box, black-box or grey-box. However this classification may vary based on the interpretation of the data.

Control system design has been progressively improved and optimized to enhance performance and reduce the cost of operations of HVAC systems and in other industries. Currently, the control methods can be categorized under the following categories: classical

control, hard control, soft control. hybrid control and other techniques [10]. Each of the following categories includes subcategories as depicted in Table 2-1 [10]. For instance, classical control includes ON-OFF and PID controls. The latter PID control is the most dominant control technique in the industry due to its simplicity, and it's the most used benchmark for scientific comparison with newer or modern control techniques such as optimal control, robust control, model predictive control and data-driven control.

Table 2-1: Some of HVAC Control Methods [10]

<u>Classical Control</u>	<u>Hard Control</u>	<u>Soft Control</u>	<u>Hybrid Control</u>	<u>Other Techniques</u>
ON/OFF	Gain Scheduling PID	Fuzzy Logic Control	Adaptive Fuzzy	Direct Feedback Linear Control
PID	Nonlinear Control	Neural Network Control	Adaptive Neuro	Pulse Modulation Adaptive Control
	Optimal Control		Neuro Fuzzy	Pattern Recognition Adaptive Control
	Robust Control		Fuzzy PID	Preview Control
	Model Predictive Control			Two Parameter Switching Control
				Reinforcement Learning Control

## 2.1 Modeling Techniques of Vapor Compression Systems

### 2.1.1 White-Box Modeling (Physical)

White-box or physics-based models of vapor compression systems can be static (or steady-state) or dynamic (transient). In static or steady-state modeling, the parameters are constant and do not vary in time. Thus, the behavior of the system from the initial point of time before applying the change to the final steady-state value is not captured. On the other hand, dynamic or transient modeling captures this behavior and the system's parameters vary with time. Since the thermal inertia of the compressor and expansion valve are much smaller – or even negligible – in comparison to the heat exchangers (condenser and evaporator) in VCS, many researchers tend to model the compressor and expansion valve in steady-state. Otherwise, compressors are modeled using Turbomachinery theory and other related physics-based equations.

The heat exchangers white-box models typically fall under three categories, namely, finite volume (FV), moving boundary (MB) and lumped-parameter [11]. In finite-volume, the heat exchanger is discretized into a finite number of independent – fixed length - control volumes. This modeling approach is known for its accuracy in dynamic (transient) and steady-state simulations. However, the order of the system is high, execution speed is slow and applying control laws on this formulation is challenging [11,12]. MB also adopts the discretization of the heat exchanger, but the number of control volumes is dependent on the number of refrigerant phases and the length of each volume varies based on the duration of each phase. The MB formulation is known for its computational speed, accuracy and relatively lower order of equations as opposed to the FV approach [11,12]. Figures 2-1 and 2-2 illustrate the discretization of a shell-and-tube heat exchanger for FV and MB analysis [12]. Lumped-parameters results in fewer number of equations compared to MB and FV formulations as it simplifies the heat exchanger further. For instance, a two-phase exchanger, such as the evaporator, and a three-phase exchanger, such as the condenser, are both modeled as a single lumped system. By doing so, this approach might neglect some important dynamics that occurs during phase change or within phases [11]. However, this approach is the easiest when it comes to controller design due to the fewer and lower order systems as well as the computational speed.

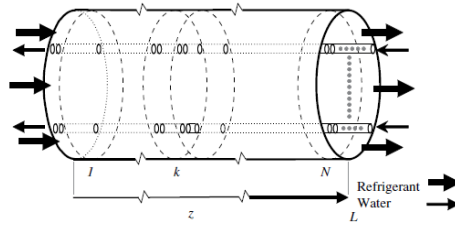


Figure 2-1: Discretization of the shell-and-tube heat exchangers for the finite-volume formulations [12]

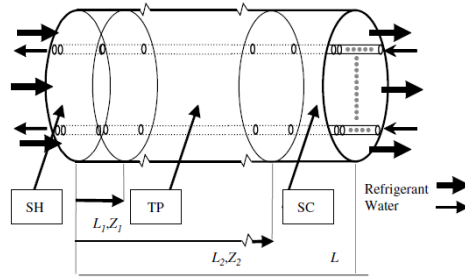


Figure 2-2: Discretization of the shell-and-tube heat exchangers for the moving boundary formulations [12]

Bendapudi et al. [13] modeled a 90 Ton centrifugal chiller running using a R134a refrigerant through finite-volume analysis. The compressor is single-stage, constant speed and with variable inlet guide vanes (IGV). Due to the fast response of the compressor, it has been modeled as quasi steady-state formulation. A simplified model was adopted that considers only the thermal inertia of the sensing element of the thermostatic expansion valve (TXV). The FV formulation of the evaporator and condenser yielded non-linear equations that were then discretized and linearized. The results of the study when compared to a test setup proved to be accurate by yielding an error of less than 10% during start-up and 27 load-change transients; the load-changes were achieved by varying the setpoint chilled water supply temperature and return water temperatures.

In a later work, Bendapudi et al. [12] modeled a shell-and-tube heat exchanger using both finite-volume and moving boundary formulations. The compressor and TXV models were identical to [13]. The modeling (or simulation) results were validated against a 300 kW water-cooled centrifugal chiller test stand running on R134a refrigerant. The study has concluded that FV formulation is more robust during start-up and all load change transients compared to MB. The MB method was stable during load-change transients, but not at start-up

(compressor and TXV models hindered the calculation process during start-up). However, the speed of execution of MB was three times as fast as FV while maintaining identical accuracies during steady-state and at load-change transients.

Lei and Zaheeruddin [14] developed a lumped-parameter dynamic model of a water-cooled chiller. The developed model was able to simulate the chiller's performance under both transient and steady-state conditions. As with other white-box modeling techniques, a modular modeling approach was adopted to model a 10.5 kW water-cooled chiller running on R22 refrigerant with shell-and-tube heat exchangers, variable speed compressor and thermostatic expansion valve (TEV). A dynamic lumped-parameter approach using mass and energy balance principles was adopted to model the heat exchangers. For the condenser, only the condensation section was accounted for. However, the evaporator's refrigerant dynamics was completely captured (i.e. the two-phase and superheated vapor regions) in the modeling process because the refrigerant temperatures have a high impact on the system output. Thus, the evaporator model had six control volumes in total, three for each section. The control volumes are the refrigerant inside and outside the tubes, tube walls and the water inside and outside the tubes. A steady-state compressor model developed considering that the set speed is reached instantly and the effect of the compressor's shell on the performance of the system has been omitted. Finally, the TEV has been modeled as a first order dynamic equation whose output is the refrigerant flowrate at the discharge side of the TEV, whose opening angle is governed by the degree of superheated vapor temperature in the suction. The model's performance was validated through computer simulation in transient and steady-state conditions. In both cases, two subcases were studied, namely, the change in compressor's speed and the change in the TEV opening angle. The simulation yielded "that there exists a minimal feasible valve position at a given operation frequency for water chiller to work within a safe operation mode to avoid water freeze up in the secondary system". Moreover, the transient response showed that the refrigerant mass flow rate and pressure reaches steady state faster the water temperature. As this study was done only on computer simulation, the overall system's accuracy was not validated experimentally.

Li et al. [15] presented a dynamic model of a water-cooled centrifugal chiller developed in Modelica software. The shell-and-tube heat exchangers were modeled using finite volume (FV) method. The TEV was modeled as a first-order equation whose output is the refrigerant mass flow rate that depends on the opening angle of the TEV. Unlike most papers, the

variable speed centrifugal compressor was modeled based on turbomachinery theory (i.e. compressor's physical and dynamic properties). Furthermore, compressor losses were accounted for in the model. The developed model considered two ways for capacity control, namely, inlet guide vanes (IGV) and compressor's speed. Both approaches will operate together to meet the capacity set point or requirement. The model's dynamic and steady-state performance was simulated in Modelica considering an R134a refrigerant. The system's response was triggered by changing the IGV angle and the input torque. The system's predicted outputs include isentropic efficiency of the compressor, mass flow rate of the refrigerant at compressor inlet, refrigerant (superheat and subcooling) and chilled-water temperatures.

Llopis et al. [16] developed a dynamic lumped parameter model of a shell-and-tube condenser operating in a vapor compression refrigeration plant. The model was formulated using mass, heat transfer and energy principles. Furthermore, the formulation considered the effect of metal control volumes (shell-and-tube), heat transfer to the environment liquid receiver and all three states or phase changes the condenser undergoes as depicted in Figure 2-3. The model was validated using measured data of an experimental vapor compression plant with a variable speed open-type compressor running on HCFC-22 refrigerant and with shell-and-tube heat exchangers. Model validation was done in steady-state and transient conditions. The steady-state output response deviation was within  $\pm 5\%$ . The transient response was triggered by changes in compressor speed, secondary fluid inlet temperature and refrigerant mass flow rate; the results matched well with the measured data.

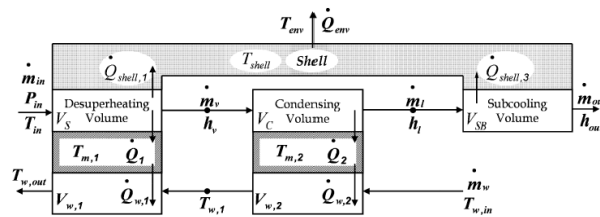


Figure 2-3: Block diagram of a condenser [16]

Koury et al. [17] presented two models to simulate the steady-state and transient behavior of a variable speed water-water type refrigeration system. Distributed (i.e. FV) method was used to model the heat exchangers. In each control volume, mass, energy and momentum

balances physical laws were applied to formulate the time-dependent partial differential equations. The other two sub-models, compressor and expansion valve, were modeled in steady-state due to their small inertia compared to the heat exchangers. Simulations - to validate the model - were done using two types of refrigerants, R12 and R134a. The VCS understudy was made up of a variable speed compressor, shell-and-tube heat exchangers and a manual expansion valve. Furthermore, secondary medium in the condenser and evaporator were water and a water-ethylene glycol mixture, respectively. Simulations and tests were done under two different cases to investigate the possibility to control the refrigeration system and the degree of superheating in the evaporator outlet. In the first case, system performance is studied during start-up of the compressor. Besides from numerical simulations, a comparison was made between the simulation values against experimental values - from another study/paper - in terms of the system's COP when the system undergoes a step increase in compressor speed. Results showed that the steady-state results were close between the two. In the second case, the response of the system was studied due a change in compressor speed and expansion valve opening angle while the system is under steady state. The transient results at terminal value predicted well when compared to steady state.

### **2.1.2 Black-Box Modeling (Data-Driven)**

To reiterate, black-box or data-driven modeling requires little or no knowledge of the system. Black-box models can be accomplished with numerous techniques including, but not limited to data mining or artificial intelligence algorithms, fuzzy logic and statistical techniques. Figure 2-4 illustrate several of these techniques - and their subcategories - commonly used in HVAC systems (not limited to chillers or vapor compression systems) [18]. As the focus is to present common literature on VCS, and more specifically chillers, papers on the modeling of liquid chillers will be presented.

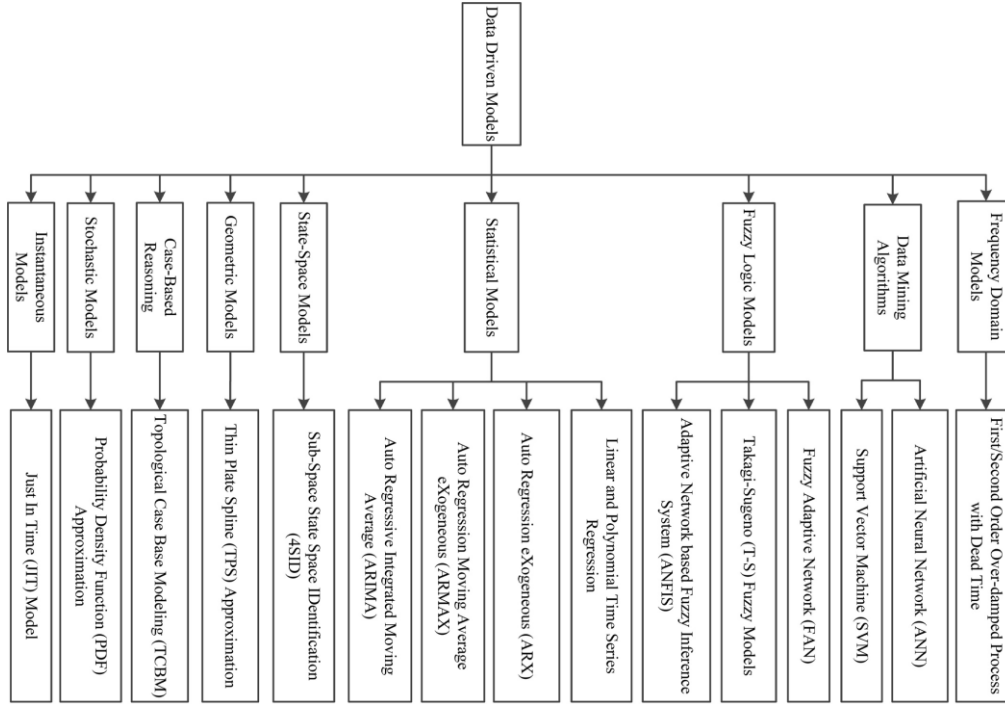


Figure 2-4: Data-driven Models in HVAC Systems [18]

Bechtler et al. [19] developed a data-driven approach to dynamic modeling of vapor compression liquid chillers using artificial neural networks (ANN). The ANN topology or type adopted was the generalized radial basis function (GRBF) with series-parallel identification structure as shown in Figure 2-5. The model inputs included the easily measured chiller data; and these were the chilled water outlet temperature, cooling tower inlet temperature and evaporator capacity. Similarly, three outputs were considered, which are the COP, compressor work and evaporator inlet temperature. As this model falls under Multi-Input-Multi-Output (MIMO) modeling, three ANN networks are created to map the three inputs with the three outputs. Each sub-network consisted of three inputs and one output. The model was trained and tested against the data of two installed chillers in the University of Auckland. Chiller A has a capacity of 650 kW, and it was equipped with a single-screw compressor and ran on R22 refrigerant. On the other hand, chiller B was 300 kW, but had a twin-screw compressor and ran on R134a. The model was trained and evaluated under two modes of operation. In the first mode, transient fluctuations in terms of a change in part-load operating capacity under normal operating conditions were examined. In the second mode, the start-up process of the chiller was modeled. Measured versus predicted results agreed; for instance, the RMS error of the COP - in both cases - was 0.3 and the RMS error of the

compressor work was less than or equal to 2.5 kW. Furthermore, it was observed that with more training data and lower sampling time, a better transient model can be attained against steep transient changes. The outcome of this study can lead to the use of this chiller model for control system design and fault detection in chillers.

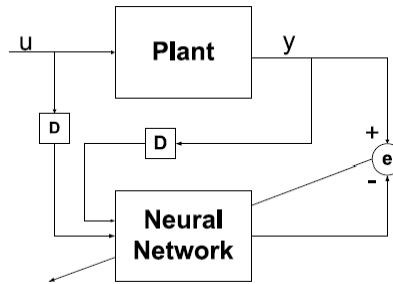


Figure 2-5: Series-parallel Identification Structure [19]

Navarro-Esbrí et al. [20] presented a black-box steady-state model of a vapor compression liquid chiller with a variable speed compressor. A radial basis function (RBF) neural network (NN) was opted to model the VCS with low-cost data input requirement – consisting of inputs that are usually available for measurement - and without extensive training set. The model had four inputs and three outputs; the inputs were carefully selected such as they provide the most information on the system. For instance, the chilled water and condenser temperatures as well as the compressor speed provide an insight into mass flow rate and the compressor’s performance, whereas the refrigerant evaporator outlet temperature describe the degree of superheating and the overall behavior of the VCS. The four inputs of the systems are the chilled water inlet temperature, condensing water temperature inlet, refrigerant evaporator outlet temperature and compressor speed. The NN outputs are the cooling capacity, electrical power consumption and the chilled water outlet temperature. Training and testing data sets were obtained from an experimental chiller setup running on R22 refrigerant in the primary loop, and the secondary fluid running in the condenser and evaporator were water and mixture of water and propylene glycol, respectively. The chiller components included shell-and-tube heat exchangers, single-stage reciprocating open-type compressor and a TEV. The RBF NN model was trained and tested at eight different steady-state conditions; in each condition, 500 measurements were used, and the measurements were split between training and testing sets. The output results generalized well with actual

measurements. For instance, the model's accuracy when predicting the chilled water output was within  $\pm 0.2$  K, and the accuracy of the power consumption was  $\pm 5\%$  of actual measurements. The positive results in accurately modeling the VCS can be further developed and used for fault detection and energy optimization of VCS.

Romero et al. [21] presented and compared four control-oriented linear statistical black-box models to predict the dynamic response of chilled water temperature in VCS liquid chillers with variable speed compressors. The first step in modeling was to select the input variables that provide the most information on the evaporator outlet water temperature as well as they must be easily measurable. The selected inputs variables are chilled water inlet temperature and compressor speed. The former is selected as the control input and the latter is selected as the disturbance input. Secondly, the model is presented through the linear discrete-time formulation describe by

$$y(t) = G(z) u(t) + H(z) e(t) \quad (2-1)$$

where  $y(t)$  is the output (chilled water temperature),  $u(t)$  are the inputs,  $e(t)$  is input noise (considered as external white noise)  $t$  is real time,  $z$  is discrete-time shift operator and lastly,  $G(z)$  and  $H(z)$  are discrete-time transfer function representing the unperturbed plant and perturbations, respectively. At different structures and configurations, four statistical models were considered as depicted in Figure 2-6. The proposed models are AutoRegressive eXogenous (ARX), AutoRegressive Moving Average eXogenous (AMX), Output Error model (OE), BoxeJenkins model (BJ). To validate the dynamic response for all models, four different experiments were executed on an experimental chiller setup under different operating conditions by varying the compressor speed. The efficiency, measured as the percentage of output variations is illustrated in Table 2-2. It can be seen that the BJ outperforms all other methods in three out of the four operating conditions. Thus, making it the most suitable model for chilled water outlet temperature control design. Moreover, Figure 2-7 compares the predicted values for all models against the measured values for validation experiment 3 (540-520 RPM). Therefore, the most suitable method for chilled water

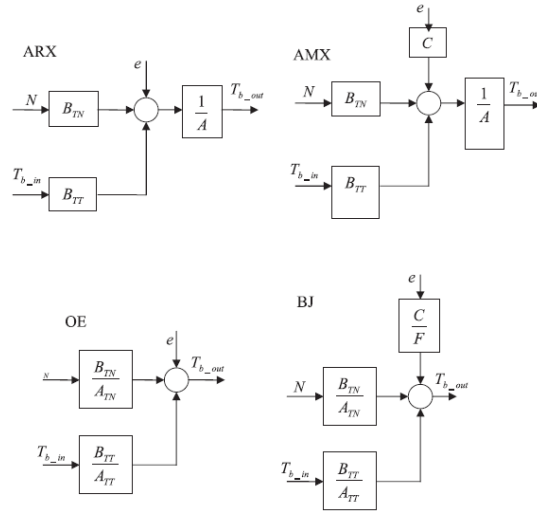


Figure 2-6: ARX, AMX, OE and BJ Model Architectures [21]

Table 2-2: Performance Comparison of the Models Under Different Experiments [21]

<u>Validation Experiment</u>	<u>ARX</u>	<u>AMX</u>	<u>OE</u>	<u>BJ</u>
1 [480-460 RPM]	69.88	71.17	68.65	69.92
2 [520-500 RPM]	63.72	70.15	71.38	73.79
3 [540-520 RPM]	65.40	68.11	65.77	68.64
4 [560-540 RPM]	52.85	62.59	66.31	76.32

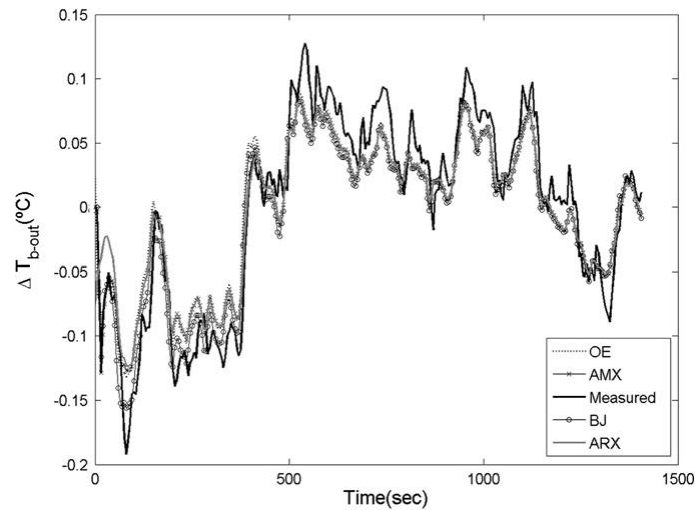


Figure 2-7: Predicted vs Actual Dynamic Response of Chilled Water Output using four methods [21]

Tudoroiu et al. [22] presented an adaptive neuro-fuzzy black-box model of a centrifugal chiller to model its nonlinear dynamics for the objective of using the model for future controller design. The chiller model under study ran on a R134a refrigerant, with variable speed centrifugal compressor and shell-and-tube heat exchanger [23]. Furthermore, the two examined outputs were the chilled water supply temperature and the refrigerant liquid level. The proposed adaptive neuro-fuzzy inference system (ANFIS) architecture is a hybrid technique combining artificial neural networks and fuzzy logic. Furthermore, the ANFIS model was simulated and compared to two other model simulations of a physics-based and ARX models. The former is a white-box model in which the heat exchangers are modeled using MB formulation [23], and the latter is a linear black-box method. Unlike the ANFIS than can model MIMO system, there were two SISO ARX models for the chiller, one for each output. Hence, the system or the two loops were decoupled. Despite the ease of use and quicker simulation time of the ARX model, the ANFIS is a more suitable approach to model systems with high non-linear dynamics and when a higher accuracy is desirable. Finally, the ANFIS modeling approach can be extended to other applications as well as deploying it in a closed-loop structure for controller design.

### **2.1.3 Grey-Box Modeling (Hybrid)**

Grey-box or hybrid models combine both white-box and black-box principles in the modeling process. For instance, the heat exchangers' fundamental formulations are laid using white-box principles such as the moving boundary, lumped-parameter or other formulation, but the coefficients or unknown parameters are determined empirically through experiments or measured data using black-box regression methods such as least-squares.

Browne and Bansal [24] developed a steady-state model of a vapor-compression centrifugal liquid chillers using physics-based formulation and empirical equations. The model was designed based on the following inputs:

- Geometric data of the chiller such as the heat exchangers and compressor dimensions.
- Temperature and flow rate of the evaporator liquid supply to the network/end-user.
- Temperature and flow rate of the condenser liquid return from the cooling tower.

The compressor was modeled using steady-state process using physical laws and geometrical data of the compressor. Furthermore, the compressor was hermitic, open-type, constant speed centrifugal compressor and with IGV capacity control. The flooded shell-and-tube type heat exchangers on the other hand were modeled using physical laws and heat transfer coefficients and solved using the effectiveness-NTU (i.e. NTU- $\epsilon$ ) methodology. Superheating and subcooling of the refrigerant in the vapor compression cycle has been accounted for in the model. The expansion valve output enthalpy was computed using the energy balance equation and efficiency assumptions within the motor and mass flow through the expansion valve. The model was designed with the following outputs:

- Condenser and evaporator capacities.
- Coefficient of Performance (COP).
- Electrical work/power of the compressor.
- Mass flow rate and refrigerant states.

The model was simulated and validated against measured data of three operational chillers at the University of Auckland. The chiller was simulated at part-load and full load conditions considering a fixed condenser liquid return temperature. In most of the operating conditions, the simulation results were within  $\pm 10\%$  of the actual measured data.

In later work, Browne and Bansal [25] developed a lumped-parameter model for a screw compressor packaged liquid chillers with modulating and on/off control. The model had several differences with respect to the model developed in [24] such as the ability to predict the dynamic or transient response during start-up, shutdown and fluctuating part-loads. The heat exchangers are modeled using thermal capacitance approach – which is a fully lumped-parameter approach – that uses physical laws and heat transfer coefficients. However, one drawback of the thermal or a lumped-parameter approach is the inability to model the refrigerant's phase changed within the heat exchangers. Furthermore, empirical relations were applied on the evaporator's tube wall mass on one of the studied chiller in order to predict its startup process. On the other hand, the screw compressor model was developed through regression models (i.e. black-box or empirical) instead of physical modeling and is also considered as a steady-state process. Overall, six dynamic variables have been considered in the modeling process and the model's outputs include compressor's electrical power, coefficient of performance (COP), water temperatures and the refrigerant states. The

model was validated against two experimental – in situ – chillers, and the output prediction was within  $\pm 10$  of the actual measured values for most operating conditions.

Wang et al. [26] developed a mechanistic model of a centrifugal chillers to study its dynamics. The compressor was modeled through the momentum, energy and mass equations as well as the equations of impeller velocity component relations. Furthermore, losses such as hydrodynamic, mechanical and electrical losses were considered in the modeling process. The heat exchangers were modeled using the classical heat exchanger efficiency method. The chiller dynamics were simulated considering lumped thermal storages at the inlet and outlets of each heat exchanger as first-order differential equations. A pre-processor was used for parameter identification of the modeled chiller using limited chiller full-load and part-load performance data. These parameters to be identified using the pre-processor included the compressor impeller geometric parameters, constants used for hydrodynamic losses of the compressor, chiller power consumption and the heat exchangers overall heat transfer coefficients. Two experimental cases were considered to validate the model's performance. In the first case, more than 200 full-load and part-load operating points from the manufacturer's data were used to validate the single-stage 2806 kW water-cooled chiller running on HCFC refrigerant. Results obtained were satisfactory, and it was concluded that the accuracy of the model increases as the parameters to be identified by the pre-processor are less. In the second case, data from site measurements from the central chilling system of a 46-storey office building were used. The plant consisted of five two-stage, indirect seawater-cooled centrifugal chillers running on R12 refrigerant. Just as case 1, both part-load and full-load capacities were simulated and the accuracy of the model, in general, was within  $\pm 10\%$ . The chiller model was then integrated into the full system to evaluate its performance once again. The simulation results matched well with the measured data in terms of power consumption and inlet and outlet temperatures of the condenser and evaporator.

Beitelmal et al. al. [27] developed a steady-state model of a centralized cooling system. Both the chiller and the cooling tower have been modeled in the study. Furthermore, the model solves the mass and energy equations and uses minimal number of inputs that are usually available. The inputs considered are the ambient conditions, condenser and chilled water flow rates, degree of superheat and sub-cool of the refrigerant, full load design conditions of the chiller and the cooling tower air flow rate. The model output includes the coefficient of performance (COP) and compressor power. The compressor's power ratio was determined

empirically - through least squares method - as a function of the cooling load and key temperatures such as the condenser and evaporator supply and return temperatures, heat load in the evaporator. Moreover, pressure drops across both heat exchangers were accounted for when computing the compressor's power. The model of the chiller and cooling towers were validated against manufacturer's data and compared with the experimental data of two water-cooled chillers feeding Hewlett-Packard campus. The first chiller was a 2286 kW and with a constant speed compressor. On the other hand, the second chiller is 2110 kW and with a variable-speed compressor. The predicted results of the model agreed with the measured data with an average deviation of 5% and maximum deviation of 18%. The study revealed that the COP of the constant speed chiller increases as the load increases and peaks at full load. In contrast, the variable-speed chiller performance peaks at part load between 40% to 80% depending on the heat load and the condenser water temperature.

Yao et al. al. [28] captured the dynamics of a liquid vapor compression chiller through a state-space model. The considered liquid chiller model had a variable speed compressor, runs on R134a refrigerant and with oil as the secondary medium in the plate type condenser and evaporator. In the proposed model, the heat exchangers were modeled using the lumped-parameter approach and the heat exchanger coefficients were determined empirically through experimental data. The compressor was modeled in steady state. With the assumption that the mass flow rate of the refrigerant is constant throughout the cycle, the expansion valve model was neglected. The developed dynamic differential equations were linearized using first order Taylor series and represented in state-space. The model had 5 inputs, 8 states and 7 output variables. The inputs are the inlet coolant temperature and flow rate of the condenser, the inlet chilled liquid temperature and flow rate of evaporator and refrigerant flow rate. The state variables were all considered as the temperatures of the condensation and evaporation of the refrigerant, outlet coolant of the condenser, chilled liquid of the evaporator, shell wall of the condenser and evaporator. Some of the state variables were also used as output variables, the 7 output variables are the outlet coolant temperature and flow rate of the condenser, outlet chilled liquid temperature and flow rate of the evaporator, compressor electric work, cooling capacity and the coefficient of performance (COP). The relationship between the input, state and output variables are illustrated in Figure 2-8. The developed state-space model has been validated against a series of 3 experiments at different initial conditions, and the average accuracy of the predicted outputs

are less than 10%. The model was then simulated under three different simulation cases, each having three subcases to study the transient behavior of the system.

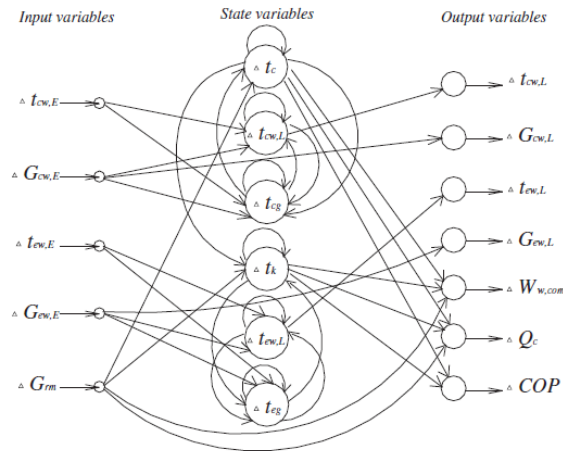


Figure 2-8: State-space chiller model directed graph [28]

In later work, Yao et al. [29] developed a state-space dynamic model of a vapor compression refrigeration system based on moving-boundary formulation. The model was more sophisticated in comparison with [28] as it gained more insight into the internal parameters of the system. The heat exchangers (i.e. condenser and evaporator) were modeled using the moving boundary technique by dividing the condenser and evaporator to three and two control volumes, respectively. For each control volume, physical laws (mass, heat and energy balance) using the lumped parameter approach were applied on each region. Moreover, heat transfer coefficients were determined through empirical relations from experiments. On the other hand, steady-state models were adopted for the compressor and electronic expansion valve (EEV). The equations of each model were then linearized and represented in state-space format. The input-output relationship between the four sub-model or module are as depicted in the block diagram in Figure 2-9.

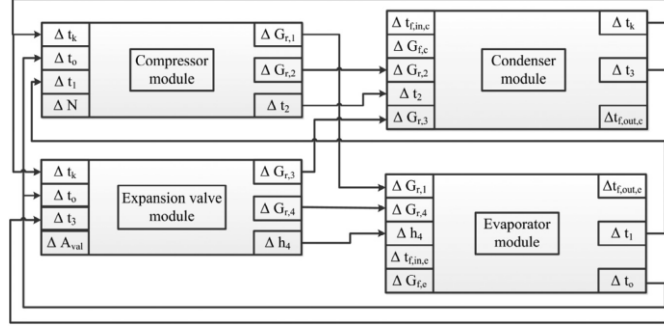


Figure 2-9: Block diagram for the dynamic simulation of refrigeration system [29]

The model was validated through an experimental setup running on R134a refrigerant and oil as the secondary medium in the heat exchangers. Moreover, a variable speed scroll compressor, electronic expansion valve and plate-fin heat exchangers were used. The proposed model was validated against three set of testing conditions, namely, a step change on the EEV degree of opening, step change in the evaporator's heat load (return temperature of the oil) and ramp change of inlet of the condenser (return coolant oil). For each test type, multiple experiments were conducted with modifications in operating conditions. The input-output relations between the modules/sub-models along with the overall's system output were examined; and in most cases, the error was less than 10%. Advantages of state-space with MB formulation included the representation (which is a very useful tool in describing MIMO systems), control system design, simulates faster (linearized system and modeled using the MB method) and gaining an insight into the transient behavior of the refrigerant states.

Liu et al. [30] presented an optimal chiller sequencing control in an office building considering chiller maximum cooling capacity. In the study, both the chiller and the cooling tower were modeled together to compute the maximum cooling capacity per chiller. In the study, the cooling tower was modeled using the effective-NTU method. On the other hand, Gordon-Ng (GN) models were adopted to model the screw compressor chiller. The Gordon-Ng models falls under the category of grey or semi-empirical models as the fundamental equation to determine the chiller's COP is governed by regression coefficients that are determined by measured or manufacturer's data. The GN fundamental model is a function of chilled water supply and condenser water return temperatures, COP and the chiller's cooling load

and is given in Equation 2-2 as

$$\left(\frac{1}{\text{COP}_i} + 1\right) \frac{T_{\text{chws},i}}{T_{\text{cwr},i}} - 1 = a_{1,i} \frac{T_{\text{chws},i}}{Q_{\text{ch},i}} + a_{2,i} \frac{(T_{\text{cwr},i} - T_{\text{chws},i})}{T_{\text{cwr},i} Q_{\text{ch},i}} + a_{3,i} \frac{\left(\frac{1}{\text{COP}_i} + 1\right)}{T_{\text{cwr},i}} Q_{\text{ch},i} \quad (2-2)$$

where  $a_1$ ,  $a_2$  and  $a_3$  are the unknown coefficients to be determined through regression techniques. The power consumption per chiller can then be determined using the COP and the chiller's cooling load. Both constant variable and variable speed compressors were modeled. The model was then deployed to develop an algorithm for the optimal chiller sequencing – to maximize the COP - under different cases and conditions.

Huang et al. [31] developed a novel approach of feature-recognition based modeling of liquid chillers to predict the chiller's capacity under different working conditions. The model used physical based formulation such as fluid mechanics, heat transfer and thermodynamics to lay the fundamental equations for each main components, namely, condenser, evaporator, compressor and the throttle valve. Then chiller measured experimental data were utilized to compute the lumped model characteristics parameter. A total of 15 characteristics were computed using Least-squares. For heat exchangers, heat transfer equations were formulated for each phase. In other words, three and two heat equations were developed for the condenser (i.e. subcooled, two-phase and overheat regions) and evaporator (two-phase and overheat regions), respectively. Both the compressor and the throttle valve were modeled using steady-state equations. An experimental water-cooled chiller setup running on R22 refrigerant was built. The setup had a variable-speed compressor, a plate type heat exchanger and an expansion type throttling device. A series of four experiments were conducted to evaluate the performance of the model under different conditions. In each working condition, the flow rate or temperature of the chilled water or condenser water per circuits were varied. The model predicted the refrigerating capacity and the COP successfully with a maximum deviation of 10%.

## 2.2 Control Techniques of Vapor Compression Systems

In this section, the control techniques of vapor compression systems will be presented. Due to the limited literature on control system design for liquid chillers, control techniques applied to VCS are also presented as the dynamics and operation are similar. Perhaps the major difference would be the secondary medium passing in the condenser and/or evaporator. That is, instead of liquid passing through the evaporator, condenser or both, the secondary medium would be air. For example, direct expansion air conditioning unit which has air as

the secondary medium. The most common control techniques applied on VCS include PID, Optimal Control, Robust Control and Model Predictive Control. Other newly emerging techniques that fall under the umbrella of machine learning or hybrid control are also presented. These include genetic algorithms, neural networks, neuro-fuzzy or neuro PID controllers. This section is divided into three subsections. Subsection 1 covers classical control techniques such as ON/OFF and PID, section 2 covers hard control techniques such as Optimal, Robust and Model Predictive Control and lastly, subsection 3 includes soft and hybrid control techniques.

In some research, the controller type is not specified, however, the feedback loop is configured to improve the system performance at a given criterion. For instance, Jia and Reddy [32] proposed a model-based feed forward controller scheme to improve the accuracy of chilled water temperature. In their study, the capacity control of the centrifugal chiller was achieved using inlet guide vanes. The traditional feedback temperature readings of chilled water will adjust the IGV position. However, in the proposed scheme, feedback control is replaced with feedforward control. The first step to achieve this was done by developing a physics-based model of the evaporator that describes the dynamic relationship between outlet and inlet chilled water temperatures. The physics-based model was described by partial differential equations with initial and boundary conditions that is solved analytically. Secondly, using transient data of a 1580 kW actual chiller, the unknown parameters of the physics-based model was determined. The model was then validated against actual data before applying the new control scheme. Finally, computer simulations were done to test the proposed feedforward control scheme and compare it with the existing feedback control scheme. It was found that the new proposed scheme improved the accuracy of chilled water supply by 28% on the given understudy chiller model.

### **2.2.1 Classical Control**

The most classical form of control is ON-OFF control, Jian and Zaheeruddin [33] investigated sub-optimal ON-OFF switching control strategies for chilled water cooling (CWC) systems with storage. First, a dynamic mathematical model of the system based on modular component models of the compressor, condenser, evaporator, expansion valve, evaporative cooler and thermal energy storage tank was done using physics-based equations such as energy balance. Empirical correlations of refrigerant properties were determined through data. The response of the open-loop model was validated through a series of tests by varying

the cooling load requirements and the compressor's speed. As the response of the system was validated, the final step was to design an algorithm and 24-hour profiles for ON-OFF control. Using a reduced-order model, ON-OFF control strategies were developed using a heuristic method. The 24 hours ON-OFF control profiles were simulated on the full-order model of a 15.8 kW CWC system. Moreover, it was concluded that the proposed ON-OFF control method is optimal when the chiller load varies with time, multiple applications of unconstrained optimal ON-Off control can provide adequate control over the chilled water supply temperature given minor fine tuning and the maximum chilled water supply temperatures difference between full-order and reduced order was less than or equal to 0.3 °C for short time load configurations and daily load profiles. Thus, this simple technique was proven to be effective for chilled water supply temperature control on CWC systems.

Tudoroiu et al. [23] applied several PI control strategies on linear and non-linear ARMAX models of water-cooled centrifugal chillers. In their study, the chiller was mathematically modeled using physical principles such as moving boundary conditions. The developed nonlinear differential equations were then linearized, discretized and represented in state-space. Two inputs and two outputs were considered. The control inputs are the compressor speed and the expansion valve opening angle. Hence, the system under study falls under MIMO systems. On the other hand, the outputs were the chilled water temperature supply and the refrigerant liquid level in the condenser. The open-loop simulations of the MIMO system determined that the model can be decoupled due to the weak link between the two outputs. Thus, the system can be converted to a Single-Input-Single-Output (SISO) system. The simulation results of the SISO model were used to build two ARMAX SISO models of the chiller, one for the evaporator and the other for the condenser. A new Proportional Integral Plus (PIP) controller was applied on the ARMAX SISO models to test its performance against traditional PI controllers applied on both the MIMO systems and the ARMAX SISO models. It was concluded after various testing scenarios – such as applying disturbances on the cooling load and noise in feedback sensors – that the proposed PIP outperforms the traditional the PI controllers and exhibit better reference trajectory tracking, robustness, convergency and percent overshoot.

### **2.2.2 Hard Control**

He et al. [34] investigated the use of a Linear-Quadratic Gaussian (LQG) with Integral MIMO controller on a residential direct expansion air conditioner. Using a linearized low-order (5<sup>th</sup>

order) lumped parameter model, an LQG controller has been designed on a two input and two output MIMO model. The model inputs included the compressor speed and expansion valve opening angle. The first input regulates the output air temperature (first output), whereas the second input controls the degree of superheat in the system. Moreover, an LQG controller deploys a Kalman filter to estimate unmeasured state variables using measured variables. Due to the nonlinear dynamics of any VCS at different operating conditions, a gain scheduling approach has been taken to adjust the controller gains based on the current operating conditions as depicted in Figure 2-10. The proposed LQG MIMO controller performance was evaluated analytically – through computer simulation – and experimentally against a traditional SISO controller. The performance of the proposed controller was evaluated based on its ability to reject disturbance, track a reference trajectory and its stability robustness when a model error is present. It was concluded that the LQG with Integral MIMO outperforms traditional SISO control. Since the decoupling of the loops was not weak. Thus, the performance of a SISO controller would be compromised.

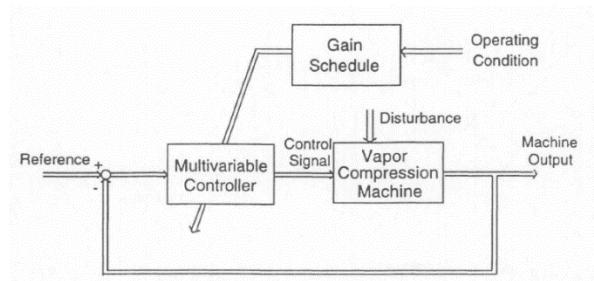


Figure 2-10: Control System Block Diagram with Gain Scheduling [34]

Leducq et al. [35] implemented a non-linear predictive controller on a water-water chiller to optimize multiple variable such as energy efficiency and refrigerating capacity at a reference set-point temperature. The proposed controller was implemented on a reduced-order (7<sup>th</sup> order) non-linear distributed plant model. In contrast to most controller designs of VCS which control each component in a VCS separately, a global control is investigated. The overall general block diagram of the proposed controller is depicted in Figure 2-11. The controller design cost function was based on the weighted sum of partial criterions and constraints. A total of four weighted quadratic cost were considered, and their weights were computed empirically. The first partial cost function penalized the difference between the actual and predicted refrigeration capacity, the second cost function minimized the coefficient of

performance, the third minimized the rapid input changes in the control signal and the fourth ensured that the controlled or secondary variables upper and lower constraint bounds are not violated. The proposed was validated on a small scale 4 kW experimental chiller with variable speed compressor. Two different experimental cases were investigated, namely, chiller partial and global optimization. The global predictive controller regulated multiple inputs such as the compressor speed and condenser flow rated; and a PID control is used to control the expansion valve opening angle Furthermore, the cost function and the controlled inputs for both were not the same. For instance, chiller global control considered constraints and it had an additional control parameter to be regulated. That is, the evaporator flow rate (in partial optimization, this was considered as a perturbation input rather than a control input). Experimental results presented an increase of 8% to 20% in terms of COP. Furthermore, the predictive controller design was implemented at an industrial level on three different dairy chiller plants. The optimal predictive controller was deployed as a supervisory controller to determine the steady-state optimal settings for the local controllers to follow; and an 8% performance increase was reported.

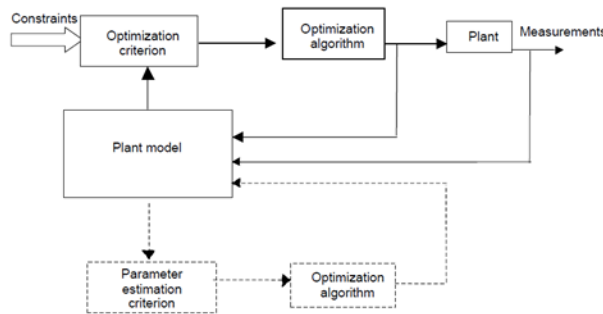


Figure 2-11: Block diagram of the non-linear predictive control system

Schurtet al. [36] presented a model-based MIMO LQG controller to assess the controlling envelope of liquid vapor compression systems. A modular approach was adopted to model each component of the VCS. For each sub-model, dynamic mathematical models were derived using physics-based principles such as the mass and energy conversion principles with moving boundary formulation for heat exchangers. The models' coefficients were computed empirically using experimental data. The experimental data were gathered by setting up a VCS running on HFC134a refrigerant, hermetic variable-speed reciprocating type compressor, tube-in-tube heat exchangers with water and brine as the secondary mediums

in the condenser and evaporator, respectively. Furthermore, the mathematical model was validated using the experimental setup. The ordinary differential equations of each sub-model were linearized using Taylor expansion series, discretized – with sample speed of 2 seconds - and represented in state-space form. The state-space representation had six state variables (i.e. evaporating and condensing pressure, evaporator and condenser boundary positions and the enthalpies at the outlet of the evaporator and condenser), two control input variables (i.e. compressor speed and expansion valve opening angle), two perturbation inputs (i.e. secondary coolant flow rates at the condenser and evaporator) and two outputs variables (i.e. superheating degree and outlet secondary coolant in the evaporator). The designed LQG controller is designed according to the separation principle. That is, it is a combination of a Linear Quadratic Regulator and optimal state estimator. In addition, an integrator was used along with LQG controller. The unmeasured state variables were computed using the Kalman Filter and they included the condenser and evaporator boundary positions. The controller's performance was assessed using the experimental setup through three performance criterions, namely, reference tracking, disturbance rejection and assessment of the controlling envelope. In the latter and the main criterion, the maximum and minimum controlled states and controllable thermal loads states were determined by applying step changes on the reference signal and varying the evaporator flow rate, respectively.

Wallace et al. [37] investigated the use of a linear offset-free model predictive controller (OF-MPC) for regulating a vapor compression cycle (VCC). The VCC linear model – running on R134a refrigerant - was developed using system identification using data from first principles model. The VCC model was interfaced with a building simulation, EnergyPlus, to form a non-linear model. The design objectives of the controller were to regulate the supply air temperature of a zone, ensure that the refrigerant temperature leaving the evaporator is superheat vapor and to operate within energy efficient ranges whenever possible. The control inputs of the VCC were the compressor speed and the expansion valve opening angle. Since the overall plant model is nonlinear and the proposed controller was linear, model-mismatch can cause the closed-loop system performance to perform poorly. To overcome this issue, a model predictive controller with 'offset-free' feature was selected to eliminate the steady-state discrepancy. Furthermore, the proposed controller included an Lueberger observer and accounted for disturbances through an augmented model. The overall block diagram of the proposed closed-loop system containing the plant model, EnergyPlus model and OF-MPC is

depicted in Figure 2-12. The proposed controller was compared to PI controller, and the results showed trajectory tracking and energy efficiency improvements.

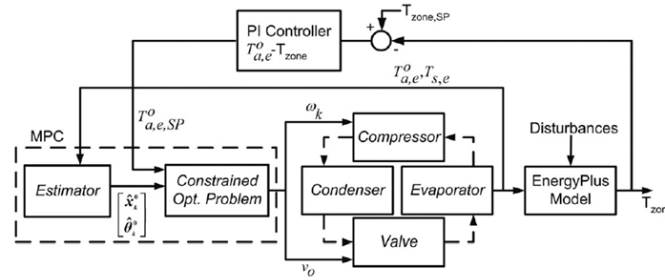


Figure 2-12: Block diagram of the closed-loop system [37]

Jaine and Alleyne. [38] investigated the use of exergy-based (also known as availability) model predictive control on a VCS that undergoes frequent load changes such as in refrigerated transport applications. A modular modeling approach was adopted to model each component of the VCS. The heat exchangers were modeled using the lumped parameter MB formulation, while a quasi-steady approach was used to model the compressor and expansion valve. The VCS nonlinear model was validated experimentally in earlier work. The experimental setup had a rated cooling capacity of 1 kW running on R134a, and it consisted of a variable-speed semi-hermetic reciprocating compressor, EEV, condenser, evaporator and a variable-speed heat exchangers fan. For each sub-model of the VCS, the rate of exergy destruction was derived from the nonlinear mathematic equations and summed all together to form an overall system exergy destruction rate that will then be used as the minimization metric in controller design. A linear MPC – considering a receding horizon - was adopted to reduce the overall system complexity. Hence, the nonlinear dynamic equations and the total exergy destruction rate were linearized, discretized and represented in state-space form. Furthermore, the length of the prediction horizon and the control horizon were both chosen to be the same (i.e. 15 samples with a sampling time of 1 second). The objective function was formulated as the sum of performance and efficiency objective functions with a weighting parameter to prioritize one over the other. Furthermore, the performance function considered the L2 norm between the difference in the required and the VCS output cooling capacity. Constraints were introduced as both linear and nonlinear on the input and state variable. They included, but not limited to having nonzero superheat and nonzero subcooling at the outlets of the evaporator and the condenser, respectively. The performance of the proposed

second law (exergy based) MPC was validated through computer simulation and compared with first law MPC. On average the COP of the first law MPC was higher by 3.95%, nevertheless. The exergetic efficiency in the second law MPC was greater than the first law MPC by more than 40%. In other words, despite the higher COP in the proposed controller, the energy used in the system was more efficient as in the system runs with fewer irreversibilities such as refrigerant flow friction and heat transfer losses.

Alfaya et al. [39] performed controllability analysis and investigated the use of  $H_\infty$  controller on one-stage refrigeration system. A simplified linear sub-model for each component in the VCS was formulated. Heat exchangers were dynamically modeled using the MB formulation. On the contrary, statistical models were adopted for the compressor, expansion valve and the thermal behavior of secondary fluxes. Two controlled inputs and two outputs were considered for the overall system model. Control inputs were the compressor speed and expansion valve opening angle. The two controlled variable - or outputs – were the superheating degree of the refrigerant and the secondary flux temperature at the evaporator's outlet. Controllability analysis was done on the simplified linear model to investigate the closed-loop limitations of the system. Despite the results showing a stable system, a transmission zero on the right half plane (RHP) imposes performance limitations and constraints. Eight modes of operation were setup based on the refrigerant enthalpy conditions at the inlet and outlet of the evaporator and condenser. One of which was the nominal operating point, whilst the others are considered as structured uncertainties. Given the outcome of the controllability study of the system as well multiple operating points, a multivariable  $H_\infty$  robust controller based on the S/KS/T Mixed Sensitivity Problem was selected. A secondary objective - besides from controlling the two output variables – was to maximize the system's COP while meeting the cooling load requirements. Computer simulations were carried out to assess the performance of the proposed  $H_\infty$  controller under the nominal and nonnominal operating points in terms of reference tracking, disturbance rejection and coupling measurements. The results of the proposed controller were compared with a MPC and a decentralized PID controller. It was concluded that the proposed controller outperforms the other two.

Yin and Li [40] presented multiple reduced-order vapor compression cycle (VCC) models using the Proper Orthogonal Decomposition (POD) and investigated the use of a multivariable MPC on the optimized low-order model. First, a full-order model of a VCC air conditioning unit was derived from sub-models of each component in the VCC. The heat

exchangers were modeled using the lumped parameter MB formulation, whereas the variable-speed compressor and expansion valve were modeled as static components. The full-order model was linearized, discretized and represented in state-space form. Furthermore, Using the POD approach, the 12<sup>th</sup> order (or full-order) model was reduced into 2<sup>nd</sup>, 3<sup>rd</sup> and 4<sup>th</sup> order models upon analyzing and considering the most influential variables that affect the system performance. The full-order model analysis revealed that the most significant variables for controller design are the evaporator pressure and the superheat of the evaporator. An experimental setup was used to evaluate the accuracy of each reduced order model. The MPC controller was designed on the 2<sup>nd</sup> and 3<sup>rd</sup> reduced-order models, since the 4<sup>th</sup> order model was still complicated for controller design. For the 2<sup>nd</sup> order model, evaporator pressure and superheat are the controlled outputs, whereas the compressor speed and expansion valve opening angle. The 3<sup>rd</sup> order model included an additional output depicted by the condenser pressure and an additional input in the form of air mass flow rate through the condenser. Moreover, Upper and lower bound constraints were applied on the inputs and outputs of the system. The objective function of the controller was formulated for the reduced order models to compute the most suitable control signal within a finite-horizon. The performance of the proposed MPC controller on the 2<sup>nd</sup> and 3<sup>rd</sup> order models were assessed experimentally in terms of trajectory tracking and disturbance rejection; and the results indicated an improved response for both, especially for the 3<sup>rd</sup> order system that tracked the reference signal faster and was more robust against disturbances.

Prášek et al. [41] studied the use of range control MPC in vapor compression cycles. Component based modeling of a heat pump VCC was done, and a complete model was formed through physical relations between these components. The heat exchangers were modeled using the MB method, whereas static models were adopted for the compressor and expansion valve. The 4-way valve – that are used in heat pumps to reverse the direction of flow – was omitted in the model. Furthermore, the secondary flux in the evaporator and condenser are air and water, respectively. The 12<sup>th</sup> order non-linear model with two controlled variables (CV), three manipulated variables (MV) and three disturbance input variables were linearized using Taylor series around a setpoint, discretized and represented in state-space form. The system model was augmented with a disturbance model to have an offset free MPC design. The disturbances include both real and modeling errors; and an observer was designed to estimate these disturbances in addition to unmeasured states. A low-order model

was derived in order to reduce the computation time of the MPC controller since the main objective is to embed this controller in a microcontroller unit. In addition, blocking (MV and CV) sets, and range control is proposed to further reduce the computational time and complexity. The range control is when the reference output or controlled variable set-point is replaced with a set-range (also known as funnel). The set-range or funnel was designed such as the closed-loop performance is robust. Simulation and experiments on a commercial small scale heat pump system with nominal heating power of 17 kW was done to validate the performance of the controller. The criterion used to validate the controller's performance was set-range reference tracking and disturbance rejection. It was noted that the proposed control algorithm had a smoother control waveform. Thus, increasing the lifetime expectancy of the VCC components. In addition, the COP of the proposed controller was compared a high-end commercial solution. The results showed that the proposed controller yielded a better reference tracking performance and a higher COP.

### **2.2.3 Soft and Hybrid Controls**

Ming. [42] presented an integrated model, performed uncertainty analysis and developed a hybrid-based control algorithm to optimize the performance of a two-zone variable air volume (VAV) and water-cooled vapor compression chiller. A modular physics-based approach was considered to model the VAV and the water-cooled chiller. Then through physical relations between the modules of the VAV and the chiller, an interface was done. The VAV model comprised of a variable-speed fan operated by a DC motor, cooling and dehumidifying coils, zone-model and an air flow model. The chiller model contained a compressor, condenser, evaporator and an expansion valve. Furthermore, MB formulation was selected to model the chiller's heat exchangers. To analyze uncertain parameters of the model's such as the chilled-water mass flow rate and inlet water to the condenser, an extended transformation approach was opted to identify these uncertainties. The uncertain parameters were considered as fuzzy variables with triangular membership function. In addition, a transformation approach was also used to perform sensitivity analysis on control variables to assess the system's coupling effects. Similar to uncertain parameters, the control inputs were treated as fuzzy variables. A neural network supervisory controller and local controllers were fitted to find the most optimal operating points for the chilled water supply temperature, discharge air temperature and air handling unit fan static pressure such that the indoor environment is maintained with the least chiller and fan energy consumption at

full-load and part-load conditions. The three-layer feed forward neural network was trained in unsupervised mode to determine the most optimal operating points in the form of control inputs. Moreover, neural network weights were update on-line and penalties were imposed when constraints were violated. Five local or low-level proportional integral (PI) controller were used - in each loop – to track optimal and zone air temperature set-points. The weights of the PI controllers were not fixed but were updated on-line using Lyapunov stability analysis. Hence, they were “adaptive on-line PI controllers”. The simulation experiments concluded that on average, the energy efficiency is increased by 10% and 19% under full-load and part-load conditions, respectively.

To improve a central chiller plant’s efficiency, Ma and Wang. [43] proposed an optimal strategy to model and control the chiller plant. The chiller plant understudy is feeding multiple superhigh rise tower, the plant included six centrifugal chillers, rated at 7230 kW. Apart from the chiller, the plant included cooling towers, condenser, primary and secondary water pumps, air handling units and heat exchangers. Simplified linear models for each equipment were formulated, and the parameters of these models were identified and updated online using the recursive least squares (RLS) estimation technique with exponential forgetting. Furthermore, a supervisory controller based on Genetic Algorithm (GA) was developed to compute the optimized operating setpoints for each equipment. Figures 2-13 and 2-14 illustrate the overall block diagram of the proposed GA controller optimization process and the overall block diagram of the prediction model with a GA trial computation. The proposed models and control algorithm were tested through computer simulation and compared with a reference strategy that adopted traditional or conventional settings. One zone was considered to analyze the system’s performance, and up to 2.5% of energy savings (in terms of electric kilo Watt hours) per day were observed under three test cases, spring, mid-summer and sunny-summer season loads.

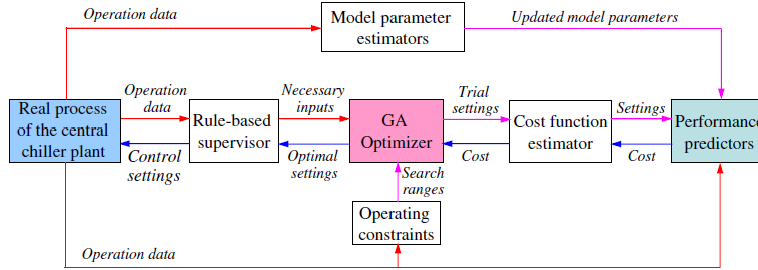


Figure 2-13: Overall GA Optimization Controller Process [43]

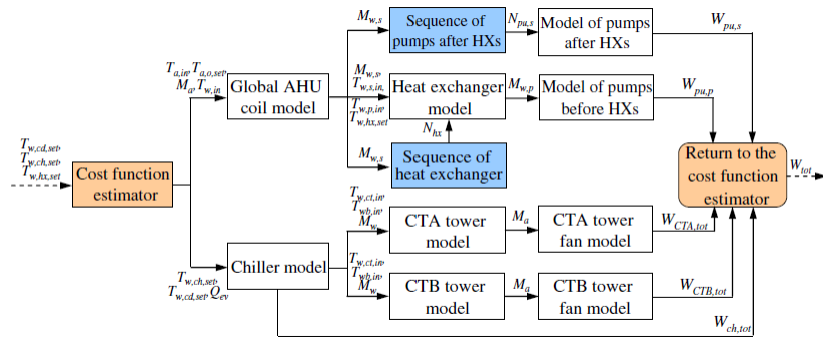


Figure 2-14: Overall Block diagram of the Prediction System with GA Trial Computations [43]

Ursu et al. [44] implemented a Fuzzy Supervised Neuro Control (FSNC) on an HVAC system. The system model was formulated using physics-based relations to model an HVAC system serving a thermal space. Two controllers were designed to synthesize the HVAC system, both of which will be working in parallel. The optimization problem is to minimize the energy consumption whilst achieving thermal comfort of an HVAC system depicted by a variable-air-volume-system (VAV). The neuro-fuzzy controllers were implemented together, and their duties were clearly identified. The neuro-controller – that was designed as a single neuron/neuro – generated the control inputs in the form of volumetric flow rate of air and the flow rate of chilled or heated water. On the contrary, the fuzzy logic - Mamdani type - controller was fitted as supervisory controller to counteract in case the neural network controller saturates.

Al-Badri and Al-Hassani [45] investigated three control types and three control techniques to maximize the COP of a chiller. The system's outputs were the evaporators' degree of superheat (DS) and chilled-water outlet temperature. The compressor in the chiller was operated by a variable-speed type DC motor, and the expansion valve was electronically

operated (also referred to as EEV). Furthermore, a R410a refrigerant was used in the system. The three investigated control types were single control loop (SCL) with adaptive EEV opening, two-control loops (TCL) with adaptive and constant DS settings (DS7). In the single control loop, the mutual coupling or physical relationship between the compressor speed and EEV opening angle were taken into consideration, and a single controller is used. On the contrary, the TCL method deploys two controllers, one for the EEV angle and the other for the compressor speed. Hence, the evaporator output water temperature and DS are controlled separately. Moreover, three control techniques were designed on each of the proposed control methods. A proportional fuzzy (PF) controller was proposed, and its performance was experimentally compared with PI and PID controllers. Experimental results revealed that not only the control technique is the pivot factor, but the control system architecture. In other words, irrespective of the controller type, the SCL experienced the highest COP when compared to TCL and D7S. In addition, experimental findings supported showed that the performance of the PF controller in the SCL configuration achieved the highest average COP as illustrated in Figure 2-15.

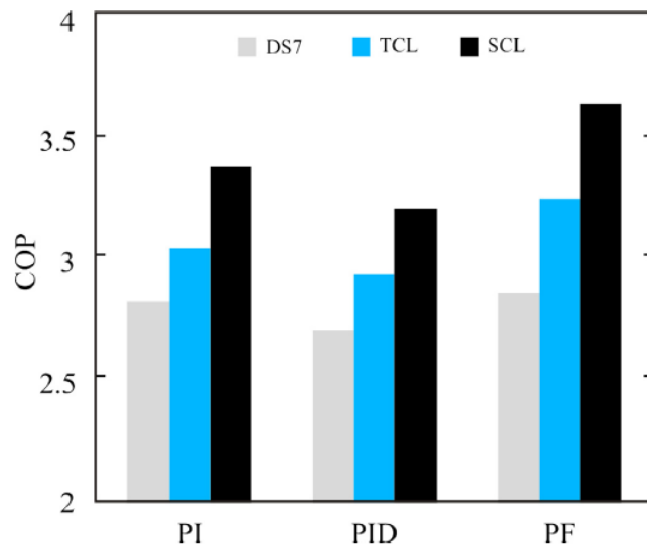


Figure 2-15: Average COP according to the control method [45]

## Chapter 3 Dynamic Modeling of Single-stage Liquid Chiller

As discussed in chapter 1, the dynamic model of a liquid chiller includes several inputs and outputs as well as three dependent circuits. In this chapter, the developed dynamic model of a vapor compression liquid chiller by Yao et al. [28,46] will be presented along with the open-loop responses. The published linearized model's data -represented in state-space -will be used to design the controllers as shown in the subsequent chapters. However, selected number of outputs were chosen from the model, and the inputs were categorized based on their type. There are two types of controlled inputs, the first type can be labeled as “direct” controlled inputs whereas the second type can be labeled as “indirect” controlled inputs. In the direct controlled inputs, the compressor's speed, IGV and/or the expansion valve opening angle are adjusted to achieve the reference output. On the other hand, the indirect controlled inputs are the outputs of the other surrounding equipment to the chiller's secondary circuits of the condenser and the evaporator. These include the condenser inlet temperature and the inlet flow rates of the evaporator and condenser (applicable to variable primary and variable compressor configurations). The flow rates of the evaporator and condenser secondary circuit liquid are varied using the primary and condenser pumps, whereas the entering condenser's coolant liquid temperature is varied using the cooling tower. Disturbance input includes the return temperature of the evaporator's chilled liquid.

### 3.1 Model Formulation

#### 3.1.1 Working Principles of Vapor Compression Cycle in Liquid Chillers

A typical single-stage liquid chiller – including the main components (i.e. evaporator, condenser, compressor and expansion valve) – and the Pressure-Enthalpy plot are depicted in Figures 3-1 and 3-2. As stated in chapter 1, the main circuit of any VCS is the refrigerant circuit, and there are secondary circuits liquid circuits in the condenser and evaporator. The medium or fluid in the secondary circuits is usually water, but it can also be oil or a mixture of water and other substance(s).

In the refrigerant circuit, the heat from the load (i.e. HVAC equipment such as a fan coil unit of an air handling unit) is exchanged in the evaporator. In other words, the liquid heat load enters the evaporator's secondary circuit, and the heat is absorbed by the low pressure and temperature two-phase (liquid vapor) refrigerant, and the secondary liquid fluid passing through the evaporator will leave the chiller back to the load at preset lower temperature. The refrigerant leaves the evaporator and enters the compressor in the gaseous or superheated vapor represented as 'state 1' in Figure 3-1. The refrigerant leaves the compressor in 'state 2' also as vapor, but at a higher pressure as shown in Figure 3-2 and a higher temperature.

The heat in the superheated vapor represented in 'state 2' entering the condenser is rejected through the secondary fluid passing through the condenser. The refrigerant leaves the condenser as high-pressure subcooled liquid and represented as 'state 3' in Figures 3-1 and 3-2. Furthermore, the temperature of the secondary fluid leaving the condenser is decreased using the cooling tower. Hence, unlike the evaporator, the condenser exhibits three phase changes in the following order: superheated vapor, two-phase and subcooled liquid. Finally, the expansion valve decreases the pressure of the refrigerant before entering the evaporator as represented in 'state 4' in Figures 3-1 and 3-2.

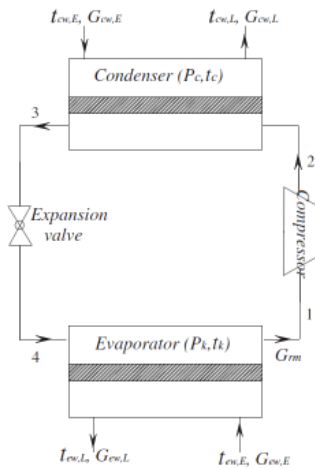


Figure 3-1: Block-diagram of a single-stage vapor compression liquid chiller [28]

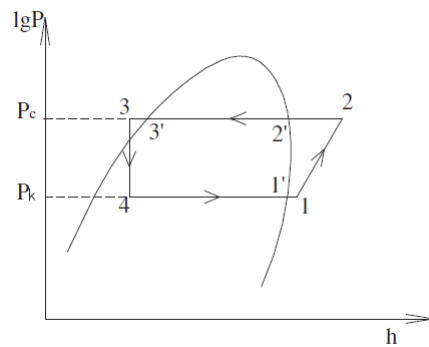


Figure 3-2: Pressure-enthalpy plot of a single-stage vapor compression system [28]

### 3.1.2 Modeling Approach and Assumptions

The heat exchangers are modeled using the lumped parameter approach, compressor as a static component and the expansion valve model is neglected (the dynamics is considered to vary linearly without any external input/control on the expansion valve opening angle). Furthermore, the fundamental equations of the heat exchangers and compressors are developed by Yao et al. [28,46] are based on the following assumptions and considerations:

1. The transition from 'state 1' to 'state 2' or the compression process is isentropic. That is, entropy at 'state 1' is equal to 'state 2'.
2. The transition from 'state 3' to state '4' or the expansion process is isenthalpic. That is, enthalpy at 'state 3' is equal to 'state 4'.
3. Friction in the refrigerant circuit is neglected.
4. The compressor model is static, and its working performance remained the same during the open-loop response simulation.
5. Temperature of the secondary fluid passing through the condenser and evaporator circuits change linearly from the input and the output.
6. Condenser and evaporator shell wall temperatures variables are described by lumped parameters.
7. The temperature of the refrigerant at the outlets of the condenser (sub-cooled liquid state) and evaporator (superheated vapor) are considered to be constant and equal to the initial conditions during the open-loop simulations.
8. A heat conduction oil is used as the secondary fluid in the heat exchangers. Within a temperature bound of -40 °C to +60 °C, the density and kinematics viscosity of the heat conduction oil is a constant value of 1084 kg/m<sup>3</sup> and 6.5 x 10<sup>-6</sup> m<sup>2</sup>/s, respectively.
9. The cooling capacity of the chiller can be adjusted using the compressor rotational speed through a variable frequency drive (or other means).
10. The chiller uses R134a as the working refrigerant.

### 3.1.3 Fundamental Equations

According to the principle of energy and mass conservation, the equations governing the refrigerant, secondary liquid and the heat exchanger's shell are developed through first-order non-linear differential equations. Note that that for all equations, 't' depicts temperature in degree Celsius and 'τ' is the time in seconds.

### Condenser Equations

The energy equation of the refrigerant passing through the condenser is given by [28,46] as

$$c_{cr}M_{cr} \frac{dt_c}{d\tau} = G_{rm}(h_{r,2} - h_{r,3}) + a_{co}A_{co}(t_{cg} - t_c) \quad (3-1)$$

where  $c_{cr}$  and  $M_{cr}$  are the specific heat and mass of the refrigerant in the condenser,  $t_c$  and  $t_{cg}$  are the condensing and condenser shell wall temperatures,  $G_{rm}$  is the refrigerant mass flow rate,  $h_{r,2}$  and  $h_{r,3}$  are the enthalpies of the refrigerant at states 2 and 3,  $a_{co}$  and  $A_{co}$  are the coefficient of convection heat transfer and the area between the condenser and refrigerant.

The mass flow rate of the coolant liquid in the condenser is given by [28,46] as

$$G_{cw,E} = G_{cw,L} = G_{cw} \quad (3-2)$$

where the subscript of the mass flow rate, 'G', refers to the entering and leaving coolant of condenser (secondary fluid)

The energy equation for the coolant liquid passing through the condenser is given by [28,46] as

$$\frac{1}{2}c_{cw}M_{cw} \frac{d(t_{cw,L} + t_{cw,E})}{d\tau} = c_{cw}G_{cw,E}(t_{cw,E} - t_{cw,L}) + a_{cw}A_{cw} \left( t_{cg} - \frac{t_{cw,E} + t_{cw,L}}{2} \right) \quad (3-3)$$

where  $c_{cw}$  and  $M_{cw}$  are the specific heat and mass of the condenser's coolant,  $t_{cw,L}$  and  $t_{cw,E}$  are the coolant liquid temperature in the outlet and inlet,  $a_{cw}$  and  $A_{cw}$  are the coefficient of convection heat transfer and the area of the condenser's secondary fluid.

The energy equation for shell of the condenser is given by [28,46] as

$$c_{cg}M_{cg} \frac{dt_{cg}}{d\tau} = a_{co}A_{co}(t_c - t_{cg}) + a_{cw}A_{cw} \left( \frac{t_{cw,E} + t_{cw,L}}{2} - t_{cg} \right) \quad (3-4)$$

where  $c_{cg}$  and  $M_{cg}$  are the specific heat and mass of the condenser's shell wall.

### Evaporator Equations

The same equations applied previously on the condenser apply on the evaporator. The energy equation for the refrigerant is given by [28,46] as

$$c_{er}M_{er} \frac{dt_k}{d\tau} = G_{rm}(h_{r,3} - h_{r,1}) + a_{eo}A_{eo}(t_{eg} - t_k) \quad (3-5)$$

where  $c_{er}$  and  $M_{er}$  are the are the specific heat and mass of the refrigerant in evaporator,  $t_k$  and  $t_{eg}$  are the evaporating and evaporator shell wall temperatures,  $h_{r,1}$  and  $h_{r,3}$  are the

enthalpies of the refrigerant at states 1 and 3,  $a_{eo}$  and  $A_{eo}$  are the coefficient of convection heat transfer and the area between the evaporator and refrigerant.

The mass equation of the chilled liquid is given by [28,46] as

$$G_{ew,L}=G_{ew,E}=G_{ew} \quad (3-6)$$

where the subscript of the mass flow rate, 'G', refers to the entering and leaving chilled liquid.

The energy equation for chilled liquid passing through the evaporator is given by [28,46] as

$$\frac{1}{2}c_{ew}M_{ew}\frac{d(t_{ew,L}+t_{ew,E})}{d\tau}=c_{ew}G_{ew,E}(t_{ew,E}-t_{ew,L})+a_{ew}A_{ew}\left(t_{eg}-\frac{t_{ew,E}+t_{ew,L}}{2}\right) \quad (3-7)$$

where  $c_{ew}$  and  $M_{ew}$  are the specific heat and mass of the chilled liquid in evaporator,  $t_{ew,L}$  and  $t_{ew,E}$  are the leaving and entering temperatures of the chilled liquid,  $a_{ew}$  and  $A_{ew}$  are the coefficient of convection heat transfer and the area of the chilled liquid in the evaporator.

The energy equation for the evaporator's shell is given by [28,46] as

$$c_{eg}M_{eg}\frac{dt_{eg}}{d\tau}=a_{eo}A_{eo}(t_k-t_{eg})+a_{ew}A_{ew}\left(\frac{t_{ew,E}+t_{ew,L}}{2}-t_{eg}\right) \quad (3-8)$$

where  $c_{eg}$  and  $M_{eg}$  are the specific heat and mass of the evaporator's shell wall.

### **Power Consumption and Cooling Capacity Equations**

As mentioned earlier, the process from state '3' to 'state 4' is considered as isenthalpic. Therefore, the energy equation in the expansion process is given by [28,46] as

$$h_{r,3}=h_{r,4} \quad (3-9)$$

where the subscript of the enthalpy, 'h', refers to the refrigerant's enthalpy at state '3' and at state '4'.

The electric power consumed by the compressor is given by equation 3-10 [28,46], and is a function of several variables such as the mass flow rate, compressor efficiency, evaporating temperature, evaporating and condensing pressures and adiabatic compression process index.

$$N_{com}=\frac{G_{rm}}{\eta_{com}}\frac{R_r T_1}{k_s-1}\left[\left(\frac{p_c}{p_k}\right)^{\frac{k_s-1}{k_s}}-1\right]=\frac{G_{rm}}{\eta_{com}}\frac{R_r(t_k+\Delta t_{e,shr}+273.15)}{k_s-1}\left[\left(\frac{f_p(t_c)}{f_p(t_k)}\right)^{\frac{k_s-1}{k_s}}-1\right]=G_{rm}f_{N_{com}}(t_k,t_c) \quad (3-10)$$

The chiller's cooling capacity is given by equation 3-11 [28,46], and it is represented as the product of the refrigerant flow rate with the energy difference between states '1' and '4' (i.e. the enthalpy different across the evaporator's outlet and inlet), or as the product of the refrigerant flow rate with the difference between a enthalpy function of the evaporating temperature and an enthalpy function of the condensing temperature.

$$Q_c = G_{rm}(h_{r,1} - h_{r,4}) = G_{rm}(f_h(t_k) - f_h(t_c)) = G_{rm}f_{Q_c}(t_k, t_c) \quad (3-11)$$

The coefficient of performance or COP is a performance evaluation metric of the chiller. The COP of the chiller is represented as the quotient of the chiller's cooling capacity with the compressor's input power and is given by equation 3-12 [28,46]. Moreover, the higher the COP, the more efficient the chiller. In other words, as the COP increases, it indicates that the chiller can provide more cooling at a lower electric power consumption.

$$COP = \frac{Q_c}{N_{com}} = \frac{f_{Q_c}(t_k, t_c)}{f_{N_{com}}(t_k, t_c)} = f_{COP}(t_k, t_c) \quad (3-12)$$

### 3.1.4 Key Parameters Determination

Equations 3-1 through 3-12 lay the foundation of the chiller model. Nevertheless, there are unknown coefficients or empirical constants that need to be computed through experimental data [28,46].

The equations to compute these coefficients as described by [28,46] are presented in this subsection. They include used to compute the refrigerant's enthalpy at different key states, heat transfer coefficients (U values) and the adiabatic compression index.

#### Enthalpy Calculation of the Refrigerant

The refrigerant physical state changes across different states as mentioned earlier. For instance, the refrigerant is in the form of superheated vapor at the evaporator's outlet (state '1') and compressor's outlet (state '2'). On the other hand, the refrigerant is ideally subcooled liquid at the condenser's outlet (state '3') and evaporator's outlet (state '4'). Furthermore, the enthalpy of the refrigerant at these key states ('1' through '4') are presented through semi-empirical equations.

At the gaseous state, the refrigerant's enthalpy in terms of pressure and temperature are given by Equation 3-13 [28,46]; and the refrigerant's pressure at the gaseous state is given by Equation 3-14 [28,46].

$$h_{\text{vapor}} = h_0 + (p_{r,g} v_{r,g} - R_r T_{r,g}) + \sum_{n=1}^4 \frac{c_n T_{r,g}^n}{n} + c_5 \ln T_{r,g} - \frac{c_6}{T_{r,g}} + \sum_{n=2}^5 \frac{A_n}{(n-1)(v_{r,g}-b)^{n-1}} + e^{-K_1 T_{r,g}/T_{cc}(1+K_1 T_{r,g}/T_{cc})} \times \sum_{n=2}^5 \frac{C_n}{(n-1)(v_{r,g}-b)^{n-1}} \quad (3-13)$$

$$p_{r,g} = \frac{R_r T_{r,g}}{v_{r,g} - b} + \sum_{n=2}^5 \frac{A_n + B_n T_{r,g} + C_n e^{-K_1 T_{r,g}/T_{cc}}}{(v_{r,g} - b)^n} \quad (3-14)$$

The saturated vapor (or gas) pressure of refrigerant is computed as [28,46]

$$\ln p_{r,bg} = A + \frac{B}{T_{r,bg}} + C T_{r,bg} + D T_{r,bg}^2 + \frac{E(F - T_{r,bg})}{T_{r,bg}} \ln(F - T_{r,bg}) + G \ln T_{r,bg} \quad (3-15)$$

The temperature of the gaseous refrigerant,  $T_{r,g}$ , and saturated gas refrigerant,  $T_{r,bg}$ , at states '1' and '2', correspond to the evaporating,  $T_k$ , and condensing,  $T_c$  temperatures, respectively.

At the liquid state, the enthalpy of the sub-cooled liquid refrigerant (states '3' and '4') is given by Equation 3-16.

$$h_{r,\Delta t} = h_{r,bl} - \frac{p_{r,bl} - p_{\text{atm}}}{q_r} \quad (3-16)$$

where the heat of vaporization,  $q_r$ , is given by the Clausius-Clapeyron equation.

$$q_r = T_{r,q} (v_{r,bl} - v_{r,bg}) p_{r,q} \left[ -\frac{B}{T_{r,q}^2} + C + 2D T_{r,q} - \frac{EF}{T_{r,q}^2} \times \ln(F - T_{r,q}) - \frac{EF}{T_{r,q}} \times \frac{1}{F - T_{r,q}} + E \times \frac{1}{F - T_{r,q}} + \frac{G}{T_{r,q}} \right] \quad (3-17)$$

The enthalpy of the saturated liquid refrigerant is given by equation 3-18. Furthermore, the density of the saturated liquid refrigerant is given by equation 3-19.

$$h_{r,bl} = h_{r,bg} - q_r \quad (3-18)$$

$$\rho_{r,bl} = \rho_{cc} + \sum_{n=1}^6 D_n (1 - T_{r,bl}/T_{cc})^{\frac{n}{3}} \quad (3-19)$$

To summarize, the gaseous enthalpies at states ‘1’ and ‘2’ are computed using equations 3-13 and 3-14. Furthermore, the gaseous pressures at states ‘1’ and ‘2’ corresponding to saturated evaporating and saturated condensing pressures, respectively, are computed from equation 3-15. Considering an isenthalpic process between states ‘3’ and ‘4’ as given in equation 3-9, the sub-cooled liquid refrigerant enthalpies at states ‘3’ and ‘4’ are the equal; and the equation to compute the enthalpy at this state is given by equations 3-14, 3-16, 3-17, 3-18 and 3-19. Moreover, the enthalpy at these states only depends on the condensing temperature,  $T_c$ .

The unknown constants/coefficients from equations 3-13 through 3-19 are A, B, C, D, E, F, G,  $K_1$ , b,  $c_1 \sim c_6$ ,  $A_2 \sim A_5$ ,  $B_2 \sim B_5$ ,  $C_2 \sim C_5$  and  $D_1 \sim D_6$ . These coefficients are determined through refrigerant property software.

### Heat Transfer Coefficients

The four coefficients of convection heat transfer considered in this chiller model are:

1. Condensation heat transfer coefficient between the condenser and refrigerant ( $a_{co}$ ).
2. Boiling heat transfer coefficient between the evaporator and refrigerant ( $a_{eo}$ ).
3. Convection heat transfer coefficient between the coolant liquid and condenser ( $a_{cw}$ ).
4. Convection heat transfer coefficient between the chilled liquid and evaporator ( $a_{ew}$ ).

The above coefficients are determined through the Equations 3-20 through 3-23 [28,46]; and the constants  $C_1$ ,  $C_2$ ,  $C_3$ ,  $n_1$ ,  $n_2$ ,  $n_3$  are determined through experimental data.

$$a_{co} = C_1 (t_c - t_{cg})^{n_1} \quad (3-20)$$

$$a_{eo} = C_2 (t_{eg} - t_k)^{n_2} \quad (3-21)$$

$$Nu_d = C_3 Re_d^{n_3} = \frac{a_{cw} d_{ci}}{\lambda_w} = C_3 \left( \frac{u_{cw} d_{ci}}{v_w} \right)^{n_3} \quad (3-22)$$

$$Nu_d = C_3 Re_d^{n_3} = \frac{a_{ew} d_{ei}}{\lambda_w} = C_3 \left( \frac{u_{ew} d_{ei}}{v_w} \right)^{n_3} \quad (3-23)$$

Furthermore, Equations 3-20 through 3-23 are formulated to compute these coefficients and constants using Equations 3-24 through 3-26 [28,46].

$$G_{rm} (h_2 - h_3) = a_{co} A_{co} (t_c - t_{cg}) = C_1 A_{co} (t_c - t_{cg})^{n_1+1} \quad (3-24)$$

$$G_{rm} (h_4 - h_1) = a_{eo} A_{eo} (t_{eg} - t_k) = C_2 A_{eo} (t_{eg} - t_k)^{n_2+1} \quad (3-25)$$

$$c_{cw} G_{cw} (t_{cw,L} - t_{cw,E}) = a_{cw} A_{cw} \left[ t_{cg} - \frac{(t_{cw,L} + t_{cw,E})}{2} \right] = A_{cw} \frac{C_3 \lambda_w}{d_{ci}} \left[ t_{cg} - \frac{(t_{cw,L} + t_{cw,E})}{2} \right] Re_d^{n_3} \quad (3-26)$$

where the measured data include the refrigerant and secondary fluid mass flow rates ( $G_{rm}$ ,  $G_{cw}$ ,  $G_{ew}$ ) secondary fluid temperatures at the inlet and outlet of the condenser and evaporator ( $t_{cw,E}$ ,  $t_{cw,L}$ ,  $t_{ew,E}$ ,  $t_{ew,L}$ ) and the shell wall temperatures of the condenser and evaporator ( $t_{cg}$ ,  $t_{eg}$ ).

Equations 3-24 through 3-26 are further re-arranged and presented by Equations 3-27 through 3-29 [28,46].

$$\ln[G_{rm}(h_2 - h_3)] = \ln(C_1 A_{co}) + (n_1 + 1) \ln(t_c - t_{cg}) \quad (3-27)$$

$$\ln[G_{rm}(h_4 - h_1)] = \ln(C_2 A_{eo}) + (n_2 + 1) \ln(t_{eg} - t_k) \quad (3-28)$$

$$\ln[c_{cw} G_{cw} (t_{cw,L} - t_{cw,E})] = \ln \left[ A_{cw} \frac{C_3 \lambda_w}{d_{ci}} \left[ t_{cg} - \frac{(t_{cw,L} + t_{cw,E})}{2} \right] \right] + n_3 \ln Re_d \quad (3-29)$$

#### Adiabatic Compression process index (ks)

The adiabatic compression process index of the gaseous refrigerant is given by

$$k_s = \frac{Z}{Z_p - \frac{R_r Z_T^2}{c_{r,p}}} = \frac{Z}{\left( Z_p \left( \frac{\partial Z}{\partial p} \right)_T \right) - \frac{R_r \left( Z + T \left( \frac{\partial Z}{\partial T} \right)_p \right)^2}{c_{r,p}}} \quad (3-30)$$

where  $Z$  is the compressibility factor, the subscript 'p' and "T" correspond to the isobaric and isothermal processes respectively.

### 3.2 State-Space Representation

The differential equations presented earlier are non-linear. To represent these equations in a linear state-space representation as shown in Equation 3-31 in its compact form as well as the block diagram description in Figure 3-3, these equations must be linearized first. Prior to linearization, the selection of the state variables, inputs and outputs must be determined. The variables are classified into two groups, fundamental and lumped. The fundamental variables will classify as state variables, inputs and outputs. The lumped variables such as the heat transfer coefficients, enthalpy and pressures will be embedded (implicit) within these fundamental variables [28,46].

$$\begin{cases} \dot{x}(t)=Ax(t)+Bu(t) \\ y(t)=Cx(t)+Du(t) \end{cases} \quad (3-31)$$

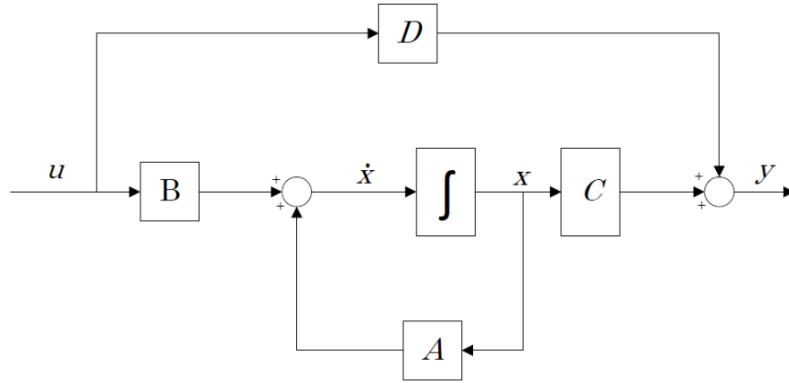


Figure 3-3: State-space Representation Block Diagram

Considering a disturbance input,  $w$ , to the system as shown in Figure 3-4, the state-space Equation in 3.31 will, thus, be given in Equation 3-32.

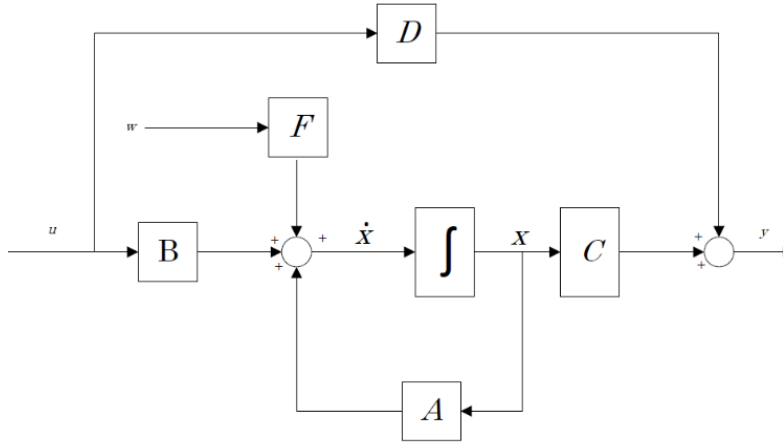


Figure 3-4: State-space Representation with Disturbance Input Block Diagram

$$\begin{cases} \dot{x}(t)=Ax(t)+Bu(t)+Fw(t) \\ y(t)=Cx(t)+Du(t) \end{cases} \quad (3-32)$$

A total of six state variables, in the form of temperatures of the system, are considered as given in equation 3-32 in vector notation. The selected state variables will represent the dynamic operations of the chiller. The chosen state variables are the condensing temperature, leaving condenser coolant liquid temperature, shell wall temperature of the condenser, evaporating temperature, leaving evaporator chilled liquid temperature and shell wall temperature of the evaporator. The system state variables are given in 3-33 as

$$\text{state variables} = \Delta x_{\text{chiller}} = [\Delta t_c, \Delta t_{\text{cw,L}}, \Delta t_{\text{cg}}, \Delta t_k, \Delta t_{\text{ew,L}}, \Delta t_{\text{eg}}]^T \quad (3-33)$$

The same inputs as considered by Yao et al. [28][46] are considered. However, the inputs in this thesis will be divided into controlled and disturbance inputs. The controlled inputs are the condenser entering coolant liquid temperatures and flow rate, evaporator entering chilled liquid flow rate and the refrigerant flow rate (which is manipulated by varying the compressor's rotational speed). Note that only the latter input is direct or within the chiller model, and the other controlled inputs are indirect or external. That is, controlled through other equipment of the DCP such as cooling towers and pumps. The considered measured disturbance input to the system is the temperature of the evaporator's entering chilled liquid, because we can measure this temperature through sensors, but we don't have a control on its value. Moreover, as this value increases, the load to the system increases since more heat is rejected from the customer load. The controlled input vector and the measured disturbance input vector are given in 3-34 and 3-35, respectively.

$$\text{controlled inputs} = \Delta u_{\text{chiller}} = [\Delta t_{\text{cw,E}}, \Delta G_{\text{cw,E}}, \Delta G_{\text{ew,E}}, \Delta G_{\text{rm}}]^T \quad (3-34)$$

$$\text{disturbance input} = \Delta w_{\text{chiller}} = [\Delta t_{\text{ew,E}}]^T \quad (3-35)$$

The outputs are the leaving condenser coolant liquid temperature and flow rates, leaving evaporator chilled liquid temperature and flow rates, power consumption by the compressor, cooling capacity and the COP. Yao et al. [28,46] has also considered the condenser coolant and evaporator chilled liquids flow rates in the outputs. However, these will be omitted as they are already considered as outputs. The outputs are represented in vector notion in 3-36.

$$\text{controlled variables (outputs)} = \Delta y_{\text{chiller}} = [\Delta t_{\text{cw,L}}, \Delta t_{\text{ew,L}}, \Delta W_{\text{com}}, \Delta Q_C, \Delta \text{COP}]^T \quad (3-36)$$

The  $\Delta$  symbol shown in equations 3-33 through 3-36 depict the 'difference' between the initial conditions and final values after the system exhibits a change input.

The linearization process begins by considering the fundamental variable,  $\theta$ , to be the sum of the initial value,  $\theta_0$ , and small increment  $\Delta\theta$  as shown in 3-37.

$$\theta = \theta_0 + \Delta\theta \quad (3-37)$$

Using first-order Taylor series expansion as given by Equation 3-38, Equations 3-1 through 3-12 will be linearized, and the results are depicted in Equations 3-39 to 3-49.

$$\sigma = \sigma_o + \left( \frac{\partial \sigma}{\partial \theta'} \right)_o \Delta \theta' \quad (3-38)$$

$$T_{cr} \frac{d\Delta t_c}{d\tau} = X_{cr,1} \Delta t_c + X_{cr,2} \Delta t_{cg} + X_{cr,3} \Delta G_{rm} \quad (3-39)$$

where,

$$\begin{aligned} T_{cr} &= (c_{cr} M_{cr})_o \\ X_{cr,1} &= \left[ \left( \frac{\partial h_{r,2}}{\partial t_c} \right)_o - \left( \frac{\partial h_{r,3}}{\partial t_c} \right)_o \right] (G_{rm})_o + A_{co} (t_{cg} - t_c)_o \left( \frac{\partial a_{co}}{\partial t_c} \right)_o - (a_{co} A_{co})_o \\ X_{cr,2} &= A_{co} (t_{cg} - t_c)_o \left( \frac{\partial a_{co}}{\partial t_{cg}} \right)_o + (a_{co} A_{co})_o \\ X_{cr,3} &= (h_{r,2} - h_{r,3})_o \end{aligned}$$

$$T_{cw} \frac{d\Delta t_{cw,L}}{d\tau} = X_{cw,1} \Delta t_{cw,L} + X_{cw,2} \Delta t_{cg} + X_{cw,3} \Delta t_{cw,E} + X_{cw,4} \Delta G_{cw,E} + \xi_{\Delta t_{cw,L}} \quad (3-40)$$

where,

$$\begin{aligned} T_{cw} &= \frac{c_w M_{cw}}{2} \\ X_{cw,1} &= -c_w (G_{cw,E})_o - \frac{A_{cw}}{2} (a_{cw})_o \\ X_{cw,2} &= A_{cw} (a_{cw})_o \\ X_{cw,3} &= c_w (G_{cw,E})_o - \frac{A_{cw}}{2} (a_{cw})_o \\ X_{cw,4} &= c_w (t_{cw,E} - t_{cw,L})_o + A_{cw} \left( t_{cg} - \frac{t_{cw,E} + t_{cw,L}}{2} \right)_o \left( \frac{\partial a_{cw}}{\partial G_{cw,E}} \right)_o \\ \xi_{\Delta t_{cw,L}} &= -\frac{1}{2} c_w M_{cw} \frac{\partial \Delta t_{cw,E}}{\partial \tau} \end{aligned}$$

$$T_{cg} \frac{d\Delta t_{cg}}{d\tau} = X_{cg,1} \Delta t_c + X_{cg,2} \Delta t_{cw,L} + X_{cg,3} \Delta t_{cg} + X_{cg,4} \Delta t_{cw,E} + X_{cg,5} \Delta G_{cw,E} \quad (3-41)$$

where,

$$\begin{aligned} T_{cg} &= c_{cg} M_{cg} \\ X_{cg,1} &= A_{co} (t_c - t_{cg})_o \left( \frac{\partial a_{co}}{\partial t_c} \right)_o + (a_{co} A_{co})_o \\ X_{cg,2} &= X_{cg,4} = \frac{A_{cw}}{2} (a_{cw})_o \\ X_{cg,3} &= A_{co} (t_c - t_{cg})_o \left( \frac{\partial a_{co}}{\partial t_{cg}} \right)_o - (a_{cw} A_{cw} + a_{co} A_{co})_o \\ X_{cg,5} &= -A_{cw} \left( t_{cg} - \frac{t_{cw,E} + t_{cw,L}}{2} \right)_o \left( \frac{\partial a_{cw}}{\partial G_{cw,E}} \right)_o \end{aligned}$$

$$T_{er} \frac{d\Delta t_k}{d\tau} = X_{er,1} \Delta t_k + X_{er,2} \Delta t_{eg} + X_{er,3} \Delta G_{rm} \quad (3-42)$$

where,

$$\begin{aligned}
T_{er} &= (c_{er} M_{er})_o \\
X_{er,1} &= \left( \frac{\partial h_{r,1}}{\partial t_k} \right)_o (G_{rm})_o + A_{eo} (t_{eg} - t_k)_o \left( \frac{\partial a_{eo}}{\partial t_k} \right)_o - (a_{eo} A_{eo})_o \\
X_{er,2} &= A_{eo} (t_{eg} - t_k)_o \left( \frac{\partial a_{eo}}{\partial t_{eg}} \right)_o - (a_{eo} A_{eo})_o \\
X_{er,3} &= (h_{r,4} - h_{r,1})_o
\end{aligned}$$

$$T_{ew} \frac{d\Delta t_{ew,L}}{d\tau} = X_{ew,1} \Delta t_{ew,L} + X_{ew,2} \Delta t_{eg} + X_{ew,3} \Delta t_{ew,E} + X_{ew,4} \Delta G_{ew,E} + \xi_{\Delta t_{ew,L}} \quad (3-43)$$

where,

$$\begin{aligned}
T_{ew} &= \frac{c_w M_{ew}}{2} \\
X_{ew,1} &= -c_w (G_{ew,E})_o - \frac{A_{ew}}{2} (a_{ew})_o \\
X_{ew,2} &= A_{ew} (a_{ew})_o \\
X_{ew,3} &= c_w \rho_w (G_{ew,E})_o - \frac{A_{ew}}{2} (a_{ew})_o \\
X_{ew,4} &= c_w (t_{ew,E} - t_{ew,L})_o + A_{ew} \left( t_{eg} - \frac{t_{ew,E} + t_{ew,L}}{2} \right)_o \left( \frac{\partial a_{ew}}{\partial G_{ew,E}} \right)_o \\
\xi_{\Delta t_{ew,L}} &= -\frac{1}{2} c_w M_{ew} \frac{\partial \Delta t_{ew,E}}{\partial \tau}
\end{aligned}$$

$$T_{eg} \frac{d\Delta t_{eg}}{d\tau} = X_{eg,1} \Delta t_k + X_{eg,2} \Delta t_{ew,L} + X_{eg,3} \Delta t_{eg} + X_{eg,4} \Delta t_{ew,E} + X_{eg,5} \Delta G_{ew,E} \quad (3-44)$$

where,

$$\begin{aligned}
T_{eg} &= c_{eg} M_{eg} \\
X_{eg,1} &= A_{eo} (t_k - t_{eg})_o \left( \frac{\partial a_{eo}}{\partial t_k} \right)_o + (a_{eo} A_{eo})_o \\
X_{eg,2} &= X_{eg,4} = \frac{A_{ew}}{2} (a_{ew})_o \\
X_{eg,3} &= A_{eo} (t_k - t_{eg})_o \left( \frac{\partial a_{eo}}{\partial t_{eg}} \right)_o - (a_{ew} A_{ew} + a_{eo} A_{eo})_o \\
X_{eg,5} &= -A_{ew} \left( t_{eg} - \frac{t_{ew,E} + t_{ew,L}}{2} \right)_o \left( \frac{\partial a_{ew}}{\partial G_{ew,E}} \right)_o
\end{aligned}$$

$$\Delta G_{cw,L} = \Delta G_{cw,E} = \Delta G_{cw} \quad (3-45)$$

$$\Delta G_{ew,L} = \Delta G_{ew,E} = \Delta G_{ew} \quad (3-46)$$

$$\Delta N_{com} = X_{EW,1} \Delta t_c + X_{EW,2} \Delta t_k + X_{EW,3} \Delta G_{rm} \quad (3-47)$$

where,

$$\begin{aligned}
X_{EW,1} &= (G_{rm})_o \left( \frac{\partial f_{N_{com}}(t_k, t_c)}{\partial t_c} \right)_o \\
X_{EW,2} &= (G_{rm})_o \left( \frac{\partial f_{N_{com}}(t_k, t_c)}{\partial t_k} \right)_o \\
X_{EW,3} &= \left( f_{N_{com}}(t_k, t_c) \right)_o
\end{aligned}$$

$$\Delta Q_c = X_{Q,1} \Delta t_c + X_{Q,2} \Delta t_k + X_{Q,3} \Delta G_{rm} \quad (3-48)$$

where,

$$\begin{aligned}
X_{Q,1} &= (G_{rm})_o \left( \frac{\partial f_{Q_c}(t_k, t_c)}{\partial t_c} \right)_o \\
X_{Q,2} &= (G_{rm})_o \left( \frac{\partial f_{Q_c}(t_k, t_c)}{\partial t_k} \right)_o \\
X_{Q,3} &= \left( f_{Q_c}(t_k, t_c) \right)_o
\end{aligned}$$

$$\Delta COP = X_{COP,1} \Delta t_c + X_{COP,2} \Delta t_k \quad (3-49)$$

where,

$$\begin{aligned}
X_{COP,1} &= \left[ \frac{\partial f_{COP}(t_k, t_c)}{\partial t_c} \right]_o \\
X_{COP,2} &= \left[ \frac{\partial f_{COP}(t_k, t_c)}{\partial t_k} \right]_o
\end{aligned}$$

Equations 3-39 through 3-49 are all linear, and hence, they can be arranged in matrix format in the following state-space arrangement.

$$\Delta \mathbf{x}_{chiller} = \mathbf{A}_{chiller} \Delta \mathbf{x}_{chiller} + \mathbf{B}_{chiller} \Delta \mathbf{u}_{chiller} + \boldsymbol{\xi} \quad (3-50)$$

$$\Delta \mathbf{y}_{chiller} = \mathbf{C}_{chiller} \Delta \mathbf{x}_{chiller} + \mathbf{D}_{chiller} \mathbf{u}_{chiller} \quad (3-51)$$

The variable,  $\boldsymbol{\xi}$ , given by equation 3-52 can be removed from equation 3-50 through mathematical manipulation as illustrated in equation 3-53.

$$\boldsymbol{\xi} = \left[ 0, \boldsymbol{\xi}_{\Delta t_{cw,L}}, 0, 0, \boldsymbol{\xi}_{\Delta t_{ew,L}}, 0 \right]^T \quad (3-52)$$

$$\Delta \mathbf{X}_{chiller} = \Delta \mathbf{x}_{chiller} + \mathbf{A}_{chiller}^{-1} \boldsymbol{\xi}_{chiller} \quad (3-53)$$

Finally, the state-space representation of the liquid chiller is as given by equations 3-54 and 3.55 in compact form.

$$\Delta \dot{X}_{\text{chiller}} = A_{\text{chiller}} \Delta X_{\text{chiller}} + B_{\text{chiller}} \Delta u_{\text{chiller}} \quad (3-54)$$

$$\Delta y_{\text{chiller}} = C_{\text{chiller}} \Delta X_{\text{chiller}} + D_{\text{chiller}} u_{\text{chiller}} - C_{\text{chiller}} A_{\text{chiller}}^{-1} \xi_{\text{chiller}} \quad (3-55)$$

In matrix form, the state matrices A, B, C, D and F of the liquid chiller are as depicted below.

$$A_{\text{chiller}} = \begin{bmatrix} \frac{X_{\text{cr},1}}{T_{\text{cr}}} & 0 & \frac{X_{\text{cr},2}}{T_{\text{cr}}} & 0 & 0 & 0 \\ 0 & \frac{X_{\text{cw},1}}{T_{\text{cw}}} & \frac{X_{\text{cw},2}}{T_{\text{cw}}} & 0 & 0 & 0 \\ \frac{X_{\text{cg},1}}{T_{\text{cg}}} & \frac{X_{\text{cg},2}}{T_{\text{cg}}} & \frac{X_{\text{cg},3}}{T_{\text{cg}}} & 0 & 0 & 0 \\ \frac{X_{\text{er},4}}{T_{\text{er}}} & 0 & 0 & \frac{X_{\text{er},1}}{T_{\text{er}}} & 0 & \frac{X_{\text{er},2}}{T_{\text{er}}} \\ 0 & 0 & 0 & 0 & \frac{X_{\text{ew},1}}{T_{\text{ew}}} & \frac{X_{\text{ew},2}}{T_{\text{ew}}} \\ 0 & 0 & 0 & \frac{X_{\text{eg},1}}{T_{\text{eg}}} & \frac{X_{\text{eg},2}}{T_{\text{eg}}} & \frac{X_{\text{eg},3}}{T_{\text{eg}}} \end{bmatrix};$$

$$B_{\text{chiller}} = \begin{bmatrix} 0 & 0 & 0 & \frac{X_{\text{cr},3}}{T_{\text{cr}}} \\ \frac{X_{\text{cw},3}}{T_{\text{cw}}} & \frac{X_{\text{cw},4}}{T_{\text{cw}}} & 0 & 0 \\ \frac{X_{\text{cg},4}}{T_{\text{cg}}} & \frac{X_{\text{cg},5}}{T_{\text{cg}}} & 0 & 0 \\ 0 & 0 & 0 & \frac{X_{\text{er},3}}{T_{\text{er}}} \\ 0 & 0 & \frac{X_{\text{ew},4}}{T_{\text{ew}}} & 0 \\ 0 & 0 & \frac{X_{\text{eg},5}}{T_{\text{eg}}} & 0 \end{bmatrix} \quad F_{\text{chiller}} = \begin{bmatrix} 0 \\ 0 \\ 0 \\ \frac{X_{\text{ew},3}}{T_{\text{ew}}} \\ \frac{X_{\text{eg},4}}{T_{\text{eg}}} \end{bmatrix};$$

$$C_{\text{chiller}} = \begin{bmatrix} 0 & 1 & 0 & 0 & 0 & 0 \\ 0 & 0 & 0 & 0 & 1 & 0 \\ X_{\text{EW},1} & 0 & 0 & X_{\text{EW},2} & 0 & 0 \\ X_{\text{Q},1} & 0 & 0 & X_{\text{Q},2} & 0 & 0 \\ X_{\text{COP},1} & 0 & 0 & X_{\text{COP},2} & 0 & 0 \end{bmatrix}; \quad D_{\text{chiller}} = \begin{bmatrix} 0 & 0 & 0 & 0 \\ 0 & 0 & 0 & 0 \\ 0 & 0 & 0 & X_{\text{EW},3} \\ 0 & 0 & 0 & X_{\text{Q},3} \\ 0 & 0 & 0 & 0 \end{bmatrix};$$

### 3.3 Simulation Results of the Open-Loop Model

The experimental cases presented by Yao et al. [28][46] as tabulated in Tables 3-1, 3-2, 3-3 and 3-4, the total number of simulation cases are 10, and they are divided into 4 main cases. Furthermore, there are three subcases under cases 2, 3 and 4. The open-loop response is simulated given a change on a single input and its effect on each output. Case 1 and two other cases (not shown in this report) were simulated and validated experimentally by Yao et al. [28][46] as mentioned earlier in Chapter 2. Furthermore, a unique A, B, C, D, and F coefficient matrices are derived at different initial conditions.

Table 3-1: Initial Conditions of Case 1 [28][46]

<u>Initial Conditions</u>	<u>Unit</u>	<u>Case 1</u>
Evaporating temperature ( $t_k$ ) <sub>0</sub>	°C	14.5
Entering chilled liquid temperature of evaporator ( $t_{ew,E}$ ) <sub>0</sub>	°C	24.8
Leaving chilled liquid temperature of evaporator ( $t_{ew,L}$ ) <sub>0</sub>	°C	19.5
Shell wall temperature of evaporator ( $t_{eg}$ ) <sub>0</sub>	°C	22.5
Chilled liquid flow rate of evaporator ( $G_{ew}$ ) <sub>0</sub>	kgs <sup>-1</sup>	1.45
Condensing temperature ( $t_c$ ) <sub>0</sub>	°C	36.3
Entering coolant liquid temperature of condenser ( $t_{cw,E}$ ) <sub>0</sub>	°C	29.5
Leaving coolant liquid temperature of condenser ( $t_{cw,L}$ ) <sub>0</sub>	°C	37.2
Coolant liquid flow rate of condenser ( $G_{cw}$ ) <sub>0</sub>	kgs <sup>-1</sup>	1.16
Shell wall temperature of condenser ( $t_{cg}$ ) <sub>0</sub>	°C	33.9
Compressor inlet temperature ( $t_{com,E}$ ) <sub>0</sub>	°C	24.1
Compressor exhaust temperature ( $t_{com,L}$ ) <sub>0</sub>	°C	58.1
Refrigerant flow rate ( $G_{rm}$ ) <sub>0</sub>	kgs <sup>-1</sup>	0.116

Table 3-2: Initial Conditions of Case 2 and its Subcases [28][46]

<u>Initial Conditions</u>	<u>Unit</u>	<u>Case 2a</u>	<u>Case 2b</u>	<u>Case 2c</u>
Inlet chilled liquid temperature of evaporator ( $t_{ew,E}{}_0$ )	°C	24.6	29.3	36.2
Compressor inlet temperature ( $t_{com,E}{}_0$ )	°C	24.1	28.2	34.5
Compressor exhaust temperature ( $t_{com,L}{}_0$ )	°C	56.1	61.5	67.8
Evaporating temperature ( $t_k{}_0$ )	°C	16.3		
Chilled liquid flow rate of evaporator ( $G_{ew}{}_0$ )	kgs <sup>-1</sup>	1.45		
Condensing temperature ( $t_c{}_0$ )	°C	36.7		
Inlet chilled liquid temperature of condenser ( $t_{cw,E}{}_0$ )	°C	29.3		
Coolant flow rate of condenser ( $G_{cw}{}_0$ )	kgs <sup>-1</sup>	1.16		
Refrigerant flow rate ( $G_{rm}{}_0$ )	kgs <sup>-1</sup>	0.13		

Table 3-3: Initial Conditions of Case 3 and its Subcases [28][46]

<u>Initial Conditions</u>	<u>Unit</u>	<u>Case 3a</u>	<u>Case 3b</u>	<u>Case 3c</u>
Inlet chilled liquid temperature of condenser ( $t_{cw,E}{}_0$ )	°C	29.6	40.7	49.7
Compressor inlet temperature ( $t_{com,E}{}_0$ )	°C	51.5	57.5	59.7
Compressor exhaust temperature ( $t_{com,L}{}_0$ )	°C	37.1	49.5	55.2
Condensing temperature ( $t_c{}_0$ )	°C	37.1	49.5	55.2
Evaporating temperature ( $t_k{}_0$ )	°C	18.8		
Chilled liquid flow rate of evaporator ( $G_{ew}{}_0$ )	kgs <sup>-1</sup>	1.45		
Inlet chilled liquid temperature of evaporator ( $t_{ew,E}{}_0$ )	°C	24.1		
Coolant flow rate of condenser ( $G_{cw}{}_0$ )	kgs <sup>-1</sup>	1.16		
Refrigerant flow rate ( $G_{rm}{}_0$ )	kgs <sup>-1</sup>	0.13		

Table 3-4: Initial Conditions of Case 4 and its Subcases [28][46]

<u>Initial Conditions</u>	<u>Unit</u>	<u>Case 4a</u>	<u>Case 4b</u>	<u>Case 4c</u>
Refrigerant flow rate ( $G_{rm}$ ) <sub>0</sub>	kg s <sup>-1</sup>	0.176	0.199	0.238
Evaporating temperature ( $t_k$ ) <sub>0</sub>	°C	15.1		
Inlet chilled liquid temperature of evaporator ( $t_{ew,E}$ ) <sub>0</sub>	°C	24.7		
Chilled liquid flow rate of evaporator ( $G_{ew}$ ) <sub>0</sub>	kg s <sup>-1</sup>	2.14		
Condensing temperature ( $t_c$ ) <sub>0</sub>	°C	41.2		
Inlet chilled liquid temperature of condenser ( $t_{cw,E}$ ) <sub>0</sub>	°C	33.4		
Coolant flow rate of condenser ( $G_{cw}$ ) <sub>0</sub>	kg s <sup>-1</sup>	2.14		
Compressor inlet temperature ( $t_{com,E}$ ) <sub>0</sub>	°C	23.7		
Compressor exhaust temperature ( $t_{com,L}$ ) <sub>0</sub>	°C	71.3		

### 3.3.1 Open-loop Response of Case 1

By manipulating one input variable at a time by applying a step change with values as tabulated in Table 3.5, the open-loop response for each output variable is closely examined and the transient simulations for case 1 are illustrated in Figures 3-5 to 3-11. Note that the results of cases 2, 3 and 4 are not shown due to the high number of plots.

Table 3-5: Applied Changes on Input Value of the Open-loop System

<u>Input Name</u>	<u>Unit</u>	<u>Applied Change</u>
Inlet Coolant Temperature of Condenser ( $\Delta t_{cw,E}$ )	°C	Step, +1.0
Coolant Flow Rate of Condenser ( $\Delta G_{cw}$ )	kg s <sup>-1</sup>	Step, +0.1
Inlet Chilled liquid Temperature of Evaporator ( $\Delta t_{ew,E}$ )	°C	Step, +1.0
Chilled liquid Flow Rate of Evaporator ( $\Delta G_{ew}$ )	kg s <sup>-1</sup>	Step, +0.1
Refrigerant Flow Rate ( $\Delta G_{rm}$ )	kg s <sup>-1</sup>	Step, +0.01

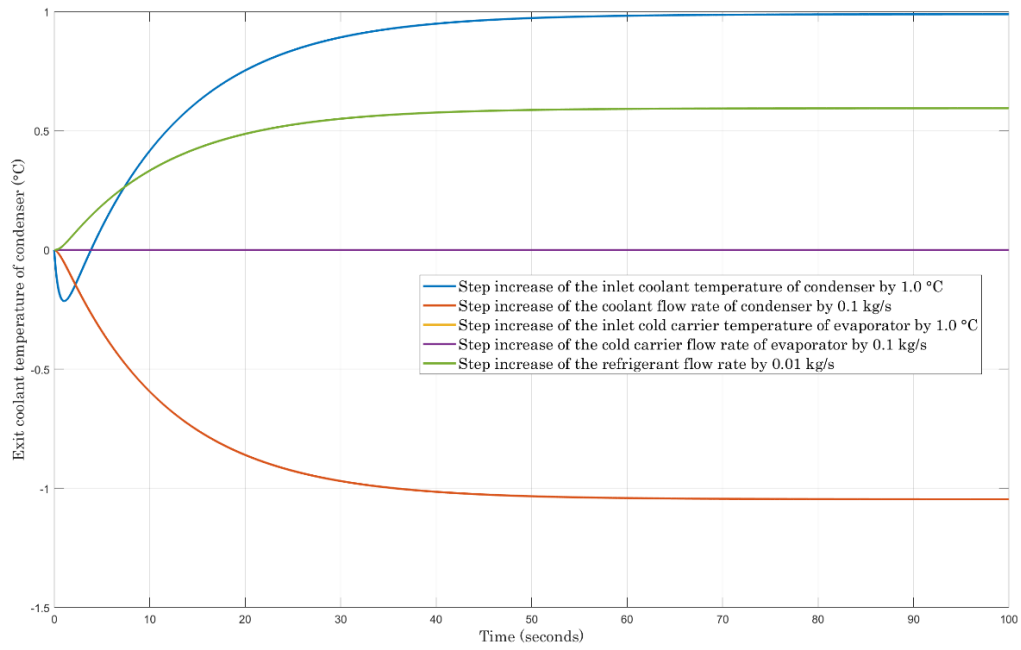


Figure 3-5: Output Responses of Exit Coolant Temperature of Condenser at Different Inputs

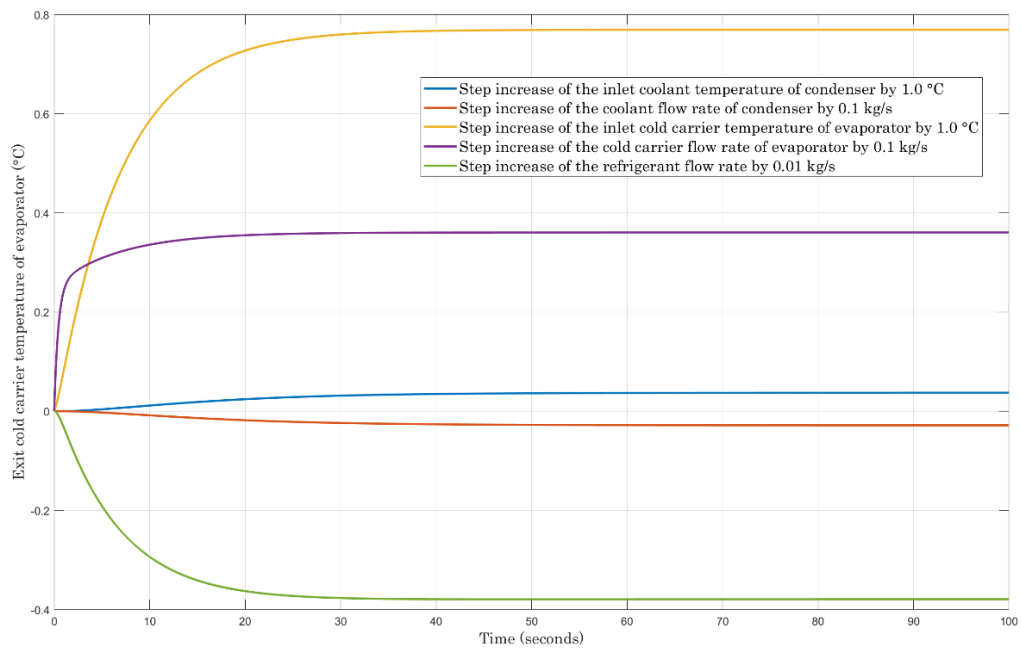


Figure 3-6: Output Responses of Exit Chilled liquid Temperature of Evaporator at Different Inputs

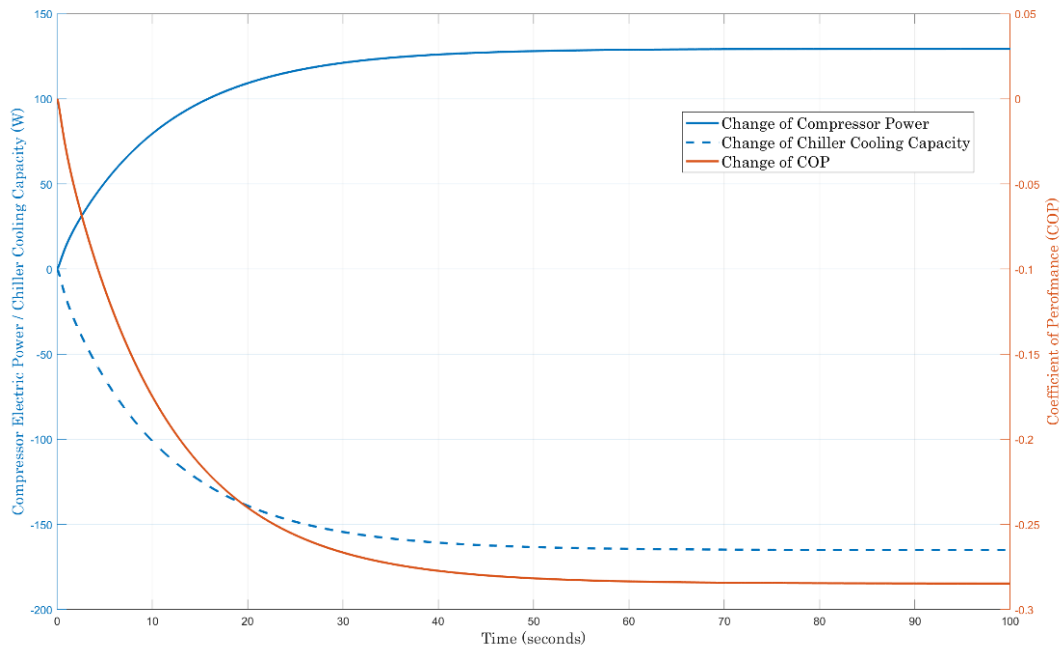


Figure 3-7: Output Responses of Compressor Electric Power, Chiller Cooling Capacity and COP due to Step Increase of Inlet Coolant Temperature of Condenser

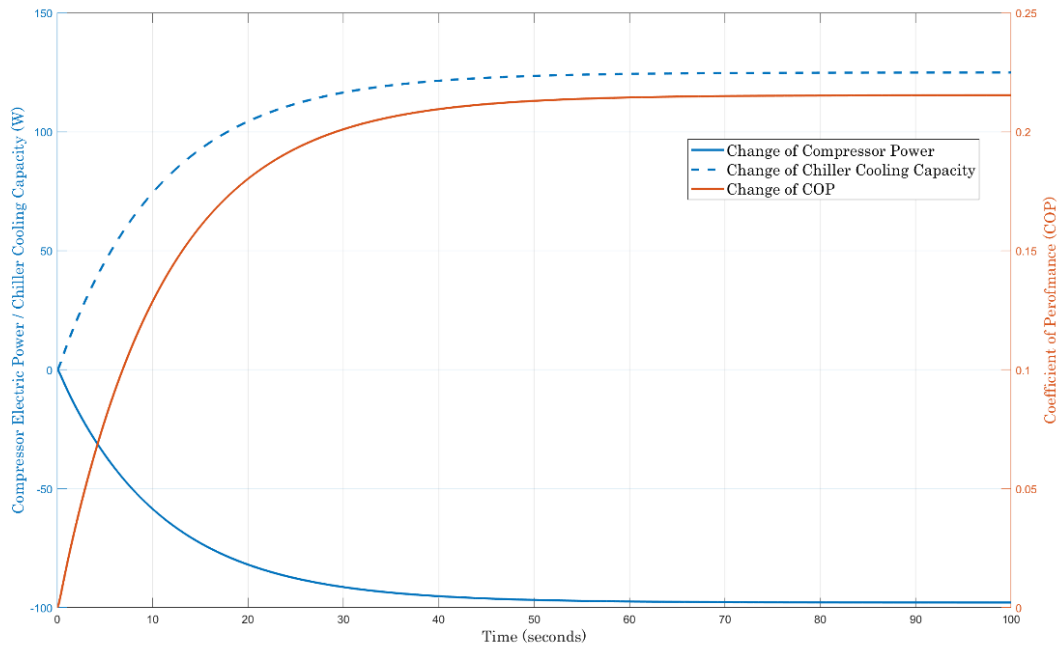


Figure 3-8: Output Responses of Compressor Electric Power, Chiller Cooling Capacity and COP due to Step Increase of Coolant Flow Rate of Condenser

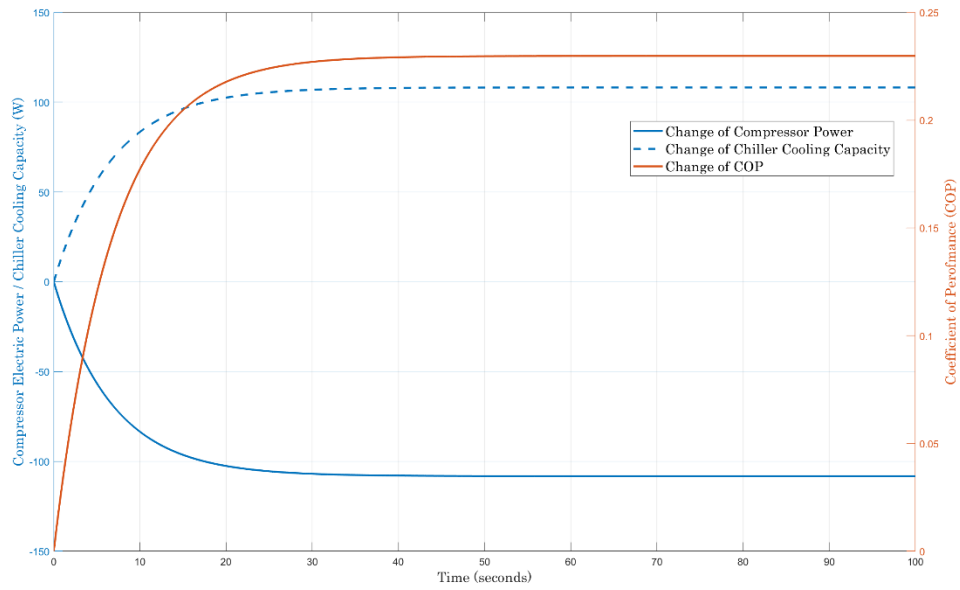


Figure 3-9: Output Responses of Compressor Electric Power, Chiller Cooling Capacity and COP due to Step Increase of Inlet Chilled liquid Temperature of Evaporator

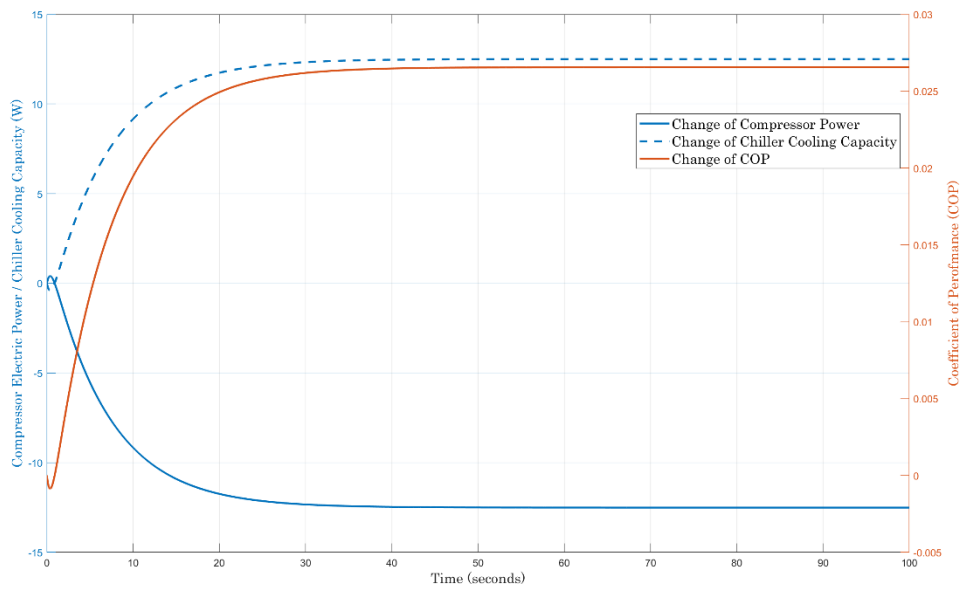


Figure 3-10: Output Responses of Compressor Electric Power, Chiller Cooling Capacity and COP due to Step Increase of Chilled liquid Flow Rate of Evaporator

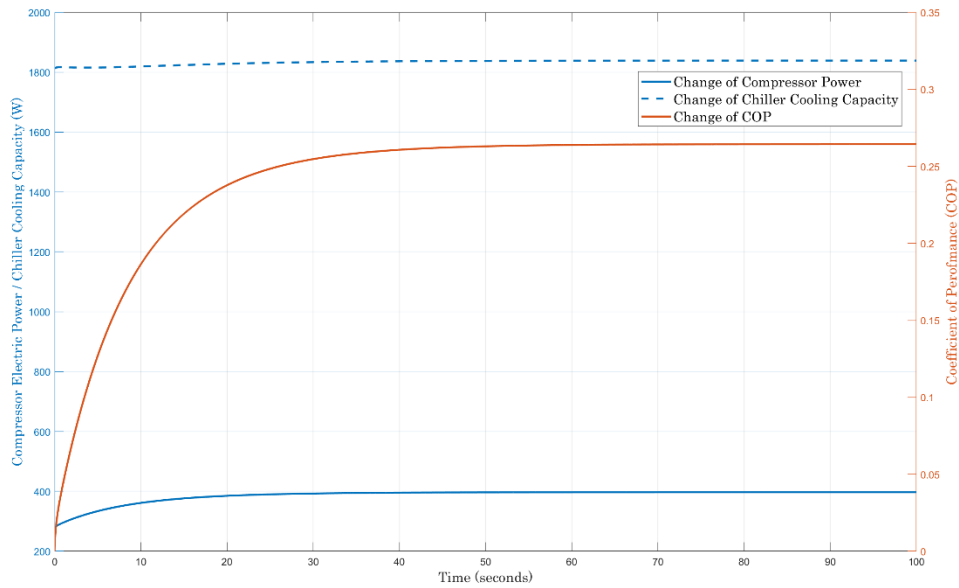


Figure 3-11: Output Responses of Compressor Electric Power, Chiller Cooling Capacity and COP due to Step Increase of the Refrigerant Flow Rate

As seen from Figure 3-5, the outlet coolant temperature of the condenser can be increase by increasing the inlet coolant temperature and the refrigerant mass flow rate, whereas increasing the condenser coolant mass flow rate will decrease the outlet coolant temperature. Furthermore, it also shown that evaporator circuit’s mass flow rate and inlet temperature of the chilled liquid liquids have no effect on the coolant temperature of the condenser.

As illustrated in Figure 3-6, the evaporator’s chilled liquid temperature at the outlet exhibits an acute increase in temperature when the inlet chilled liquid temperature and mass flow rate of the evaporator increases. However, the temperature drops considerably as the refrigerant flow rate increases. Similar to the effect of the evaporator variables on the condenser chilled liquid temperatures, the same can also be seen as shown in Figure 3-6. Nevertheless, the evaporator – unlike the condenser – shows as small change in temperature when condenser parameters are increased.

The performance parameters of the chiller, namely, the compressor’s electric work/power, chiller’s cooling capacity and the COP plots against every input to the chiller are shown in Figures 3-7 to 3-11. As shown in Figure 3-7, the chiller experiences a marginal increase in the compressor power and marginal decay in the cooling capacity as the condenser liquid

increases. The increase in the inlet temperature of the condenser causes the temperature overall temperature in the condenser to increase. Therefore, the pressure of the compressor at its outlet increases, and subsequently, the compressor's power increases, and the cooling capacity reduces [28,46]. On the contrary, it can be entailed from Figure 3-8 that as the flow rate of the condenser increases, the ability of the chiller to reject more heat increases and the compressor's outlet pressure decreases. Thus, the cooling capacity increases whilst the compressor's power decreases.

On the evaporator's side, an increase in the chilled liquid temperature or mass flow rate as shown in Figures 3-9 and 3-10, respectively causes a slight increase in the order of 10 W to 100 W of cooling. As the increase of cooling was caused by external equipment, the compressor's suction temperature and pressure increased [28,46]. Hence, the compressor's power decreases. Figure 3-11 shows that as the refrigerant mass flow rate increases, the chiller's cooling capacity and the compressor power both increase.

To reiterate, the compressor's electric power marginally increases or decreases on all applied inputs except when the refrigerant flow rate is varied. This is in line with the fact stated earlier that the only direct input to this chiller model is the refrigerant flow rate, which is proportional to the compressor rotational speed. Since all other indirect or disturbance inputs are associated with other equipment such as the cooling tower, pumps and client load. Moreover, it is seen that as the inlet chilled liquid temperature of the evaporator, the cooling capacity decreases. On the contrary, increasing all other inputs to the chiller increases the cooling capacity of the chiller.

### Stability Analysis

The outputs of all plots demonstrate the same behavior. That is, once the input is applied to the chiller, the output increases/decreases – with minimal overshoot, if any - until a steady-state value is reached. The system's stability can also be analyzed by computing the eigenvalues of the A-matrix and plotting the result in the pole-zero map as shown in Figure 3-12. It is seen that all system eigenvalues for matrix A of Case 1 are real and negative. Thus, the system is proven to be stable with minimal or no overshoot. Using the open-loop chiller model – without the COP output -presented in this chapter, several automatic control techniques will be applied to the system including PID, LQI and MPC.

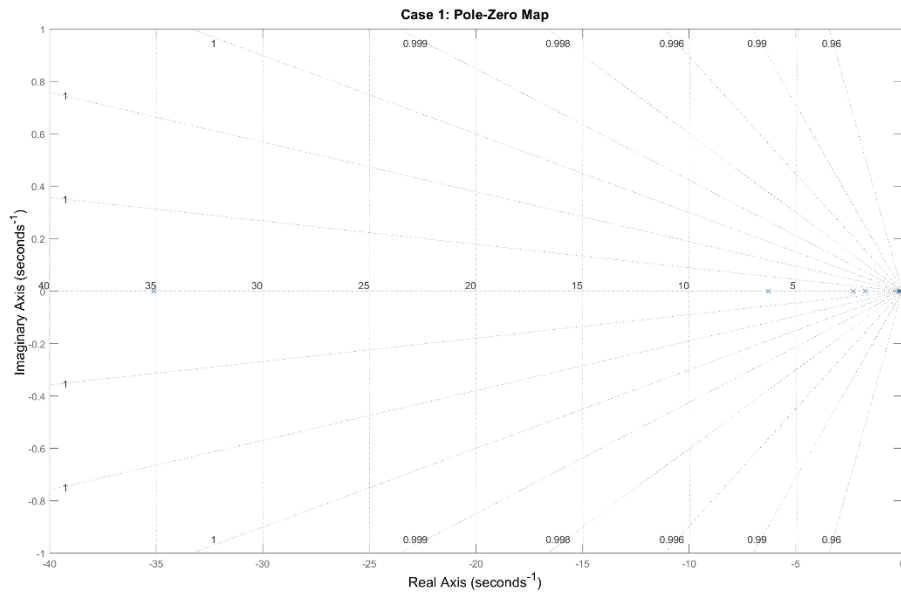


Figure 3-12: Pole-Zero Map of Case 1 illustrating that all the eigenvalues of the open-loop chiller model are negative and real

## Chapter 4 Liquid Chiller Control using PID Controllers

This chapter begins by introducing the detailed methodology of the control problem including, but not limited to simulation cases and the evaluation criterion. Then, the closed-loop control using PID controllers are applied to the MIMO liquid chiller model developed in Chapter 3. Finally, the simulation results of the closed-loop system using PID controllers are presented.

### 4.1 The Control Problem

To recap, the liquid chiller model presented in chapter 3 was derived by Yao et al. [28,46] from nonlinear equations, and then linearized and presented in state-space formulation. Furthermore, the model has 4 control inputs, 5 outputs (7 as published by Yao et al.), 6 state variables and 1 disturbance input. However, the COP output will be omitted from the model. Thus, the model will have 4 control inputs, 5 outputs, 6 state variables. Since the model is nonlinear, there exists N number of models based on the current initial conditions of the system. By applying linear control techniques on the linearized liquid chiller model, the use of adaptive control techniques - such as gain-scheduling - is mandatory. In this research, three control techniques are applied to the linearized model of Case 1 (model parameters of Table 3-1) as the same can be easily generalized to the other cases (or initial conditions). The linearized state-space model data for these cases were published by Yao et al. [28,46] to design the controllers. The control design techniques described herein are Proportional-Integral-Derivative (PID) control, Linear Quadratic Integral (LQI) control and Model Predictive Control (MPC).

The performance of the controller is evaluated based on its ability to track a defined trajectories and to reject input disturbance to the system. Further details on the methodology of trajectory tracking and disturbance rejection simulations are presented in Sections 4.1.1 and 4.1.2, respectively. Note that the input disturbance to the system in this model is measured, and the same holds true in the industry as the entering evaporator liquid temperature to the evaporator is measured using temperature transmitter. In real life cooling

plant, the compressor, cooling tower and pumps all have performance limitation in terms of flow rate or temperature. Thus, saturation (lower and upper limits) is applied on the controlled inputs. The saturation values are tabulated in Table 4-1.

Table 4-1: Saturations of the Control Input Signals

<u>Input Name</u>	<u>Unit</u>	<u>Saturation Limit</u>
Inlet Coolant Temperature of Condenser ( $\Delta t_{cw,E}$ )	°C	±1.0
Coolant Flow Rate of Condenser ( $\Delta G_{cw}$ )	kgs <sup>-1</sup>	±0.5
Chilled liquid Flow Rate of Evaporator ( $\Delta G_{ew}$ )	kgs <sup>-1</sup>	±0.7
Refrigerant Flow Rate ( $\Delta G_{rm}$ )	kgs <sup>-1</sup>	±0.07

#### 4.1.1 Trajectory Tracking

The trajectory tracking performance was tested under two simulation conditions. The first simulation case is to test the controller performance to track the change in cooling capacity of the system. In this case, the leaving chilled liquid temperature from the chiller is to be maintained at 0 °C. On the contrary to first simulation test, the cooling capacity to be maintained at 0 W while the leaving evaporator liquid temperature is tracked. For both tests, the other output reference setpoints (i.e. leaving condenser coolant temperature and compressor electric power) are varied to achieve the desired cooling capacity requirement. Therefore, the leaving condenser coolant temperature and compressor's electric power are set points variables that are adjusted by the plant's operator, while the other two outputs are set points that are decided by the cooling load. Furthermore, the input disturbance, entering evaporator liquid temperature, for both tests are set to 0 °C. The tracking performance test values for both tests are illustrated in Table 4-2 and Table 4-3. It can be observed that there exist two power values in Table 4-2, which are highly dependent on the controller performance and the ability to minimize the refrigerant flow rate, which is directly related to the compressor's electrical power. Further details on this will be discussed in Chapters 7.

Table 4-2: Reference Values for Testing the Trajectory Tracking Performance of the Controller due a to Step Change in the Cooling Capacity

$\Delta t_{ew,L\_REF}$ (°C)	$\Delta t_{ew,L\_REF}$ (°C)	$\Delta W_{com\_REF}$ (W)	$\Delta Q_{c\_REF}$ (W)	$\Delta t_{ew,E\_DIST}$ (°C)
±1	0	±100/±70	±100	0
±1.2	0	±130/±100	±200	0
±1.4	0	±160/±130	±300	0
±1.4	0	±190/±150	±400	0
±1.2	0	±160/±140	±400	0
±1.25	0	±200/±180	±600	0
±1.25	0	±220/±205	±800	0
±1.35	0	±260/±248	±1000	0
±1.45	0	±310/±290	±1200	0
±1.5	0	±350/±330	±1400	0
±1.5	0	±380/±365	±1600	0
±1.5	0	±410/±400	±1800	0
±1.5	0	±445/±435	±2000	0
±1.6	0	±570/±530	±2500	0
±1.6	0	±655/±620	±3000	0
±1.55	0	±670/±620	±3000	0

Table 4-3: Reference Values for Testing the Trajectory Tracking Performance of the Controller due a to Step Change in the Exit Chilled liquid Temperature of the Evaporator

$\Delta t_{cw,L\_REF}$ (°C)	$\Delta t_{ew,L\_REF}$ (°C)	$\Delta W_{com\_REF}$ (W)	$\Delta Q_{c\_REF}$ (W)	$\Delta t_{ew,E\_DIST}$ (°C)
±0.05	±0.5	±42/0	0	0
±0.1	±1	±22/±8	0	0
±0.15	±1.5	∓18/∓15	0	0
±0.2	±2	∓18/∓20	0	0
±0.2	±2.5	∓33/∓30	0	0

#### 4.1.2 Disturbance Rejection

The controller performance was also tested on its ability to reject measured input disturbance in the form of entering evaporator liquid temperature. This temperature varies based on the load. As the load decreases, the probability of having a lower entering temperature is higher. Thus, it is of utter importance to mitigate the “Low Delta-T” phenomena as it can cause operational issues to the chiller, and subsequently the cooling plant. Considering the same principles adopted earlier, the leaving condenser liquid temperature and the compressor’s electric power are varied by the operator, whilst the cooling capacity and the leaving evaporator liquid temperature are set to 0 °C. The simulation values are given in Table 4-4.

Table 4-4: Reference Values for Testing the Disturbance Rejection of the Controller due a to Step Change in the Entering Chilled liquid Temperature of the Evaporator

$\Delta t_{cw,L\_REF}$ (°C)	$\Delta t_{ew,L\_REF}$ (°C)	$\Delta W_{com\_REF}$ (W)	$\Delta Q_{c\_REF}$ (W)	$\Delta t_{ew,E\_DIST}$ (°C)
0	0	∓30/∓15	0	±0.5
±0.33/±0.1	0	∓35	0	±1
±0.43/±0.2	0	∓60	0	±1.5
±0.3/±0.2	0	∓100/∓93	0	±2
±0.3/±0.25	0	∓140/∓120	0	±2.5

## 4.2 PID Control of Liquid Chiller

Invented in the early 1900s – by Nicholas Minorsky - and first deployed in the industry for automatic steering of ships in 1922 [47], proportional-plus-integral-plus-derivative, or simply PID are the most used feedback control technique in the industry. Despite the emergence of many advanced control techniques, PID controllers are still dominates the market due to its simplicity and ease of use. The output of a PID controller (i.e. control input) in continuous-time is given by

$$u(t) = K_p + K_i \int e(t) dt + K_d \frac{de(t)}{dt} \quad (4-1)$$

where  $e(t)$  is the error signal (i.e. difference between the desired and actual output) and  $K_p$ ,  $K_i$ , and  $K_d$  are the scalar gain terms associated with proportional, integral and derivative controls, respectively.

The block diagram of a control system with one output, one input and a PID controller is depicted in Figure 4-1 [47]. Notice that the plant and controllers are represented as transfer function. Furthermore, the PID or three-mode controller has three parameters summed parameters, one for each mode. Thus, the transfer function at the summation point of the PID controller is given by

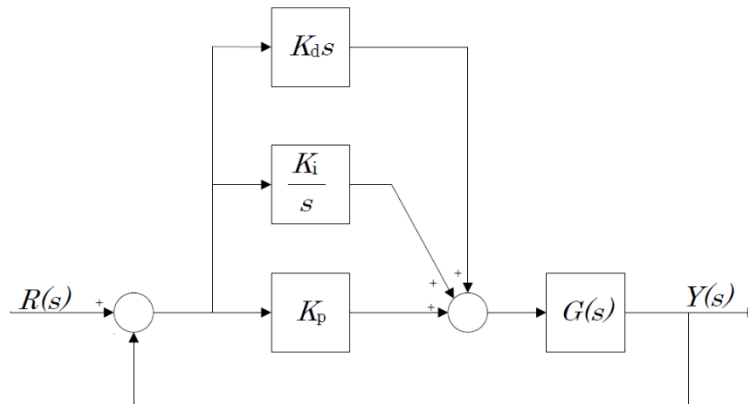


Figure 4-1: PID controller block diagram of a SISO system

$$G_c(s) = K_p + \frac{K_i}{s} + K_d s = \frac{K_p s + K_i + K_d s^2}{s} = \frac{K_d \left( s^2 + \frac{K_p}{K_d} s + \frac{K_i}{K_d} \right)}{s} \quad (4-2)$$

The controller parameters as shown in Equation 3-1 do not have to be all present. For instance, if the derivative term is set to zero, then it would just be a PI controller. Furthermore, each element in the PID controller has its own advantages and disadvantages. For example, the proportional term reduces the rise time and has a decent contribution to reduce steady-state error, but in return, it increases the overshoot and may not significantly affect the settling time. To overcome such challenges, the use of the integral term along with the proportional term would drastically improve the steady-state error, but overshoot may increase and decrease the settling time. Along with the PI terms, the addition of the derivative term reduces the overshoot and the settling time.

An array of PID controllers will be applied to the model developed in chapter 3 in a centralized manner. However, two pre-requisites need to be done to the model. First, the chiller model represented in continuous-time state-space needs to be converted to a transfer function representation. As the model includes 4 inputs and 4 outputs, the number of transfer functions would be 16. The second step is to extend the SISO feedback control system shown in Figure 4-1 to a MIMO system by adding PID controllers whose quantities are equivalent to the product of the number of inputs and outputs. Furthermore, the controllers would be divided into 4 zones, which is equivalent to the number of outputs. So, in each zone, 4 controllers would be there. Figure 4-2 shows the block diagram of PID control of the liquid chiller model.

The transfer functions and controllers shown in Figure 4-2 can be truncated by first obtaining the expression of the loop transfer functions as shown in Equation 4-3. The expression of the closed-loop system to compute the required input is as shown in Equation 4-4. Finally, plugging expression 4-4 in to 4-3 yields equation 4-5. Finally, expression 4-5 can be described by equation 4-6. The  $i$  and  $j$  terms in equation 4-6 correspond to the output and input, respectively.

$$\begin{bmatrix} Y_1 \\ Y_2 \\ Y_3 \\ Y_4 \end{bmatrix} = \begin{bmatrix} G_{11} & G_{12} & G_{13} & G_{14} \\ G_{21} & G_{22} & G_{23} & G_{24} \\ G_{31} & G_{32} & G_{33} & G_{34} \\ G_{41} & G_{42} & G_{43} & G_{44} \end{bmatrix} \begin{bmatrix} U_1 \\ U_2 \\ U_3 \\ U_4 \end{bmatrix} \quad (4-3)$$

$$\begin{bmatrix} U_1 \\ U_2 \\ U_3 \\ U_4 \end{bmatrix} = \begin{bmatrix} G_{C11} & G_{C12} & G_{C13} & G_{C14} \\ G_{C21} & G_{C22} & G_{C23} & G_{C24} \\ G_{C31} & G_{C32} & G_{C33} & G_{C34} \\ G_{C41} & G_{C42} & G_{C43} & G_{C44} \end{bmatrix} \begin{bmatrix} R_1 - Y_1 \\ R_2 - Y_2 \\ R_3 - Y_3 \\ R_4 - Y_4 \end{bmatrix} \quad (4-4)$$

$$\begin{bmatrix} Y_1 \\ Y_2 \\ Y_3 \\ Y_4 \end{bmatrix} = \begin{bmatrix} G_{11} & G_{12} & G_{13} & G_{14} \\ G_{21} & G_{22} & G_{23} & G_{24} \\ G_{31} & G_{32} & G_{33} & G_{34} \\ G_{41} & G_{42} & G_{43} & G_{44} \end{bmatrix} \begin{bmatrix} G_{C11} & G_{C12} & G_{C13} & G_{C14} \\ G_{C21} & G_{C22} & G_{C23} & G_{C24} \\ G_{C31} & G_{C32} & G_{C33} & G_{C34} \\ G_{C41} & G_{C42} & G_{C43} & G_{C44} \end{bmatrix} \begin{bmatrix} R_1 - Y_1 \\ R_2 - Y_2 \\ R_3 - Y_3 \\ R_4 - Y_4 \end{bmatrix} \quad (4-5)$$

$$Y = G_{ij} G_{Cij} (R - Y) = G_{ij} U \quad (4-6)$$

where  $i$  and  $j$  are the indices of the input and output, respectively.

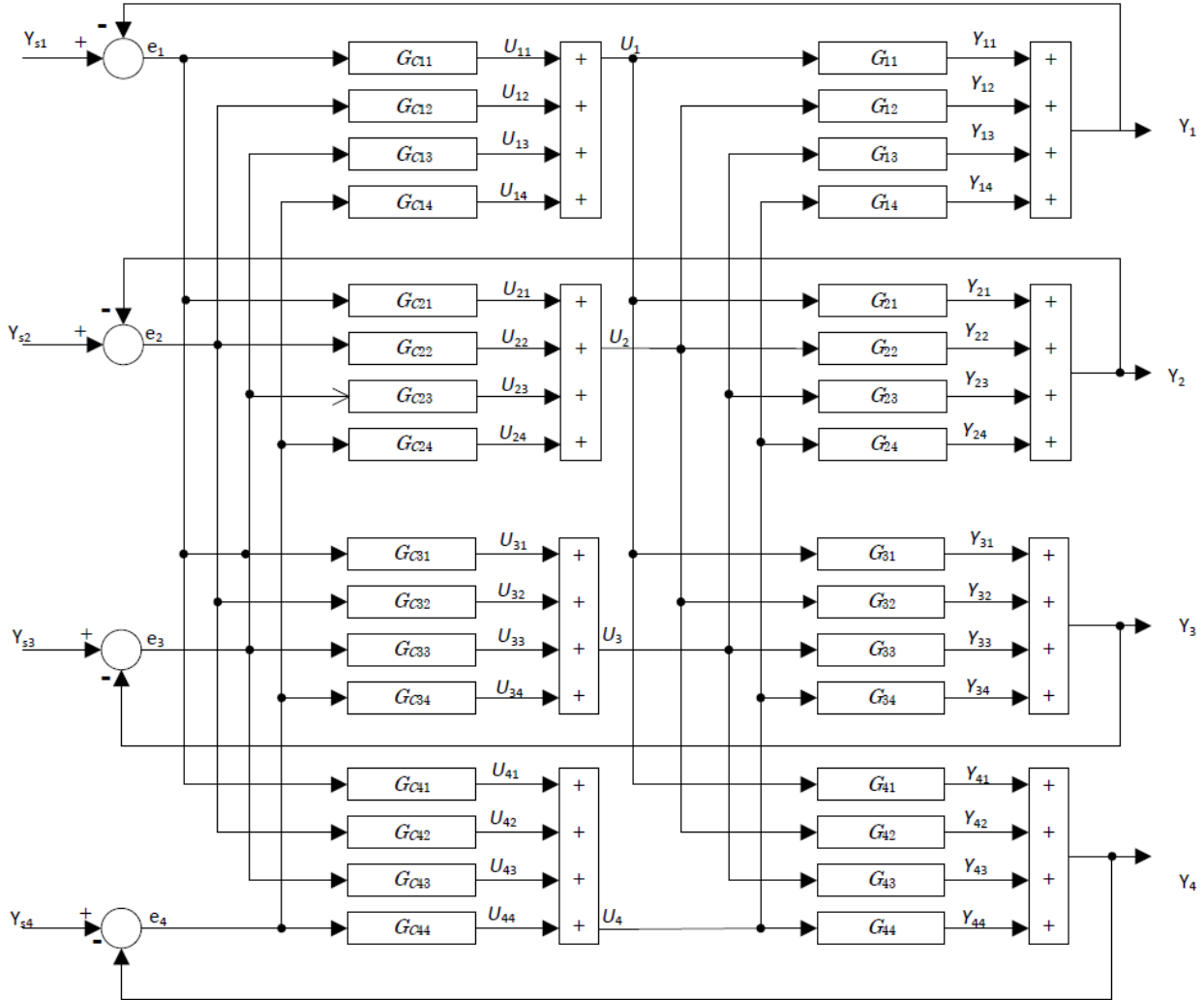


Figure 4-2: Decentralized PID control for a model with 4 inputs and 4 outputs

### 4.3 Implementation and Simulation Results of the PID Controller

The PID controllers are shown in Figure 4-2 and Equation 4-5 have been modeled using Simulink as shown in Figure 4-3. Two methods were tested to tune the PID controllers fitted in a MIMO environment. The first method, which was motivated by [48], the controllers were divided in to two types, diagonal and off-diagonal controllers. The relative gain array (RGA) was used to establish the dependence of one input with one output. Then the diagonal controllers would be tuned normally considering that output with one input. Then using algebraic closed-loop solution, the off-diagonal controllers gains were computed such as to eliminate the interference between other inputs and other outputs. In other words, the system is to be decoupled and the output input relationship is only determined by the diagonal controllers. The method proposed by [48] was implemented on a two-input-two-output (TITO) process. Extending the same to the four-input-four-output model did not prove to be successful, since the RGA on the chiller model yielded heavy interference between the variables.

The first method was not successful due to the heavy interactions between the system's inputs and outputs. Hence, we could not decouple the system and assign one input to just one output. Another method was adopted, which is motivated from the open-loop system results and the centralized configuration of the PID control closed-loop. As per Equations 4-4 and 4-5, each controller is labelled based on the output and input. Thus, in the tuning process of each controller, the system is assumed to be decoupled. Once all 16 PID controllers were tuned, they were all oriented in a centralized manner as per Figure 4-2. In Simulink, the system was modeled as illustrated in Figure 4-3. Note that some of these controllers had zero gains such as the input did not affect the output. For instance, varying the evaporator's flow had no effect on the outlet temperature of the condenser coolant.

Saturation blocks and anti-windup technique was used to ensure that the input does not exceed the allowable input limits as specified in Table 4-4. The simulation was done for 100 seconds and considering a fixed step time of 0.0001. The step time was chosen to be very low due to the simulation errors encountered when using higher step times as there were discontinuities in the system.

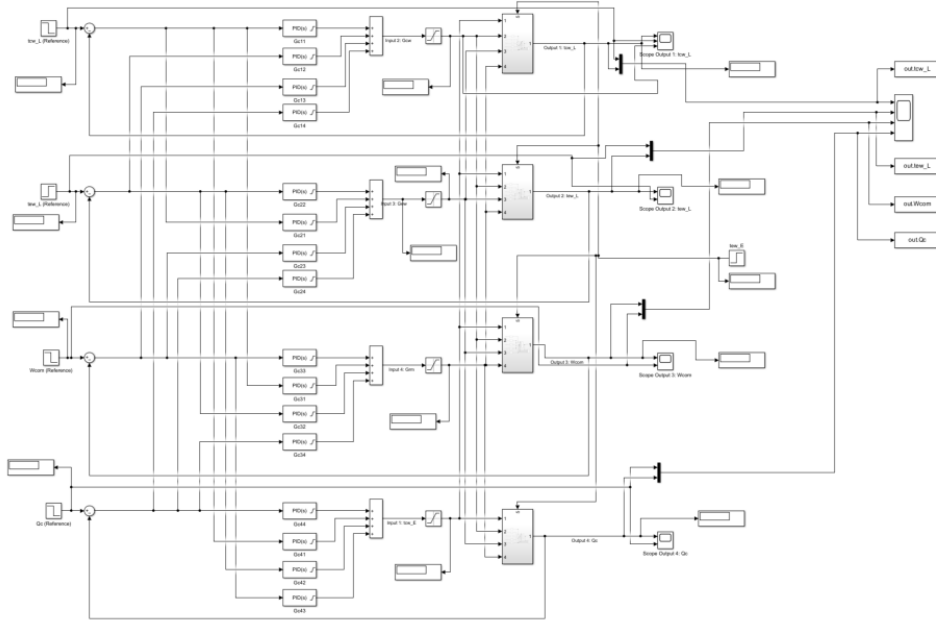


Figure 4-3: Decentralized PID control implementation on Simulink

After an exhaustive analysis and simulations of all controllers combined. It was found that some controllers have no effect on the system's output. On the contrary, the system become unstable when all controllers are present. Hence, the nondominant controllers were removed; and the Simulink closed-loop model as illustrated in Figure4-2 reduces to the block diagram shown in Figure 4-4. Finally, the general form as shown in Equations 4-3 to 4-5 are now represented in terms of actual chiller input variables, output variables and the remaining controllers are as given in Equations 4-6 through 4-8. Note that the same set of controllers will be used for both trajectory tracking and disturbance rejection.

$$\begin{bmatrix} t_{cw,L} \\ t_{ew,L} \\ W_{com} \\ Q_c \end{bmatrix} = \begin{bmatrix} G_{11} & G_{12} & G_{13} & G_{14} \\ G_{21} & G_{22} & G_{23} & G_{24} \\ G_{31} & G_{32} & G_{33} & G_{34} \\ G_{41} & G_{42} & G_{43} & G_{44} \end{bmatrix} \begin{bmatrix} G_{cw} \\ G_{ew} \\ G_{rm} \\ t_{cw,E} \end{bmatrix} \quad (4-6)$$

$$\begin{bmatrix} G_{cw} \\ G_{ew} \\ G_{rm} \\ t_{cw,E} \end{bmatrix} = \begin{bmatrix} G_{C11} & 0 & 0 & 0 \\ 0 & G_{C22} & 0 & G_{C24} \\ G_{C31} & G_{C32} & G_{C33} & G_{C34} \\ G_{C41} & 0 & 0 & G_{C44} \end{bmatrix} \begin{bmatrix} t_{cw,L,REF} - t_{cw,L} \\ t_{ew,L,REF} - t_{ew,L} \\ W_{com,REF} - W_{com} \\ Q_{c,REF} - Q_c \end{bmatrix} \quad (4-7)$$

$$\begin{bmatrix} t_{cw,L} \\ t_{ew,L} \\ W_{com} \\ Q_c \end{bmatrix} = \begin{bmatrix} G_{11} & G_{12} & G_{13} & G_{14} \\ G_{21} & G_{22} & G_{23} & G_{24} \\ G_{31} & G_{32} & G_{33} & G_{34} \\ G_{41} & G_{42} & G_{43} & G_{44} \end{bmatrix} \begin{bmatrix} G_{C11} & 0 & 0 & 0 \\ 0 & G_{C22} & 0 & 0 \\ G_{C31} & G_{C32} & G_{C33} & G_{C34} \\ G_{C41} & 0 & 0 & G_{C44} \end{bmatrix} \begin{bmatrix} t_{cw,L,REF} - t_{cw,L} \\ t_{ew,L,REF} - t_{ew,L} \\ W_{com,REF} - W_{com} \\ Q_{c,REF} - Q_c \end{bmatrix} \quad (4-8)$$

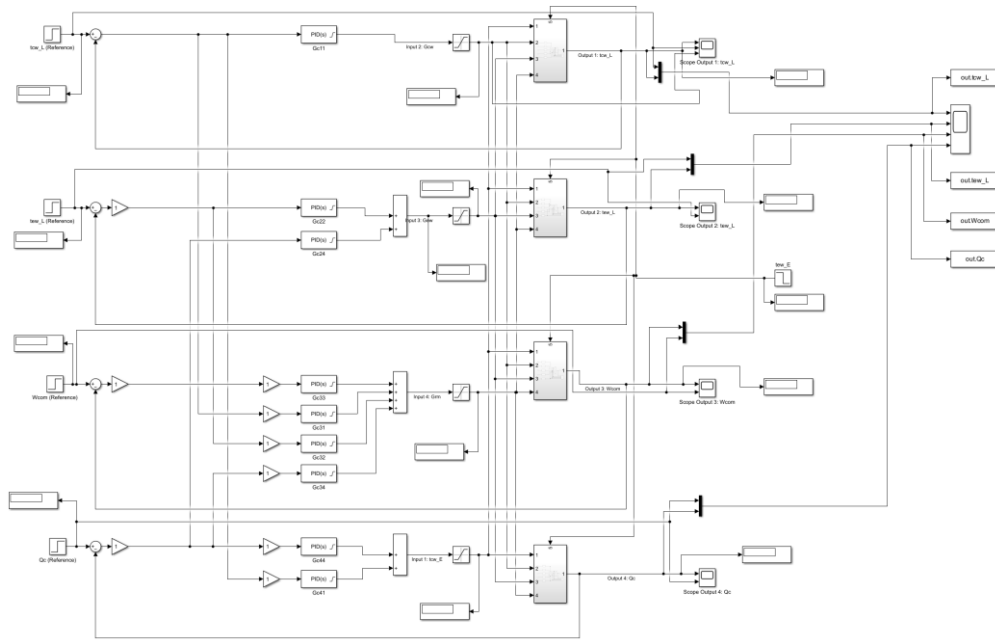


Figure 4-4: Decentralized Closed-loop System with only Dominant Controllers

### 4.3.1 Trajectory Tracking – Cooling Load

The first trajectory tracking test was done when the chiller was subjected to a change in the cooling load. The step change in the cooling load values is as reflected in Table 4-2. Furthermore, the required reference signals for the exit coolant temperature of the condenser and the chiller's output electric power have been changed to meet the change in the cooling load, whereas the reference exit chilled liquid temperature of evaporator remained at zero. In other words, the PID controllers need to reach the required cooling load whilst maintaining the exit chilled liquid temperature at zero (i.e. regulation).

The output response of the closed-loop system using PID controllers due to a step change on the cooling load by 600 W, 1200 W and 3000 W are shown on Figures 4-5, 4-6 and 4-7, respectively. Similarly, the applied control inputs to achieve the desired set points whilst regulating are illustrated in Figures 4-8, 4-9 and 4-10. It can be noted that the PID controllers reach the desired setpoint in less than 50 seconds and with a low overshoot on the evaporator exit temperature and compressor's work. However, the overshoot on the cooling load is very high. Furthermore, there are some oscillations in the system, especially on the input.

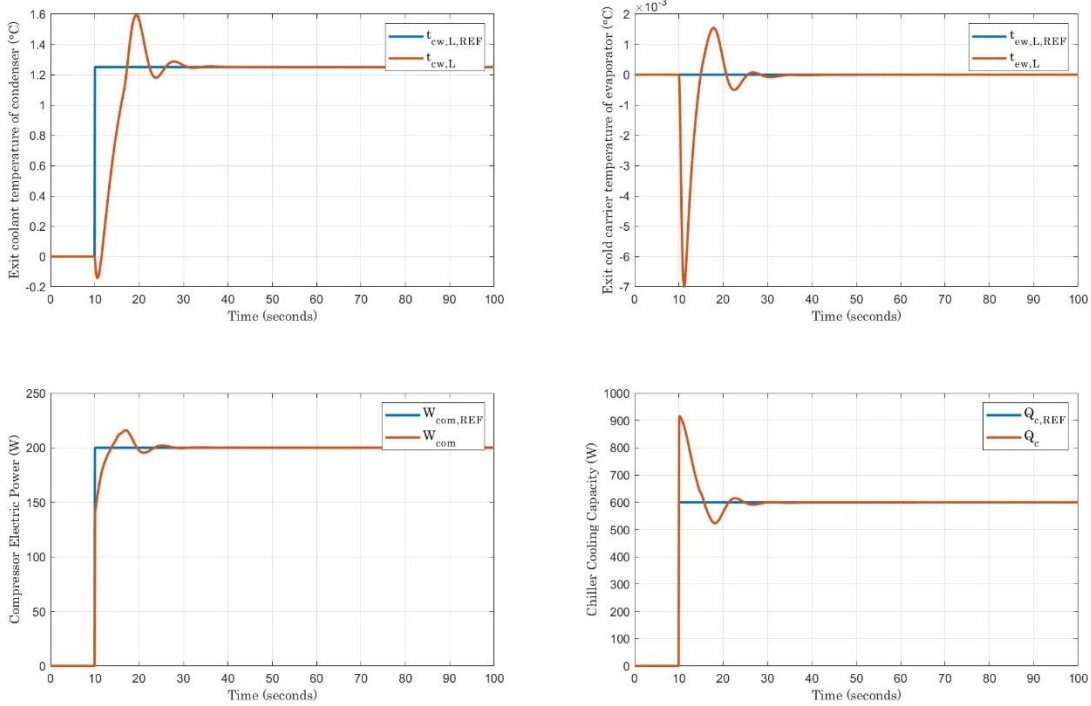


Figure 4-5: Output responses due to a step change in cooling load by 600 W

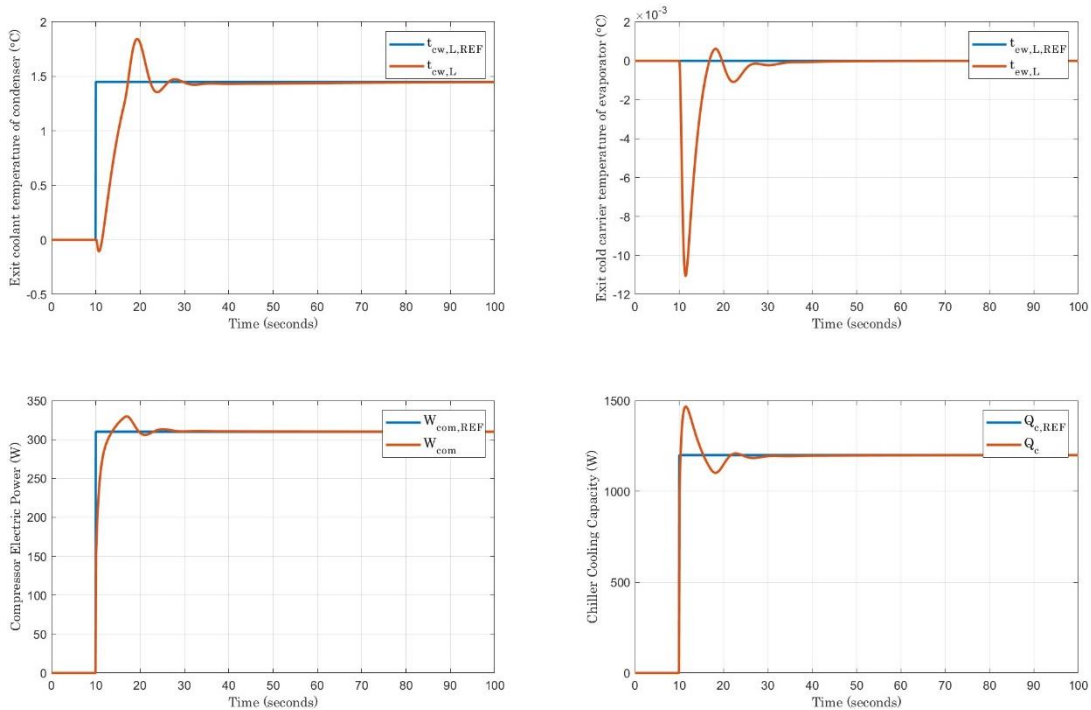


Figure 4-6: Output responses due to a step change in cooling load by 1200 W

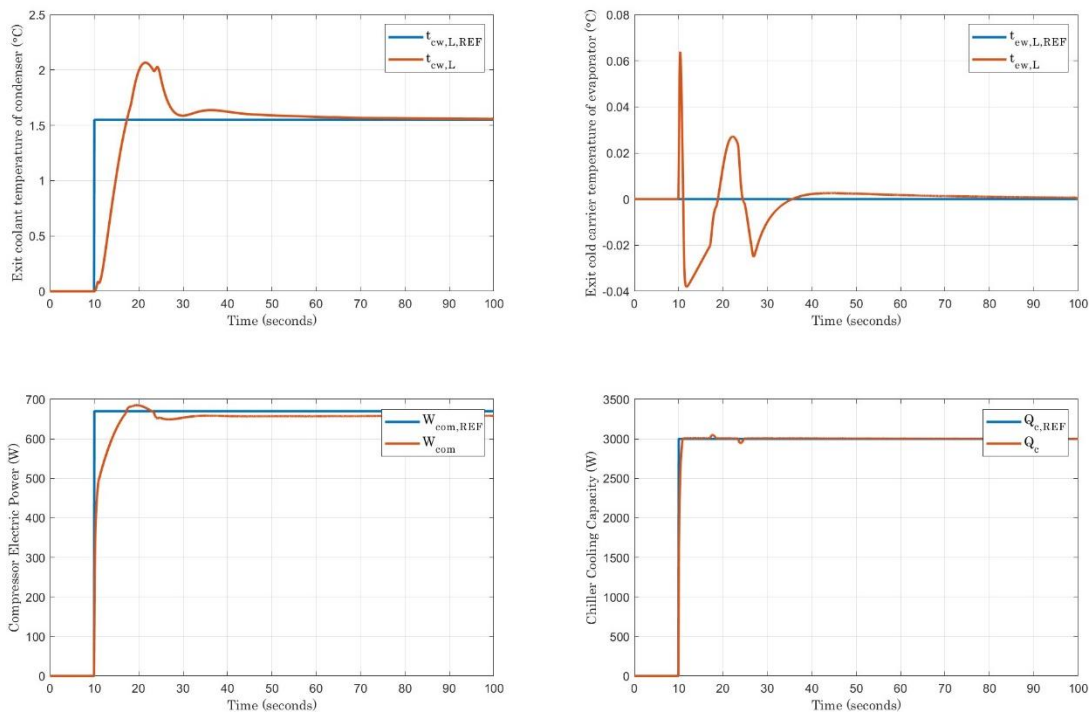


Figure 4-7: Output responses due to a step change in cooling load by 3000 W

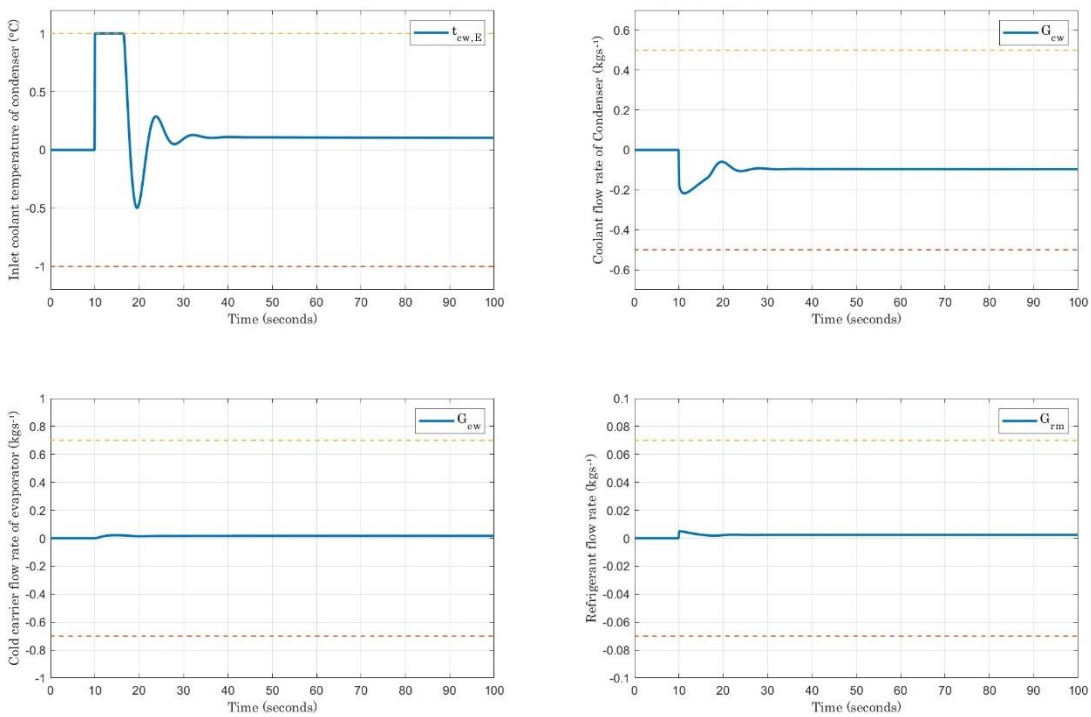


Figure 4-8: Applied control inputs signals due to a step change in cooling load by 600 W

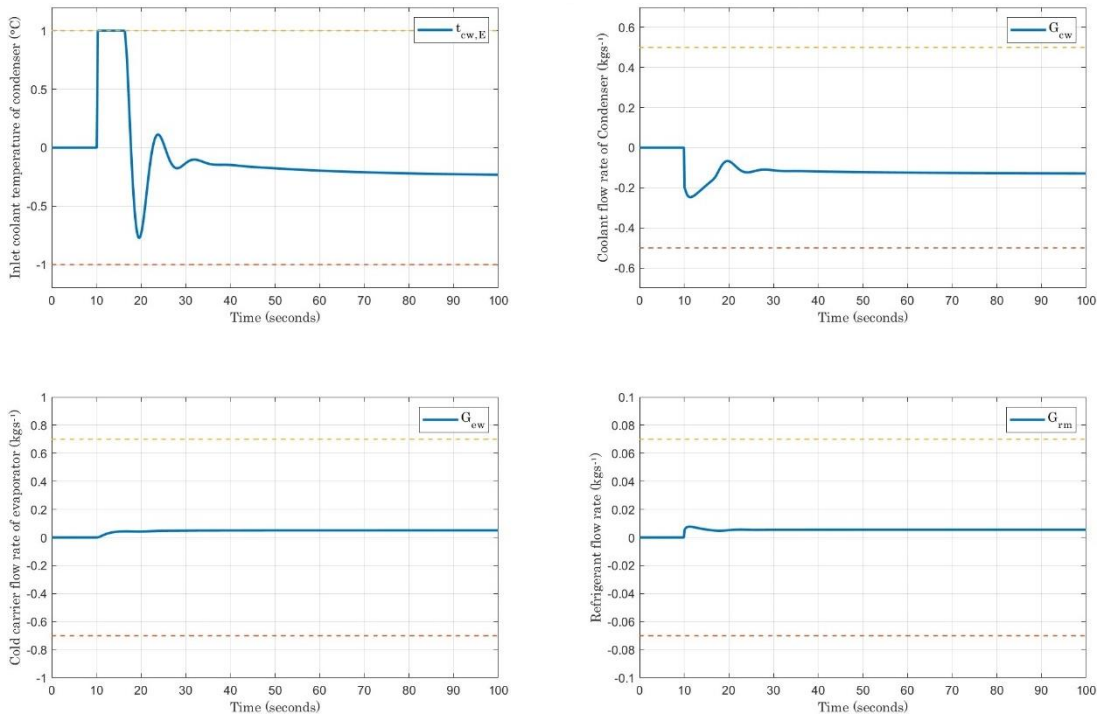


Figure 4-9: Applied control inputs signals due to a step change in cooling load by 1200 W

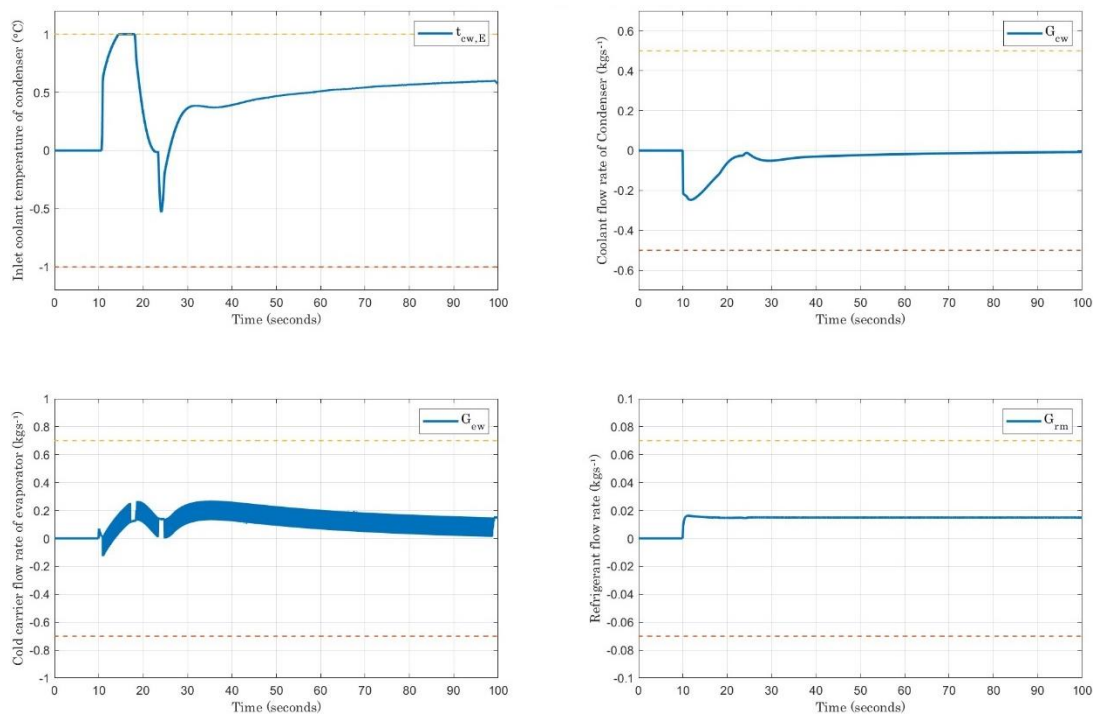


Figure 4-10: Applied control inputs signals due to a step change in cooling Load by 3000 W

### 4.3.2 Trajectory Tracking – Leaving Chilled liquid Temperature

The same procedures applied earlier in Section 4.2.2. as applied this time to the leaving chilled liquid of the evaporator by changing its setpoint whilst maintaining the cooling load at its initial state. The output response of the closed-loop system due to a step change in the leaving chilled liquid temperature of evaporator by 1 °C and 2 °C are depicted in Figures 4-11 and 4-12, respectively. The control inputs are presented in Figures 4-13 and 4-14. High overshoot is noticed in the cooling capacity and oscillatory behavior in the compressor power. Furthermore, the exit chilled liquid temperature of the evaporator exhibited oscillatory behavior for a few cycles before eventually converging to the desired value.

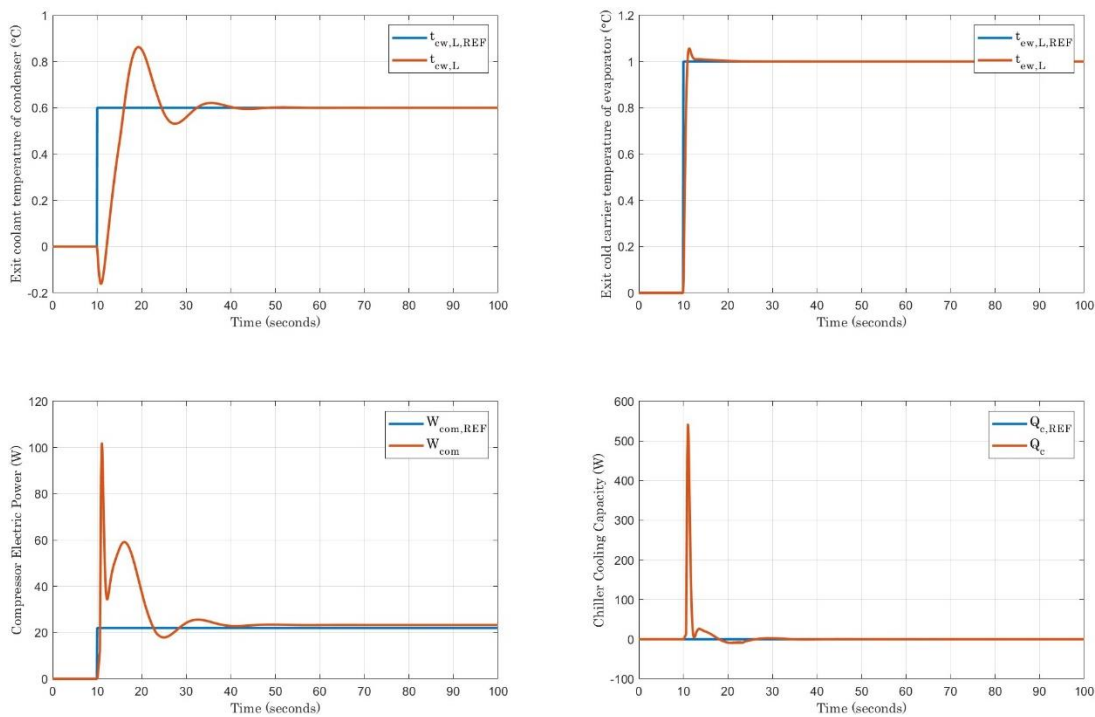


Figure 4-11: Output responses due to a step change in exit chilled liquid temperature of the evaporator by 1 °C

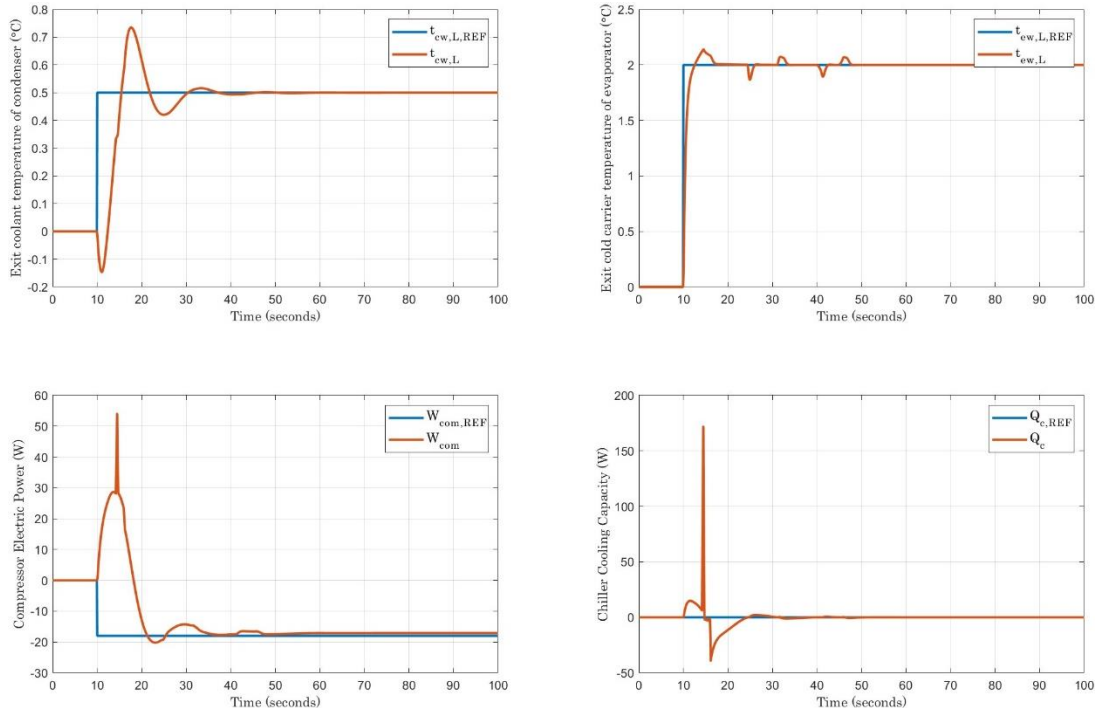


Figure 4-12: Output responses due to a step change in exit chilled liquid temperature of the evaporator by 2 °C

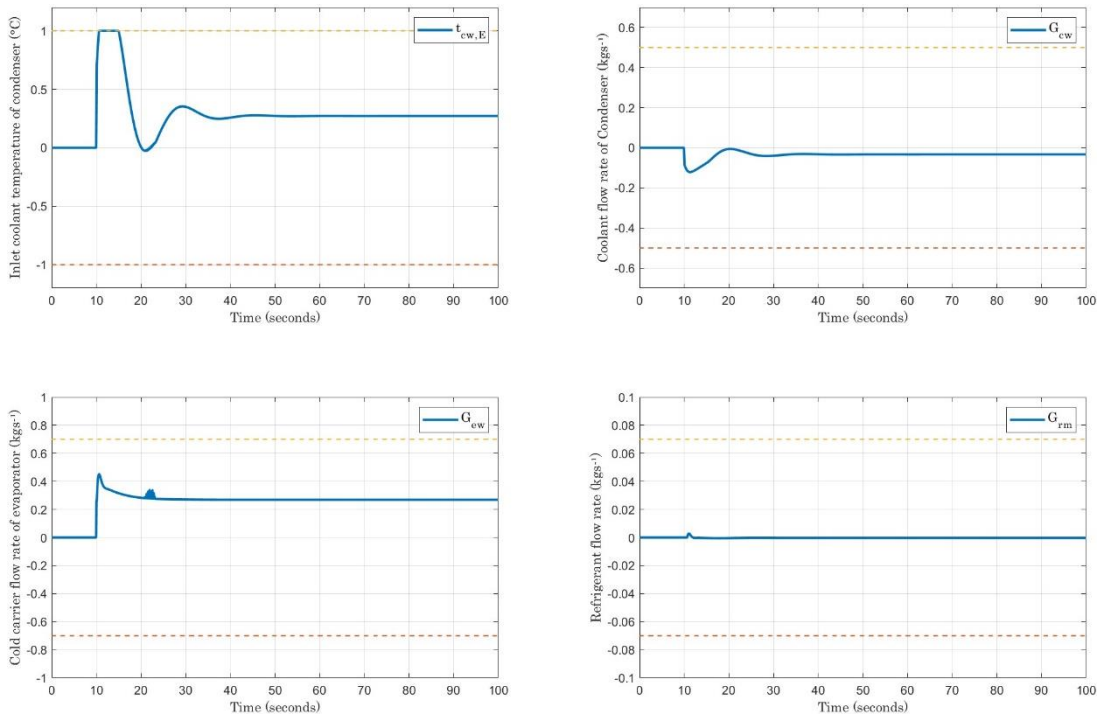


Figure 4-13: Control signals due to a step change in exit chilled liquid temperature of the evaporator by 1 °C

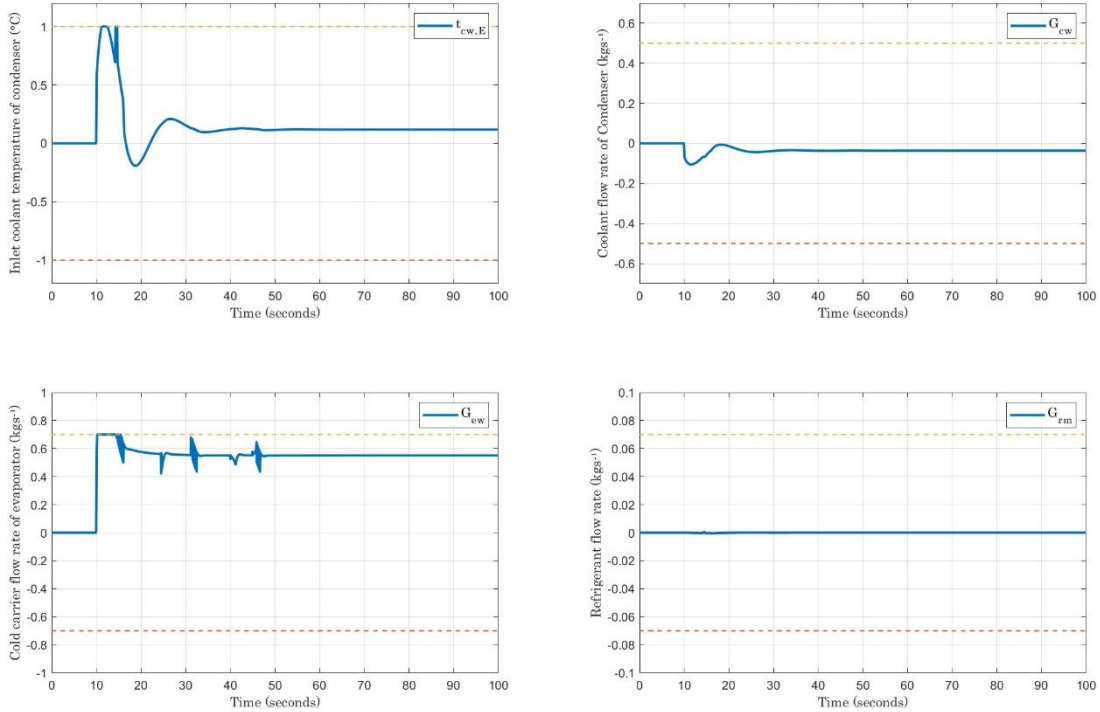


Figure 4-14: Control signals due to a step change in exit chilled liquid temperature of the evaporator by 2 °C

### 4.3.3 Disturbance Rejection – Entering Chilled liquid Temperature

The disturbance rejection performance was accomplished in a similar fashion as the trajectory tracking. In this test, the chiller model was subjected to a change in the entering chilled liquid of evaporator temperature, and the controller’s main goal is to keep the cooling load and the leaving evaporating temperature unchanged (i.e. zero). for the selected disturbance values as shown in Table 4-4 are presented in this section. The output response of the closed-loop system due to a step change in the entering chilled liquid temperature of evaporator by 0.5 °C and 2.5 °C are depicted in Figures 4-15 and 4-16, respectively. The applied control inputs to regulate the system is for the same conditions are as illustrated in Figures 4-17 and 4-18, respectively. Despite reaching steady state, the output contained high overshoot and severe oscillations.

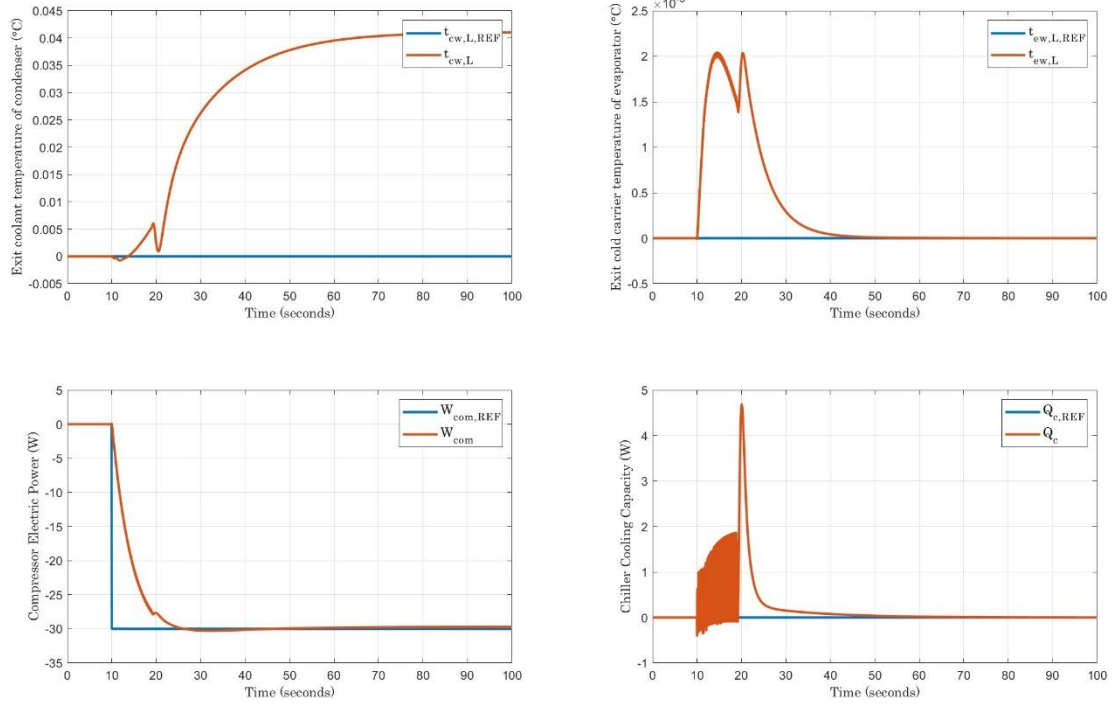


Figure 4-15: Output responses due a step change in inlet chilled liquid temperature of evaporator by 0.5 °C

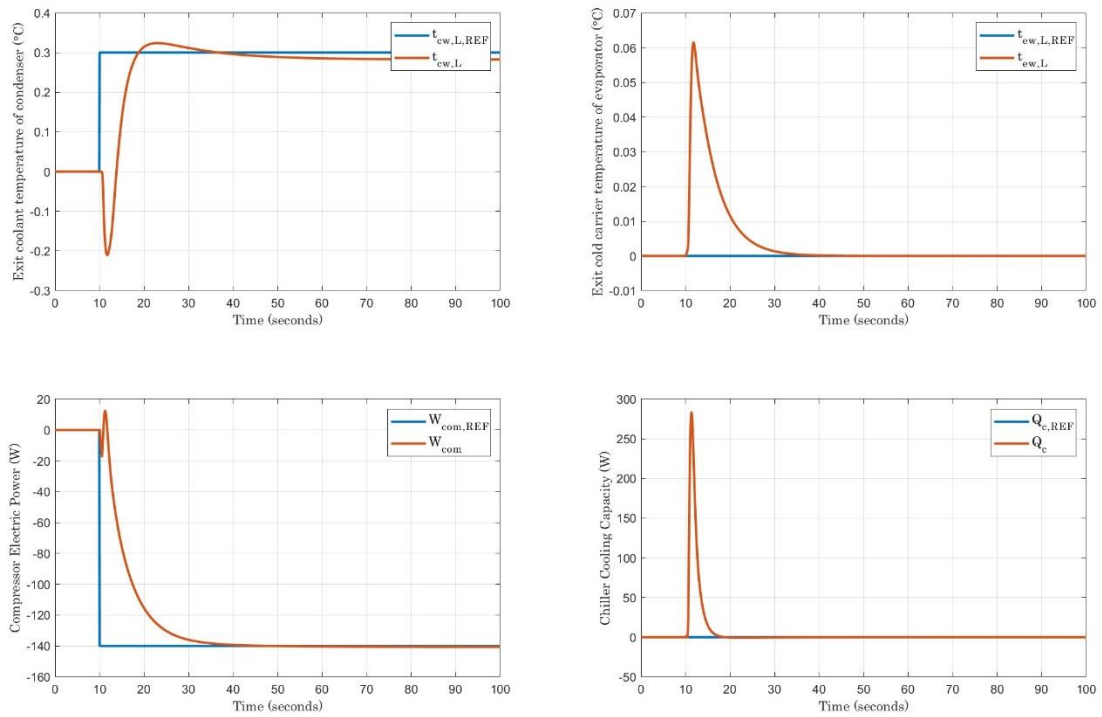


Figure 4-16: Output responses due a step change in inlet chilled liquid temperature of evaporator by 2.5 °C

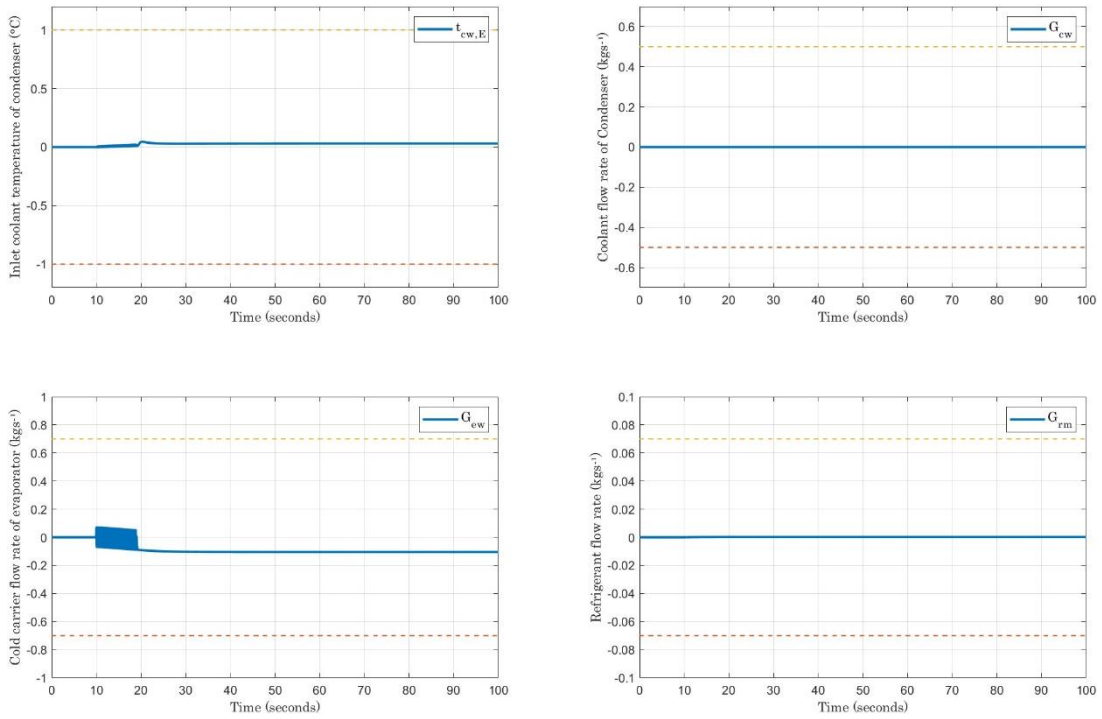


Figure 4-17: Control signals due to a step change in inlet chilled liquid temperature of evaporator by  $0.5^{\circ}\text{C}$

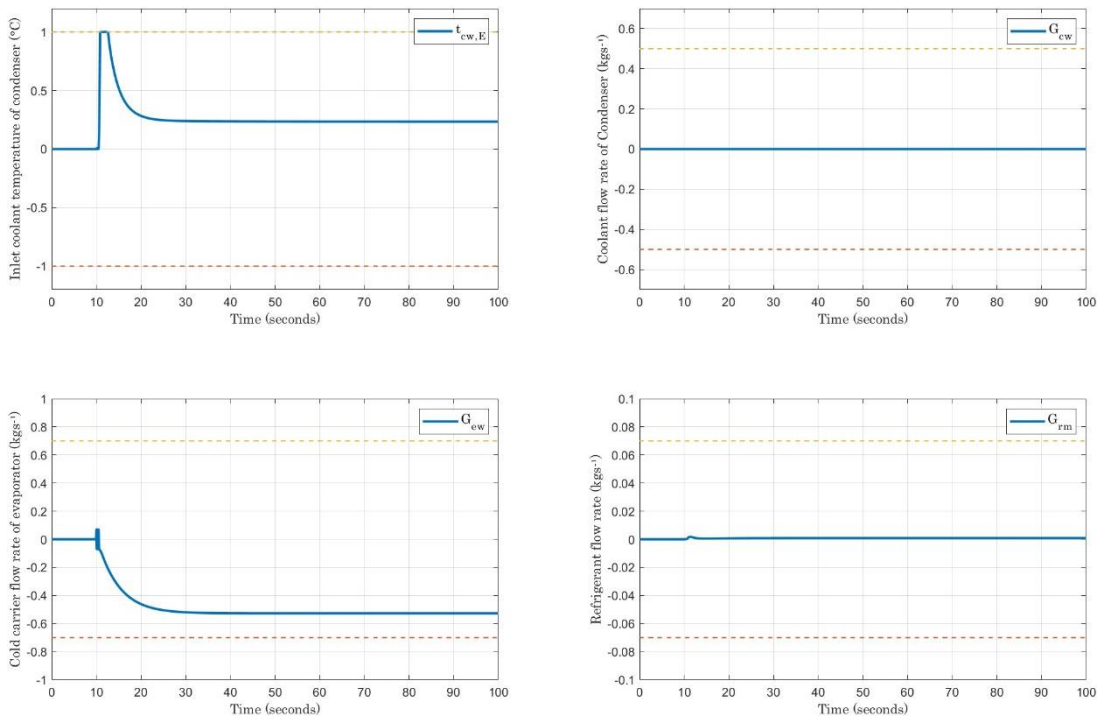


Figure 4-18: Control signals due to a step change in inlet chilled liquid temperature of evaporator by  $2.5^{\circ}\text{C}$

## Chapter 5 Linear Quadratic Integral Control of Liquid Chiller

This chapter applies a multivariable optimal control technique to the liquid chiller, namely, Linear Quadratic Integral Control (LQI). The chapter begins with the formulation of the control problem as a continuous time linear time invariant (LTI) system. Then, the LQI control will be applied on the system in discrete time rather than continuous time since it would be more practical. The closed-loop responses are presented at the end of this chapter for both trajectory tracking and disturbance rejection.

### 5.1 The Solution to the Linear Quadratic Regulator

The Linear Quadratic Integral Control (LQI) is an extension of the Linear Quadratic Regulator (LQR). Both of which are multivariable optimal control techniques that can be applied to continuous and discrete time systems, and they share the same structure of state feedback controllers. The formulation of the LQR will be introduced first, then the extension to LQI controller will be carried out.

A linear quadratic controller is a multivariable controller that computes the optimal control signal by minimizing a cost function [49]. Given an infinite-time continuous-time LTI state-space system (Equation 5-1), the cost function,  $J$ , of a general optimal control system to regulate the plant's states is given by Equation 5-2 as [49]

$$\dot{x}(t) = Ax(t) + Bu(t) \quad (5-1)$$

$$J = \frac{1}{2} \int_0^{\infty} [x^T(t)Qx(t) + u^T(t)Ru(t)] dt \quad (5-2)$$

where,  $x(t)$  is an  $n^{\text{th}}$  order state vector;  $u(t)$  is an  $r^{\text{th}}$  order control vector;  $A$  and  $B$  are the state and control matrices of orders  $n \times n$  and  $r \times n$ ;  $Q$  is a weighting matrix with an order  $n \times n$ , symmetric, positive semidefinite matrix;  $R$  is weighting matrix with an order of  $r \times r$ , symmetric positive definite matrix.

The optimal control signal,  $u^*(t)$ , solution to the problem in Equation 5-2 is given by

$$u^*(t) = -R^{-1}B^T\bar{P}x^*(t) \quad (5-3)$$

where,  $\bar{P}$ , is a  $n \times n$  positive definite and symmetric costate matrix, is the solution of the nonlinear, matrix algebraic Riccati equation (ARE) given by

$$\bar{P}A + A^T\bar{P} - \bar{P}BR^{-1}B^T\bar{P} + Q = 0 \quad (5-4)$$

and the closed-loop controller gain matrix,  $K$ , is then given by

$$K = R^{-1}B^T\bar{P} \quad (5-5)$$

The block diagram representation of an LQR controller is depicted in Figure 5-1 [49].

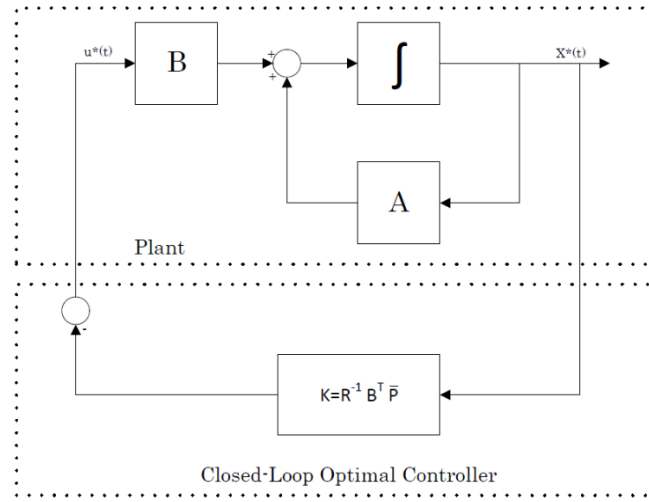


Figure 5-1: Block diagram representation of an LQR controller [49]

## 5.2 Linear Quadratic Integral Problem Formulation

The state regulation controller as explained in Section 5-1 can be extended for tracking the output of a state-space LTI model given by Equation 5-6. The disturbance term,  $w$ , will be neglected during the formulation process. To reduce or even eliminate the steady-state errors to zero, an integrator is added to the system. Hence, the controller is called a Linear Quadratic Integral (LQI) controller. Furthermore, by adding an integrator to the closed-loop system, the order of the system will be increased. Thus, the closed-loop system state matrix,  $A_{CL}$ , will have an order of the sum of the number of states and the number of outputs. In the liquid chiller case, the closed-loop state matrix has an order of  $10 \times 10$ . The block diagram representation of an LQI controller is shown in Figure 5-2.

$$\begin{cases} \dot{x}(t) = Ax(t) + Bu(t) + Fw(t) \\ y(t) = Cx(t) + Du(t) \end{cases} \quad (5-6)$$

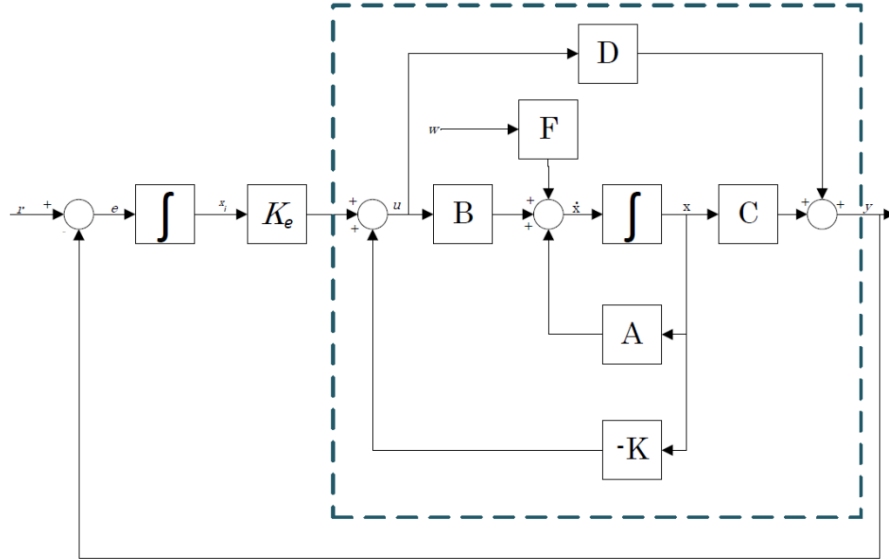


Figure 5-2: Block diagram representation of an LQI controller

The error signal is given by

$$e(t)=r(t)-y(t) \quad (5-7)$$

where  $r(t)$  is the reference signal and  $y(t)$  is the actual output.

The integral of the error signal, represented by  $x_i$  is given by

$$x_i(t)=\int [(r(t)-y(t))]dt \quad (5-8)$$

The state and output equations from Figure 5-2 are given by

$$\dot{x}(t)=Ax(t)+Bu(t) \quad (5-9)$$

$$\dot{x}_i(t)=e(t)=r(t)-y(t) \quad (5-10)$$

$$y(t)=Cx(t)+Du(t) \quad (5-11)$$

The control signal which is the summation of the nominal states (state feedback) and the integral states (integral of the error signal) are given by [47][50]

$$u(t)=K_i x_i - Kx(t) \quad (5-12)$$

where  $K_i$  are the controller gains of the integral states and  $K$  are the feedback gains of the open-loop states. Note that the feedback gain matrix,  $K$ , represent 'proportional and derivative' gains [50].

The state-space representation of the closed-loop system with an LQI controller is

$$\dot{z}(t) = \begin{bmatrix} \dot{x}(t) \\ \dot{x}_i(t) \end{bmatrix} = \begin{bmatrix} A & 0 \\ -C & 0 \end{bmatrix} \begin{bmatrix} x(t) \\ x_i(t) \end{bmatrix} + \begin{bmatrix} B \\ -D \end{bmatrix} u(t) + \begin{bmatrix} 0_{n \times n} \\ I_{n \times n} \end{bmatrix} r(t) \quad (5-13)$$

$$y = [C \quad 0] \begin{bmatrix} x(t) \\ x_i(t) \end{bmatrix} + Du(t) \quad (5-14)$$

where  $0_{n \times n}$  and  $I_{n \times n}$  are the zero and identity matrices of suitable size.

Substituting Equation 5-12 into Equations 5-13 and 5-14 to get

$$\dot{z}(t) = \begin{bmatrix} \dot{x}(t) \\ \dot{x}_i(t) \end{bmatrix} = \begin{bmatrix} A-BK & BK_i \\ -C+DK & -DK_i \end{bmatrix} \begin{bmatrix} x(t) \\ x_i(t) \end{bmatrix} + \begin{bmatrix} 0_{n \times n} \\ I_{n \times n} \end{bmatrix} r(t) \quad (5-15)$$

$$y = [C-DK \quad DK_i] \begin{bmatrix} x(t) \\ x_i(t) \end{bmatrix} \quad (5-16)$$

The cost function of the closed-loop LQI controller is given then by

$$J = \int_0^{\infty} [z^T(t)Qz(t) + u^T(t)Ru(t)] dt \quad (5-17)$$

The solution to obtain the optimal signal,  $u^*(t)$ , is obtained by solving Equation 5-17 using the algebraic Riccati equation (ARE) in a similar manner as described in Section 5.1.

### 5.3 Implementation and Simulation Results of the LQI Controller

To obtain a more realistic controller, the LQI has been implemented in discrete time. The sampling time considered is 0.1 seconds. The controller's gains were computed using MATLAB built-in function, LQI, and the simulations were done on Simulink for all the listed simulations in Tables 4-2, 4-3 and 4-4. The block diagram representation of the closed-loop system is depicted in Figure 5-2. The detailed block diagram of the chiller model sub-block is as shown in Figure 5-3.

As the chiller model has 4 inputs, 4 outputs and 6 states, the weighting input matrix,  $R$ , has an order of  $4 \times 4$ . On the other hand, the size of output weighting matrix,  $Q$ , is  $10 \times 10$ . The weights of the  $Q$  and  $R$  matrices are shown in Table 5-1. As the value of the weighing element in matrix  $R$  increases, it will be more expensive to apply this control input. Thus, the controller will be more conservative on this input, and it will prioritize inputs with lower cost. Similarly, a higher value of an element in matrix  $Q$  indicates a higher penalty on this state or output. Thus, the controller will exert more or effort in reducing the errors on this state or output.

In total, the closed-loop chiller model had 40 gains arranged as 4x10 matrix. The number of rows is equivalent to the number of inputs, whereas the number of columns is the summation of the number of states and number of outputs.

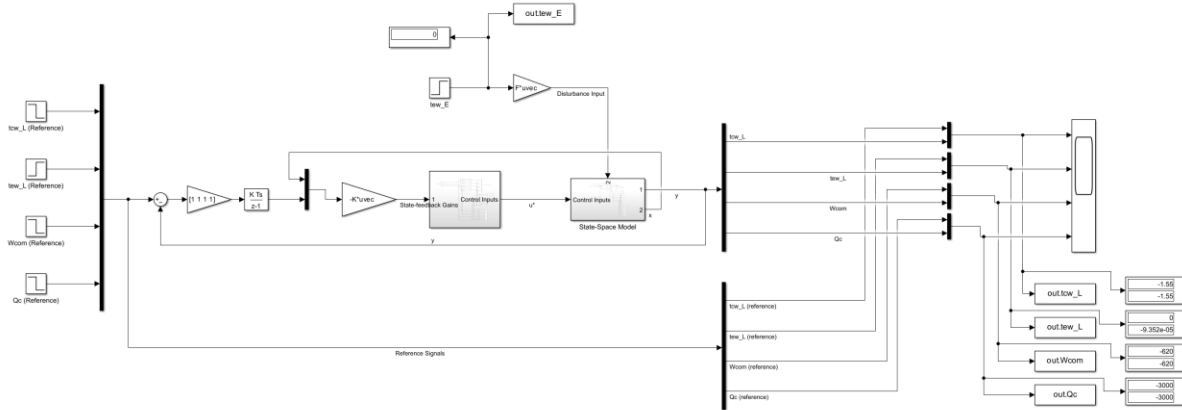


Figure 5-3: Simulink implementation of the LQI controller on the chiller model

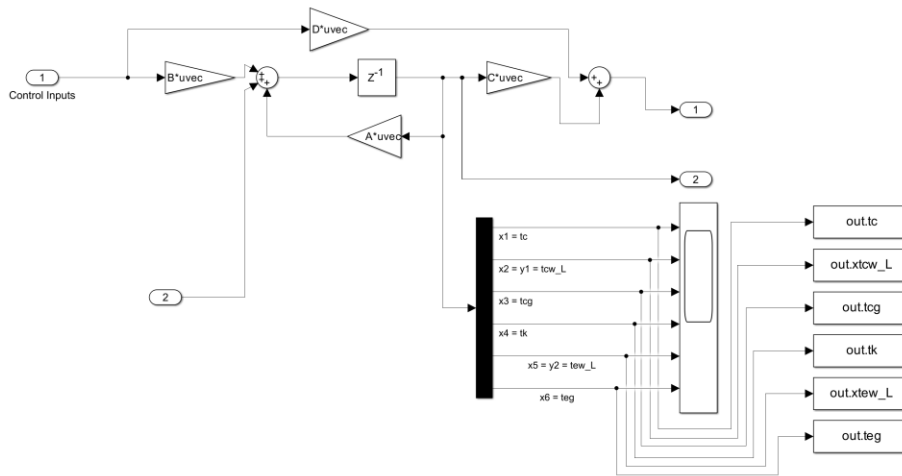


Figure 5-4: Implementation of the open-loop chiller model subblock in discrete time

The same simulation tests were also applied to the chiller model controlled by an LQI controller. Unlike the PID controller, the LQI controller was able to adjust the variable reference setpoints, namely, the condenser entering temperature and the compressor's power. Thus, reducing the overall power consumption and reducing the cost. The output and input signal responses for the tracking and disturbance cases are subsequently presented in the next subsections.

Table 5-1: Weights of Q and R Matrices of the LQI controller

<u>Weights</u>	<u>Value</u>	<u>Affected Variable</u>
q1	10	State $t_c$
q2	1	State $t_{cw,L}$
q3	10	State $t_{cg}$
q4	0.1	State $t_k$
q5	1	State $t_{ew,L}$
q6	10	State $t_{eg}$
q7	10	Time error of output $t_{cw,L}$
q8	5	Time error of output $t_{ew,L}$
q9	0.001	Time error of output $W_{com}$
q10	1	Time error of ouput $Q_c$
r1	100	Input $t_{cw,E}$
r2	1,000	Input $G_{cw}$
r3	1,000	Input $G_{ew}$
r4	1,000	Input $G_{rm}$

### 5.3.1 Trajectory Tracking – Cooling Load

The output responses of the using an LQI controller due to a step change on the cooling load by 600 W, 1200 W and 3000 W are shown on Figures 5-5, 5-6 and 5-7, respectively. Similarly, the applied control inputs to achieve the desired set points whilst regulating are illustrated in Figures 5-8, 5-9 and 5-10.

It is observed that the overshoot on the cooling load is zero; and the overshoot and oscillations on other outputs are kept at minimum, which proves the controller efficiency. Furthermore, all the control input signals are smooth and free of sharp or very rapid changes. The integral action ensured that the steady state errors are minimized, if not eliminated. Also, the settling time for all outputs was less than 80 seconds.

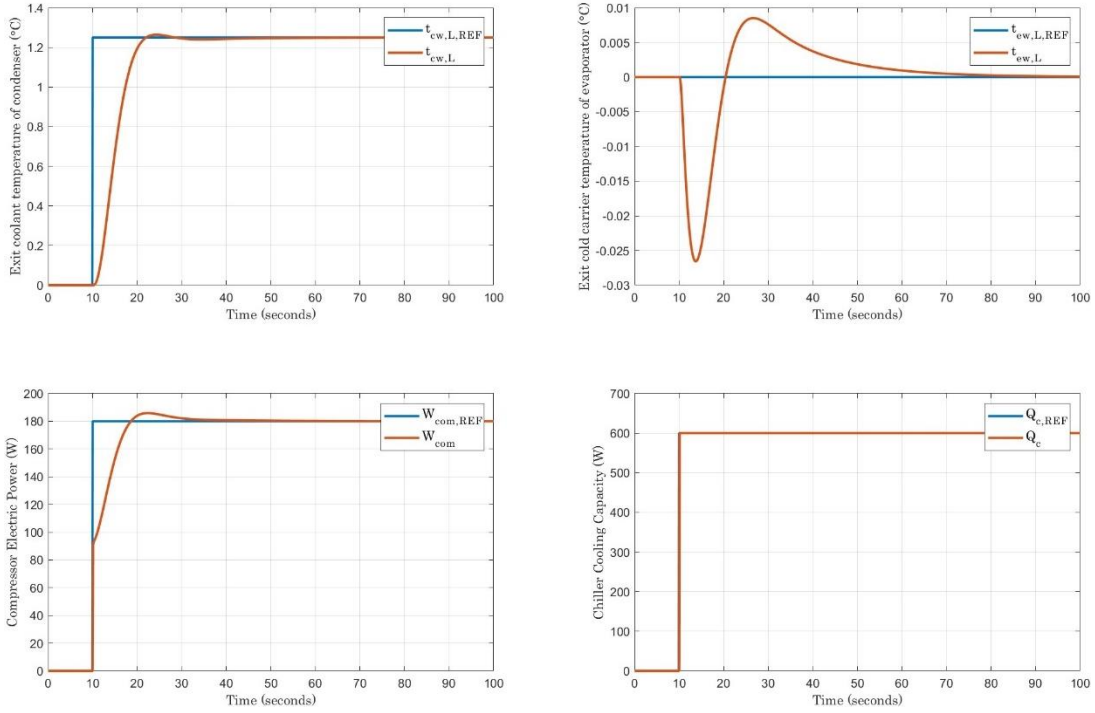


Figure 5-5: Output responses due to a step change in cooling load by 600 W

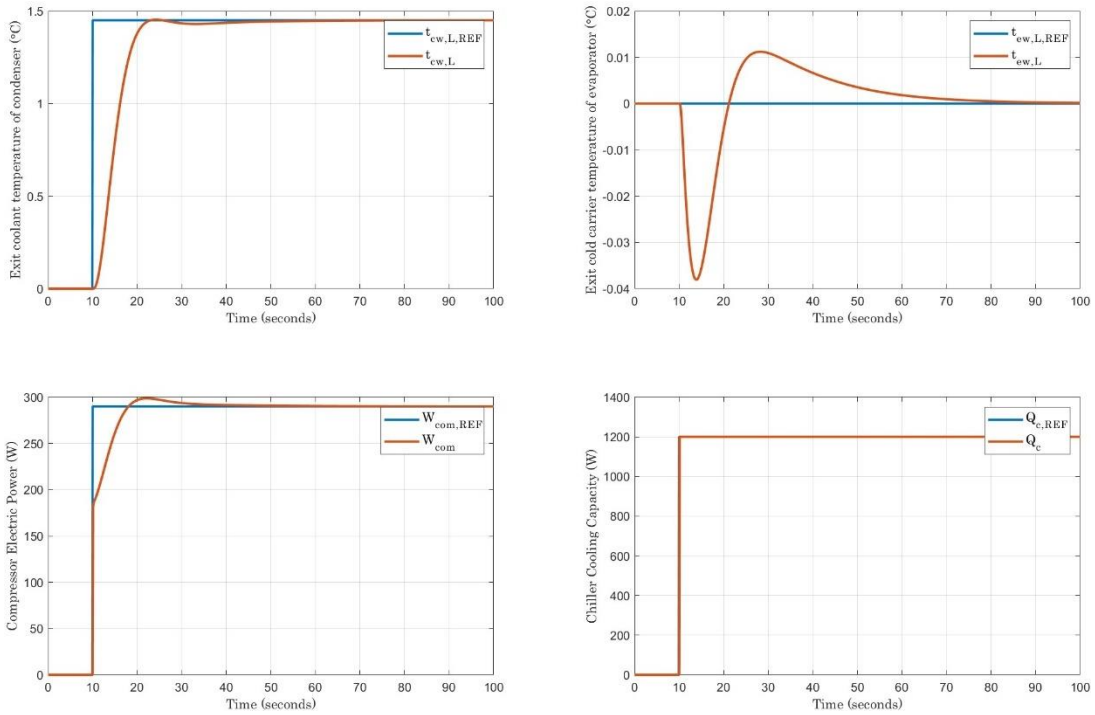


Figure 5-6: Output response due to a step change in cooling load by 1200 W

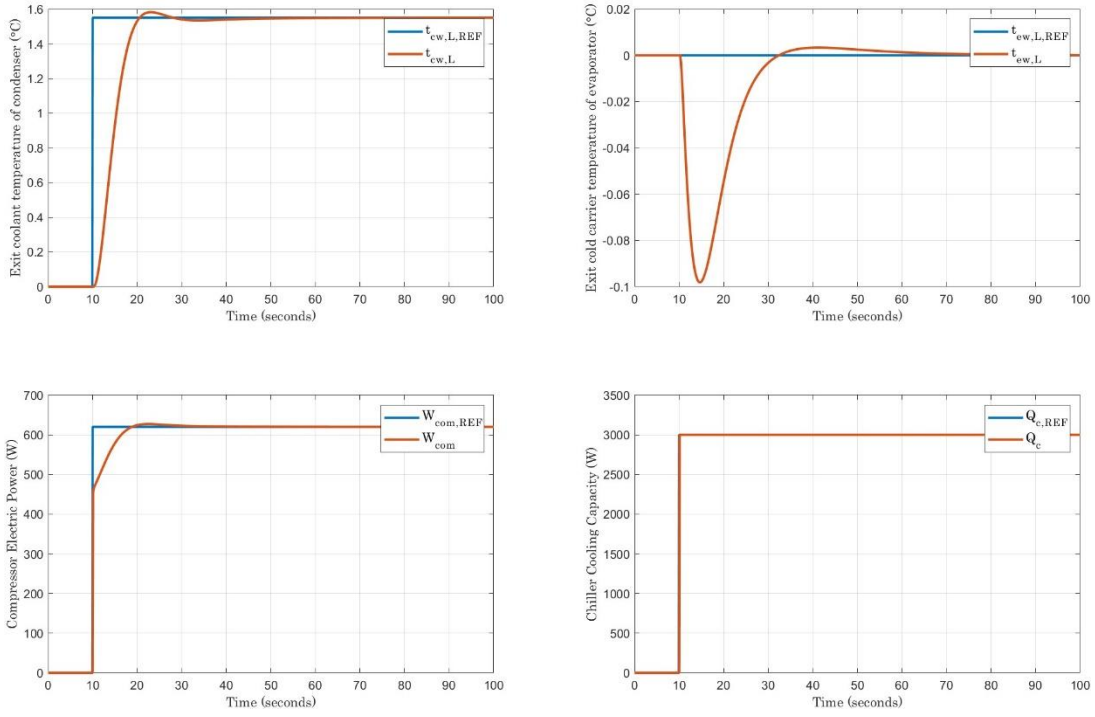


Figure 5-7: Output responses due to a step change in cooling load by 3000 W

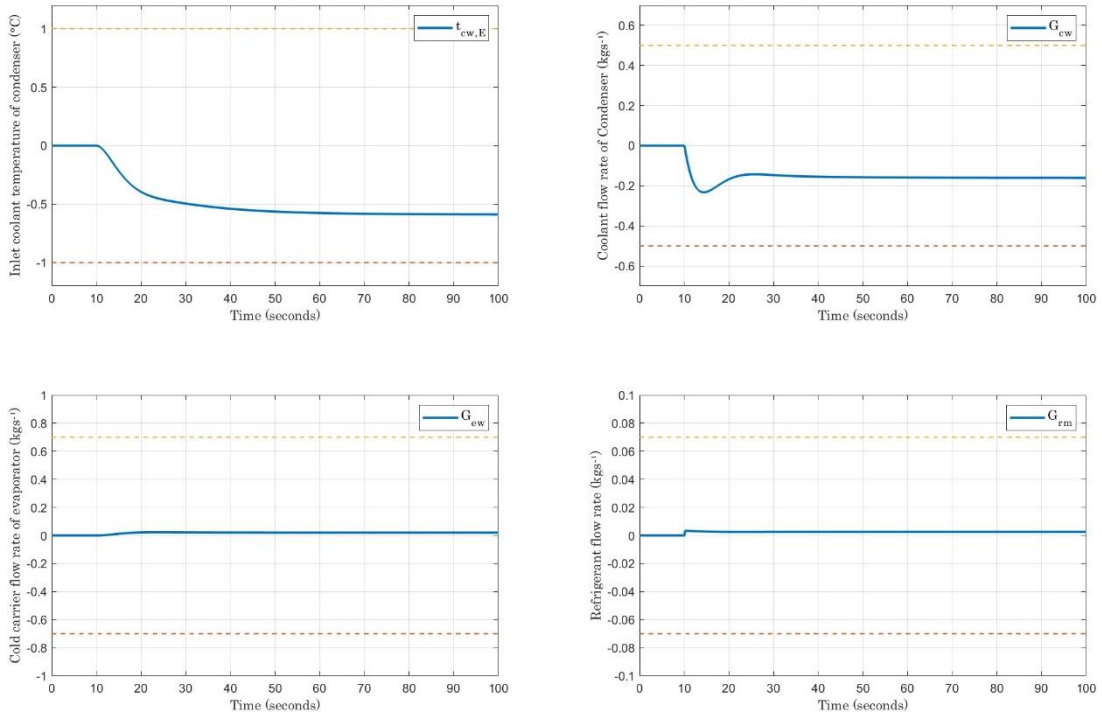


Figure 5-8: Control signals due to a step change in cooling load by 600 W

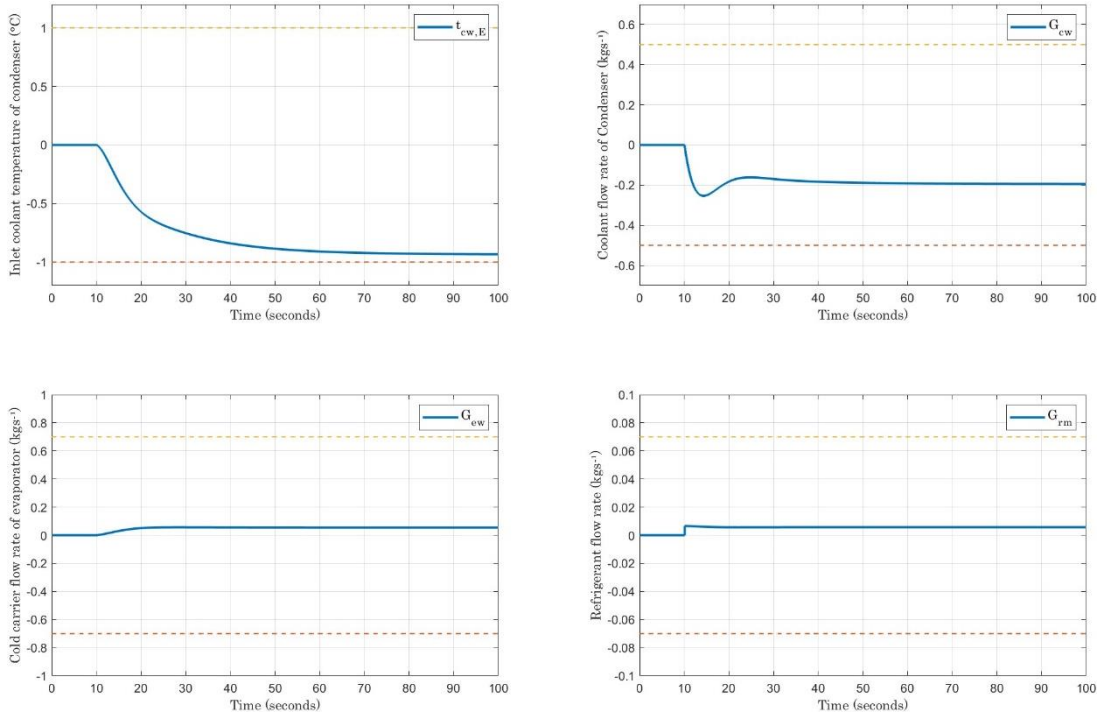


Figure 5-9: Control signals due to a step change in cooling load by 1200 W

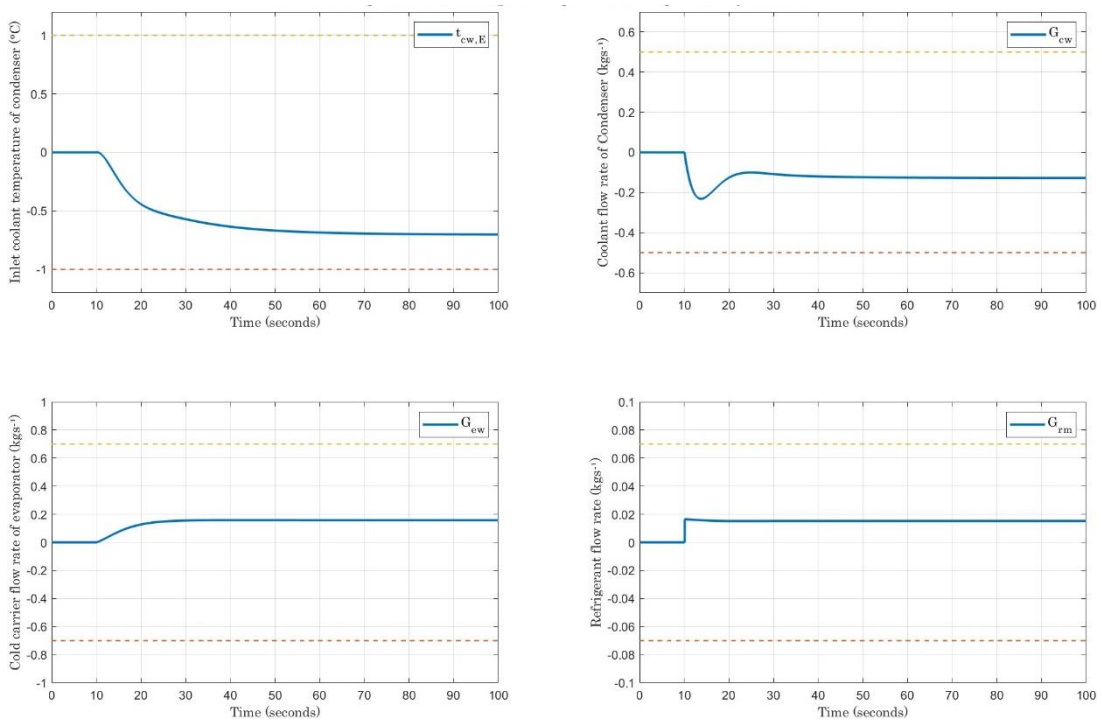


Figure 5-10: Control signals due to a step change in cooling load by 3000 W

### 5.3.2 Trajectory Tracking – Leaving Chilled liquid Temperature

The output response of the closed-loop system due to a step change in the leaving chilled liquid temperature of evaporator by 1 °C and 2 °C are depicted in Figures 5-11 and 5-12, respectively. On the other hand, the optimal control trajectory to meet the new set-points are illustrated in Figures 5-13 and 5-14, respectively.

A major observation for this test was the slow response in terms of the exit coolant temperature of condenser, compressor electric power and cooling load that the settling time is large (more than 70 seconds). Also, there were minor steady-state error when the new setpoint temperature of the exit chilled liquid of the evaporator was set at 1 °C. On the positive side, an excellent output response was achieved in terms of tracking the new setpoint temperature of the evaporator’s chilled liquid, since the output response showed 0% overshoot, no steady-state error and a settling time of less than 40 seconds. As with the previous tracking test, the control effort in transient response was smooth and free of sharp oscillation.

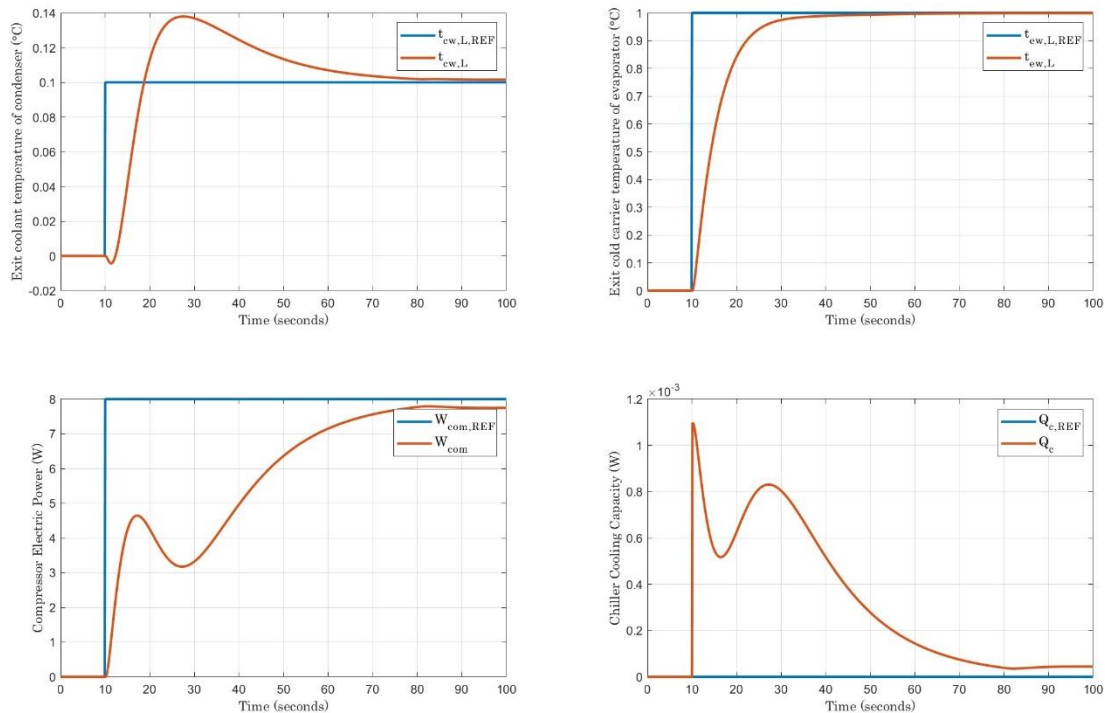


Figure 5-11: Output responses due to a step change in exit chilled liquid temperature of evaporator by 1 °C

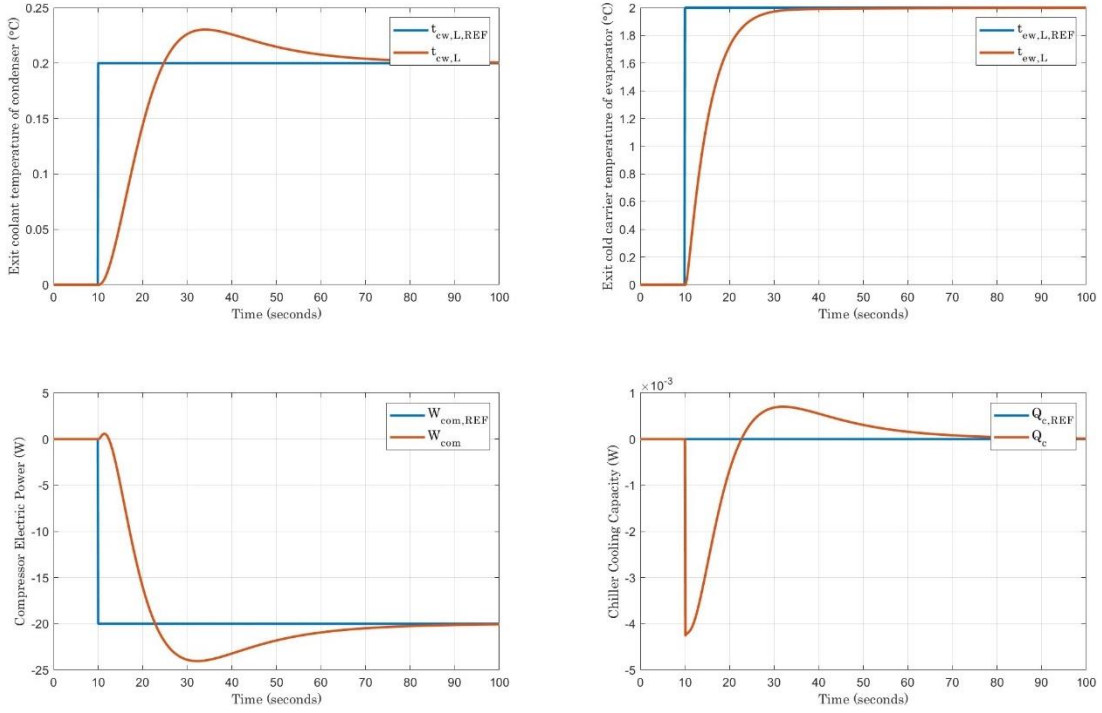


Figure 5-12: Output response due to a step change in exit chilled liquid temperature of evaporator by 2 °C

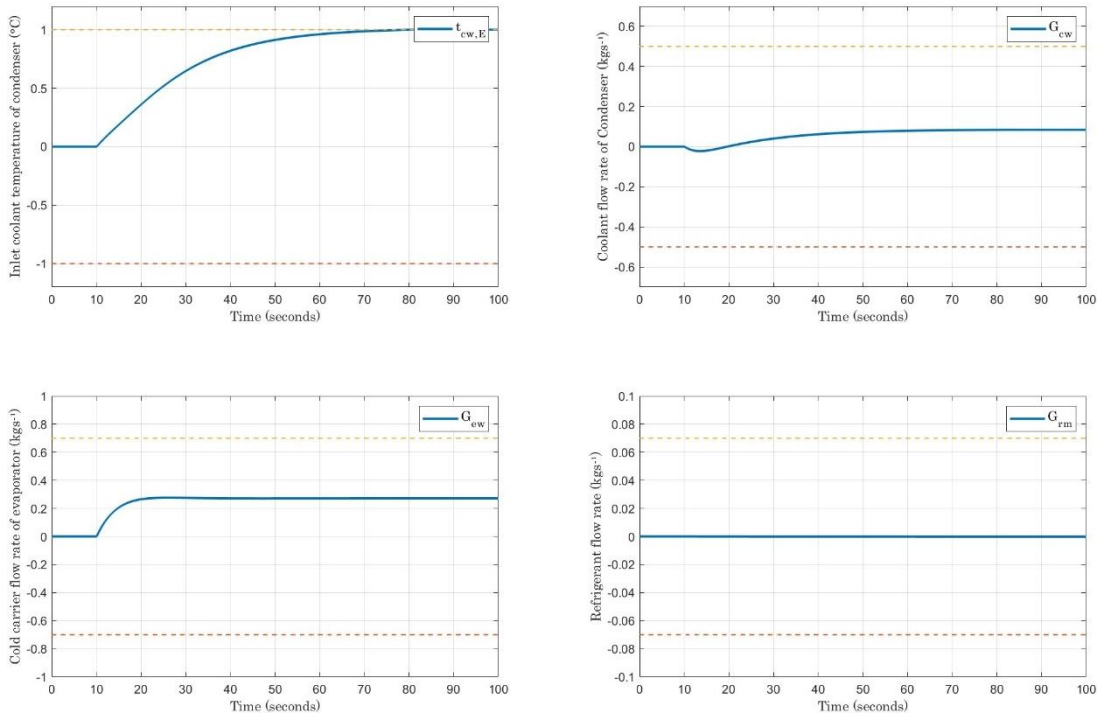


Figure 5-13: Control signals due to a step change in exit chilled liquid temperature of evaporator by 2 °C

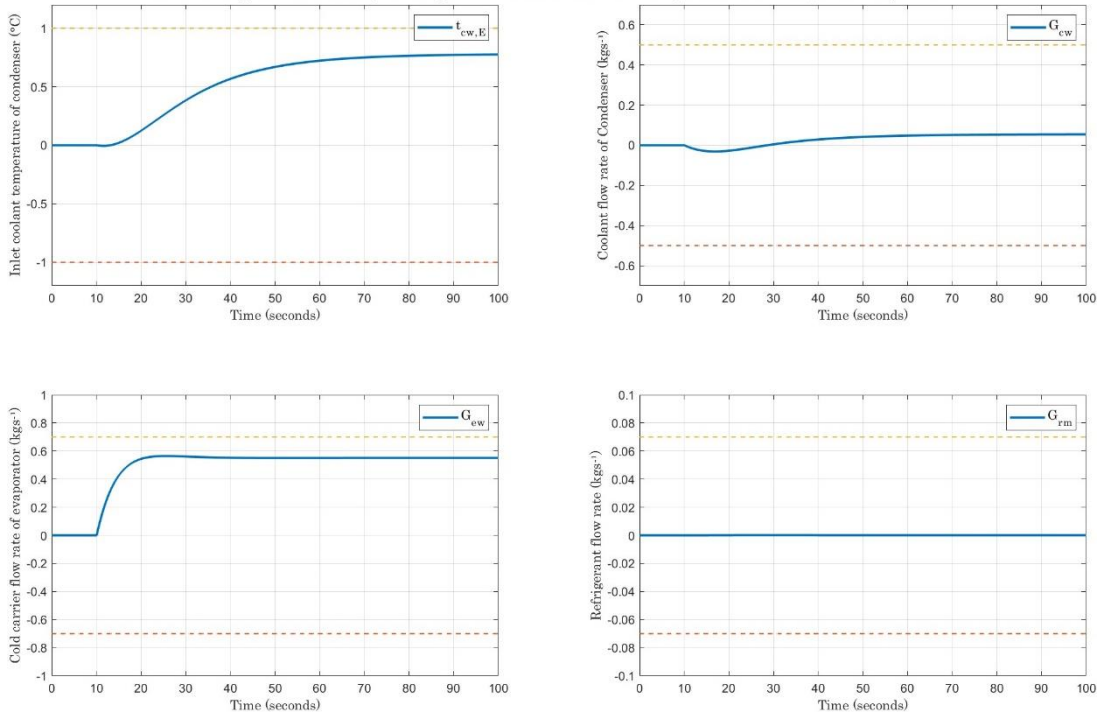


Figure 5-14: Control signals due to a step change in exit chilled liquid temperature of evaporator by 2 °C

### 5.3.3 Disturbance Rejection – Entering Chilled liquid Temperature

The LQI controller was evaluated on its ability to reject disturbances in the form of a step change in the entering chilled liquid temperature of the evaporator for the values outlined in Table 4-4. The output response due to a step change in the entering chilled liquid temperature of evaporator by 0.5 °C and 2.5 °C are shown in Figures 5-15 and 5-16, respectively. The applied control inputs to regulate the system is for the same conditions are as illustrated in Figures 5-17 and 5-18, respectively.

The controller performance in rejecting disturbance was fast with minimal overshoot, oscillations and no steady-state error. Furthermore, the settling time was decent, and the control effort exerted was smooth and within the constraint limits. Hence, the LQI controller was proven to be efficient in terms of rejecting the entering chilled liquid temperature of evaporator from values ranging from -0.5 °C to +2.5 °C.

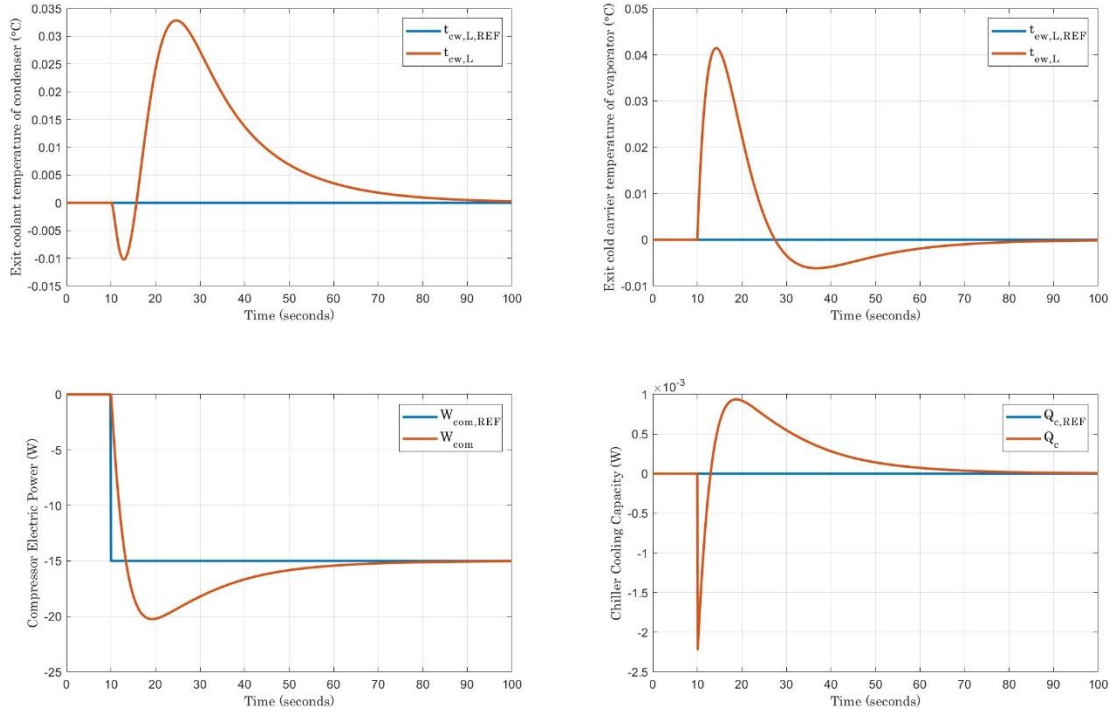


Figure 5-15: Output response due to a step change in inlet chilled liquid temperature of evaporator by 0.5 °C

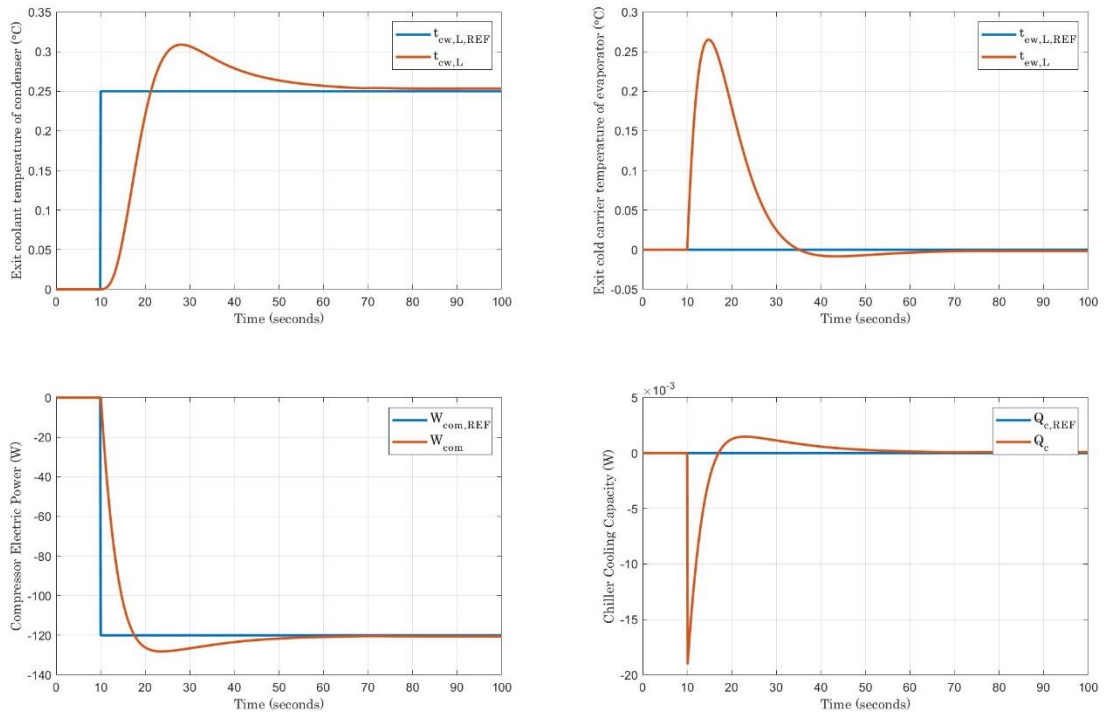


Figure 5-16: Output response due to a step change in inlet chilled liquid temperature of evaporator by 1 °C

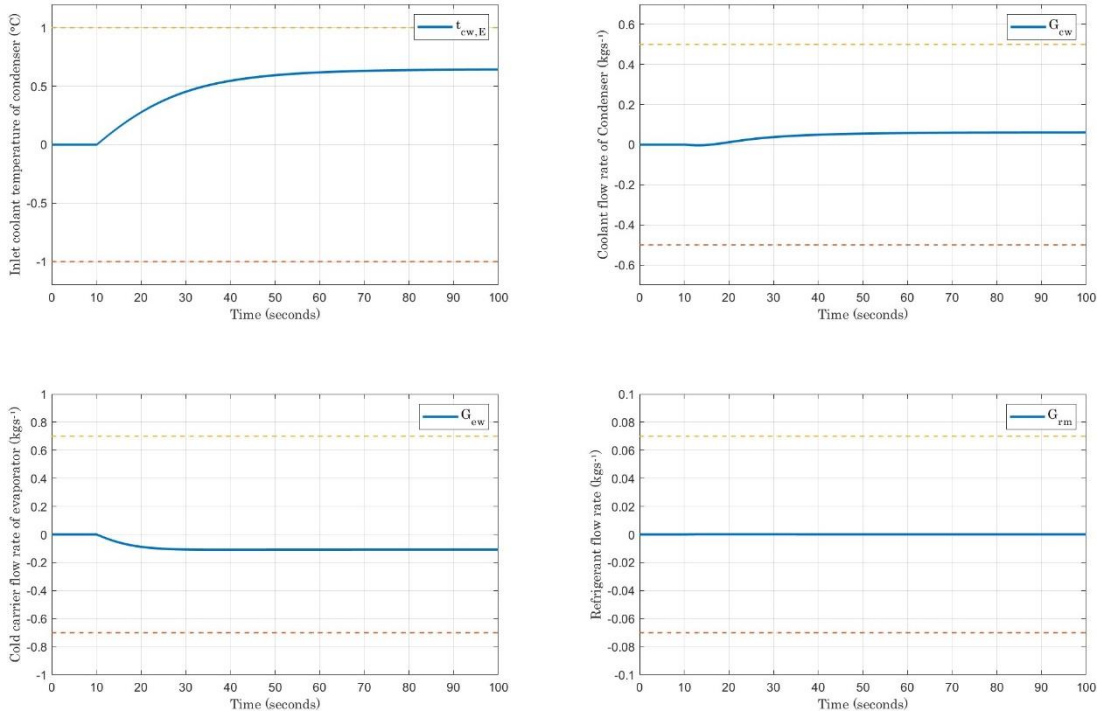


Figure 5-17: Control signals due to a step change in inlet chilled liquid temperature of evaporator by 0.5 °C

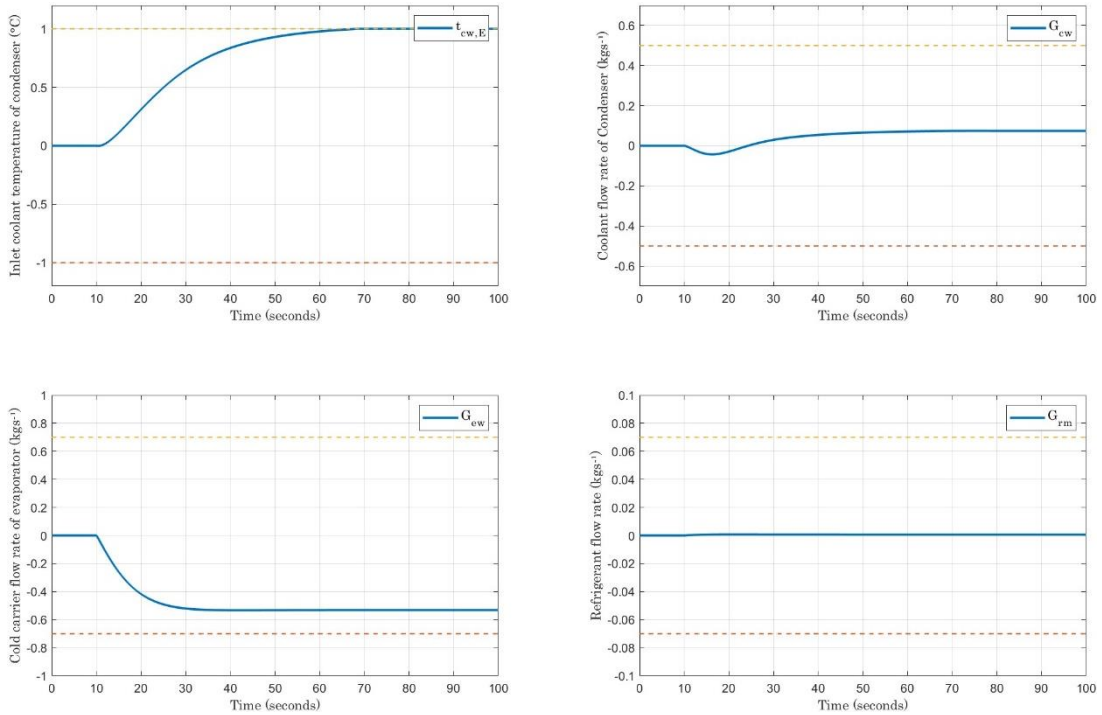


Figure 5-18: Control signals due to a step change in inlet chilled liquid temperature of evaporator by 1 °C

## Chapter 6 Model Predictive Control of Liquid Chiller and Controller Tuning using Genetic Algorithms

In this chapter, the last control technique applied on the chiller model is examined. First, the fundamentals of Model Predictive Control (MPC) are introduced. Then, a detailed derivation of the MPC for a MIMO system with direct feedthrough is presented. Due to the difficulty in tuning the controller's weights, a machine learning approach, namely, Genetic Algorithm is deployed to perform this task. The MATLAB implementation of MPC along with GA is discussed as well as the simulation results in terms of trajectory tracking and disturbance rejection are illustrated.

### 6.1 Fundamentals of Model Predictive Control (MPC)

Model Predictive Control (MPC) is an optimal multivariable feedback control technique that opts to compute the most optimal control trajectory to meet the required reference setpoint using model output prediction and iterative computation of the control trajectory as illustrated in Figure 6-1 [51][52]. The optimization is done for each time horizon window as shown in Figure 6-1. The MPC can be applied to both continuous and discrete-time systems. However, it is more natural for this type of control technique to be used in discrete-time models. Both LQR (including its derivatives such as LQT, LQG and LQI) and MPC are optimal controllers that share several similarities such as a quadratic cost function, can be applied to multivariable systems represented through a state-space model and can be applied in both continuous and discrete times. Albeit sharing common features, an LQR controller solves the control problem or computes the optimal control signal using a fixed window, whereas MPC uses a moving time horizon [51]. In other words, when a long prediction horizon is considered, an LQR can be thought of as an offline controller – as it uses one fixed control horizon – while MPC is an online controller that iteratively computes the optimal control trajectory on each window. Another critical salient feature that an MPC controller possesses lies in its ability to handle soft and hard constraints.

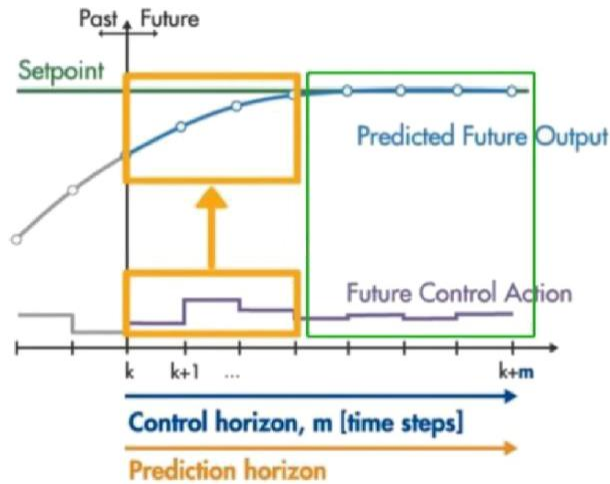


Figure 6-1: Illustration of the MPC control operation [52]

Just as with LQR, there are many variations to the MPC controller including, but not limited to, robust MPC, stochastic MPC, distributed MPC, adaptive MPC and hybrid MPC [52]. Irrespective of the MPC type, the parameters or inputs to design the controller are as outlined below [51]:

1. Plant model: MPC can be designed with a transfer function or a state-space model in either continuous or discrete time. However, the dominant model type is discrete-time state-space model (SISO or MIMO).
2. Moving horizon window,  $T_p$ : the time-dependent window in which optimization or controller computation takes place. It is measured from an arbitrary time  $t_i$  to  $t_i+T_p$ . The length of the moving horizon window is assigned by the designer and remains fixed during simulation.
3. Prediction horizon,  $N_p$ : determines the prediction window of the plant's model. It is an important parameter that contributes to the controller's performance. This parameter is varied in the tuning process of the controller. However, it should be large enough to cover the full transient response. The length of the prediction horizon window,  $N_p$ , is equal to the length of the moving horizon window.
4. Receding horizon control: the optimal control trajectory computed in the moving horizon window applied to the first sample of the control signal. Hence, the rest of the trajectory gets omitted.

5. Control Horizon,  $N_c$ : a parameter defined by the designer as to what extent the future control trajectory is predicted. The value of the control horizon is less than or equal to the value of the prediction horizon.
6. Cost function,  $J$ : the optimal control trajectory is evaluated based on a pre-defined cost function (or object function). A common cost function for MPC control is the quadratic cost function. When constraints are integrated into the cost function, quadratic programming is used to compute the optimal control signal.

## 6.2 Solution to Model Predictive Control with Direct Feedthrough

### 6.2.1 Augmented State-space Model Formulation

To align with standard practice, the MPC derivation will be done on a discrete time (DT) state-space model. However, the model derived in Chapter 3 includes a direct feedthrough term ( $D \neq 0$ ). In other words, one or more inputs have a direct impact on one or more outputs without passing through the states (i.e. the states or the internal model is bypassed). Most literature including MATLAB Model Predictive Control toolbox consider that there is no direct feedthrough in the model. Therefore, the MPC equations need to be reformulated by considering the direct feedthrough affect.

The MPC controller will have an embedded integrator [51], which is adopted to ensure that the steady-state errors are eliminated. However, the model presented in [51] considered that there is no direct feedthrough (i.e.  $D=0$ ) term. A reformulation of the state-space based MPC model with an embedded integrator and with direct feedthrough developed by [53] will be presented in this section and subsequent sections in detail. First, the state-space model given in Equation 3-32 is discretized at a suitable sampling time,  $T_s$ , and given by

$$\begin{cases} x_P(k_i+1) = A_P x_P(k_i) + B_P u(k_i) + F_P w(k_i) \\ y(k) = C_P x_P(k_i) + D_P u(k_i) \end{cases} \quad (6-1)$$

where  $x_P \in \mathbb{R}^{n \times 1}$  is the state vector,  $u \in \mathbb{R}^{m \times 1}$  is the control input vector,  $w \in \mathbb{R}^{r \times 1}$  is the measured disturbance input vector,  $y \in \mathbb{R}^{q \times 1}$  is the output vector,  $A_P \in \mathbb{R}^{n \times n}$  is the states matrix in discrete time,  $B_P \in \mathbb{R}^{n \times m}$  is the control input matrix in DT,  $F_P \in \mathbb{R}^{n \times r}$  is the measured disturbance matrix in DT,  $C_P \in \mathbb{R}^{q \times n}$  is the output matrix in DT and  $D_P \in \mathbb{R}^{q \times m}$  is the feedthrough matrix in DT.

The difference equations for the states, control inputs and the measured disturbances are given by

$$\Delta x_P(k_i+1) = x_P(k_i+1) - x_P(k_i) \quad (6-2)$$

$$\Delta x_P(k_i) = x_P(k_i) - x_P(k_i-1) \quad (6-3)$$

$$\Delta u(k_i) = u(k_i) - u(k_i-1) \quad (6-4)$$

$$\Delta w(k_i) = w(k_i) - w(k_i-1) \quad (6-5)$$

The difference of state-space equation is given as

$$\Delta x_P(k_i+1) = A_P \Delta x_P(k_i) + B_P \Delta u(k_i) + F_P \Delta w(k_i) \quad (6-6)$$

The predicted output is described by

$$y(k_i+1) = C_P A_P \Delta x_P(k_i) + C_P B_P \Delta u(k_i) + C_P F_P \Delta w(k_i) + D_P \Delta u(k_i+1) + y(k_i) \quad (6-7)$$

Let the closed-loop augmented state vector be

$$x(k_i) = \begin{bmatrix} \Delta x_P(k_i) \\ y(k_i) \end{bmatrix}^T \quad (6-8)$$

The augmented state-space model is then represented as

$$\begin{bmatrix} \Delta x_P(k_i+1) \\ y(k_i+1) \end{bmatrix} = \begin{bmatrix} A_P & O_m^T \\ C_P A_P & I_{qq} \end{bmatrix} \begin{bmatrix} \Delta x_P(k_i) \\ y(k_i) \end{bmatrix} + \begin{bmatrix} B_P \\ C_P B_P \end{bmatrix} \Delta u(k_i) + \begin{bmatrix} O_m^T \\ D_P \end{bmatrix} \Delta u(k_i+1) + \begin{bmatrix} F_P \\ C_P F_P \end{bmatrix} \Delta w(k_i) \quad (6-9)$$

$$y(k_i) = \begin{bmatrix} O_m & I_{qq} \end{bmatrix} \begin{bmatrix} \Delta x_P(k_i) \\ y(k_i) \end{bmatrix} \quad (6-10)$$

where,

$$x_{CL}(k) = \begin{bmatrix} \Delta x_P(k_i) \\ y(k_i) \end{bmatrix}$$

$$A_{CL} = \begin{bmatrix} A_P & O_m^T \\ C_P A_P & I_{qq} \end{bmatrix}$$

$$B_{CL} = \begin{bmatrix} B_P \\ C_P B_P \end{bmatrix}$$

$$F_{CL} = \begin{bmatrix} F_P \\ C_P F_P \end{bmatrix}$$

$$C_{CL} = [O_m \quad I_{qq}]$$

$$D_{CL} = \begin{bmatrix} O_m^T \\ D_P \end{bmatrix}$$

$O_m \in \mathbb{R}^{m \times 1}$  is the zero matrix and  $I_{qq} \in \mathbb{R}^{q \times q}$  is the identity matrix

For simplicity, the subscript, CL, will be dropped from the augmented closed-loop model variables as defined above when presenting the remaining equations.

### 6.2.2 Prediction of Controlled Inputs, States and Output Variables

In the following derivations, the disturbance term will be ignored. Now, given the control horizon,  $N_c$ , the expression for the future incremental control trajectory for a multi-input model is described by

$$\Delta U = [\Delta u(k_i)^T \quad \Delta u(k_i+1)^T \quad \dots \quad \Delta u(k_i+N_c-1)^T]^T \quad (6-11)$$

The state variables prediction, on the other hand, depends on the prediction horizon,  $N_p$ , or the length of the optimization window. The predicted state variables are expressed as

$$x(k_i+1|k_i) = Ax(k_i) + B\Delta u(k_i) + D\Delta u(k_i+1) \quad (6-12)$$

$$\begin{aligned} x(k_i+2|k_i) &= Ax(k_i+1) + B\Delta u(k_i+1) + D\Delta u(k_i+2) \\ &= A^2x(k_i) + AB\Delta u(k_i) + (AD+B)\Delta u(k_i+1) + D\Delta u(k_i+2) \end{aligned} \quad (6-13)$$

$$\begin{aligned} x(k_i+3|k_i) &= Ax(k_i+2) + B\Delta u(k_i+2) + D\Delta u(k_i+3) \\ &= A^3x(k_i) + A^2B\Delta u(k_i) + (A^2D+AB)\Delta u(k_i+1) + (AD+B)\Delta u(k_i+2) + D\Delta u(k_i+3) \end{aligned} \quad (6-14)$$

⋮

$$\begin{aligned} x(k_i+N_p|k_i) &= A^{N_p}x(k_i) + A^{N_p-1}B\Delta u(k_i) + (A^{N_p-1}D + A^{N_p-2}B)\Delta u(k_i+1) + \\ & (A^{N_p-2}D + A^{N_p-3}B)\Delta u(k_i+2) + (A^{N_p-3}D + A^{N_p-4}B)\Delta u(k_i+3) + \dots + (A^{N_p-(N_p-1)}D + A^{N_p-N_p}) \end{aligned} \quad (6-15)$$

The future predicted output is derived using the predicted state Equations 6-12 through 6-15 to obtain the following

$$y(k_i+1|k_i) = Cx(k_i+1|k_i) = CAx(k_i) + CB\Delta u(k_i) + CD\Delta u(k_i+1) \quad (6-12)$$

$$\begin{aligned} y(k_i+2|k_i) &= Cx(k_i+2|k_i) = CAx(k_i+1) + CB\Delta u(k_i+1) + CD\Delta u(k_i+2) \\ &= CA^2x(k_i) + CAB\Delta u(k_i) + (CAD+CB)\Delta u(k_i+1) + CD\Delta u(k_i+2) \end{aligned} \quad (6-13)$$

$$\begin{aligned} y(k_i+3|k_i) &= Cx(k_i+3|k_i) = CAx(k_i+2) + CB\Delta u(k_i+2) + CD\Delta u(k_i+3) \\ &= CA^3x(k_i) + CA^2B\Delta u(k_i) + (CA^2D+CAB)\Delta u(k_i+1) + (CAD+CB)\Delta u(k_i+2) \\ & + CD\Delta u(k_i+3) \end{aligned} \quad (6-14)$$

⋮

$$(6-15)$$

$$\begin{aligned}
y(k_i+N_P|k_i) &= Cx(k_i+N_P|k_i) \\
&= CA^{N_P}x(k_i) + CA^{N_P-1}B\Delta u(k_i) + (CA^{N_P-1}D + CA^{N_P-2}B)\Delta u(k_i+1) \\
&\quad + (CA^{N_P-2}D + CA^{N_P-3}B)\Delta u(k_i+2) + (CA^{N_P-3}D + CA^{N_P-4}B)\Delta u(k_i+3) + \dots \\
&\quad + (CA^{N_P-(N_P-1)}D + CA^{N_P-N_P})\Delta u(k_i+N_P-1) + CD\Delta u(k_i+N_P)
\end{aligned}$$

The output for a MIMO system is expressed in matrix form as

$$Y = [y(k_i+1|k_i)^T \quad y(k_i+2|k_i)^T \quad y(k_i+3|k_i)^T \quad \dots \quad y(k_i+N_P|k_i)^T]^T \quad (6-16)$$

The solution to Equation 6-16 is represented in a compact matrix form in terms of the current state variables, the future incremental control trajectory and two gain matrices that depend on the augmented state-space gain matrices (i.e. A, B, C and D), prediction horizon and control horizon. Thus, the output equation is given as

$$Y = Fx(k_i) + \Phi\Delta U \quad (6-17)$$

where

$$F = \begin{bmatrix} CA \\ CA^2 \\ CA^3 \\ \vdots \\ CA^{N_P} \end{bmatrix};$$

$$\Phi = \begin{bmatrix} CB & CD & 0 & \dots & 0 \\ CAB & CAD+CB & CD & \dots & 0 \\ CA^2B & CA^2D+CAB & CAD+CB & \dots & 0 \\ \vdots & \vdots & \vdots & \dots & \vdots \\ CA^{N_P}B & CA^{N_P-1}D+CA^{N_P-2}B & CA^{N_P-2}D+CA^{N_P-3}B & \dots & CAD+CA^0B \end{bmatrix}$$

It can be observed that the matrix,  $\Phi$ , includes a feedthrough gain matrix, D. Thus, the MPC has now been reformulated to include in its computation or prediction the direct-feedthrough matrix as opposed to previous formulation which neglected in the derivation the direct feedthrough term.

### 6.2.3 Optimization

Having derived the predicted output in Equation 6-17, the final step is to compute the incremental control trajectory,  $\Delta U$ . First, the solution is presented for the unconstrained case. Then, it the solution will be extended for the constrained case. In both cases, a cost function needs to be defined. A standard cost function for a model predictive controller is the quadratic cost function given by

$$J=(R_s-Y)^T(R_s-Y)+\Delta U^T\bar{R}\Delta U \quad (6-18)$$

where  $R_s \in \mathbb{R}^{N_p \times q}$  is a column vector containing all the reference or setpoint signals information, and  $\bar{R} \in \mathbb{R}^{m \times m}$  is a diagonal matrix containing the weights applied on the control inputs. The weights (or tuning parameters) is adjusted by the designer to achieve the desired closed-loop system performance. The number of weights is equal to the number of the system's control inputs.

Using Equation 6-17, Equation 6-18 is expanded as

$$J=(R_s-Fx(k_i))^T(R_s-Fx(k_i))-2\Delta U^T\Phi^T(R_s-Fx(k_i))+\Delta U^T(\Phi^T\Phi+\bar{R})\Delta U \quad (6-19)$$

In the unconstrained case, the solution for the optimal control trajectory is given as a closed form solution by minimizing  $J$ . This is achieved by taking the first derivative of  $J$  with respect to  $\Delta U$ , equate the first derivate to zero and solve for  $\Delta U$  as given in the steps below

$$\frac{\partial J}{\partial \Delta U}=-2\Phi^T(R_s-Fx(k_i))+2(\Phi^T\Phi+\bar{R})\Delta U \quad (6-20)$$

$$-2\Phi^T(R_s-Fx(k_i))+2(\Phi^T\Phi+\bar{R})\Delta U=0 \quad (6-21)$$

$$\Delta U=(\Phi^T\Phi+\bar{R})^{-1}\Phi^T(R_s-Fx(k_i)) \quad (6-22)$$

In the constrained case, a closed form solution as given in Equation 6-22 is not plausible. Instead, a suitable iterative optimization method is used. This is due to the incorporation of the input and/or output constraints to the cost function defined earlier. Furthermore, there are two types of input constraints, constraints on the amplitude and constraints on the incremental variation [51]. Thus, the optimization problem is redefined as

$$\min J=(R_s-Fx(k_i))^T(R_s-Fx(k_i))-2\Delta U^T\Phi^T(R_s-Fx(k_i))+\Delta U^T(\Phi^T\Phi+\bar{R})\Delta U \quad (6-23)$$

Subject to:

$$\begin{bmatrix} M_1 \\ M_2 \\ M_3 \end{bmatrix} \Delta U \leq \begin{bmatrix} N_1 \\ N_2 \\ N_3 \end{bmatrix}$$

where,

$$M_1=\begin{bmatrix} -C_2 \\ C_2 \end{bmatrix}; N_1=\begin{bmatrix} -U^{\min}+C_1u(k_i-1) \\ U^{\max}-C_1u(k_i-1) \end{bmatrix};$$

$$C_1 = \begin{bmatrix} \mathbf{I} \\ \mathbf{I} \\ \mathbf{I} \\ \vdots \\ \mathbf{I} \end{bmatrix}; C_2 = \begin{bmatrix} \mathbf{I} & 0 & 0 & \dots & 0 \\ \mathbf{I} & \mathbf{I} & 0 & \dots & 0 \\ \mathbf{I} & \mathbf{I} & \mathbf{I} & \dots & 0 \\ \vdots & \vdots & \vdots & \ddots & \vdots \\ \mathbf{I} & \mathbf{I} & \mathbf{I} & \dots & \mathbf{I} \end{bmatrix}$$

$$M_2 = \begin{bmatrix} -\mathbf{I} \\ \mathbf{I} \end{bmatrix}; N_2 = \begin{bmatrix} -\Delta U^{\min} \\ \Delta U^{\max} \end{bmatrix}$$

$$M_3 = \begin{bmatrix} -\Phi \\ \Phi \end{bmatrix}; N_3 = \begin{bmatrix} -Y^{\min} + Fx(k_i) \\ Y^{\max} - Fx(k_i) \end{bmatrix}$$

The size of each element in Equation 6-23 depends on several factors such as the number of constraints, control horizon and the constraint window. The constraint window sets the extent of optimization. In other words, shall the control trajectory be optimized for just the next sample or more. Also, the matrix  $\Phi^T \Phi + \bar{R}$  is called the Hessian matrix and is assumed to be positive definite [51].

Given that the cost function is quadratic and with linear inequalities constraints, the solution to Equation 6-23 is obtained numerically using Quadratic Programming (QP). Some of the common QP methods are Active-Set, Interior-Point and Hildreth Quadratic Programming Procedure. To apply of these methods, Equation 6-23 needs to be arranged in the standard form described by

$$\min J = \frac{1}{2} x^T H x + x^T f \quad (6-24)$$

Subject to:

$$\begin{bmatrix} M_1 \\ M_2 \\ M_3 \end{bmatrix} \Delta U \leq \begin{bmatrix} N_1 \\ N_2 \\ N_3 \end{bmatrix}$$

where,

$$H = 2(\Phi^T \Phi + \bar{R});$$

$$f = -2\Phi^T (R_s - Fx(k_i))$$

### 6.2.4 Block Diagram Representation of the Model Predictive Control System

The model predictive control scheme can be represented in block-diagram as illustrated in Figure 6-2. It is evident from the block diagram representation that structure is identical nature to LQI or state-feedback with output feedback integrator. However, the difference is that the value of the state and output feedback gains vary. Applying receding horizon control

to the output trajectory computed in Equation 6-22, the first sample is only considered and the equation becomes

$$\Delta U = [I_m \quad O_m \quad \dots \quad O_m] (\Phi^T \Phi + \bar{R})^{-1} (\phi^T \bar{R}_s r(k_i) - \phi^T F x(k_i)) \quad (6-25)$$

where the size of the ones and zeros matrix is  $m \times N_c$ ,  $\bar{R}_s \in \mathbb{R}^{qN_p \times q}$  is a ones matrix and  $r(k_i)$  is the reference signal column vector.

Equation 6.25 can be represented in terms of the state feedback gain,  $K_x$ , and the output feedback gain,  $K_y$ , yielding

$$\Delta U = K_y r(k_i) - K_x x(k_i) \quad (6-26)$$

where,

$$K_y = \text{first element of } \{ (\Phi^T \Phi + \bar{R})^{-1} \phi^T \bar{R}_s \};$$

$$K_x = \text{first column of } \{ (\Phi^T \Phi + \bar{R})^{-1} \phi^T F \}$$

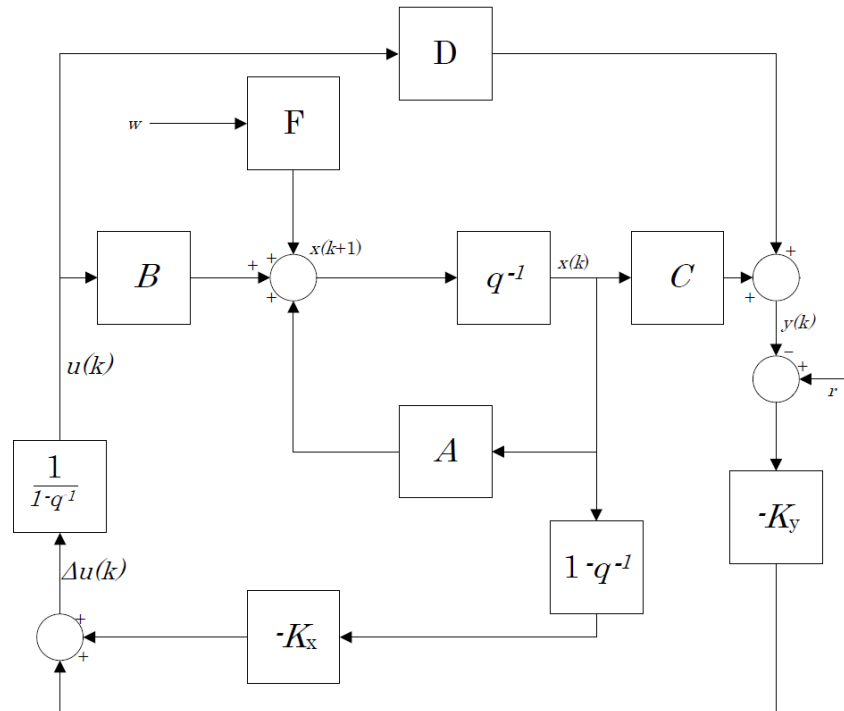


Figure 6-2: Block diagram of discrete-time predictive control system with direct feedthrough and measured input disturbance

### 6.3 Model Predictive Controller Weight Tuning using Genetic Algorithm

Genetic Algorithms (GA) is considered as one of the oldest stochastic parameter optimization or machine learning tools [54]. This makes this GA one of the available methods to controllers' tuning. Motivated by the example given by S. L. Brunton et al. [54] to tune a PID controller weights and V. Ramasamy et al. [55] to utilize GA with iterative decision trees to tune the weights of an MPC for an industrial cement kiln process, GA will be used to tune the weights of the control inputs of the MPC controller developed earlier.

As the name suggests, genetic algorithm is developed based on natural selection [55]. It uses the concept of natural selection in an iterative manner to find a nearly global optimal solution. The iterative approach of the GA is illustrated in Figure 6-3 and as described in the steps below [54][55]:

1. *Population Initialization*: this is a user defined value and in simple terms, it is the pool of solvers or individuals. The number of populations is fixed across the iteration process. For instance, for a population of 10 individuals and maximum of 5 generations (i.e. iterations), then in each generation, 10 individuals are present. Furthermore, a higher population size has a higher probability of achieving a nearly optimal solution, but at the expense of computational power.
2. *Cost function and probability of selection*: an individual will randomly have a weight value assigned to it as a binary number. The optimization problem will be solved based on these weights and a suitable cost function is used to evaluate the performance of the individual. The individuals with the highest cost function have a higher probability to qualify to the next generation that is governed by a set of natural selection rules or genetic operations as given below:
  - a. *Replication*: an individual replicates itself and advances to the next generation without undergoing any genetic operation that alters its weights. In other words, the set of weights in the first generation proceeds to the next generation to compete with different individuals than the previous generation. The individual that gets to be replicated has one of the lowest cost function values (i.e. highest probability) or has performance (i.e. elitism). Figure 6-4 depicts this operation.

- b. Crossover: in the genetic operation, two individuals are selected and part of their binary representation or code gets swapped. Figure 6-4 depicts this operation.
  - c. Mutation: in this operation, part of the individual's binary code is altered to a new random value. This process enhances diversity by exploring different set of weights as well as averts the optimizer of pointing or exploring single direction that are less optimal (i.e. local minimum) or even poor Figure 6-4 depicts this operation.
3. Number of Generation: the optimizer terminates its heuristic search operation once it reaches the maximum number of generations defined by the user or the set of individuals in that generation converge.

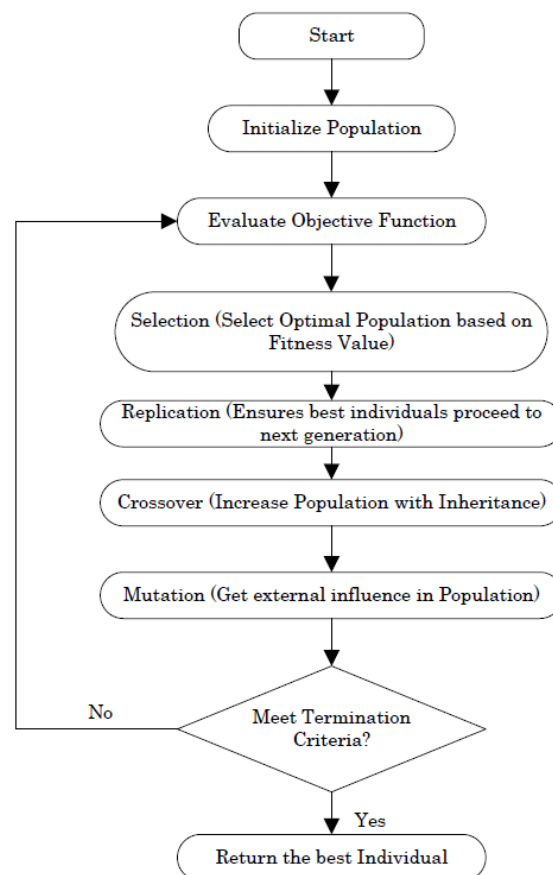


Figure 6-3: Flow chart of the Genetic algorithm optimization process [55]

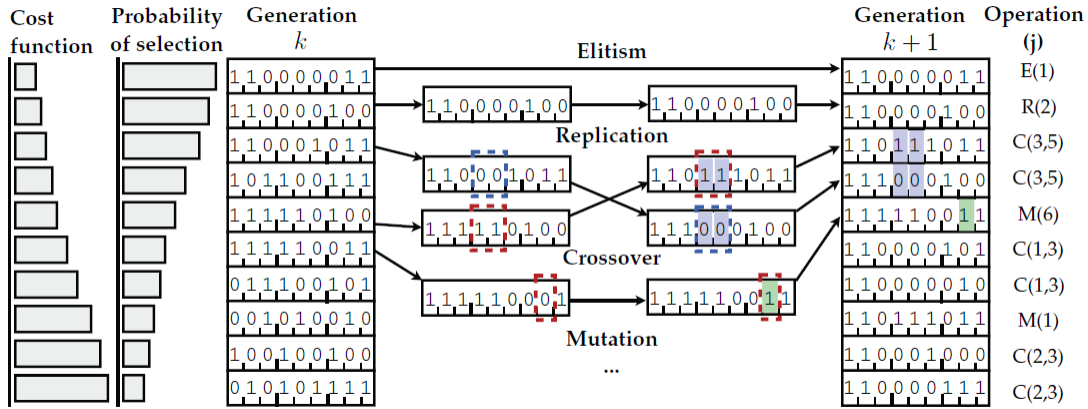


Figure 6-4: Illustration of the various steps performed by GA [54]

## 6.4 Implementation and Simulation Results of the MPC Controller

The discrete-time model predictive controller presented earlier was implemented using MATLAB by creating several functions. The considered sampling time,  $T_s$ , was 0.1 seconds. This was the optimal sampling time as going with a larger sampling time will impact the performance of the system, and having smaller sampling time increased the computational complexity of the system. For instance, a dedicated function to compute the gain matrices of Equation 6-17. Furthermore, only two linear nonequality constraints were imposed on the system, namely, constraints on the amplitude of the control signal and the rate of change of the control signal. Hence, no constraints were added to the output as it may deteriorate the controller's performance. Moreover, constraints on the rate of change of the control signal is taken as one third of the constraints on the amplitude rate of change.

The steps to compute the optimal control signal is as given below:

1. Convert the continuous time state-space model to discrete-time state space model.
2. Define  $N_P$  and  $N_C$ .
3. Load the weights of the model predictive controller (tuned through GA and stored) and select the set of weights corresponding to the application (i.e. reference tracking or rejection).
4. Compute the gain matrices,  $F$  and  $\Phi$ .
5. Define the constraint optimization window and represent the constraints in their standard form (Equation 6-22).

6. Load the reference and input disturbance signal vectors.
7. Initialize  $x(0)$  and  $u(-1)$  to zero.
8. Let the predicted  $y(k) = y(k-1)$ .
9. Compute  $\Delta U$  assuming there are no constraints on the system (Equation 6-23).
10. If the any of the elements in  $\Delta U$  violates the constraints, then solve the optimization problem using QP (Equation 6-24).
11. Compute the predicted states and outputs.
12. Repeat steps 9 through 11 until the end of the simulation.

The weights of the controller were initially tuned randomly. However, this approach was deemed not effective as instability at certain gain values were noticed. Thus, GA was used to tune the 4 controller weights. After a series of trial-and-error, it was deduced that the required population size is 50 and the maximum number of generations is 25. Another hyperparameter considered as was the minimum and maximum allowable weights value. These limits were derived from the trial-and-error manual tuning process in which the unstable or poor performance regions were defined. The tuning process took 13 hours to complete, and the weighing vectors were stored. The training of the controller for tracking purposes was done for a single tracking reference setpoint. The considered value is a change in the cooling load by 1200 W. Likewise, for disturbance rejection, the chosen training value was when the system was subjected to a measured input disturbance in the form of a step change in the inlet evaporating liquid by +2.5 °C.

The performance of the GA to find the nearly optimal controller weights is depicted in Figure 6-5. It is evident that in the beginning, most of the results had high cost as indicated in yellow, and as the algorithm advances, the GA evolves until it converges as depicted in dark blue in the last generation. Note that the number of generations needed is 17 until the algorithm converges. Furthermore, the  $\log J$  correspond to the logarithmic value of the cost function value at the end of the 100 seconds optimization window. Also, the training process of the controller

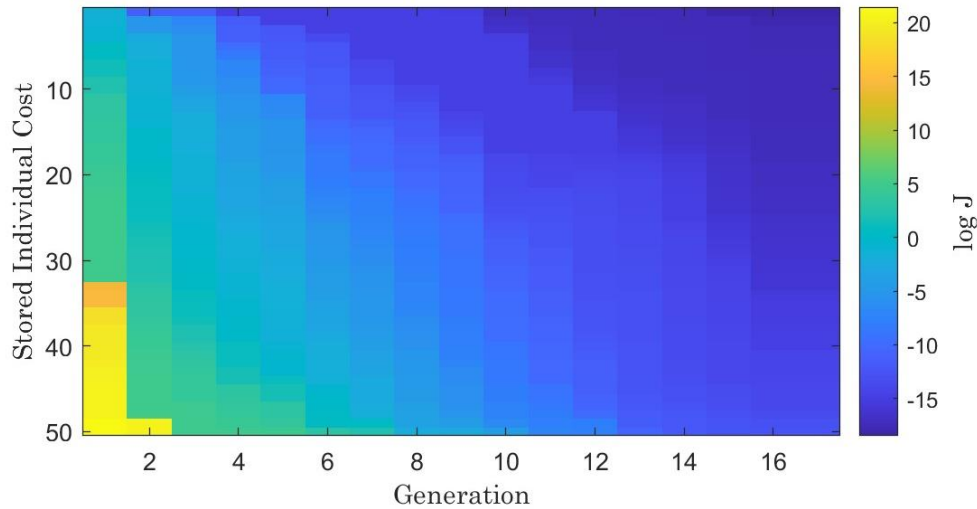


Figure 6-5: Performance of the GA on liquid chiller tuning as the generations evolve

The final set of parameters for the model predictive controller to control the liquid chiller model are given in Table 6-1. The same settling time used earlier for an LQI controller was used here. Also, reducing the settling beyond 0.1 seconds increased the computational power. Three other parameters also associated with the computation power are the prediction horizon,  $N_p$ , control horizon,  $N_c$  and the constraint optimization window, CDW. The prediction horizon was selected as to cover as much as possible the transient phase of the system. A value of 400 was selected as it complied with the prediction requirements as well as not increasing the computation power. The control horizon is usually a fraction of the prediction horizon, typically this value is between 10% and 20%. However, this range did not yield satisfactory results as compared to 30% (i.e. 120). The constraint optimization window term was used to set up the constraint matrix that was later solved using QP. After several trials, an optimization on the current time instant was sufficient instead of optimizing across the full control horizon.

The GA tuned the last 4 variables in Table 6-1 pertaining to the applied weights on the control signals. A higher input weight yields to a higher cost on that input, which means that the applied control effort is more limited. Using these parameters along with the iterative procedure defined above, the performance of the controller will be subject to the same tests done earlier on the PID and LQI controllers. The performance results in terms of trajectory tracking and disturbance rejection will be presented in the next subsections.

Table 6-1: Tuning Parameters and Weights of the MPC Controller

<u>Parameter</u>	<u>Reference Tracking</u>	<u>Disturbance Rejection</u>	<u>Affected Variable(s)</u>
$T_s$	0.1 seconds		Overall system
$N_P$	400 samples		Overall system
$N_c$	120 samples		Overall system
CDW	1 sample		Overall system
rw1	$3.0374 \times 10^3$	$3.2824 \times 10^3$	Input $t_{cw,E}$
rw2	$1.3783 \times 10^5$	$1.4497 \times 10^5$	Input $G_{cw}$
rw3	$3.0897 \times 10^5$	$3.0151 \times 10^4$	Input $G_{ew}$
rw4	$9.6895 \times 10^8$	$9.5841 \times 10^9$	Input $G_{rm}$

#### 6.41 Trajectory Tracking – Cooling Load

The output responses of the closed-loop system using an MPC controller due to a step change on the cooling load by 600 W, 1200 W and 3000 W are shown on Figures 6-6, 6-7 and 6-8, respectively. The applied control inputs to achieve the desired setpoints whilst regulating the entering chilled liquid temperature are illustrated in Figures 6-9, 6-10 and 6-11.

The overshoot in the cooling load was higher at low load conditions, but as load increased the overshoot decreased. This could be due to the interactions between the control inputs and outputs as most of them are dependent. On the other hand, the cooling load exhibited lower overshoot at low load conditions as opposed to when the load is higher. The exit coolant of condenser had a steady overshoot of around 0.2 °C to 0.5 °C, while the overshoot of the compressor power was very minimal at low loads and zero at high loads. The settling time for all outputs was less than 50 seconds and the steady state was almost zero. The control signals for all simulations were smooth with the exception of the inlet coolant temperature of the condenser, in which a sharp one oscillation was observed albeit introducing a rate of change input constraint.

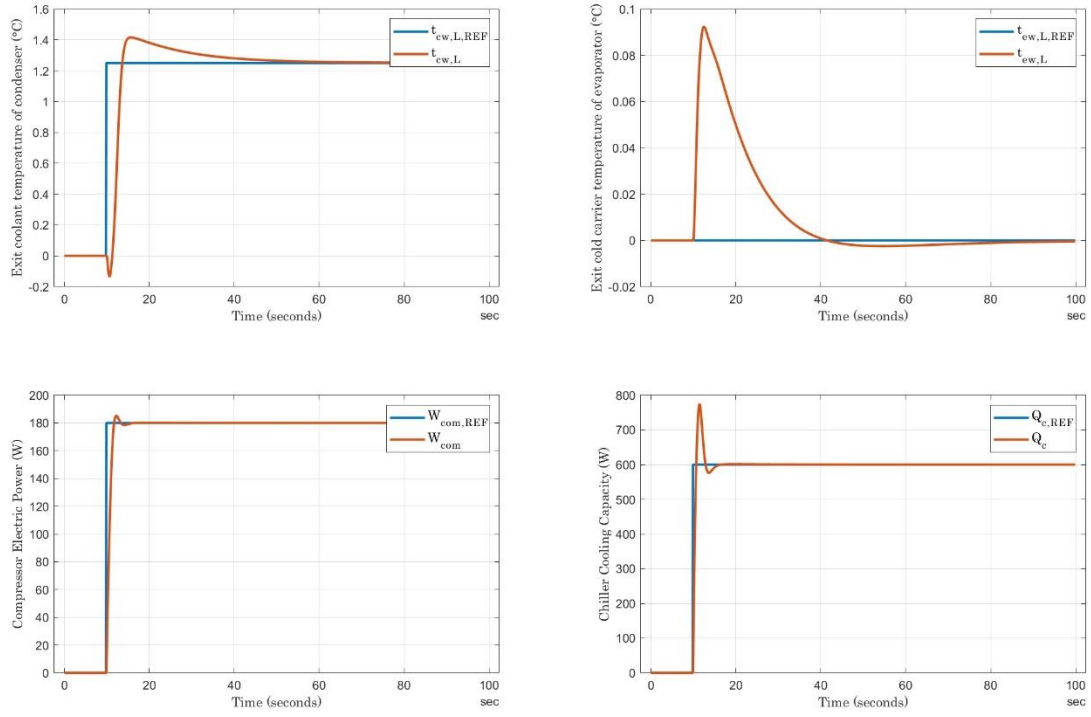


Figure 6-6: Output responses due to a step change in cooling load by 600 W

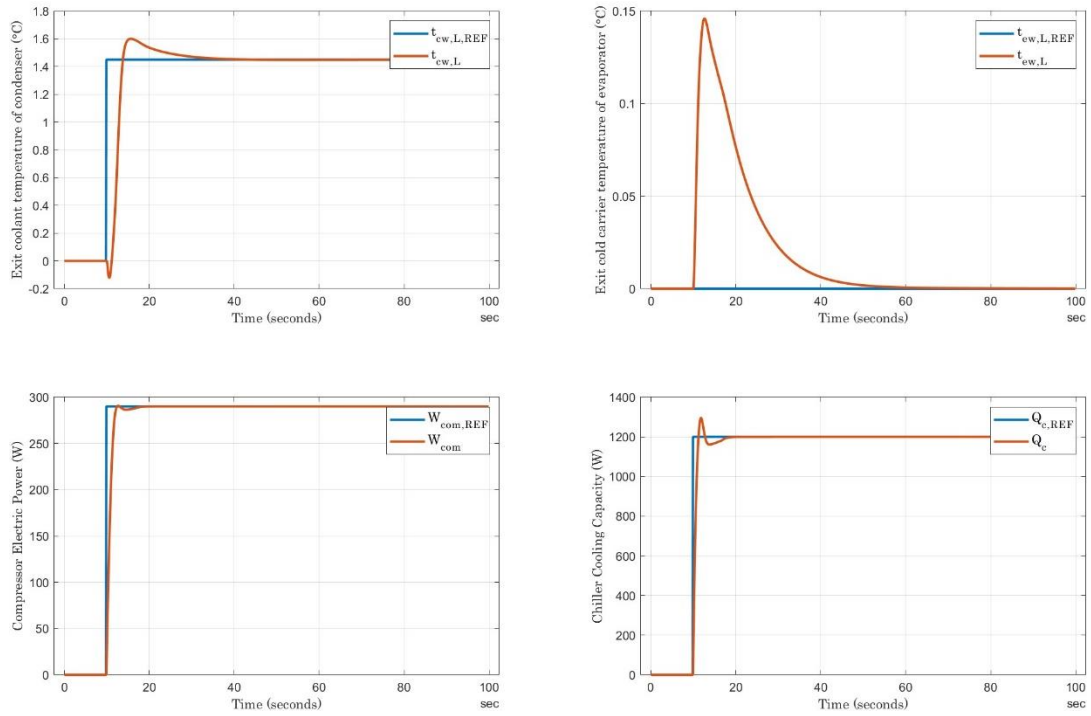


Figure 6-7: Output responses due to a step change in cooling load by 1200 W

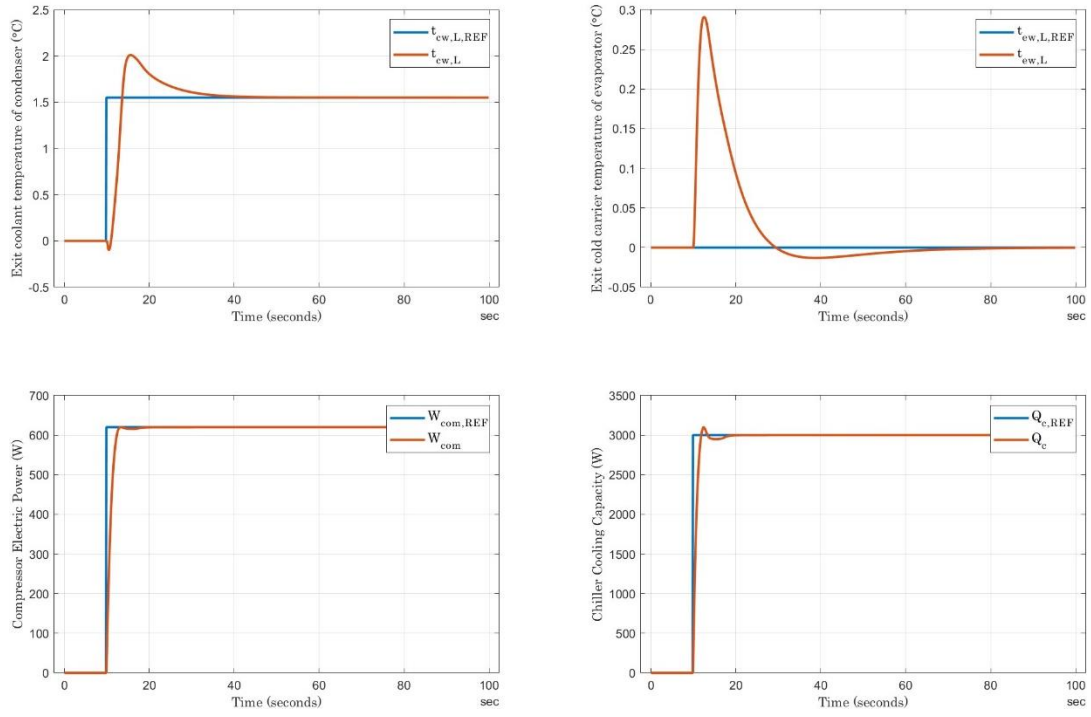


Figure 6-8: Output responses due to a step change in cooling load by 3000 W

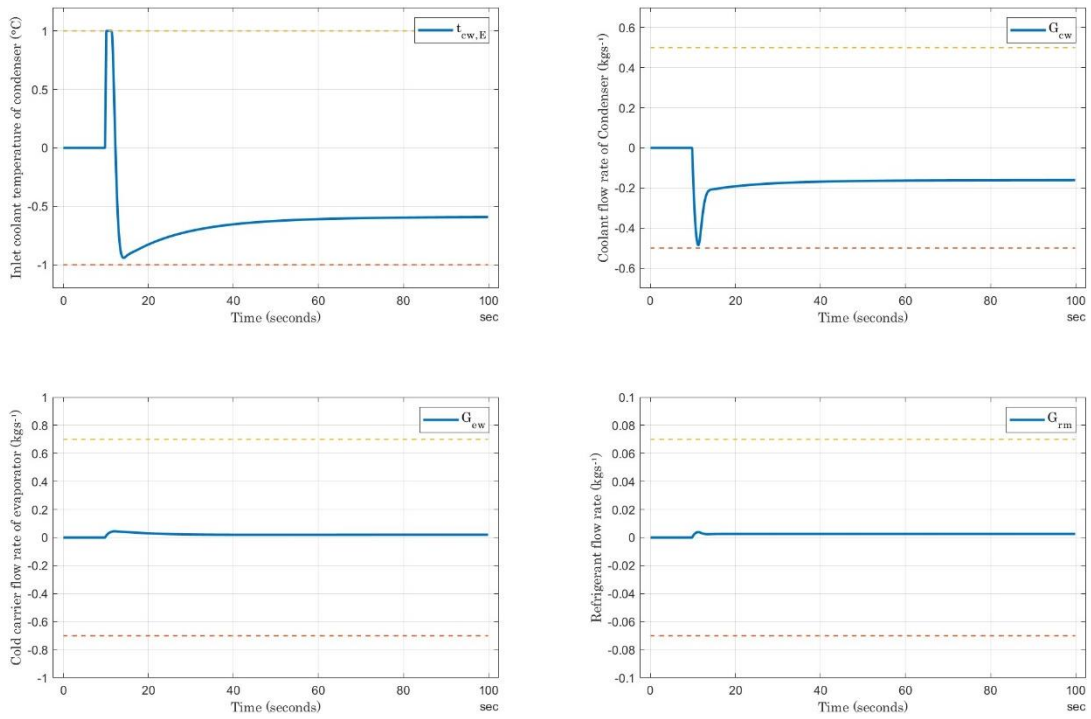


Figure 6-9: Control signals due to a step change in cooling load by 600 W

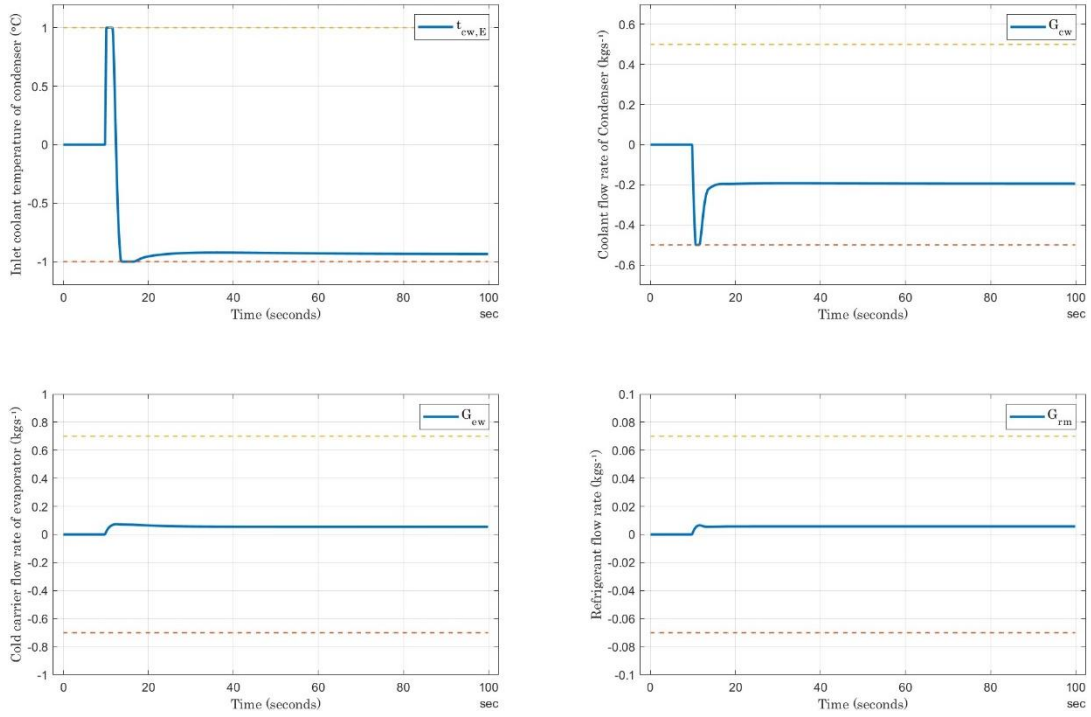


Figure 6-10: Control signals due to a step change in cooling load by 1200 W

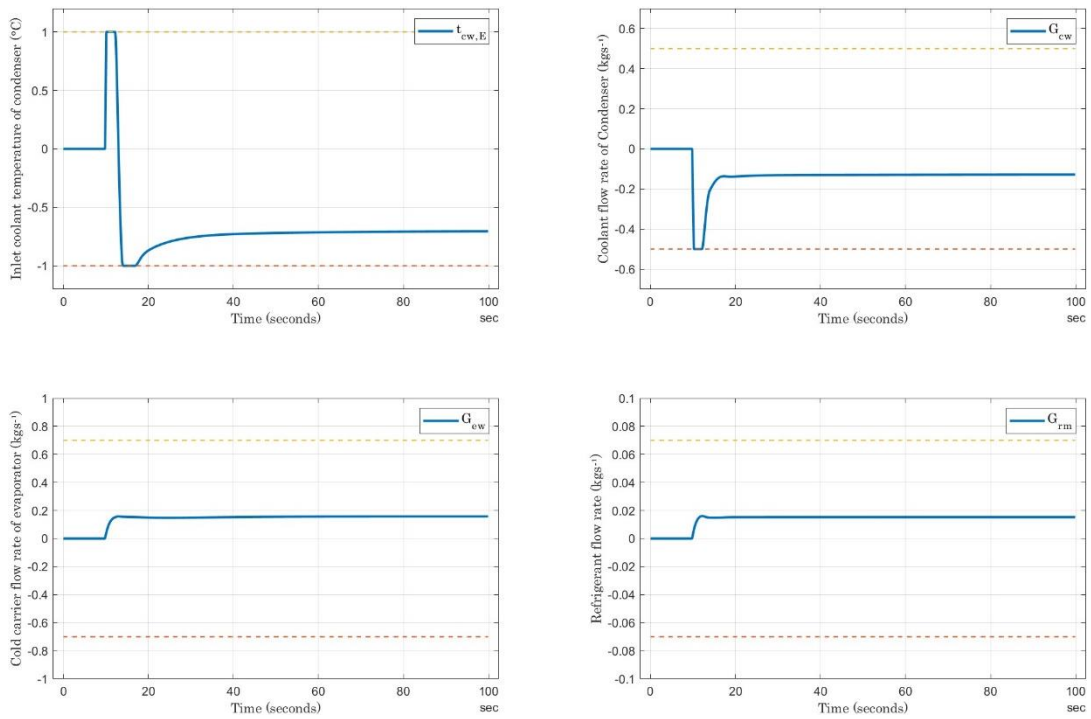


Figure 6-11: Control signals due to a step change in cooling load by 3000 W

## 6.4.2 Trajectory Tracking – Leaving Chilled liquid Temperature

The output responses of the closed-loop system due to a step change in the leaving chilled liquid temperature of evaporator by 1 °C and 2 °C are depicted in Figures 6-12 and 6-13, respectively. On the other hand, the optimal control trajectory to meet the new set-points are illustrated in Figures 6-14 and 6-15, respectively.

Aligning with the results of Section 6.3.2, the exit coolant temperature of condenser converged very slowly. It also exhibited some oscillations and small to moderate overshoots. On the other hand, the exit chilled liquid temperature of the evaporator had zero overshoot in favor of a moderate settling time. The compressor’s electric power and cooling load converged very quickly, but the overshoot was moderate and sharp. Control inputs were smooth and without sharp oscillations, except for the inlet coolant temperature of the condenser. Moreover, the refrigerant flow rate had a very small change in amplitude (less than 0.01 kg/s). This deduces that when the load remained the same whilst a change of the evaporator exit carrier temperature is required, the ancillary equipment to the chiller (i.e. cooling tower, condenser and evaporator pumps) are sufficient, and the compressor involvement is minimal.

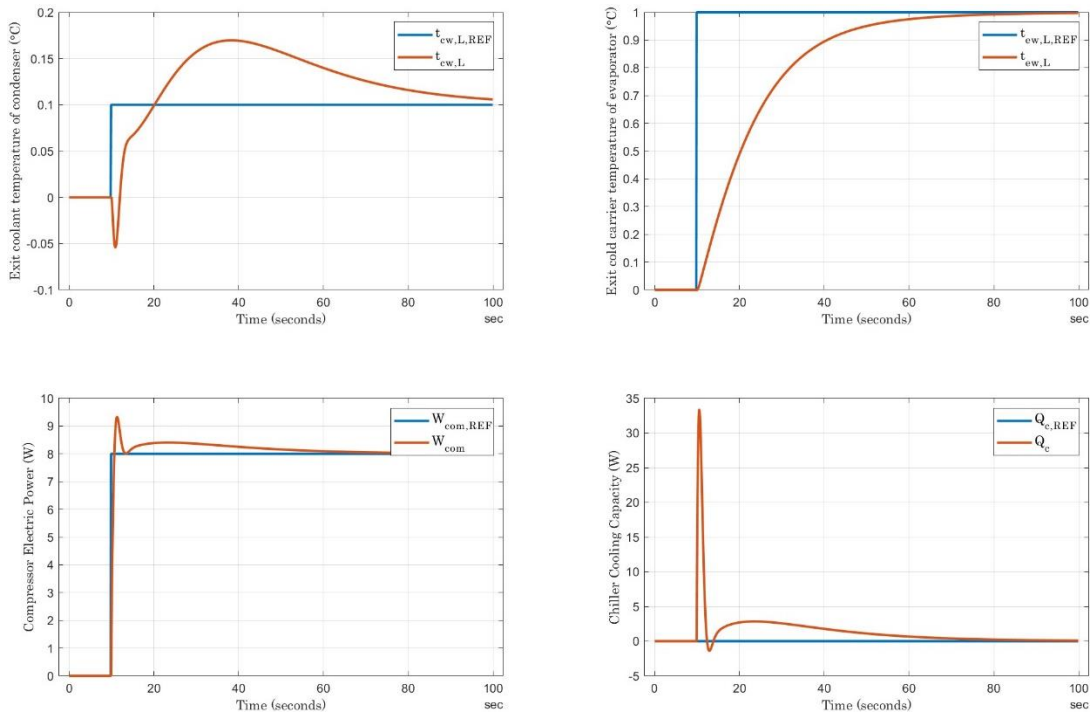


Figure 6-12: Output response due to a step change in exit chilled liquid temperature of evaporator by 1 °C

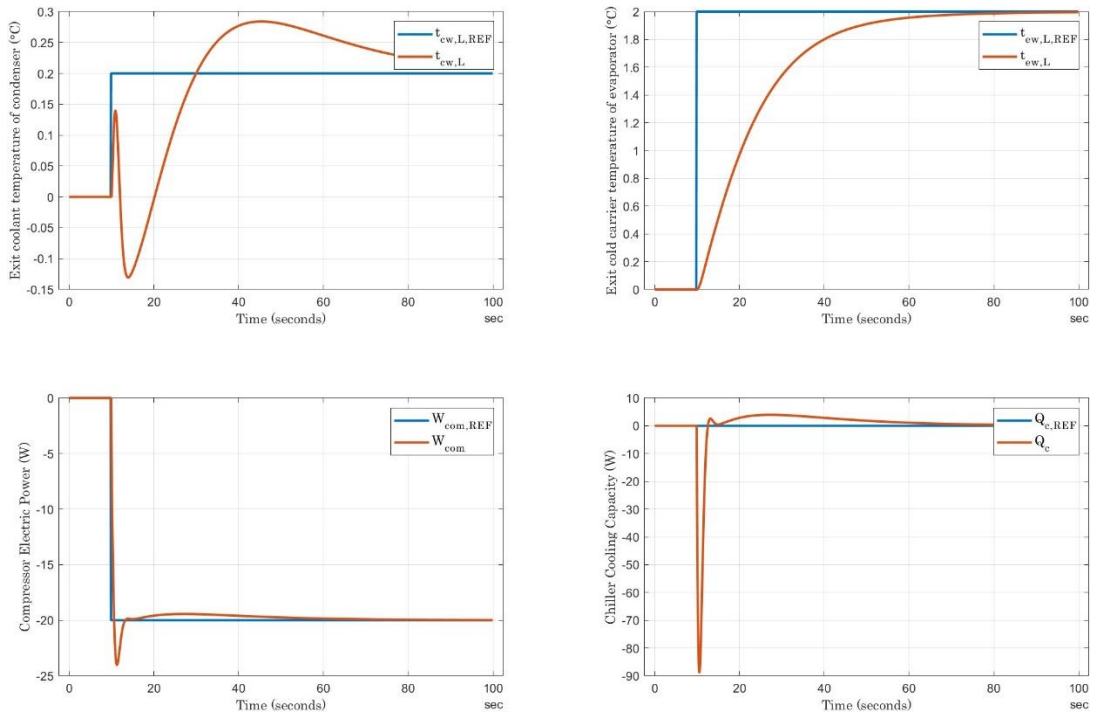


Figure 6-13: Output response due to a step change in exit chilled liquid temperature of evaporator by 2 °C

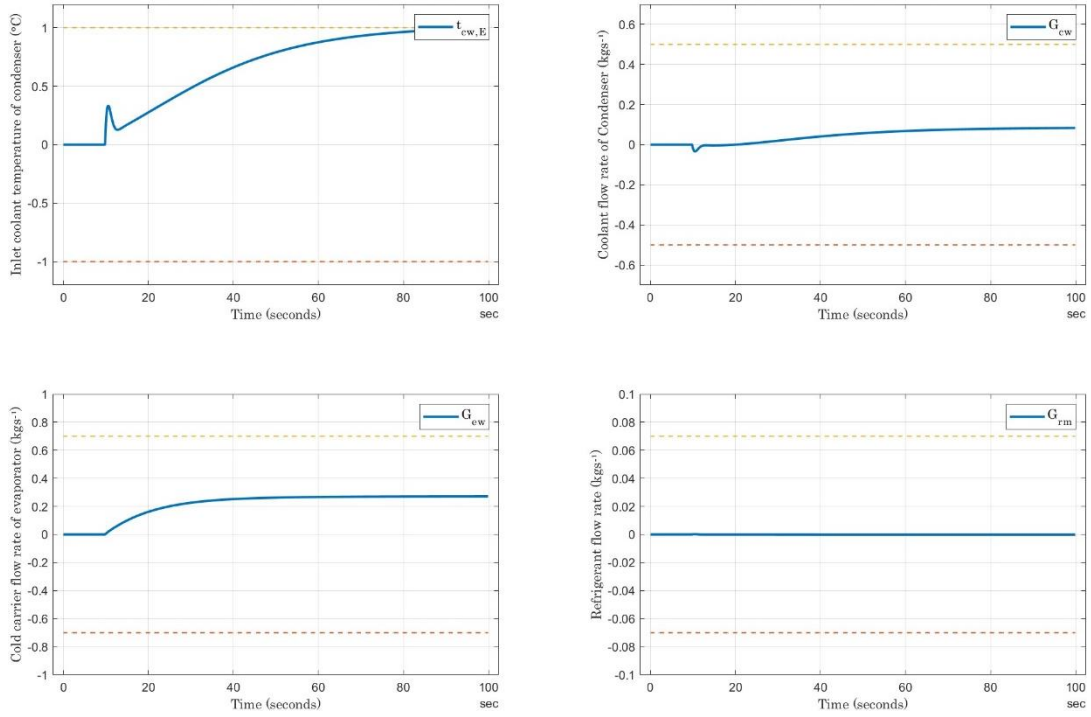


Figure 6-14: Control signals due to a step change in exit chilled liquid temperature of evaporator by 1 °C

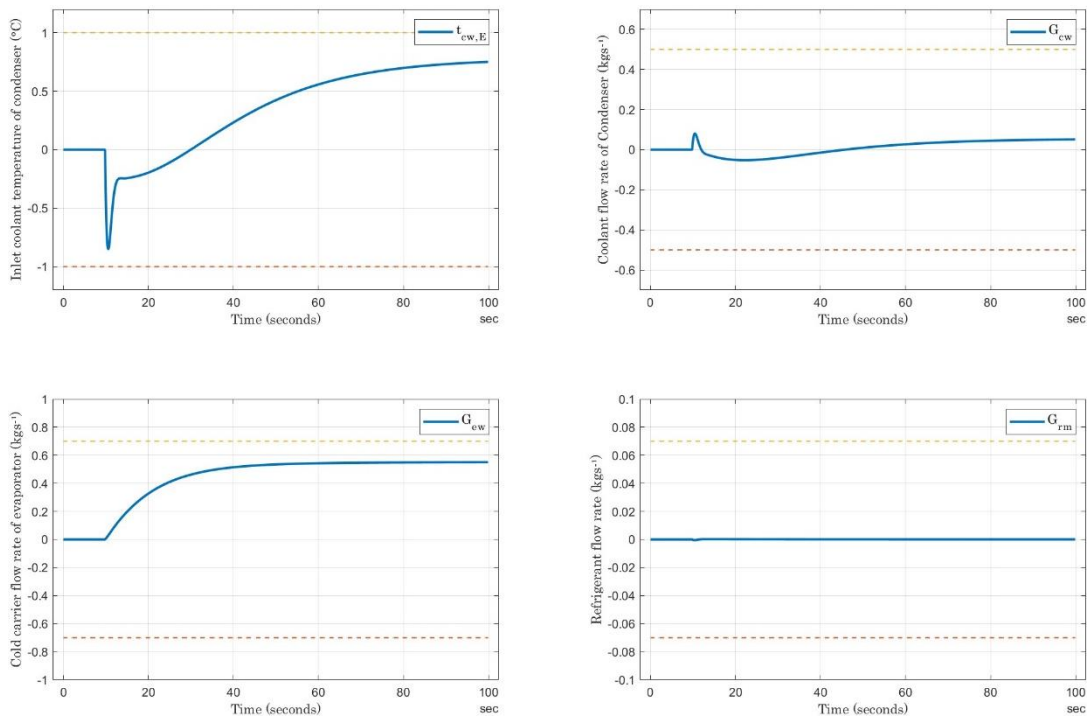


Figure 6-15: Control signals due to a step change in exit chilled liquid temperature of evaporator by 2 °C

### 6.4.3 Disturbance Rejection – Entering Chilled liquid Temperature

To further enhance the system performance, an adaptive strategy is adopted. In the disturbance rejection test, a different set of controller input weights were considered as shown in Table 6-1. The output response due to a step change in the entering chilled liquid temperature of evaporator by 0.5 °C and 2.5 °C are shown in Figures 6-16 and 6-17, respectively. The applied control inputs to regulate the system is for the same conditions are as illustrated in Figures 6-18 and 6-19, respectively.

The controller's performance in rejecting disturbance was fast with minimal overshoot of less than 10% for most outputs. However, two cycle oscillations for all outputs. Furthermore, steady-state error was zero for all outputs. As the case with trajectory tracking, inlet coolant temperature of the condenser had an oscillatory behavior. Similar effects were notice on the coolant flow rate of the condenser as well. The flow rate of the refrigerant did not change for the applied disturbance input values. Thus, the same conclusion made earlier in Section 6.4.2 holds true for this test.

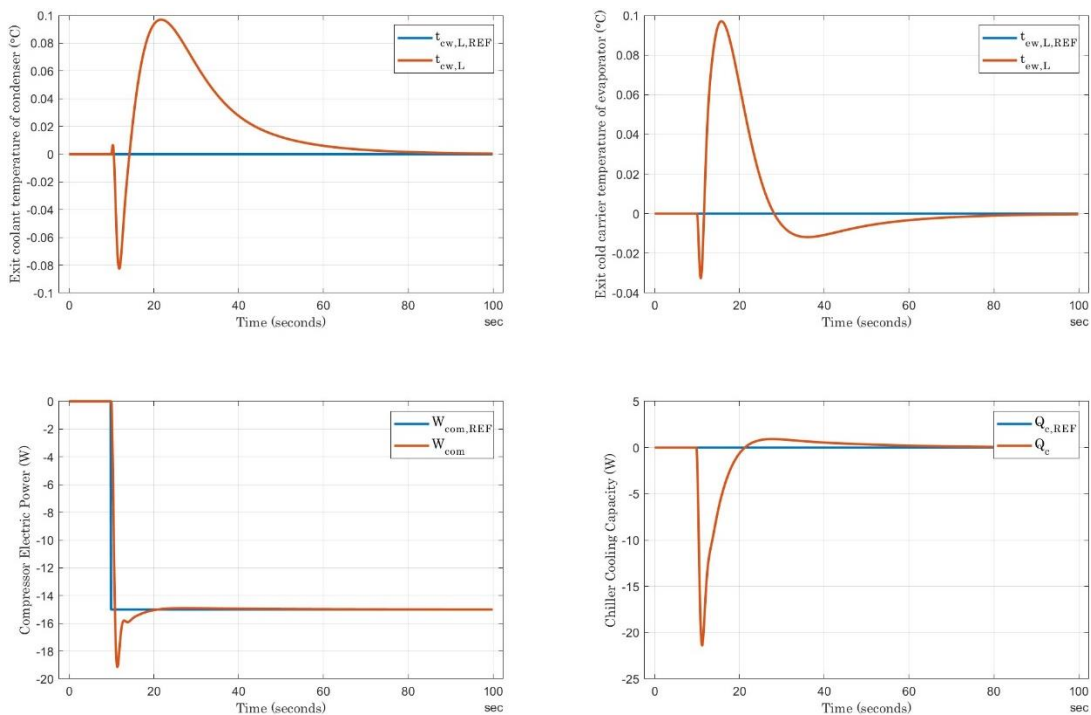


Figure 6-16: Output response due to a step change in entering chilled liquid temperature of evaporator by 0.5 °C

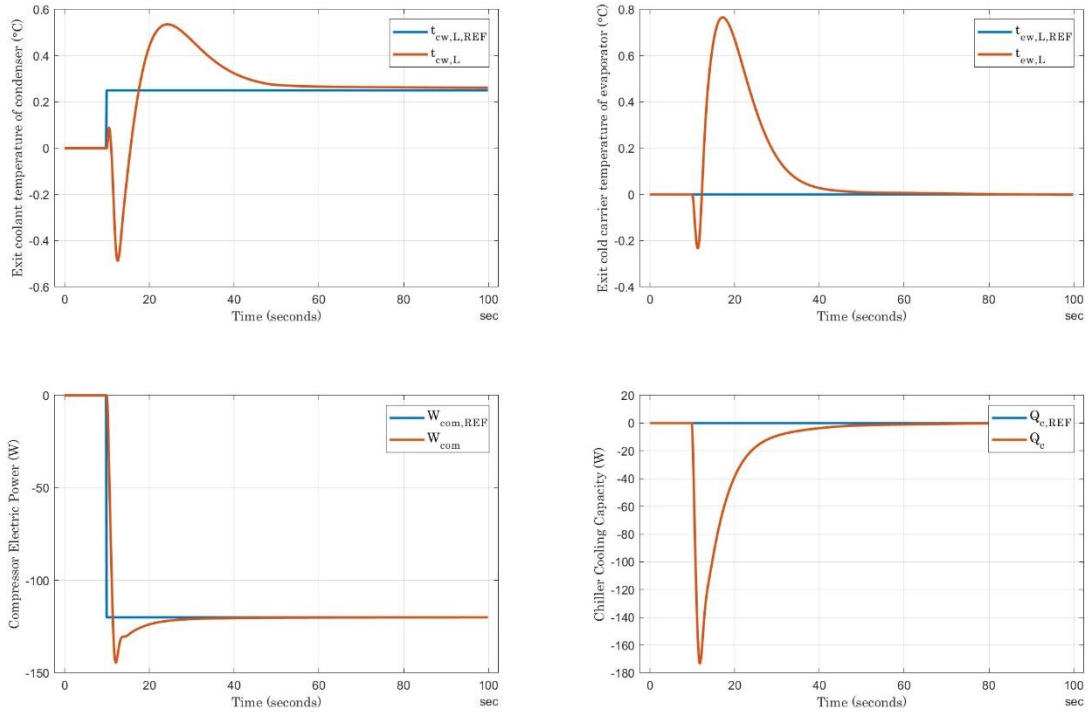


Figure 6-17: Output response due to a step change in entering chilled liquid temperature of evaporator by 2.5 °C

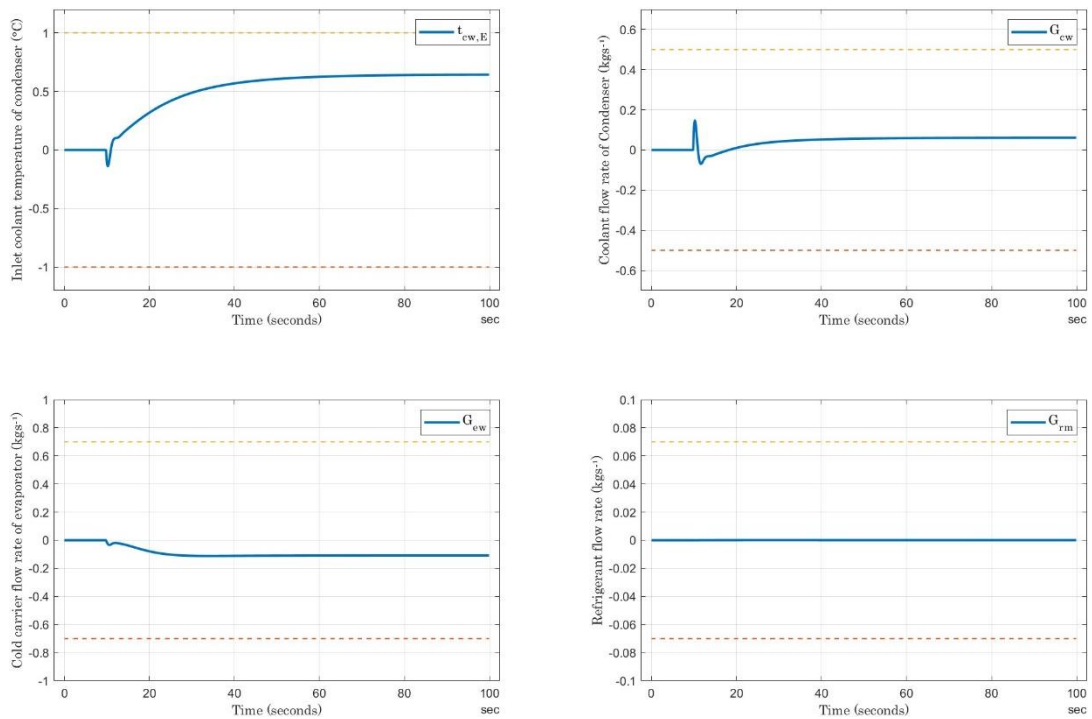


Figure 6-18: Control signals due to a step change in entering chilled liquid temperature of evaporator by 0.5 °C

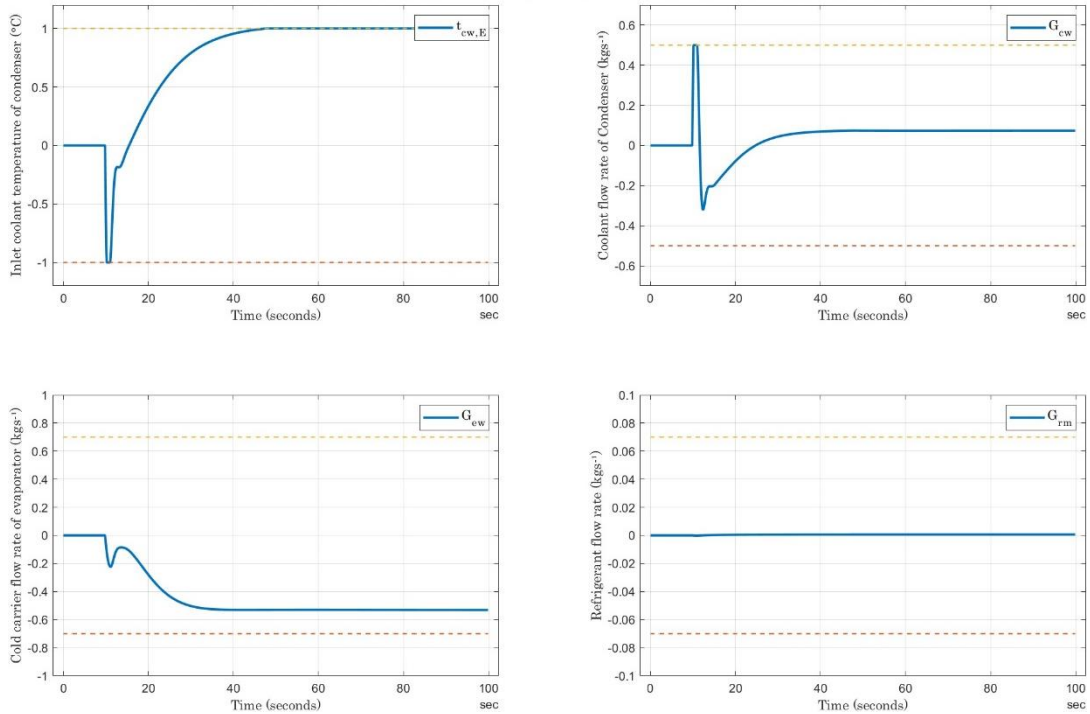


Figure 6-19: Control signals due to a step change in entering chilled liquid temperature of evaporator by 2.5 °C

## Chapter 7 Analysis and Performance Comparison between the Control Approaches

The output responses of the three control techniques presented in the previous chapters compared and analyzed in this Chapter in terms of trajectory tracking and disturbance rejection. Two cases are considered for trajectory tracking, namely, a step change in the cooling load and a step change in the exit chilled liquid temperature of the evaporator. Moreover, in the first test trajectory tracking test, the exit chilled liquid temperature shall be regulated to its nominal value (i.e. zero), and the same holds true in the second test.

In the disturbance performance test, controller performance is evaluated based on its ability to reject a measured input disturbance in the form of a step change in the entering chilled liquid temperature of the evaporator. Furthermore, the remaining two outputs, namely, the

exit coolant temperature of the condenser and the compressor's electric power are user adjustable or variable reference values that vary based on the change in the main reference outputs. The test values used for the performance tests are given in Tables 4-2, 4-3 and 4-4.

## 7.1 Trajectory Tracking – Cooling Load

The first trajectory tracking test was done when the chiller was subjected to a change in the cooling load. Five values that represent the full testing spectrum from minimum to maximum were selected from Table 4-2 for performance comparison between the controllers. The output response of the closed-loop system using PID, LQI and MPC controllers due to a step change on the cooling load - at  $t = 10$  seconds) - by 200 W, 600 W, 1200 W, 2000 W and 3000 W are shown in Figures 7-1, 7-2, 7-3, 7-4 and 7-5. Likewise, the control input signals waveforms are depicted in Figures 7-6, 7-7, 7-8, 7-9 and 7-10.

Beginning with the change in cooling load, the LQI controller response was perfect with zero overshoot, instant settling time and zero steady-state error for all the cooling loads. MPC responses had a high overshoot of 50% at low capacities, but the overshoot percentage decreased a lot at higher capacities to reach around less than 5%. Furthermore, the MPC controller settling time was fast and it exhibited fewer oscillations (less than 3) and had zero steady-state error. The PID controllers had high overshoots, good settling time and zero steady-state error.

The PID controllers produced the best results in terms of regulating the exit chilled liquid temperature of the condenser back to its initial state. LQI had a good response in general with small overshoots/undershoots (less than  $|\pm 0.1|$  °C, yet it had the highest settling time of around 50 seconds. On the other hand, MPC controller overshoot/undershoot was considerable high when compared to the other two controllers of around  $|\pm 0.3|$  °C, but had a slightly smaller settling time than the LQI controller at higher capacities. For all controllers, zero-steady state error was attained.

The other two variable reference outputs were manipulated such as to have the lowest exit coolant temperature of the condenser and less compressor power consumption. The PID performance became unstable beyond the values shown on Table 4-2 and output response figures. Hence, it can be concluded that the LQI and MPC controllers yielded the lower energy consumption. In terms of overshoot/undershoot and settling time, LQI and MPC had very similar performances overall with minimal or no overshoot/undershoot, but MPC had a better

transient speed as it converged faster, especially for the compressor's electric power. The PID controller, on the other hand, had high and multiple overshoot/undershoot cycles before reaching steady state.

The control signals shown in Figures 7-6, 7-7, 7-8, 7-9 and 7-10 show that the LQI controller had the lowest oscillations and was far away from the dashed saturation lines. The MPC controller had decent control signals for all inputs except the inlet coolant temperature of the condenser. As there were sharp single cycle oscillation that reached the saturation point. PID controller applied control inputs had the highest frequency of decaying oscillations, but with lower amplitude than the MPC controller.

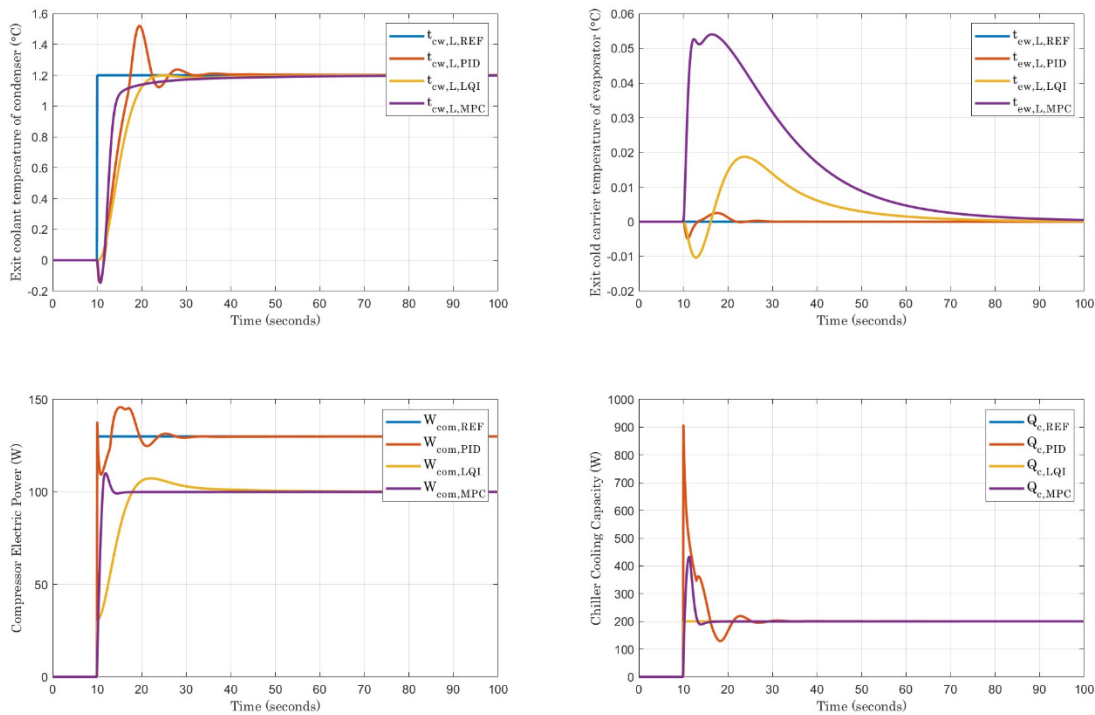


Figure 7-1: Output responses due to step change in cooling load by 200 W

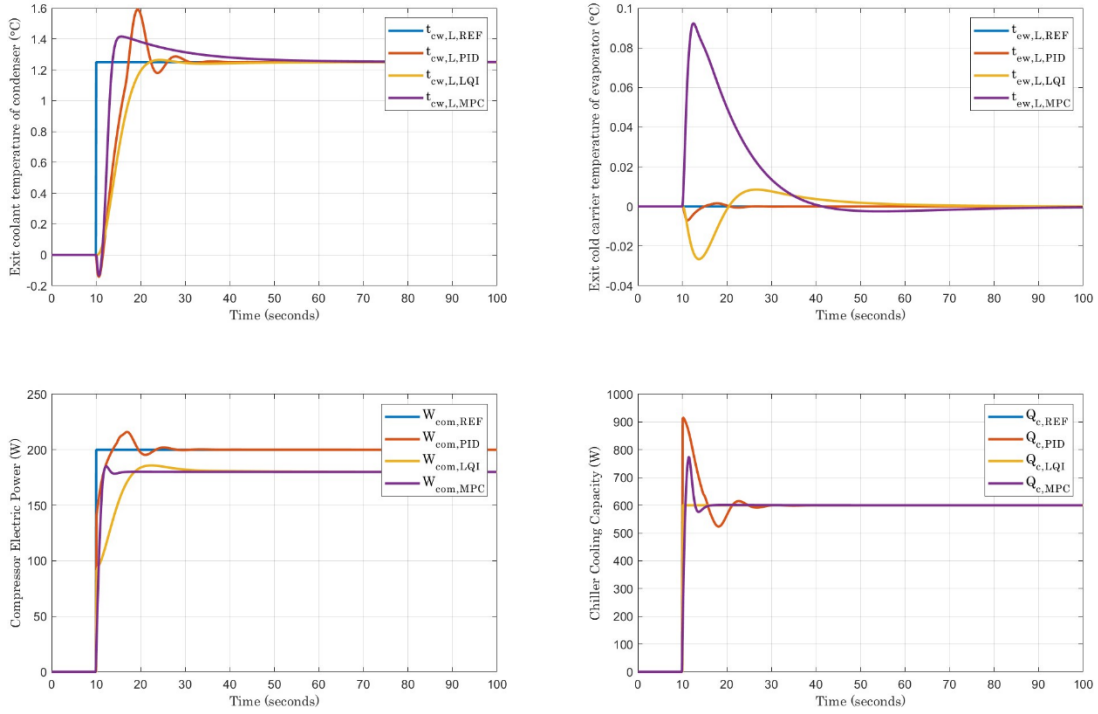


Figure 7-2: Output responses due to step change in cooling load by 600 W

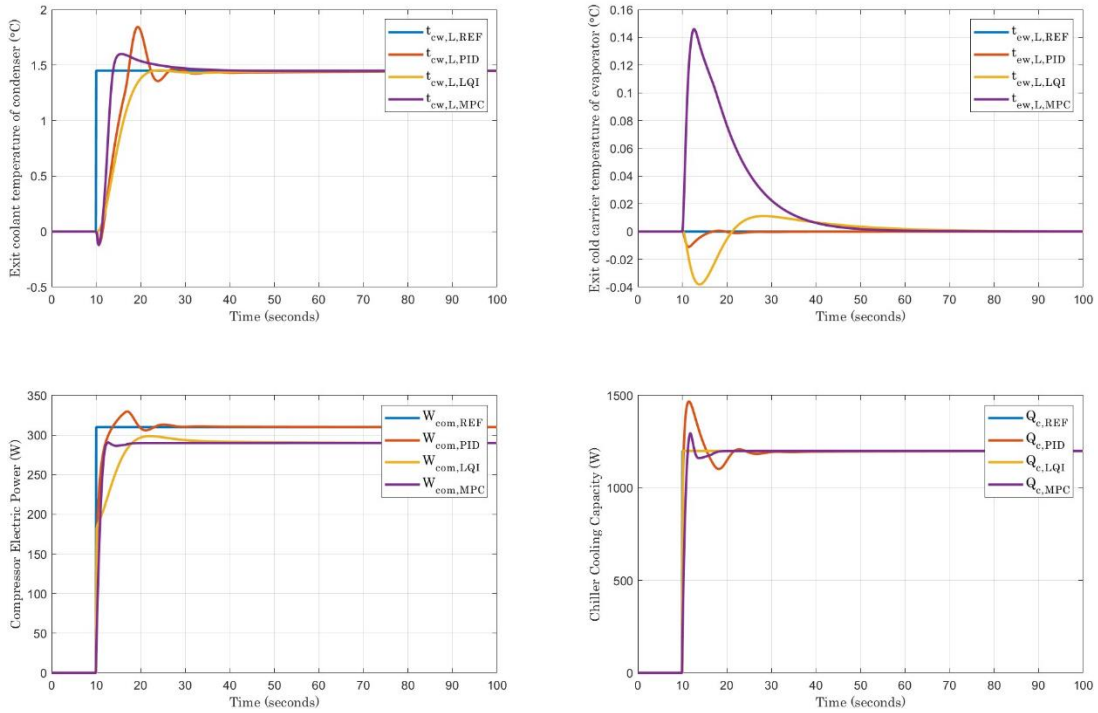


Figure 7-3: Output responses due to step change in cooling load by 1200 W

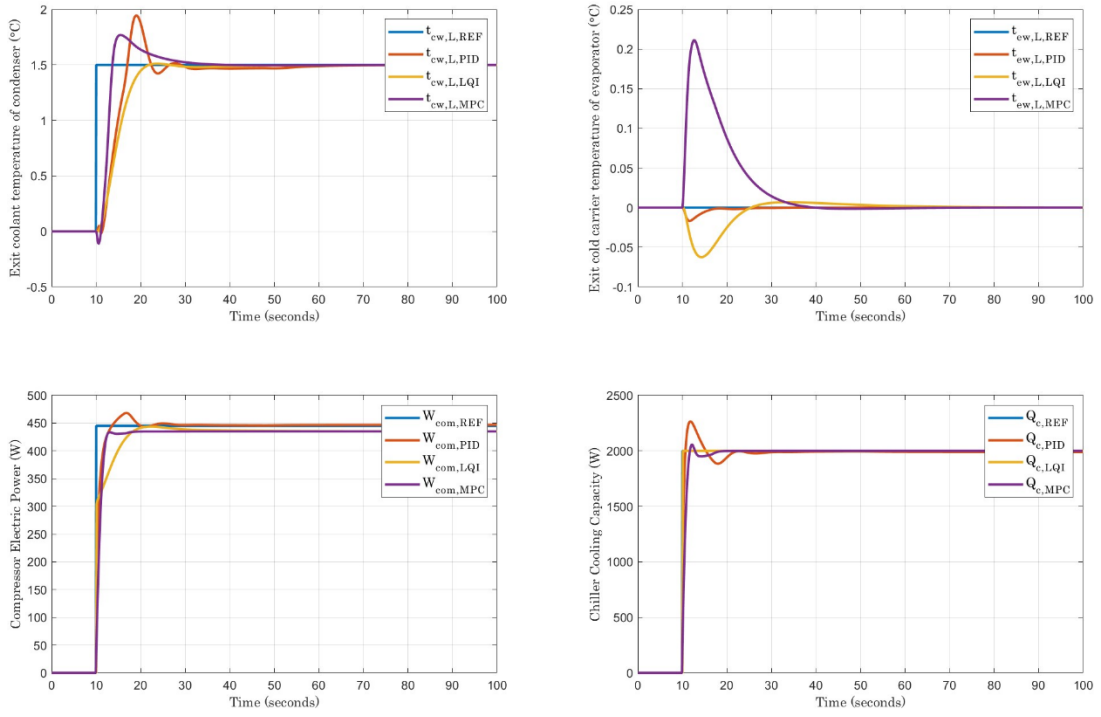


Figure 7-4: Output responses due to step change in cooling load by 2000 W

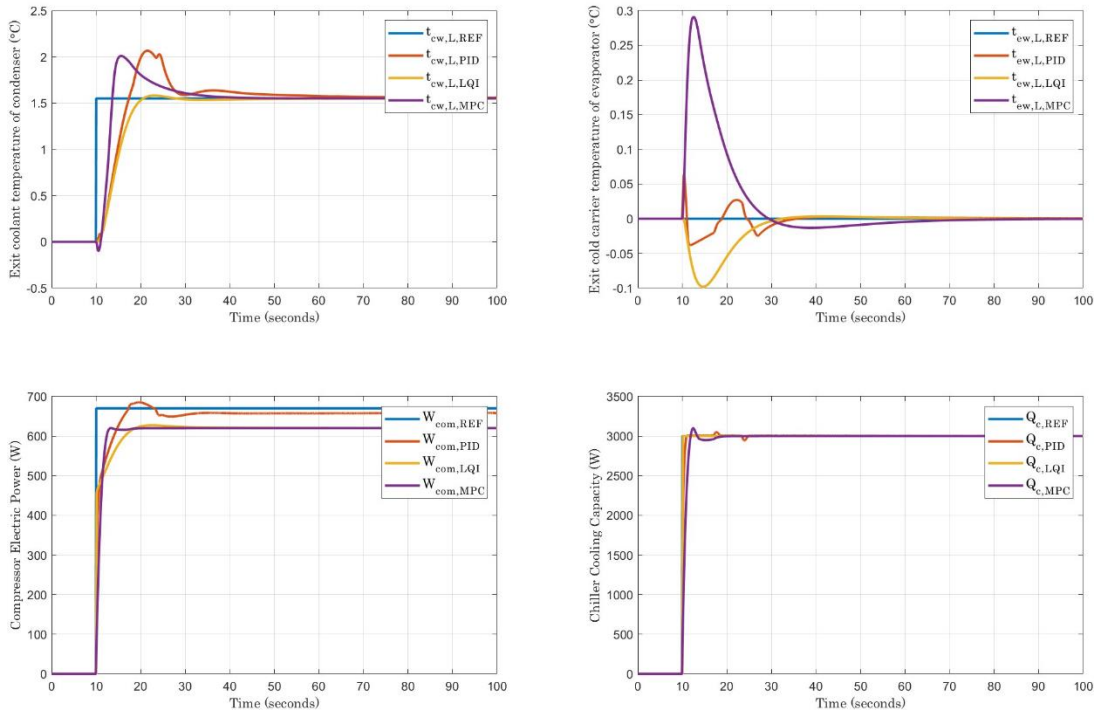


Figure 7-5: Output responses due to step change in cooling load by 3000 W

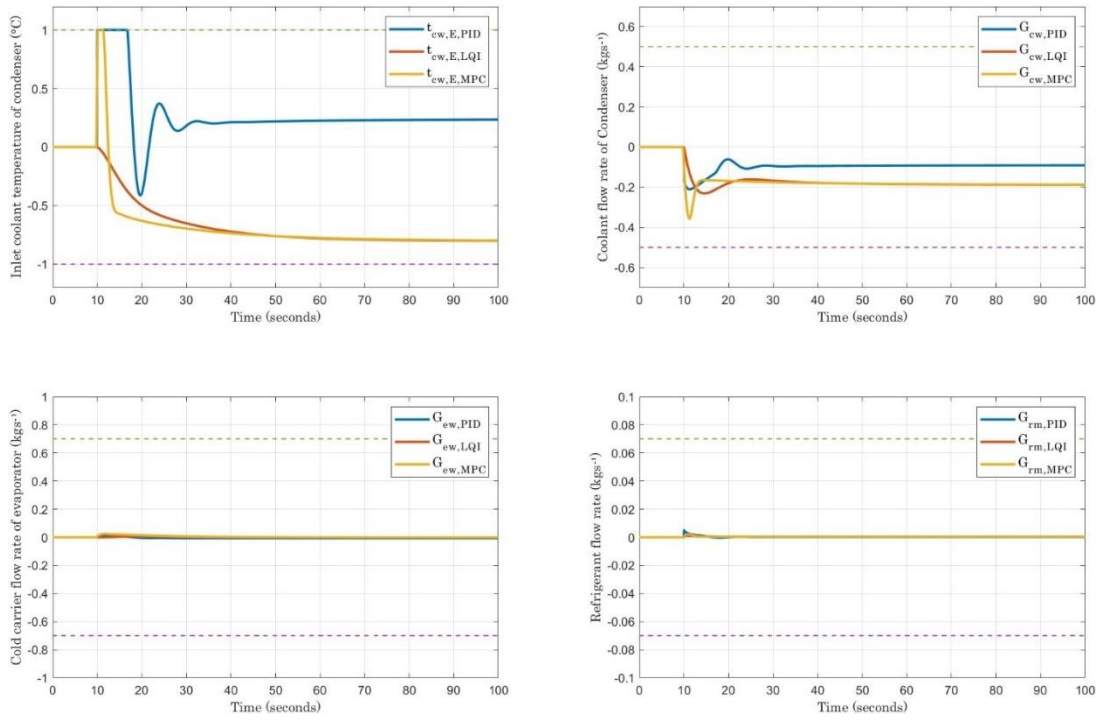


Figure 7-6: Control signals due to step change in cooling load by 200 W

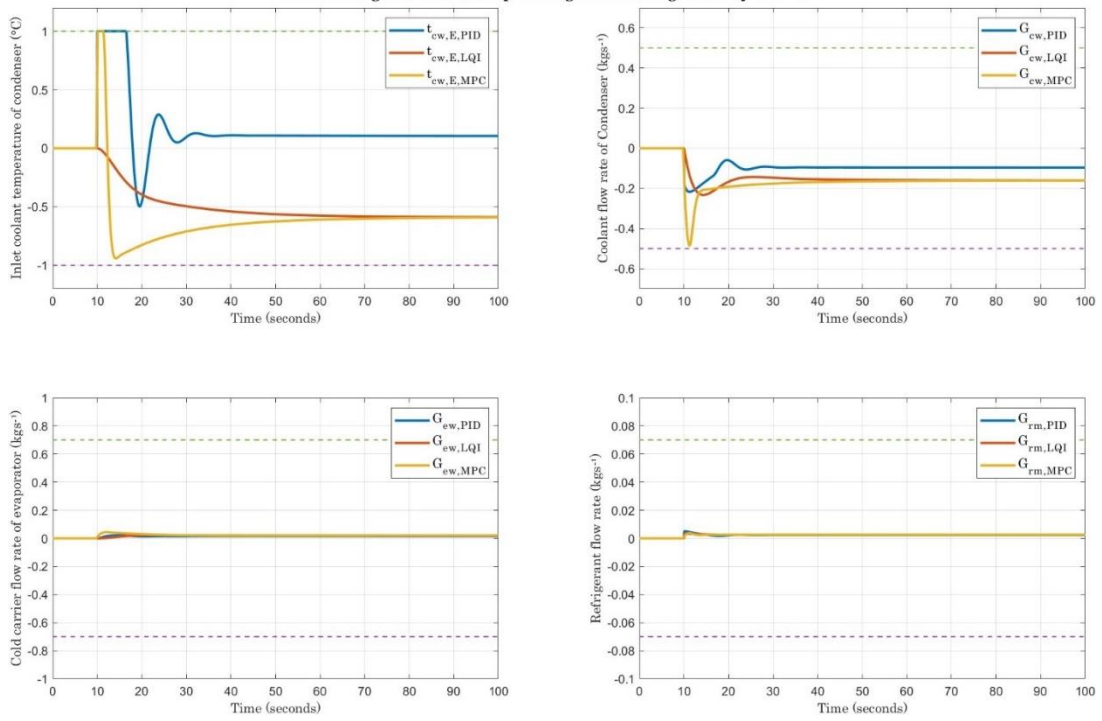


Figure 7-7: Control signals due to step change in cooling load by 600 W

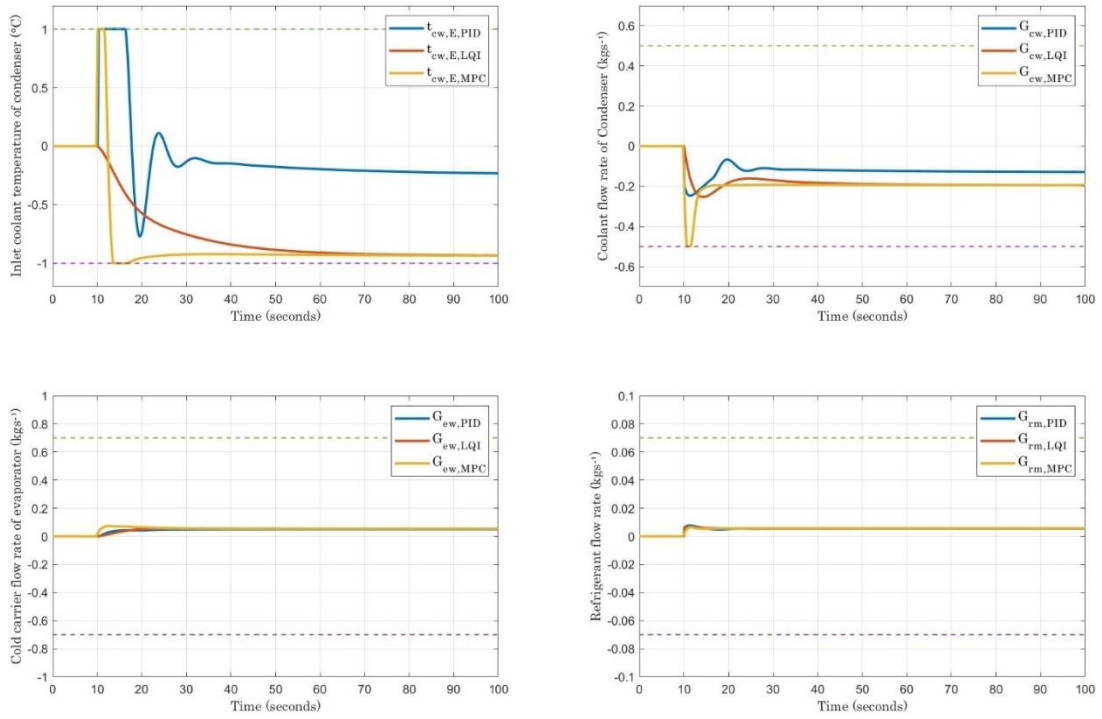


Figure 7-8: Control signals due to step change in cooling load by 1200 W

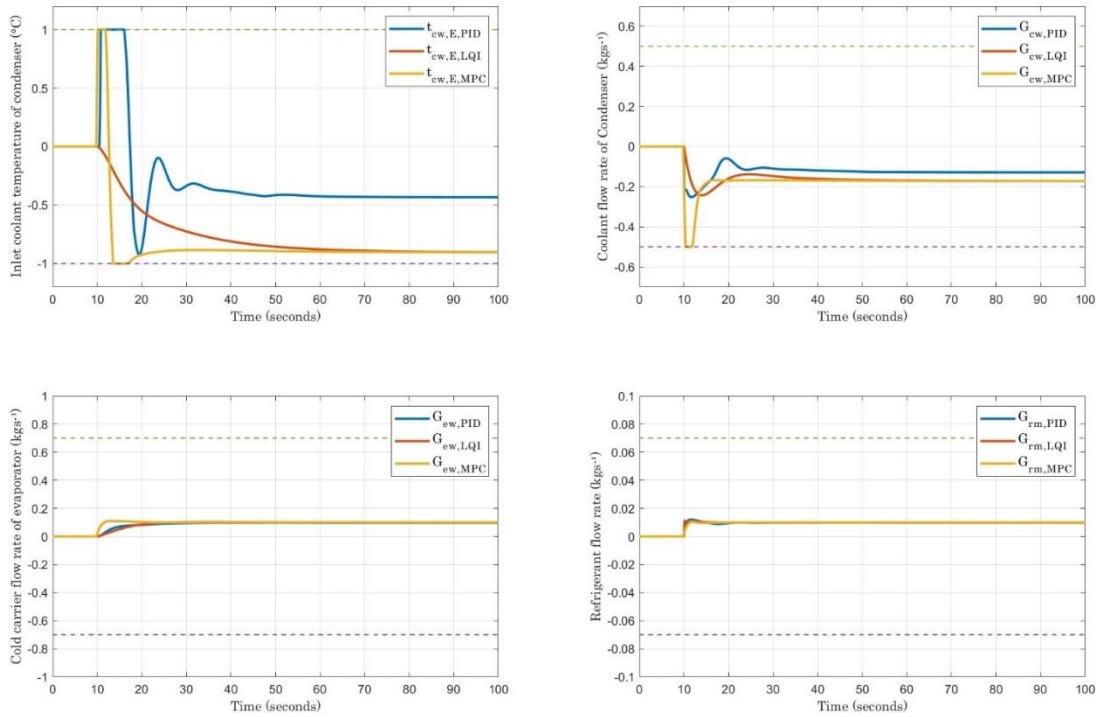


Figure 7-9: Control signals due to step change in cooling load by 2000 W

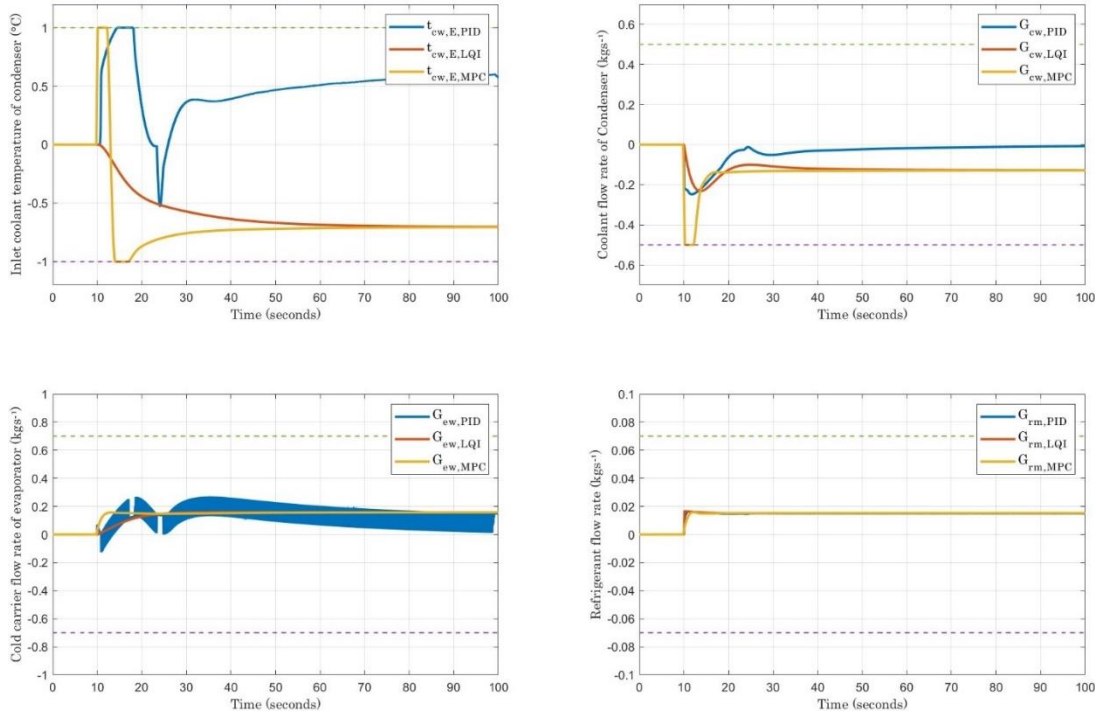


Figure 7-10: Control signals due to step change in cooling load by 3000 W

## 7.2 Trajectory Tracking – Leaving Chilled liquid Temperature

In this test, two values were selected from Table 4-3 for performance comparison between the controllers. The output response of the closed-loop system using PID, LQI and MPC controllers due to a step change on the exit chilled liquid temperature of the evaporator - at  $t = 10$  seconds) - by  $1\text{ }^{\circ}\text{C}$  and  $2\text{ }^{\circ}\text{C}$  are shown in Figures 7-11 and 7-12. The control input signals waveforms are given in Figures 7-13 and 7-14.

The output response to reach the desired new set-point temperature of the leaving evaporating liquid was accompanied with one or more oscillations when PID controllers were used. Yet, the PID controller had the fastest settling time (irrespective of the constant oscillations at  $2\text{ }^{\circ}\text{C}$ ). On the other hand, the LQI and MPC controllers had an overdamped response (i.e. 0% overshoot/undershoot). MPC were slowest among the other two controllers with a settling time of around 50 seconds. All controllers achieved zero tracking error at the end of the 100 seconds simulation window.

As with the previous test, the LQI regulated the cooling load with almost zero overshoot/undershoot and very fast settling time. MPC quickly regulated the cooling capacity but at the expense of an undershoot of less than 100 W at  $2\text{ }^{\circ}\text{C}$  exit evaporating temperature,

which is a small value. PID controller however, experienced several oscillations with high impulse shape overshoots before reaching steady state. Overall, all controllers regulated the cooling capacity with zero steady state error and settling time of less than 30 seconds.

As with the previous test, better overall energy expenditure was noticed when using an LQI and MPC controllers as opposed to PID. Furthermore, multiple high amplitude decaying oscillations were noticed when using PID controllers. In contrast, LQI and MPC controllers reached steady state at low frequency and low amplitude overshoots/undershoots.

In terms of control signals, severe and sharp oscillations were noticed in the evaporator's flow when using PID. Furthermore, oscillations were also noticed on the inlet coolant temperature of condenser when using PID controllers. On the contrary, less oscillations and more natural waveforms for all control inputs were observed when using LQI and MPC controllers. For all controllers, the refrigerant flow rate was kept at minimum; and this explains the low power consumption to achieve the new desired exit evaporating chilled liquid temperature.

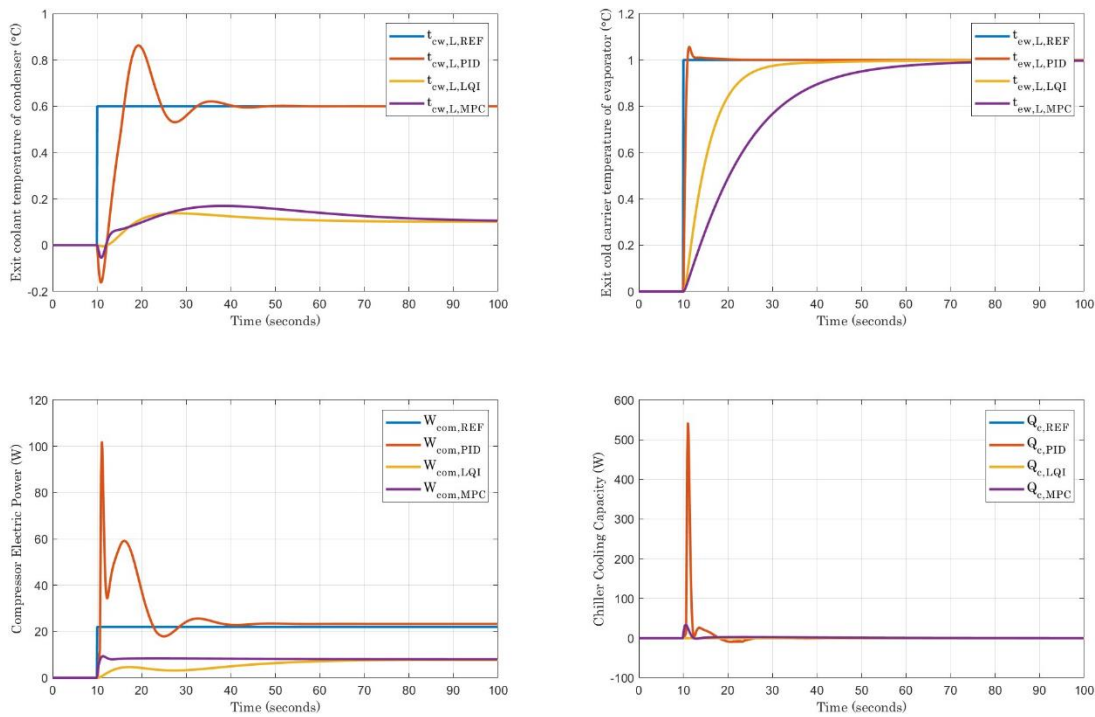


Figure 7-11: Output responses due to a step change in exit chilled liquid temperature of evaporator by 1 °C

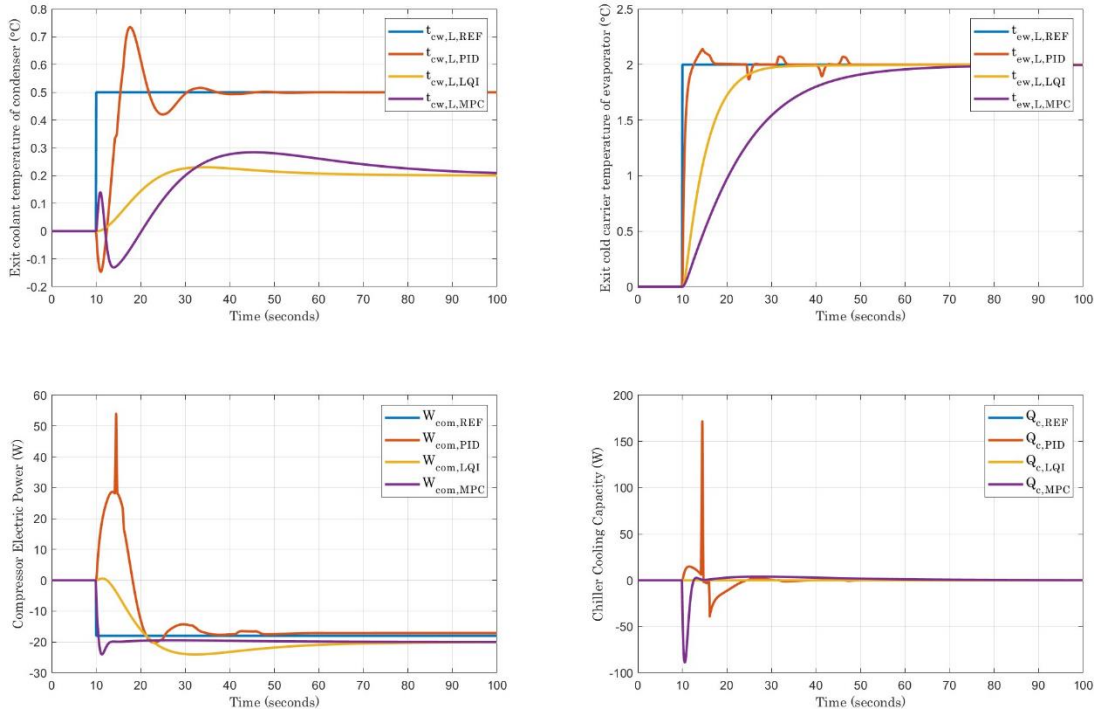


Figure 7-12: Output responses due to a step change in exit chilled liquid temperature of evaporator by 2 °C

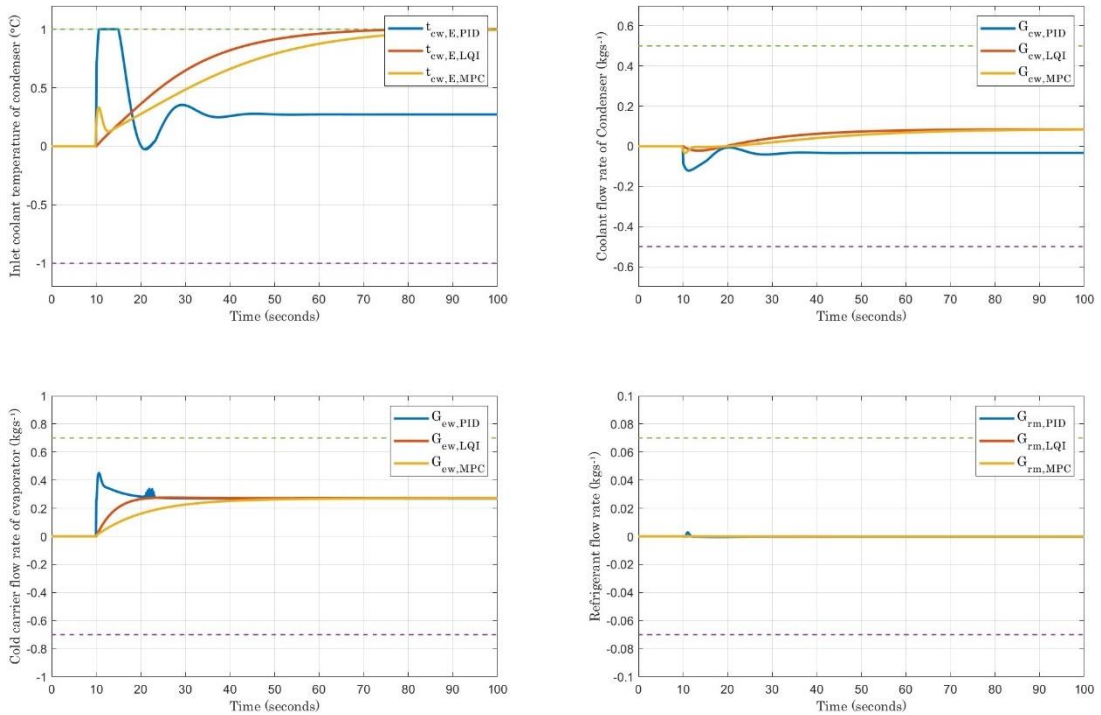


Figure 7-13: Control signals due to a step change in exit chilled liquid temperature of evaporator by 1 °C

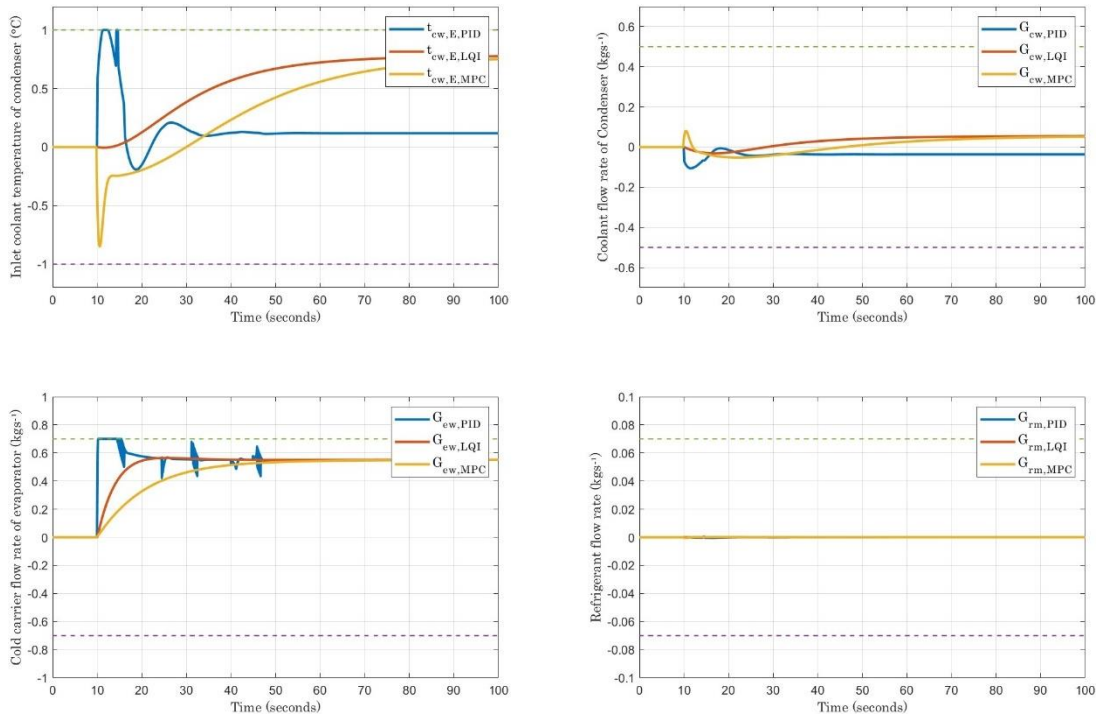


Figure 7-14: Control signals due to a step change in exit chilled liquid temperature of evaporator by 2 °C

### 7.3 Disturbance Rejection – Entering Chilled liquid of Evaporator

As the chiller undergoes measured input disturbance, the effectiveness of the controllers to reject the entering chilled liquid of the evaporator change in temperature was examined. Two input disturbance values from Table 4-4 were select to demonstrate the controllers’ performance entering chilled liquid temperature of the evaporator for the values outlined in Table 4-4. The output response of the LQI controller due to a step change in the entering chilled liquid temperature of evaporator by 0.5 °C and 2.5 °C are shown in Figures 7-15 and 7-16, respectively. The applied control inputs to regulate the system is for the same conditions are as illustrated in Figures 7-17 and 7-18, respectively.

For the two outputs that need to be regulated, namely, exit chilled liquid temperature of the evaporator and the cooling capacity, the PID controller had the best response in regulating the output in terms of overshoot and settling time for the former. However, the PID was the least effective controller to regulate the cooling capacity since high amplitude overshoot were noticed at 2.5 °C and sharp oscillations at 0.5 °C. LQI had the least overshoot/undershoot and with quick response time. MPC controller was the slowest of the three controllers to reach steady state and the highest overshoot/undershoot among the three. Despite the high

relative overshoot/undershoot in the MPC, these values are very small in comparison to the actual cooling capacity the chiller can reach.

All three controllers demonstrated similar transient behavior to meet the new setpoints on the exit coolant temperature of the condenser and compressor's electric power. However, LQI and MPC have again demonstrated their ability to minimize the energy expenditure by having lower setpoints for these two outputs.

To reject the applied input disturbance, all controllers relied on using three out of the four inputs. Hence, there were minor, if any, requirement to adjust the refrigerant flow rate of the condenser, and the system relied on changing the inlet temperature of the condenser's coolant using the cooling tower and increasing the flow rate of the evaporator's and condenser fluid to reject the input disturbance.

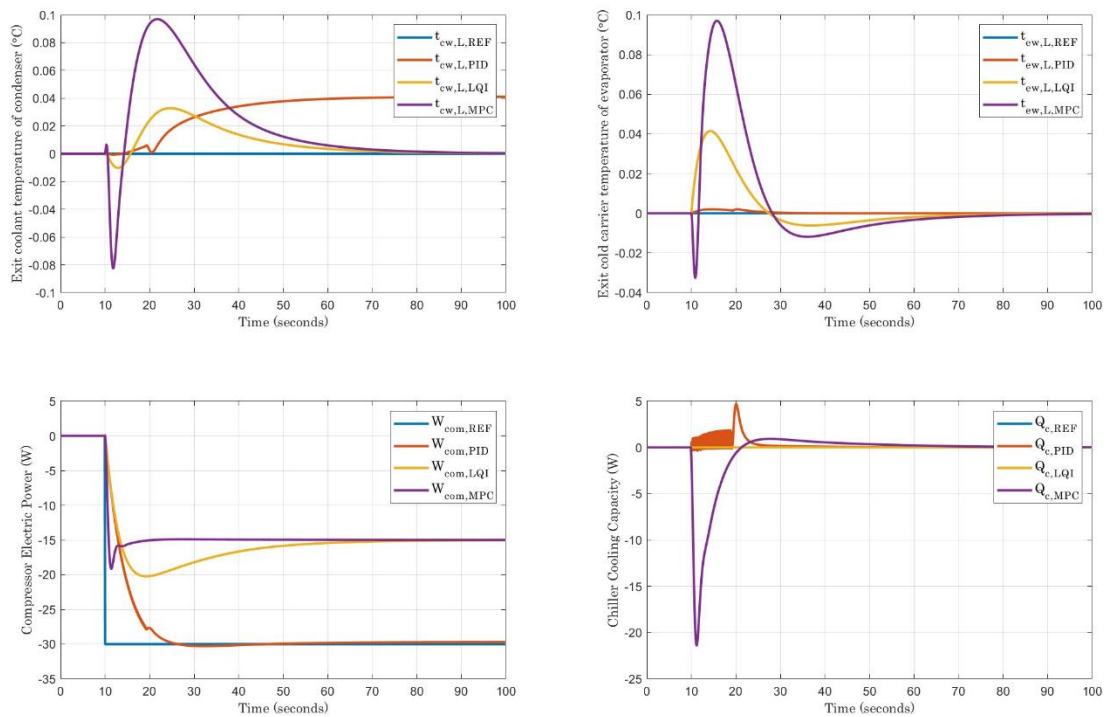


Figure 7-15: Output responses due to a step change in entering chilled liquid temperature of evaporator by 0.5 °C

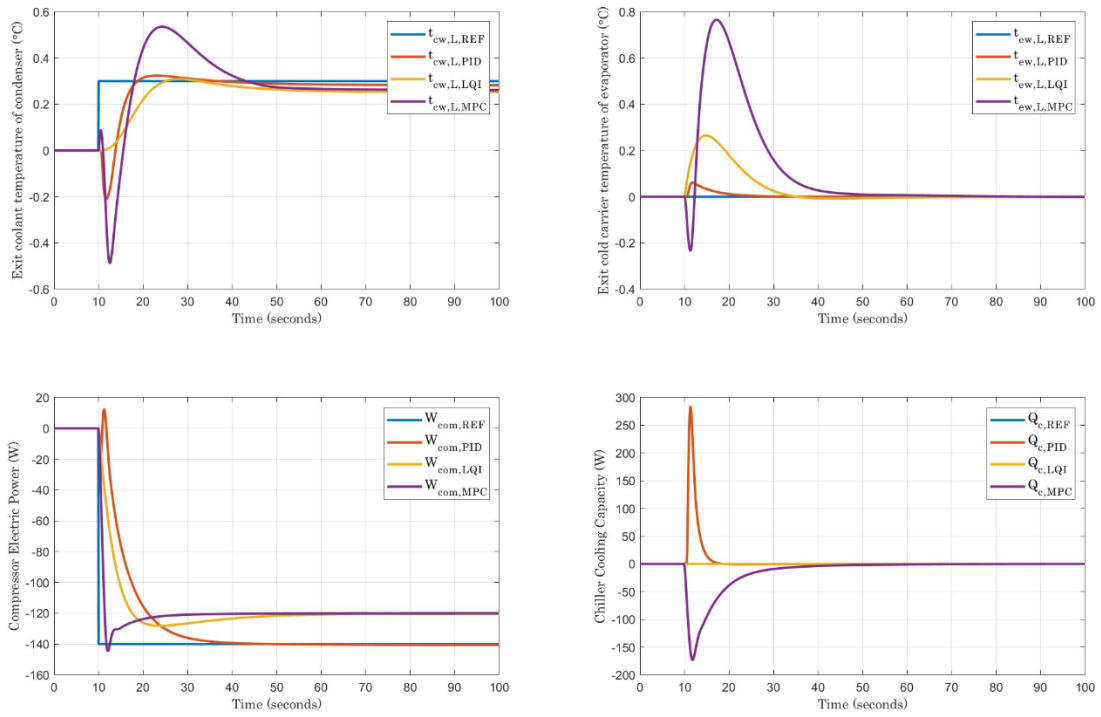


Figure 7-16: Output responses due to a step change in entering chilled liquid temperature of evaporator by 2.5 °C

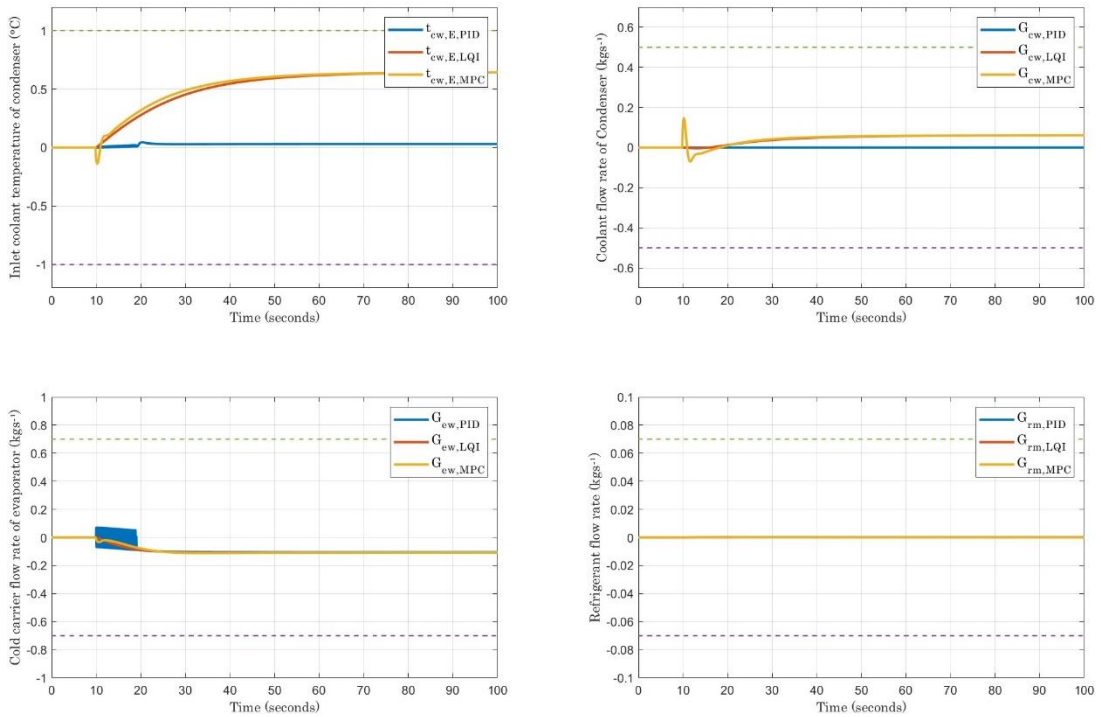


Figure 7-17: Control signals due to a step change in entering chilled liquid temperature of evaporator by 0.5 °C

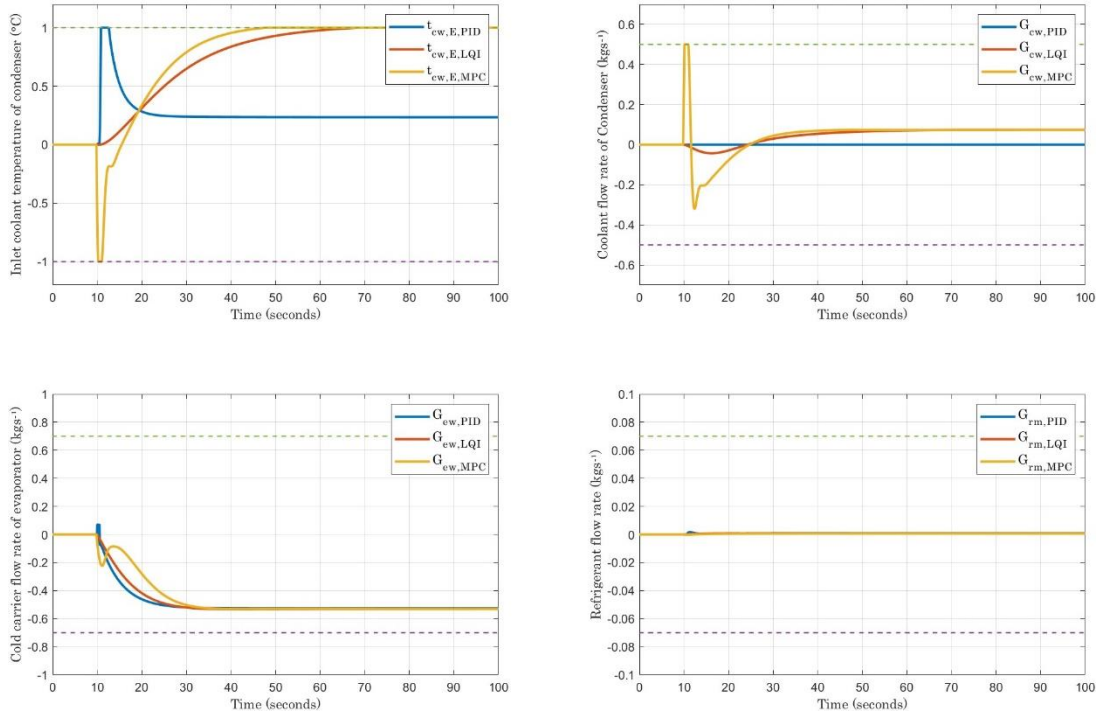


Figure 7-18: Control signals due to a step change in entering chilled liquid temperature of evaporator by 2.5 °C

## Chapter 8 Conclusions and Future Work

In the framework of this thesis, the control of a vapor compression liquid chiller was examined. The chiller model was formulated by Yao et al. [28,46] using lumped parameter formulation and the coefficients were computed empirically. Hence, it is classified as a grey-box model. The model's published data in state-space representation were used for controller design. The number of outputs from the original model were modified and the outputs were classified based on their type. Thus, the model used to design the controller included four inputs (condenser coolant liquid entering temperature and flow rate, entering chiller temperature and refrigerant mass flow rate), four outputs (leaving condenser coolant and evaporator chilled liquid temperatures, compressor power and cooling capacity) and six states (condensing and evaporating temperatures, leaving condenser coolant and evaporator chilled liquid temperatures and shell wall temperatures of the condenser and evaporator)

Given that the chiller model is MIMO, two optimal multivariable control techniques were chosen to synthesize the system. The results were compared with PID control. The first control technique is the linear quadratic integral control (LQI). This control technique is an extension of the linear quadratic regulator (LQR). The second applied technique is the model predictive control (MPC). To tune the weights of the MPC controller, genetic algorithms (GA) were used to find a nearly global optimal controller weights.

The control performance was examined under three different tests, namely, a change in the chiller cooling load, a change in the exit chilled liquid temperature and a change in the entering chilled liquid temperature. The first two tests fall under the category of reference tracking and the latter is classified under disturbance rejection. The other two outputs of the system were adjusted such as to achieve the best overall system performance. Although a change in the leaving chilled liquid temperature is not frequent as chiller is designed to operate at a fixed supply and return chilled liquid temperature setpoints, some cooling plant operators increase this leaving temperature in winter (low load season) as another means of capacity control to reduce the number of operational chillers and cut costs.

LQI yielded the best results in general, whilst MPC came in second. Many issues were encountered with PID controllers, such as tuning the system, algebraic discontinuities and instability due to the interference between the controllers. Furthermore, the LQI and MPC controller were able to lower the power consumption of the system by 10% to 20%. Although LQI controller performed better, the MPC controller introduced many features the LQI controller lacked, such as the incorporation of input amplitude and input rate of change constraints. Also, the MPC is more suited for industrial applications as the optimization is done online rather than offline. Putting the difference aside, both LQI and MPC controller proved to be very efficient in reference tracking, regulation and disturbance rejection.

For future work, a more sophisticated chiller model with more states shall be investigated. In addition, integrating the chiller model along with the ancillary equipment such as the cooling tower and pumps would give more resolution to the controller performance. With this configuration and all the equipment working with each other, the need for a supervisory and local controller is inevitable. Therefore, machine learning approaches such as neural networks and neuro-fuzzy would be a good approach to have as a supervisory controller, whilst multivariable control techniques can be deployed as local controllers. As for the presented controllers, the addition of unmeasured noise to the system can be investigated. Also, the use of a different cost function (other than the quadratic cost function) for the MPC controller or a different variation of MPC controllers - such as distributed model predictive control, adaptive model predictive control, economic MPC - could yield better overall results.

## Bibliography

- [1] American Society of Heating, Refrigerating and Air-Conditioning Engineers and Knovel (Firm), "District Cooling Guide". 2013.
- [2] A. Olama "District Cooling: Theory and Practice," CRC Press, vol. 3, (47), 2017.
- [3] Herbert W. "HVAC water chillers and cooling towers; fundamentals, application, and operation, 2d ed," Reference & Research Book News, vol. 27, (1), 2012.
- [4] R. Wiltshire, "Advanced District Heating and Cooling (DHC) Systems", 1st ed, Wood Head Publishing, Series in Energy, 2015.
- [5] V. Thomas, "Centrifugal Chiller - Fundamentals", n.d. [Online]. Available: <https://energy-models.com/centrifugal-chiller-fundamentals> [Accessed Dec. 1, 2020].
- [6] Trane (Firm), "Chiller System Design and Control", Application Engineering Manual, 2011. [Online]. Available: <https://www.tranebelgium.com/files/book-doc/12/fr/12.1hp13yp1.pdf> [Accessed Dec. 1, 2020].
- [7] L. Cline et al., "Variable-Speed Compressors on Chillers", Trane Engineers Newsletter Live, 2015. [Online]. Available: [https://www.trane.com/content/dam/Trane/Commercial/global/products-systems/education-training/continuing-education-gbci-aia-pdh/Variable-Speed-Compressors-On-Chillers/APP-CMC053-EN\\_Course\\_material.pdf](https://www.trane.com/content/dam/Trane/Commercial/global/products-systems/education-training/continuing-education-gbci-aia-pdh/Variable-Speed-Compressors-On-Chillers/APP-CMC053-EN_Course_material.pdf) [Accessed Dec 1, 2020].
- [8] M. Grant, "How to Cut Chiller Energy Costs by 30%", Yaskawa America, 2015.
- [9] Z. Afroz et al, "Modeling techniques used in building HVAC control systems: A review," Renewable & Sustainable Energy Reviews, vol. 83, pp. 64-84, 2018.
- [10] A. Afram and F. Janabi-Sharifi, "Theory and applications of HVAC control systems – A review of model predictive control (MPC)," Building and Environment, vol. 72, pp. 343-355, 2014.
- [11] B. P. Rasmussen, "Dynamic Modeling and Advanced Control of Air Conditioning and Refrigeration Systems." , ProQuest Dissertations Publishing, 2005.
- [12] S. Bendapudi, J. E. Braun and E. A. Groll, "A comparison of moving-boundary and finite-volume formulations for transients in centrifugal chillers," International Journal of Refrigeration, vol. 31, (8), pp. 1437-1452, 2008.
- [13] S. Bendapudi, J. E. Braun and E. A. Groll, "Dynamic Model of a Centrifugal Chiller System-Model Development, Numerical Study, and Validation," ASHRAE Trans, vol. 111, pp. 132-148, 2005.
- [14] Z. Lei and M. Zaheeruddin, "Dynamic simulation and analysis of a water chiller refrigeration system," Applied Thermal Engineering, vol. 25, (14), pp. 2258-2271, 2005.

- [15] P. Li, Y. Li and J.E. Seem, "Modelica Based Dynamic Modeling of Water- Cooled Centrifugal Chillers, " International Refrigeration and Air Conditioning Conference, Paper 1091, pp 1-8, 2010
- [16] R. Llopis, R. Cabello and E. Torrella, "A dynamic model of a shell-and-tube condenser operating in a vapour compression refrigeration plant," International Journal of Thermal Sciences, vol. 47, (7), pp. 926-934, 2008.
- [17] R. N. N. Koury, L. Machado and K. A. R. Ismail, "Numerical simulation of a variable speed refrigeration system," International Journal of Refrigeration, vol. 24, (2), pp. 192-200, 2001.
- [18] A. Afram and F. Janabi-Sharifi, "Review of modeling methods for HVAC systems," Applied Thermal Engineering, vol. 67, (1-2), pp. 507-519, 2014.
- [19] H. Bechtler et al, "New approach to dynamic modelling of vapour-compression liquid chillers: artificial neural networks," Applied Thermal Engineering, vol. 21, (9), pp. 941-953, 2001.
- [20] J. Navarro-Esbrí et al, "A low data requirement model of a variable-speed vapour compression refrigeration system based on neural networks," International Journal of Refrigeration, vol. 30, (8), pp. 1452-1459, 2007.
- [21] J. A. Romero, J. Navarro-Esbrí and J. M. Belman-Flores, "A simplified black-box model oriented to chilled water temperature control in a variable speed vapour compression system," Applied Thermal Engineering, vol. 31, (2-3), pp. 329-335, 2011.
- [22] R. Tudoroiu, M. Zaheeruddin, N. Tudoroiu and D. Dan burdescu, "MATLAB Implementation of an Adaptive Neuro-Fuzzy Modeling Approach Applied on Nonlinear Dynamic Systems - a Case Study," 2018 Federated Conference on Computer Science and Information Systems (FedCSIS), Poznan, 2018, pp. 577-583.
- [23] N. Tudoroiu, M. Zaheeruddin, S. Li and R. Tudoroiu, "Design and Implementation of Closed-loop PI Control Strategies in Real-time MATLAB Simulation Environment for Nonlinear and Linear ARMAX Models of HVAC Centrifugal Chiller Control Systems," Advances in Science, Technology and Engineering Systems Journal, vol 3, No. 2, pp. 283-308, 2018
- [24] M. W. Browne and P. K. Bansal, "Steady-state model of centrifugal liquid chillers," International Journal of Refrigeration, vol. 21, (5), pp. 343-358, 1998.
- [25] M. W. Browne and P. K. Bansal, "Transient simulation of vapour-compression packaged liquid chillers," International Journal of Refrigeration, vol. 25, (5), pp. 597-610, 2002.
- [26] S. Wang, J. Wang and J. Burnett, "Mechanistic model of centrifugal chillers for HVAC system dynamics simulation," Building Services Engineering Research & Technology, vol. 21, (2), pp. 73-83, 2000.

- [27] A. H. Beitelmal and C. D. Patel, "A steady-state model for the design and optimization of a centralized cooling system," *International Journal of Energy Research*, vol. 34, (14), pp. 1239-1248, 2010.
- [28] Y. Yao, M. Huang and J. Chen, "State-space model for dynamic behavior of vapor compression liquid chiller," *International Journal of Refrigeration*, vol. 36, (8), pp. 2128-2147, 2013.
- [29] Y. Yao, W. Wang and M. Huang, "A state-space dynamic model for vapor compression refrigeration system based on moving-boundary formulation," *International Journal of Refrigeration*, vol. 60, pp. 174-189, 2015.
- [30] Z. Liu et al, "Optimal chiller sequencing control in an office building considering the variation of chiller maximum cooling capacity," *Energy and Buildings*, vol. 140, pp. 430-442, 2017.
- [31] T. Huang et al, "Study on the feature-recognition-based modeling approach of chillers," *International Journal of Refrigeration*, vol. 100, pp. 326-334, 2019.
- [32] Jia , Y., and Reddy, T. A. (February 7, 2005). "A Model-Based Feed-Forward Controller Scheme for Accurate Chilled Water Temperature Control of Inlet Guide Vane Centrifugal Chillers ." *ASME. J. Sol. Energy Eng.* February 2005; 127(1): 47–52. <https://doi-org.ezproxy.rit.edu/10.1115/1.1775225>
- [33] W. Jian and M. Zaheeruddin, "Sub-optimal on–off switching control strategies for chilled water cooling systems with storage," *Applied Thermal Engineering*, vol. 18, (6), pp. 369-386, 1998.
- [34] X. He et al, "Multivariable Control of Vapor Compression Systems," *HVAC&R Research*, vol. 4, (3), pp. 205-230, 1998.
- [35] D. Leducq, J. Guilpart and G. Trystram, "Non-linear predictive control of a vapour compression cycle," *International Journal of Refrigeration*, vol. 29, (5), pp. 761-772, 2006.
- [36] L. C. Schurt, C. J. L. Hermes and A. Trofino Neto, "Assessment of the controlling envelope of a model-based multivariable controller for vapor compression refrigeration systems," *Applied Thermal Engineering*, vol. 30, (13), pp. 1538-1546, 2010.
- [37] M. Wallace et al, "Offset-free model predictive control of a vapor compression cycle," *Journal of Process Control*, vol. 22, (7), pp. 1374-1386, 2012.
- [38] N. Jain and A. Alleyne, "Exergy-based optimal control of a vapor compression system," *Energy Conversion and Management*, vol. 92, (C), pp. 353-365, 2015.
- [39] J. A. Alfaya et al, "Controllability analysis and robust control of a one-stage refrigeration system," *European Journal of Control*, vol. 26, pp. 53-62, 2015.
- [40] X. Yin and S. Li, "Model Predictive Control for Vapor Compression Cycle of Refrigeration Process," *International Journal of Automation and Computing*, vol. 15, (6), pp. 707-715, 2016;2018;.

- [41] J. Prášek et al, "Range control MPC with application to Vapor Compression Cycles," *Control Engineering Practice*, vol. 96, pp. 104309, 2020.
- [42] M. Ning, "Neural Network Based Optimal Control of HVAC&R Systems," Ph.D. dissertation, The Department of Building, Civil and Environmental Engineering, Concordia University, 2008.
- [43] Ma, Z. & Wang, S. 2011, "Supervisory and optimal control of central chiller plants using simplified adaptive models and genetic algorithm", *Applied energy*, vol. 88, no. 1, pp. 198-211.
- [44] U. Ioan et al, "Intelligent control of HVAC systems. Part I: Modeling and synthesis," *INCAS Bulletin*, vol. 5, (1), pp. 103-118, 2013.
- [45] A. R. Al-Badri and A. H. Al-Hassani, "A control method using adaptive setting of electronic expansion valve for water chiller systems equipped with variable speed compressors," *International Journal of Refrigeration*, vol. 119, pp. 102-109, 2020.
- [46] Y. Yao, Y. Yu and SpringerLink (Online service), "Modeling and Control in Air-Conditioning Systems". (1st 2017. ed.) 2017.
- [47] N. S. Nise, "Control Systems Engineering". (8th ed.) Hoboken, NJ: John Wiley & Sons Inc, 2019.
- [48] B. E. Park, S. W. Sung and I. Lee, "Design of centralized PID controllers for TITO processes," 2017.
- [49] D. S. Naidu, "Optimal Control Systems". Boca Raton, Fla: CRC Press, 2003.
- [50] P. C. Young and J. C. Willems, "An approach to the linear multivariable servomechanism problem," *Legacy CDMS*, 1972.
- [51] L. Wang, "Model Predictive Control System Design and Implementation using MATLAB". (1st. ed.), Springer, 2009.
- [52] Y. Yao and D. K. Shekhar, "State of the art review on model predictive control (MPC) in Heating Ventilation and Air-conditioning (HVAC) field," *Building and Environment*, vol. 200, pp. 107952, 2021.
- [53] C. L. Charm et al, "Model Predictive Control with Direct Feedthrough with Application on a Mist Reactor", *IFAC-PapersOnLine*, vol. 53, Issue 1, pp. 183-188, 2020
- [54] S. L. Brunton, J. N. Kutz, "Data-Driven Science and Engineering Machine Learning, Dynamical Systems", and Control, (1st. ed.), Cambridge University Press, 2019
- [55] V. Ramasamy et al, "Optimal Tuning of Model Predictive Controller Weights Using Genetic Algorithm with Interactive Decision Tree for Industrial Cement Kiln Process," *Processes*, vol. 7, (12), pp. 938, 2019.